EX LIBRIS
UNIVERSITATIS
ALBERTENSIS

The Bruce Peel
Special Collections
Library

Digitized by the Internet Archive
in 2025 with funding from
University of Alberta Library

https://archive.org/details/0163020225351

UNIVERSITY OF ALBERTA

LIBRARY RELEASE FORM

NAME OF AUTHOR	Brigida I. Meza Diaz
TITLE OF THESIS	Experimental Investigation of Sand Production into a Horizontal Well Slot
DEGREE	Master of Science

YEAR THIS DEGREE GRANTED: 2001

Permission is hereby granted to THE UNIVERSITY OF ALBERTA LIBRARY to reproduce single copies of this thesis and to lend or sell such copies for private, scholarly or scientific research purposes only.

The author reserves other publication rights, and neither the thesis nor extensive extracts from it may be printed or otherwise reproduced without the author' s written permission.

University of Alberta

EXPERIMENTAL INVESTIGATION OF SAND PRODUCTION INTO A HORIZONTAL WELL SLOT

By

Brigida Inmaculada Meza Diaz

A thesis submitted to the Faculty of Graduate Studies and Research in partial fulfillment of the requirements for the degree of Master of Science

in

Petroleum Engineering

Department of Civil and Environmental Engineering

Edmonton, Alberta

Fall 2001

University of Alberta

Faculty of Graduate Studies and Research

The undersigned certify that they have read, and recommend to the Faculty of Graduate Studies and Research, for acceptance, a thesis entitled Experimental Investigation of Sand Production into a Horizontal Well Slot submitted by Brigida I. Meza Diaz in partial fulfillment of the requirements for the degree Master Science in Petroleum Engineering.

To my family

To Özgür

ABSTRACT

Reducing sand cleanout cost by controlling sand production into horizontal wells while enhancing the surrounding permeability of the formation is an important aspect in optimizing cold production from unconsolidated heavy oil reservoirs

The objective of this experimental investigation is to study the sand flow behavior in the vicinity of a slot in a horizontal well under different conditions. The parameters studied include slot size (0.018 in to 0.048 in), saturation fluid (air and dead synthetic oil), flow rates (50 - 150 cm^3/h), and sand properties (morphology and grain size distribution).

The results suggest that sand production through the slots can be controlled, depending more on the sand grain sorting than the morphology of the grain or its average diameter. Sand production behavior is strongly influenced by the arrangements of the sand grains in the vicinity of the slot including the formation of sand bridges, arches, or plugging. Significant changes in the permeability and porosity were determined in the vicinity of the slot. The changes in the parameters were less significant away from the slot.

ACKNOWLEDGEMENTS

The author wishes to express her sincere gratitude to her supervisors, Dr Bernard Tremblay, Dr Quang Doan and Dr Ergun Kuru, for their guidance, advice and encouragement throughout this study.

The technical assistance and suggestions provided by Kaz Oldakowski, Clare McCarthy Nina Sitek, Gerard Korpany and Valerie Pinkoski is greatly appreciated.

The patience and moral support provided by friends during the research years merits great appreciation. I wish to give particular thanks to Ludmilla Schmidt and Özgür Ökte for their understanding, encouragement and irrepressible willingness to help in all situations and under any conditions.

The financial support for My Master degree provided by PDVSA-INTEVEP, Alberta Research Council (ARC) and the Natural Sciences and Engineering Research Council (NSERC) is gratefully acknowledged.

TABLE OF CONTENTS

1 Introduction 1

2 Literature Review 2

2.1 Cold Production 2
2.2 Sand Production 3
2.2.1 Sand Production Mechanism 5
2.2.2 Parameters influencing sand production 8
2.3 Sand Arching 9
2.3.1 Theoretical development 10
2.3.2 Effect of grain morphology, grain size distribution and opening diameter 13
2.3.3 Effect of confining stress 19
2.3.4 Effect of flow rate and other parameters 24
2.4 Stress Field Around a Slotted Liner 28

3 Statement of the Problem 37

4 Experimental Equipment, Materials and Procedure 39

4.1 Materials Used and their Properties 39
4.1.1 Fluids 39
4.1.2 Sands 39
4.1.2.1 Grain Size Analysis 40
4.1.2.2 Solids Density Measurement 42
4.1.2.3 Morphology Analysis 43
4.1.2.4 Shear Strength: Shear box test 45
4.2 Description of the apparatus and experimental procedure 47
4.2.1 Air Tests 47
4.2.2 Liquid Tests 49
4.2.2.1 Scaling flow rates to field conditions 51
4.2.2.2 Absolute Permeability of the Pack 52
4.2.2.3 Measurement of the produced sand 52
4.2.3 Sand Arch Visualization Using Thin Sections 56
4.2.4 X-ray Computed Tomography 58
4.2.4.1 Dry Sand Tests 59
4.2.4.2 Epoxied Cores 60

5 Discussion of the Experimental Results 79

5.1 Air Test Experiments 79
5.1.1 History of a Typical Air Test 80
5.1.1.1 Sil-1 Sand 80
5.1.1.2 Husky Sand 81
5.1.2 Effect of the Slot Size 81
5.1.2.1 Sil-1 Sand 82

5.1.2.2 Husky Sand 82
5.1.3 Effect of the Initial Flow Rate 83
5.1.3.1 Sil-1 Sand 84
5.1.3.2 Husky Sand 85
5.1.4 Size Distribution of the produced sand 86
5.1.5 Effect of Initial Porosity on sand production 87
5.1.6 Reproducibility of the Tests 87
5.1.7 Comparison Between Sands 88
5.1.8 Summary of the section 88
5.2 Liquid Experiments 111
5.2.1 Data Analysis Procedure 111
5.2.1.1 Slot width to equivalent diameter ratio 111
5.2.1.2 Pressure Gradients Calculations 112
5.2.1.3 Determination of the variations in the properties of the sand pack .. 114
5.2.2 History of a Typical Liquid Test 116
5.2.2.1 Sil-1 Sand 116
5.2.2.2 Husky Sand 119
5.2.2.3 Glass Beads 126
5.2.3 Effect of the Slot Size 128
5.2.3.1 Sil-1 Sand 128
5.2.3.2 Husky Sand 132
5.2.4 Effect of Morphology and Size Distribution 135
5.2.4.1 Shape 135
5.2.4.2 Size distribution 138
5.2.5 Reproducibility Test: Sil-1 sand 139
5.2.6 Summary of the section 142
5.3 Thin Sections 176
5.3.1 Sil-1 sand 176
5.3.2 Husky sand 177
5.3.3 Glass beads less fines (GBLF) 178
5.4 X-ray Computed Tomography 187
5.4.1 Dry Sand Tests 187
5.4.1.1 Sil-1 Sand 187
5.4.1.2 Husky Sand 188
5.4.1.3 Glass Beads with Less Fines 188
5.4.2 Epoxied Sand Packs 189
5.4.2.1 Sil-1 190
5.4.2.2 Husky sand 191
5.4.2.3 Glass beads 191

6 Conclusions 207

7 Recommendations for Future Work 208

8 References 209

A. Appendix: Numerical Simulation of Stress Field around a Slotted Liner [42].....216

B. Appendix: Sample Calculations.....220

B.1 Sieve Analysis data.....220
B.2 Density measurements (From equations 4.3 and 4.4).....222
B.3 Effective stress calculations.....223
B.4 Shear box test.....224
B.5 Calculation of the air flow rate.....229
B.6 Calibration of the pump.....234
B.7 Calculation of porosity in the pack.....237
B.8 Compressibility Tests.....238
B.8.1 Procedure.....238
B.8.2 Calculations.....238
B.9 Determination of absolute permeability.....240

LIST OF FIGURES

Figure 2.1: Micromechanical forces exerted on a grain lying on the borehole wall. After A. Charlez [4] 31

Figure 2.2: Difference between sand bridging and sand arching. After Tippie et al. [30] 31

Figure 2.3: Sand arching experiment. After A. Charlez [4] 31

Figure 2.4: Rules of particle stability. After McCormack [32] 32

Figure 2.5: Stability diagram for 3-particle arches when the gap opening is 2 x the particle diameter. After McCormack [32] 32

Figure 2.6: Stability diagram for 3-particle of different particle sizes. After McCormack [32] 33

Figure 2.7: Calculation of gap opening size from sand fraction arrangement probability. After McCormack [32] 33

Figure 2.8: System of an arch that can stabilize friable sand. After Stein et al. [39] 34

Figure 2.9: Radial stress versus distance at different compressibilities and gas saturation. After Yuan [44] 34

Figure 2.10: Tangential stress versus distance at different compressibilities and gas saturation. After Yuan [44]. 35

Figure 2.11: Axial stress versus distance at different compressibilities and gas saturation. After Yuan [44] 35

Figure 2.12: Porosity versus distance at different compressibilities. After Yuan [44] 36

Figure 4.1: Particle size distribution curves 67

Figure 4.2: Reproducibility of the sieve analysis. Sil-1 sand, two different samples 67

Figure 4.3: Roundness scale of Maurice Powers [52] 68

Figure 4.4: SEM photomicrograph of the Sil-1 sand. MAG: X50. 68

Figure 4.5: SEM photomicrograph of a Sil-1 grain. MAG X500 69

Figure 4.6: SEM photomicrograph of the Husky sand. MAG: X50. 69

Figure 4.7: SEM photomicrograph of the Husky sand showing the difference between the grain sizes. MAG:50 70

Figure 4.8: SEM photomicrograph of a Husky grain. MAG X450. 70

Figure 4.9: SEM photomicrograph of the Glass Beads. MAG: X50. 71

Figure 4.10: SEM photomicrograph of a Glass Bead. MAG X500. 71

Figure 4.11: Shear stress displacement curve for Husky sand. σ_n=40.56 kPa 72

Figure 4.12: Mohr-Coulomb failure envelope Sil-1 sand 72
Figure 4.13: Mohr-Coulomb failure envelope Husky sand 73
Figure 4.14: Mohr-Coulomb failure envelope Glass Beads with less fines sand 73
Figure 4.15: Schematic of Sand Production Apparatus for the Air Tests (not to scale)..... 74
Figure 4.16: Dimensions of the Vessel used in the Air Experiments (not to scale). 74
Figure 4.17: Slot plates used in the air experiments 75
Figure 4.18: Schematic of Sand Production Apparatus for Liquids Tests (not to scale)..... 75
Figure 4.19: Slot plates used in the sand production liquid experiments 76
Figure 4.20: Equipment for the liquid experiments 76
Figure 4.21: Experimental apparatus to prepare the epoxied core for the thin sections..... 77
Figure 4.22: Pictures of epoxied core obtained for the thin sections 77
Figure 4.23: Overview of the thin sections 78
Figure 5.1: Cumulative sand production versus time. Sand: Sil-1. Gravity flow. Slot size: 0.028 in (0.71 mm). Runs 6 and 16..... 99
Figure 5.2: Sand production rate versus time. Gravity flow and 10 psi (69 kPa) injection pressure. Sand: Sil-1. Slot size: 0.028 in (0.711 mm). Run 6. 99
Figure 5.3: Sand production rate versus time. Gravity flow and 10 psi (69 kPa) injection pressure. Sand: Husky. Slot size: 0.028 in (0.711 mm). Run16..... 100
Figure 5.4: Sand flow rate versus time. Sil-1 sand. Slot width: 0.040 in (1.02 mm). Run 13 100
Figure 5.5: Sand flow rate Vs time. Husky sand. Slot width: 0.040 in (1.02 mm). Run 26 101
Figure 5.6: Effect of initial air delivery pressure. Sand production rate versus time. Sil-1 sand. Slot size: 0.028 in (0.71 mm). Different flow rates..... 101
Figure 5.7: Effect of initial air delivery pressure. Sand production versus time Sil-1 sand. Slot size: 0.028 in (0.71 mm). Different flow rates. 102
Figure 5.8: Effect of initial air delivery pressure. Sand production rate versus time. Husky sand. Slot size: 0.028 in (0.71 mm). Different flow rates. 102
Figure 5.9: Effect of initial air delivery pressure. Sand production versus time. Husky sand. Slot size: 0.028 in (0.71 mm). Different flow rates..... 103
Figure 5.10: Effect of flow rate: Sand production rate versus time. Husky sand. Slot size: 0.040 in (1.02 mm). Run 27. Initial flow rate 5.66 l/min..... 103
Figure 5.11: Effect of initial flow rate: Sand production rate versus time at initial conditions for runs 26 and 27. Husky sand. Slot size: 0.040 in (1.02 mm)..... 104
Figure 5.12: Sand production rate versus time at the air threshold flow rate for runs 26 and 27. Husky sand. Slot size: 0.040 in (1.02 mm). 104

Figure 5.13: Particle size distribution curves for the sand produced by gravity flow test 39. Sand: Sil-1. Slot size: 0.028 in (0.711 mm). 105

Figure 5.14: Particle size distribution curves for the sand produced with a flow rate of 5.66 l/min @10 psi (68.90 kPa). Sand: Sil-1. Slot size: 0.028 in (0.711 mm)..... 105

Figure 5.15: Particle size distribution curves for the sand produced with a flow rate of 13.68 l/min @ 40 psi (275.79 kPa). Sand: Sil-1. Slot size: 0.028 in (0.711 mm)..... 106

Figure 5.16: Effect of porosity in the sand production rate. Tests 6, 37 and 40. Sand: Sil-1. Slot size: 0.028 in (0.711 mm). 106

Figure 5.17: Sand produced versus of time. Tests: 6, 21, 22, 24, 30, and 38. Sil-1 Sand. Gravity flow. Slot size: 0.028 in (0.711 mm). 107

Figure 5.18: Sand flow rate versus time. Tests: 6, 21, 22, 24, 30, and 38. Gravity flow. Sil-1 Sand. Slot size: 0.028 in (0.711 mm)..... 107

Figure 5.19: Sand Production rate versus time. Tests: 7, 8 and 28. Air flow rate: 9.53 l/min @ 20 psi (137.90 kPa). Sil-1 Sand. Slot size: 0.028 in (0.711 mm)..... 108

Figure 5.20: Sand Production rate versus time. Tests: 9 and 29. Air flow rate: 13.68 l/min @ 40 psi (275.79 kPa) Sil-1 Sand. Slot size: 0.028 in (0.711 mm)..... 108

Figure 5.21: Sand Production rate versus time. Tests: 16, 25, 31 and 34. Gravity flow. Husky Sand. Slot size: 0.028 in (0.711 mm). 109

Figure 5.22: Sand Production rate versus time. Tests: 17, 18 and 35. Air flow rate: 9.53 l/min @ 20 psi (137.90 kPa). Husky Sand. Slot size: 0.028 in (0.711 mm). 109

Figure 5.23: Sand produced versus time at different air flow rates. Slot size: 0.028 in (0.711 mm). 110

Figure 5.24: Sand flow rate, cumulative sand production and sand concentration versus time for Run 2. Sil-1 sand, slot size: 0.022 in (0.56 mm). Flow rate: 50 cm^3/h. 152

Figure 5.25: Pressure versus time for test # 2. Sil-1 sand, slot size: 0.022 in (0.56 mm). Flow rate: 50 cm^3/h. 152

Figure 5.26: Pressure gradients versus time for Run 2. Sil-1 sand, slot size: 0.022 in (0.56 mm). Flow rate: 50 cm3/h 153

Figure 5.27: Pressure versus time for test # 2. Sil-1 sand, slot size: 0.022 in (0.56 mm). Flow rate: 100 cm^3/h. 153

Figure 5.28: Pressure gradients versus time for test # 2. Sil-1 sand, slot size: 0.022 in (0.56 mm). Flow rate: 100 cm3/h 154

Figure 5.29: Pressure versus time for test # 2. Sil-1 sand, slot size: 0.022 in (0.56 mm). Flow rate: 150 cm3/h. 154

Figure 5.30: Pressure gradients versus time for test # 2. Sil-1 sand, slot size: 0.022 in (0.56 mm). Flow rate: 150 cm^3/h. 155

Figure 5.31: View of the slot producing Sil-1 sand at the beginning of Run 2. Slot size 0.022 in (0.56 mm). Flow rate: 50 cm^3/h 155

Figure 5.32: View of the slot producing Husky sand. Run 7. Slot size: 0.040 in (1.02 mm). Flow rate 50 cm^3/h. 156

Figure 5.33: Sand flow rate, cumulative sand production and sand concentration versus time for run 7. Husky sand, slot size: 0.040 in (1.02 mm). Flow rate: 50 cm^3/h 157

Figure 5.34: Pressure versus time for run 7. Husky sand, slot size: 0.040 in (1.02 mm). Flow rate: 50 cm^3/h. 157

Figure 5.35: Pressure gradients versus time for run 7. Husky sand, slot size: 0.040 in (1.02 mm). Flow rate: 50 cm^3/h. 158

Figure 5.36: Sand flow rate, cumulative sand production and sand concentration versus time for run 7. Husky sand, slot size: 0.040 in (1.02 mm). Flow rate: 100 cm^3/h 158

Figure 5.37: Pressure versus time for run 7. Husky sand, slot size: 0.040 in (1.02 mm). Flow rate: 100 cm^3/h. 159

Figure 5.38: Pressure gradients versus time for run 7. Husky sand, slot size: 0.040 in (1.02 mm). Flow rate: 100 cm^3/h. 159

Figure 5.39: Sand flow rate, cumulative sand production and sand concentration versus time for run 7. Husky sand, slot size: 0.040 in (1.02 mm). Flow rate: 150 cm^3/h 160

Figure 5.40: Pressure versus time for run 7. Husky sand, slot size: 0.040 in (1.02 mm). Flow rate: 150 cm^3/h. 160

Figure 5.41: Pressure gradients versus time for run 7. Husky sand, slot size: 0.040 in (1.02 mm). Flow rate: 150 cm^3/h. 161

Figure 5.42: Bridging of two sand grains within a slot. Arrows indicated forces acting on right hand side grain. 161

Figure 5.43: View of the slot producing Glass Beads sand. Run 9. Slot size 0.028 in (0.71 mm). Flow rate: 50 cm^3/h. 162

Figure 5.44: Sand flow rate, cumulative sand production and sand concentration versus time for run 9. Glass Beads with less fines, slot size: 0.028 in (0.71 mm). Flow rate: 50 cm^3/h 162

Figure 5.45: Pressure versus time for run 9. Glass Beads less fines, slot size: 0.028 in (0.71 mm). Flow rate: 50 cm^3/h. 163

Figure 5.46: Pressure gradients versus time for run 9. Glass Beads with less fines, slot size: 0.028 in (0.71 mm). Flow rate: 50 cm3/h. 163

Figure 5.47: Pressure versus time for run 9. Glass Beads less fines, slot size: 0.028 in (0.71 mm). Flow rate: 100 cm^3/h. 164

Figure 5.48: Pressure gradients versus time for run 9. Glass Beads with less fines, slot size: 0.028 in (0.71 mm). Flow rate: 100 cm3/h. 164

Figure 5.49: Pressure versus time for run 9. Glass Beads with less fines, slot size: 0.028 in (0.71 mm). Flow rate: 150 cm3/h. 165

Figure 5.50: Pressure gradients versus time for run 9. Glass Beads with less fines, slot size: 0.028 in (0.71 mm). Flow rate: 150 cm3/h. 165

Figure 5.51: Sand cut versus time for different slot sizes. Sil-1 sand. Flow rate: 50 cm^3/h. 166

Figure 5.52 Sand cut versus time for different slot sizes. Sil-1 sand. Flow rate: 100 cm^3/h. 166

Figure 5.53: Sand cut versus time for different slot sizes. Sil-1 sand. Flow rate: 150 cm^3/h. 167

Figure 5.54: Pressure gradient between ports 2 and 3 versus time for different slot sizes and flow rates. Sil-1 sand. 167

Figure 5.55: Pressure gradient between ports 5 and 6 versus time for different slot sizes and flow rates. Sil-1 sand. 168

Figure 5.56: Sand cut versus time for different flow rates. Sil-1 sand and slotted plate 0.040 in (1.02 mm). 168

Figure 5.57: Pressure gradient between ports 2 and 3 versus time for different slot sizes and flow rates. Husky sand. 169

Figure 5.58: Pressure gradient between ports 5 and 6 versus time for different slot sizes and flow rates. Husky sand. 169

Figure 5.59: Pressure gradient ratio versus time for different sands and slot sizes 170

Figure 5.60: Pressure gradient between ports 2 and 3 versus time for different sands and flow rates. Slot size: 0.028 in (0.71 mm). 170

Figure 5.61: Pressure gradient between ports 5 and 6 versus time for different sands and flow rates. Slot size: 0.028 in (0.71 mm). 171

Figure 5.62: Sand cut versus time. Run 5. Sil-1 sand. Slot size 0.028 in (0.71 mm). Different Flow rates. 171

Figure 5.63: Pressure versus time for run 5. Sil-1 sand, slot size: 0.028 in (0.71 mm). Flow rate: 50 cm^3/h. 172

Figure 5.64: Pressure gradients versus time for run 5. Sil-1 sand, slot size: 0.028 in (0.71 mm). Flow rate: 50 cm^3/h. 172

Figure 5.65: Pressure versus time for run 5. Sil-1 sand, slot size: 0.028 in (0.71 mm). Flow rate: 100 cm^3/h. 173

Figure 5.66: Pressure gradients versus time for run 5. Sil-1 sand, slot size: 0.028 in (0.71 mm). Flow rate: 100 cm^3/h. 173

Figure 5.67: Pressure versus time for run 5. Sil-1 sand, slot size: 0.028 in (0.71 mm). Flow rate: 150 cm^3/h. 174

Figure 5.68: Pressure gradient versus time for run 5. Sil-1 sand, slot size: 0.028 in (0.71 mm). Flow rate: 150 cm^3/h. 174

Figure 5.69: Sand cuts for Runs 3 and 5. Sil-1 sand. 0.028 (0.71 mm) slot width. Flow rate: 50 cm^3/h. 175

Figure 5.70: Pressure gradients versus time. Sil-1 sand. Slot size: 0.028 in (0.71 mm). Flow rate 50 cm^3/h. 175

Figure 5.71: Microphotograph of the Sil-1 sand thin section showing a wide arch structure. Slot size 0.022 in (0.56 mm). Magnification: 32x 180

Figure 5.72: Microphotograph of the Sil-1 sand thin section showing a narrow arch structure. Slot size 0.022 in (0.56 mm). Magnification: 32x 181

Figure 5.73: Microphotograph of the Sil-1 sand thin section showing the arch and surrounded area. Slot size 0.022 in (0.56 mm). Magnification: 16x 181

Figure 5.74: Microphotograph of a Sil-1 sand thin section. Sand bulk above the arch. Slot size 0.022 in (0.56 mm). Magnification: 32x 182

Figure 5.75: Microphotograph of Sil-1 sand. Thin section showing gaps in the sand structure in the vicinity of the slot. Slot size: 0.028in (0.71mm). Magnification: 16x 182

Figure 5.76: Microphotograph of a slot showing grains bridging. Sil-1 sand thin section. Sand Slot size 0.028 in (0.71 mm). Magnification: 16x 183

Figure 5.77: Microphotograph of a Sil-1 sand thin section. Incipient sand arch. Slot size 0.028 in (0.56 mm). Magnification: 32x 183

Figure 5.78: Microphotograph of a Husky sand thin section. Arch 1. Slot size 0.028 in (0.56 mm). Magnification: 32x 184

Figure 5.79: Microphotograph of a Husky sand thin section. Arch 2. Slot size 0.028 in (0.56 mm). Magnification: 32x 184

Figure 5.80: Microphotograph of a Husky sand thin section. Arch 1, lower magnification. Slot size 0.028 in (0.56 mm). Magnification: 16x 185

Figure 5.81: Microphotograph of a Husky sand thin section. Sand grain plugging the slot. Slot size 0.028 in (0.56 mm). Magnification: 32x 185

Figure 5.82: Microphotograph of a Glass beads with less fines sand. Arch structure and surrounded areas. Slot size 0.028 in (0.56 mm). Magnification: 16x 186

Figure 5.83: Microphotograph of a Glass bead with less fines sand. Arch structure at higher magnification. Slot size 0.028 in (0.56 mm). Magnification: 32x 186

Figure 5.84: Transversal sections of the sand pack. Gravity flow experiments. Sand: Sil-1. Slot size: 0.028 in (0.71 mm)..... 194

Figure 5.85: Cross section of the sand pack at different heights from the slot. Gravity flow experiments. Sand: Sil-1. Slot size: 0.028 in (0.71 mm). 195

Figure 5.86: Transversal sections of the sand pack. Gravity flow experiments. Sand: Husky. Slot size: 0.028 in (0.71 mm). 196

Figure 5.87: Cross section of the sand pack at different heights from the slot. Gravity flow experiments. Sand: Husky. Slot size: 0.028 in (0.71 mm)..... 197

Figure 5.88 Transversal sections of the sand pack. Gravity flow experiments. Sand: glass beads less fines. Slot size: 0.028 in (0.71 mm)..... 198

Figure 5.89: Cross section of the sand pack at different heights from the slot. Gravity flow experiments. Sand: Glass beads less fines. Slot size: 0.028 in (0.71 mm). 199

Figure 5.90: Cross section of the sand pack at different heights from the slot. Epoxied core: Sil-1. Slot size: 0.022 in (0.56 mm). 200

Figure 5.91: Percentage of the surface area of the slice within the indicated ..... porosity change at various locations above the slot. Sil-1. 0.022 in (0.56 mm) slot size 201

Figure 5.92: Cross section of the sand pack at different heights from the slot. ..... Epoxied core: Husky sand (I). Slot size: 0.028 in (0.71 mm)..... 202

Figure 5.93: Cross section of the sand pack at different heights from the slot. Epoxied core: Husky sand (II). Slot size: 0.028 in (0.71 mm). 203

Figure 5.94: Percentage of the surface area of the slice within the indicated porosity change at various locations above the slot. Husky sand. 0.028 in (0.71 mm) slot size. 204

Figure 5.95: Cross section of the sand pack at different heights from the slot. Epoxied core: Glass beads less fines. Slot size: 0.028 in (0.71 mm)..... 205

Figure 5.96: Percentage of the surface area of the slice within the indicated porosity change at various locations above the slot.. Glass beads. 0.028 in (0.71 mm) slot size 206

Figure A.1: Mechanical boundary condition at the sand face u_r is the total radial displacement at the sand face. After Yuan [42] 218

Figure A.2: Hydraulic boundary condition at the sand face. After Yuan [42]..... 218

Figure A.3: Variation of the formation permeability with the porosity. 219

Figure B.1: Size distribution graph: Reproducibility of the sieve analysis for Husky, and glass bead sands. 221
Figure B.2: Z factor versus pressure for air @ 20 °C 233
Figure B.3: Calibration graph for pump 1 235
Figure B.4: Calibration graph for pump 2 236

LIST OF TABLES

Table 4.1: Typical Data for Viscasil 12M 61

Table 4.2: Sieve opening sizes [20] 61

Table 4.3: Sand equivalent diameters and uniformity coefficients 62

Table 4.4: Sieve analysis data 62

Table 4.5: Sieve analysis for two different samples of the Sil-1 Sand 63

Table 4.6: Butanol and Solid Densities 63

Table 4.7: Roundness classes (after Schneiderhöhn, 1954) [51] 64

Table 4.8: Effective stress at the bottom of the pressure vessel found in the liquid experiments 64

Table 4.9: Normal stresses applied during the shear box tests. Rate of displacement: 0.10 mm/min. 65

Table 4.10: Injection pressure and flow rates used in the air experiments 65

Table 4.11: Porosity and permeability of the sand packs used in the liquid tests 66

Table 4.12: Porosity of the sand packs used for the thin sections and dry sand CT scanner tests 66

Table 5.1: Slot width to equivalent diameter ratio for different percentiles 90

Table 5.2: Effect of Slot Width: Sil-1 sand (runs 6, 11, and 12) 90

Table 5.3: Effect of Slot Width: Husky sand (runs 14, 16, and 26) 91

Table 5.4: Effect of initial air delivery pressure (p_{inj}): Summary of results with Sil-1 sand for runs 6, 8, 9 and 10. Slot size 0.028 in (0.711 mm) 91

Table 5.5: Effect of initial air delivery pressure: Summary of results with Husky sand for runs 16, 17, 19 and 23. Slot size 0.028 in (0.711 mm) 92

Table 5.6: Summary of results with Husky sand for runs 26 and 27. Slot size 0.04 in (1.02 mm) 93

Table 5.7: Mass of sand produced (test 39). Sil-1 sand. Slot size 0.028 in (0.71 mm). 94

Table 5.8: Size distribution of the sand produced. Sieve analysis data. Test 39 95

Table 5.9: Effect of porosity in sand production behaviour. Summary of results for Runs 6, 37, 40, 34 and 41. Slot size: 0.028 in (0.711 mm). 96

Table 5.10: Summary of the reproducibility tests for the Sil-1 sand 97

Table 5.11: Summary of the reproducibility tests for the Husky sand 98

Table 5.12: Summary of the changes in permeability and porosity (in % of original values) for the liquid Runs. 116

Table 5.13: Slot width to equivalent diameter ratio for different percentiles for all sand evaluated in the liquid test. 143
Table 5.14: Distance between pressure ports and identification of the estimated pressure gradients 144
Table 5.15: Calculated values for the Kozeny constant "*c*" 144
Table 5.16: Results of Run 2 (Sil-1 Sand) 145
Table 5.17: Results of Run 7 (Husky Sand) 145
Table 5.18: Sand produced in Run 7 (Husky sand) 146
Table 5.19: Results of Run 9 (Glass Beads Less Fines) 147
Table 5.20: Sand produced in run 9 (Glass Beads Less Fines) 147
Table 5.21: Sand produced in the Liquid experiments 148
Table 5.22: Changes in the properties of the pack. Sil-1 sand. Different slot sizes 149
Table 5.23: Changes in the properties of the pack. Husky and Glass Beads sand. Different Slot sizes 150
Table 5.24: Summary of results for Runs 3 and 5. Sil-1 sand. Slot size: 0.028 in (0.71 mm) 151
Table 5.25: Epoxied cores characteristics 179
Table 5.26: Dry CT scanner tests. Characteristic of the sand pack and sand produced 193
Table A.1: Input Parameters Specified by ARC. After Yuan [42] 217
Table B.1: Reproducibility tests of the sieve analysis. Husky sand 220
Table B.2: Reproducibility tests of the sieve analysis. Glass Beads Like Husky 220
Table B.3: Reproducibility tests of the sieve analysis. Glass with less fines 221
Table B.4: Sand density calculations 222
Table B.5: Effective stress calculations 223
Table B.6: Data from a typical shear box test. Sand evaluates: Husky 224
Table B.7: Constants used in the air flow rate calculations 231
Table B.8: Data for air flow rate calculations. ADP = air delivery pressure 231
Table B.9: Air flow rate calculations 232
Table B.10: Z factor for air at different pressures[64]. Temperature 20 ^{o}C 233
Table B.11: Pump 1 calibration data 235
Table B.12: Pump 2 calibration data 236
Table B.14: Sample data for compressibility test. Oil Run # 5: Husky Oil sand. Slot size 0.028 in 242

Table B.15: Sample data and calculations for permeability tests. Oil run # 5: Husky Sand. Slot size: 0.028 in (0.712 mm) 244

NOMENCLATURE

A	Area (cm^2)
ARC	Alberta Research Council
b	Depth of the slot (thickness of the plate) (mm)
B	Formation volume factor (vol/vol)
BP	Bottom plate of a stacked set of sieves
c	Kozeny constant (m^{-2})
c_f	Coefficient of friction at the wall (dimensionless)
c_F	Compressibility of the fluid (kPa^{-1})
c_g	Gas compressibility (kPa^{-1})
c_o	Oil compressibility (kPa^{-1})
c_T	Total compressibility (kPa^{-1})
c_u	Cohesion (kPa)
C_u	Uniformity coefficient (dimensionless)
C_D	Drag coefficient (dimensionless)
CT	Computed tomography
dm	Differential mass (g)
dm_{oi}	Differential mass of injected oil (g)
dm_{op}	Differential mass of produced oil (g)
dm_{ot}	Differential mass of oil in the cell (g)
dm_{slurry}	Differential mass of slurry (g)
dm_{sp}	Differential mass of produced sand (g)
dm_{st}	Differential mass of sand in the cell (g)
$\partial p / \partial$	Partial derivative of pressure
$(dp/dL)_{1,2}$	Pressure gradient between ports 1 and 2 (kPa/cm)
$(dp/dL)_{2,3}$	Pressure gradient between ports 2 and 3 (kPa/cm)
$(dp/dL)_{3,4}$	Pressure gradient between ports 3 and 4 (kPa/cm)
$(dp/dL)_{4,5}$	Pressure gradient between ports 4 and 5 (kPa/cm)
$(dp/dL)_{5,6}$	Pressure gradient between ports 5 and 6 (kPa/cm)
$(dp/dL)_{6,7}$	Pressure gradient between ports 6 and 7 (kPa/cm)
$(dp/dL)_{6,slot}$	Pressure gradient between ports 6 and slot (kPa/cm)
dt	Time increment (s or h)
dV	Differential volume (cm^3 or cc)
$\partial V / \partial$	Partial derivative of volume
dV_{ot}	Differential Volume of oil at time t (cm^3 or cc)
dV_{st}	Differential Volume of slurry at time t (cm^3 or cc)
D	Diameter (cm or mm)
D_w	Outer Diameter of the pipe (in or cm)
D_{10}	Sieve size at which 10 % by weight of the sand will go through (mm)
D_{50}	Sieve size at which 50 % by weight of the sand will go through (mm)
D_{60}	Sieve size at which 60 % by weight of the sand will go through (mm)
D_{90}	Sieve size at which 90 % by weight of the sand will go through (mm)
$D_{99.9}$	Sieve size at which 99.9 % by weight of the sand will go through (mm)
E	Young's modulus (MPa or psi)

E_S	Shear modulus (MPa or psi)
F	Force (N)
F_f	Friction force (N)
F_h	Hydrodynamic force (N)
F_N	Normal intergranular force (N)
F_h^1	Drag force related to the pressure gradient (N)
F_h^2	Drag force related to the fluid viscosity (N)
G	Mass picnometer + sand + butanol (g)
GBLF	Glass beads less fines
GBLH	Glass beads with similar size distribution as Husky sand
h_{cz}	Height of the converging zone (cm)
$h_{sand\ in\ the\ cylinder}$	Height of the sand in the cylinder (cm)
$h_{small\ cylinder}$	Height of the small cylinder (cm)
K	Mass picnometer + butanol – mass of picnometer (g)
k	Permeability (Darcy or m^2)
k_p	Permeability in the sand pack (Darcy or m^2)
k_s	Permeability at the slot (Darcy or m^2)
L	Length of the pack (m, cm or mm)
L_s	Length of the slot (cm)
L_w	Length of the horizontal well (m or cm)
m_{H2O+P}	Mass of water + mass of picnometer (g)
m_{load}	Load Mass (kg)
m_P	Mass of picnometer (g)
m_{TSP}	Total mass of sand produced (g)
m_s	Mass of sand (g)
m_{S+P}	Mass of sand + mass of picnometer (g)
min.	Minute
M	Molecular weight (g/mol)
n	Moles
N	Number of perforations
p	Pressure (kPa, MPa or psi)
P	Mass of sand = m_{S+P} - m_P (g)
p_{atm}	Atmospheric pressure (kPa or psi)
p_B	Pressure at the end of the slot (kPa)
p_F	Final pressure (kPa)
p_{inj}	Pressure at inlet (kPa)
p_{prod}	Pressure at outlet (kPa)
p_s	pressure at the slot (kPa)
PV	Pore volume (cm^3 or cc)
PVC	Polyvinylchloride
q_s	Mass sand flow rate (g/s or g/h)
q_{ST}	Total sand flow rate (g/s or g/h)
Q	Volumetric fluid Flow rate (cm^3/h or cc/h)
Q_A	Volumetric air flow rate (l/min)
Q_i	Initial Volumetric flow rate (l/min, cm^3/h or cc/h)
Q_o	Volumetric oil flow rate (cm^3/h or cc/h)

Q_{slot}	Volumetric slot flow (l/min, cm^3/h or cc/h)
Q_T	Threshold air flow rate (l/min)
Q_{well}	Volumetric well flow rate (m^3/day)
r	Contact radius (mm)
r_s	Radius of the small cylinder of the liquid tests cell (cm)
R	universal gas constant (Pa m^3 K^{-1} mol^{-1})
R_c	Radius of the Coulomb zone (mm)
Re	Reynolds number (dimensionless)
R_I	Radius of the arch (mm)
R_g	Radius of a grain (mm or µm)
R_L	Radius of the large cylinder of the liquid tests cell (cm)
R_s	Value of R at the maximum effective stress (mm)
S	Butanol density (g/cc or g/cm^3)
S_{co}	Inherent shear strength of the material (cohesive strength)
S_g	Gas saturation (dimensionless)
S_o	Oil saturation (dimensionless)
S_s	Slot surface area (cm^2)
S_T	Total surface area of the horizontal well (cm^2)
Sil-1	Synthetic silica sand
SMS	Scientific Measurement Systems
t_{TSP}:	Elapsed time during which sand was produced (s or h)
T	Temperature (K or °C)
T_α	Parameter dependent on failure angle
T_{cell}	Cell temperature (K or °C)
T_{room}	Room temperature (K or °C)
TET	Total elapsed time (s or h)
v_f	Superficial velocity (cm/h)
V	Volume (l, cc or cm^3)
$V_{@atm}$	Volume at atmospheric pressure (cc or cm^3)
V_{air}	Air volume (cc or cm^3)
V_{cell}	Cell volume (cc or cm^3)
$V_{cilynder}$	Volume of the cylinder (cc or cm^3)
V_{cs}	Volume of the circumscribed sphere (cc or cm^3)
V_{cz}	Volume of the converging zone (cc or cm^3)
V_g	Gas volume (cc or cm^3)
V_o	Oil Volume (cc or cm^3)
V_p	Volume of the particle (cc or cm^3)
V_s	Sand Volume (cc or cm^3)
$V_{small\ cilynder}$	Volume of the small cylinder (cc or cm^3)
V_T	Total volume (cc or cm^3)
w	Weight of water (g)
W	Width of the slot (cm or mm)
W_s	Mass of sand produced (g)
x	Distance where the effective stress is calculated (cm)
Z	Compressibility factor (dimensionless)

GREEK SYMBOLS

α	Failure angle (degrees)
ΔL	Length increment (cm)
Δp	Pressure drop (kPa or psi)
ΔV	Volume increment (cm^3)
ϕ	Porosity (fraction or %)
ϕ_p	Porosity in the sand pack (fraction or %)
ϕ_s	Porosity at the slot (fraction or %)
φ	Friction angle (Degrees)
μ	Viscosity (cP)
μ_o	Oil viscosity (cP)
μ_r	Relative viscosity (cP)
μ_{Slurry}	Viscosity of the sand-oil slurry (cP)
ν	Poisson's ratio (dimensionless)
ρ	Density (g/cm^3 or g/cc)
ρ_f	Fluid density (g/cm^3 or g/cc)
ρ_{H2O}	Density of water (g/cm^3 or g/cc)
ρ_o	Density of oil (g/cm^3 or g/cc)
ρ_s	Density of sand (g/cm^3 or g/cc)
σ	Standard deviation
σ_{eff}	Effective stress (MPa, kPa or psi)
σ_n	Normal stress (MPa, kPa or psi)
σ_{pp}	Total radial stress (MPa, kPa or psi)
σ_r	Radial stress (MPa, kPa or psi)
σ_T	Tensile stress (MPa, kPa or psi)
$\sigma_{\theta\theta}$	Total hoop stress (MPa, kPa or psi)
$\sigma'_{\theta\theta}$	Effective hoop stress (MPa, kPa or psi)
τ_f	Maximum shearing resistance (MPa, kPa or psi)
ψ_w	Sphericity (dimensionless)

1 Introduction

Heavy oil production is becoming more important in Canada, due to the depletion of conventional oil reserves. The bulk of heavy oil production is from cold production of unconsolidated reservoirs in eastern Alberta and south-western Saskatchewan. In this process, oil production is enhanced by sand production. Many horizontal wells have been used in these reservoirs mainly to extend the access of the wellbore to the reservoir. While the use of horizontal wells has been mostly successful in improving the ultimate recovery in the reservoirs, the cost of sand cleanout is quite significant, and affects the economics of the operations.

Many studies have been done in the past on different aspects of sand production. However, they have mainly concentrated on finding effective methods to avoid sand production due to the high operation costs involved. Recent success in cold production has rekindled interest in sand production. Rather than avoiding sand production the emphasis should be on control and management of the produced sand. This new focus opens a wide area for research, especially in the case of the horizontal well technology as mentioned above.

This study focused on the experimental investigation of the flow of oil and sand in the vicinity of a heavy oil horizontal well under cold production. Specifically, it models physically the flow of oil and sand into a slot in a horizontal well liner. Emphasis was placed on obtaining measurements of flow-related variables (including pressures) inside the porous medium, including around the slot. Different types of experiments were conducted, and the data (including pressures and pressure gradients) were analyzed to improve the understanding of the mechanisms involved in the flow of oil and sand around, into, and through the slot and the response of the porous medium to sand production. It is envisioned that the findings from this work will contribute to effective sand control strategies, from the viewpoint of slot size selection for reservoir sands of given distribution and morphology.

2 Literature Review

2.1 Cold Production

Cold production is a primary non-thermal process used in unconsolidated heavy oil reservoirs in Alberta and Saskatchewan, Canada. In this process sand and oil are produced together in order to enhance the oil recovery [1,2,3]. In addition, this process has proven to be very profitable for these types of reservoir when vertical wells are used [4].

Cold production is characterized by high oil flow rates up to10 times higher than the flow rates predicted by using Darcy's radial flow equation [5,6,7]. Primary production recovery has also been reported to be significantly higher than predicted by classical flow models [8].

It is believed that two main mechanisms might explain the unexpectedly high primary oil recovery observed in these reservoirs. The first one is associated with gas evolution from the heavy oil (foamy oil) and the second one with sand production [8,9]. A comprehensive review of cold production has been presented by Tremblay et al. [1].

The presence of foamy oil in primary production reservoirs has been the subject of numerous studies since Smith [10] postulated its presence based on observations of bubbles in the produced oil. The foamy behaviour is considered to be a highly efficient solution gas drive mechanism relatively more complex than the conventional solution gas drive [11]. The foamy oil phenomenon will not be discussed in detail in the present literature review since the experimental work presented in this thesis is related to the second mechanism involved in cold production, i.e. sand production. More information about foamy oil process can be found in references [11,12,13,14,15].

Cold production has proven to be success when vertical wells are used. However, applications of cold production technology to horizontal wells has been less profitable. This has been mainly due to sand cleanout costs which significantly increase the production costs [8,16,17]. Therefore, efforts have been made to optimize sand

production in horizontal wells. In order to accomplish this objective, factors affecting sand production and control should be defined.

2.2 Sand Production

Sand production is defined as the production of small or large amounts of solids together with the reservoir fluids [18]. Traditionally sand production in oil wells has been seen as a problem that had to be avoided. Some of the negative effects associated with sand production have been [16,18,19,20]:

- Wear and erosion of the production equipment both downhole and on the surface.
- Problems with the stability of the wellbores and the production cavities, which, in the extremes cases, may lead to sand up and the abandonment of a well. Casing collapse may also result from excessive sand production.
- The necessity to handle significant amounts of sands at the wellsite and as a result the environmental problems of disposing of the dirty sand.

On the other hand, Dusseault et al [3] have reported that sanding in cold production is not necessarily a negative factor in oil well management. Some positive aspects mentioned by these authors are:

- Completion costs reduction
- Improved production rates
- Continued improvements in Productivity Index through the removal of the skin effect
- Elimination of expensive workovers to remove scale and other sources of near-well blockage

These positive aspects have been observed in many field case studies of cold production reported recently in the literature. Moreover, field observations have shown that blocking

sand production causes a strong decrease in oil production in shallow unconsolidated levels [3,4,6,21].

It is considered that sand production improves the efficiency of the other drive mechanisms by altering the fluid flow characteristics into the wells in heavy oil reservoirs. It is also thought that this might be one of the main reasons for the high production rates observed in the field [5]. A summary of the literature on field observations as well as the experimental studies performed to understand the field behaviour are given next.

McCaffrey and Bowman [5] analysed the performance of the Elk point and Lindbergh Amoco's fields. They considered that sand production enhanced the productivity of the producing interval allowing greater fluid flow rates to the wells. The presence of high permeable zones was inferred after loss circulation material during an infill drilling program was detected. Similar results were found in a program accomplished by Amoco Canada [22]. The program was planned to investigate the communication between wells. Tracer material (fluorescein dye) was pumped into the casing of the selected well. The results indicated that the tracer flowed through channel systems over 2 km in length that connected up to 12 wells. These results were also supported by Yeung's [23] findings in the study performed in the Burnt Lake cold production pilot project in the Cold Lake field operated by Suncor. The observed high oil productivity was believed to be a consequence of three main factors: 1) The sand failure and its removal from the wellbore area which provides a larger effective radius. 2) The viscosity of the bitumen which allows the sand to be suspended in the bitumen and carried out of the formation and improves the solution gas mechanism by avoiding the coalescence of the bubbles formed below the bubble point. 3) The creation of high permeability channels (wormholes) which improves the overall permeability of the reservoir.

Metwally and Solanki [8] evaluated cold production in the Lindbergh and Frog Lake heavy oil reservoirs in order to investigate the recovery mechanisms that contribute to improve primary production. They indicate that sand production leads to the creation of a high porosity disturbed zone that supplies a slurry of sand and fluid to the wellbore. It

was also pointed out that sand production reduces in situ stresses around the wellbore and was assumed jointly with the foamy oil behaviour to make the disturbed zone grow into channels of unknown geometry. These channels provide low resistance drainage paths, supply most of the produced fluids and function like fractures.

Recently, Huang et al. [7] reported the success of the Frog lake pilot project conducted under cold production by Texaco Canada Petroleum Inc. The project showed the feasibility of developing the field with horizontal wells. Oil flow rates three to four times higher than for vertical wells under cold production were reported. In spite of the technical success of the project, in order to have a profitable project the operative costs associated with sand production had to be reduced.

Laboratory studies have also been conducted to determine how sand production enhances oil production in heavy oil fields under Cold Production [24,25,26,27]. Two possible explanations have been given: formation of high permeability channels (wormholes) [24-26] or compact growth of a remolded zone (cavity formation) [3,27].

From the literature review, it is clear that cold production represents a feasible alternative to exploit thin shallow heavy oil reservoirs. However, more efforts need to be spent in overcoming the negative factors associated with sand production, especially for horizontal wells. In the following sections, the sand production mechanisms close to perforations and slots as well as the theory and practical work performed regarding sand arching will be discussed.

2.2.1 Sand Production Mechanism

Sand production analysis requires coupling of geomechanics (stress, strength, liquefaction), fluid flow (hydrodynamic drag, pressure, slurry rheology) and solution gas processes (bubble formation, phase behaviour)[3].

Sand failure occurs when the stresses on the formation exceed the strength of the formation. In order for the failed zone to grow significantly the sand must be transported. The formation cohesive strength is due mainly to the cohesive forces between the

immobile formation water and the oil surrounding the sand grains. The stress on the formation sand grains is due to many factors, notably, tectonic stresses, overburden stress, pore pressures, stress changes from drilling and the drag forces due to the producing fluids. The forces due to overburden stress however act differently in horizontal wells than they would in the case of vertical wells. Sand production is known to be rate sensitive [16].

For low cohesion materials, fluid flow can mobilize the grains. The condition for a grain to move under this situation was derived in reference [4].

Consider a grain A between two adjacent grains B and C (Figure 2.1). Assuming zero cohesion for the material, the grain is kept in place by contact (friction) through the action of the effective hoop stress:

(2.1) $$\sigma'_{\theta\theta} = \sigma_{\theta\theta} - p$$

where: $\sigma_{\theta\theta}$' = the effective hoop stress
$\sigma_{\theta\theta}$ = the total hoop stress
p = the pore pressure

The effective radial stress is null ($\sigma_{pp} = p$). The condition for a grain to move is written as:

(2.2) $$F_h \geq F_f = F_N \tan\varphi$$

where F_h = Hydrodynamic force related to the fluid velocity
F_f = Friction force
F_N = Normal intergranular force
φ = Internal friction angle

The normal mean contact force is defined to be the product of the mean stress by the contact surface:

(2.3) $$F_N = \bar{p}\pi r^2$$

where r = contact radius.

The hydrodynamic force F_h that tends to displace the grain towards the well can be separated in two components: a pressure component connected to the pressure gradient (F_h^1) and a drag force related to the fluid viscosity (F_h^2):

(2.4) $$F_h^1 = \frac{4}{3}\pi v_f \frac{\mu}{k} R_g^3$$

where R_g = grain radius (sphere in this case)
v_f = fluid velocity
μ = fluid viscosity
k = permeability of the porous media

The drag force of a viscous fluid on any submerged solid is proportional to the kinetic energy of the fluid:

(2.5) $$F_h^2 = C_D A\left(\frac{\rho_f v_f^2}{2}\right)$$

where: A = cross sectional area in the direction of flow
ρ_f = fluid density
C_D = drag coefficient depending on the Reynolds number.

In the specific case of laminar flow, Eq. (2.5) can be written as:

(2.6) $$F_h^2 = 6\pi v_f \mu R$$

Adding the expressions (2.4) and (2.6) the total drag force F_h is obtained:

(2.7) $$F_h = 2\pi v_f R\mu\left(\frac{2}{3}\frac{R^2}{k} + 3\right)$$

Using Darcy's law:

(2.8) $$v_f = -\frac{k}{\mu}\frac{\partial p}{\partial x}$$

Equation 2.8 can be rewritten as:

(2.9) $$F_h = 2\pi k R\left(\frac{2}{3}\frac{R^2}{k} + 3\right)\left(\frac{\partial p}{\partial x}\right)$$

Therefore, the hydrodynamic force acting on a sand grain is directly proportional to the pressure gradient ($\partial p / \partial x$).

It has been stated that there are two main mechanisms involved in sand production [18]:

Shear failure is related to too low well pressure. This means that some plane in the near wellbore region is subjected to higher shear stress than it can sustain. This mechanism is important mainly for cemented sands.

Tensile failure, basically related to high production rate. The sand production is then related to fluid drag forces on the grains of the formation. This is the main mechanism for the development of the high permeability channels or 'wormhole'.

In practice, the two mechanisms will work together and interact. A formation altered by shear failure may be much more susceptible to fluid drag. Even in the case of shear as basic mechanism, fluid flow is important in bringing the material into the well. Shear failure is the mechanism that can give the catastrophic amounts of sand production.

In addition to the above mechanisms, fines migration can also occur. This consists of the movement of fine particles such as clays in the formation. Fines migration can lead to the reduction of the permeability in the near wellbore region (a type of formation damage), which in turn will increase the fluid drag forces and may thus initiate sand production.

2.2.2 Parameters influencing sand production

The study of sand production control is very complex given the numerous parameters that can influence this process. McCormack [28] has classified the possible parameters that influence sand control as follows:

- *Formation properties*, such as degree of consolidation, grain size distribution, sand morphology, clay content, sand strength, overburden pressure, cohesion, wellbore stress concentration.

- *Fluid Flow*, fluid saturation, fluid production rates, oil gravity, temperature, flow transients and pressure.

- *Formation Alteration,* silica dissolution, clay dissolution and reprecipitation, fines movement.

- *Control techniques,* gravel pack sand specifications, wire wrap screen or slotted liner dimensions, consolidation of the wellbore zone by chemical methods, prepack screens, pumping equipment mechanics.

On the other hand Chalaturnik et al. [19] claimed that to evaluate the mechanisms controlling sand production it is important to follow the evolution of sand production during the different stages in the life of an oil well. This includes the drilling period, followed by completion, production and workovers. Specifically, the authors divide sand production in two interrelated categories: mechanisms governing sand production initiation and mechanisms governing sustained sand production. Moreover, initiation was defined as being strongly controlled by the disturbance from drilling and completion; it is dominated by near-wellbore effects. Sustained sand production was said to be controlled by global reservoir factors such as geology, in situ stress regimes and multiphase flow. Furthermore, it was stated that as for any other production process, sand production is intimately linked to the pressure behaviour in the well and to the flow processes in the reservoir.

2.3 Sand Arching

Sand arching seems a natural way to control sand production. An arch is a curved structure spanning an opening, serving to support a load by resolving external stresses into tangential and radial stresses [29]. Sand arching in a well completion is different from sand bridging. Sand bridging refers to blockage of an opening to sand movement

through the opening by an interlocking of a few grains and stress transfer between grains within or at the mouth of the opening. Arching refers to a structure formed entirely outside the opening [30]. In some instances, bridging and arching may occur simultaneously [17]. Figure 2.2 shows the difference between sand arching and bridging in a schematic form.

A means to visualize the arching phenomenon is through the experiment sketches in Figure 2.3. A cylindrical vessel with a perforated bottom floor is filled with an unconsolidated sand pack (Figure 2.3-1). The overburden stress is simulated by applying a vertical load to the vessel. Fluid is injected into the vessel through the top part at an increasing flow rate. Some sand is produced through the hole and a stable arch is formed (Figure 2.3-2). The flow rate can then be increased without any further production of solid until another critical value corresponding to a new arch is reached (Figure 2.3-3). The second arch is less stable than the first. The experiment was repeated until the cylinder was almost emptied (Figure 2.3-4).

Given the importance of sand production in the petroleum industry, both as a problem and more recently as an advantage in cold production, the phenomenon of sand arching over an opening has been the subject of numerous studies. Factors that influence the formation of the arches and their stability have been two of the topics most studied.

2.3.1 Theoretical development

Bratli and Risness [31] studied the arching phenomenon occurring in unconsolidated sands due to stresses imposed by a flowing fluid. They proposed a theoretical model, which established a stability criterion for sand arches. The model was validated with experimental work.

The laboratory model used by these authors consisted of a steel cylinder with a central hole at the bottom to simulate a perforation. The cylinder was filled with unconsolidated sand and compressed with a piston vertically to simulate overburden. Fluid was injected into the vessel at the top beneath the piston, with a wrapped wire screen diffuser. The

flow rate Q was increased steadily during the experiments. Air and oil were used as flowing fluid. Two types of sands, 20-40 mesh US and 80-100 Mesh US, were used.

From their experimental and theoretical work, they distinguished two modes of failure as the flow rate increased:

1. *Collapse of a thin inner shell.* A new stable arch radius is formed. The new arch has a larger radius which leads to a reduction in the stresses imposed by the flowing fluid under controlled flow rate conditions. Usually a series of such collapses occurred in an experiment.

2. *Total failure of the sand.* Critical values for flow rate and arch radius exists, and when reached, total failure of the sand results, leading to continuous sand production.

The stability criterion developed relates the drag forces and the strength parameters of the sand in the Coulomb failure zone. The criterion is given by:

(2.10) $$\frac{\mu Q}{4\pi k R_1} \geq \frac{T_\alpha + 1}{T_\alpha} 4 S_{co} \tan\alpha$$

where: T_α is given by: $T_\alpha = 2\left(\tan^2\alpha - 1\right)$

R_1= radius of the arch
μ= viscosity of the fluid
Q= fluid flow rate
S_{co}= inherent shear strength of the material (cohesive strength)
α = failure angle given by $\frac{\pi}{4} + \frac{\varphi}{2}$
φ: internal friction angle of the material

If the permeability in the Coulomb failure zone is varying, an effective permeability k_e has to be introduced in a stability criterion of the same form. From the stability criterion, the flow rate at which sand production starts can be obtained.

Collapse of an inner shell of the Coulomb failure zone by a tensile fracturing mechanism will take place if the fluid pressure exceeds the radial stress and the difference becomes equal to the uniaxial tensile strength σ_T as is shown by Eq. (2.11):

(2.11) $$p - \sigma_r = \sigma_T$$

Inserting the expression for σ_r and the fluid pressure p in Eq. (2.11) and after rearranging they came up with an expression for the flow forces at shell collapse (failure mode 1):

(2.12) $$\frac{\mu q}{4\pi k R_1} \geq \frac{T_\alpha + 1}{T_\alpha} 4 S_{co} \tan\alpha \frac{1}{1 + \frac{1}{T_\alpha}\left(\frac{R_1}{R_s}\right)^{T_\alpha + 1}}$$

where R_s= value of R at the maximum effective stress

The stability criterion also indicated that rates causing shell collapse would have values close to the critical flow rate for total collapse. Whether shell collapse or total collapse occurs will depend on the uniaxial tensile strength σ_T.

(2.13) $$\sigma_T < \frac{4 S_{CO} \tan\alpha}{T_\alpha}$$

This condition relating the strength parameters of the material must be fulfilled to make shell collapses occur.

If thin shells starts to fall in, this failure mechanism will continue with increasing flow rate until the radius of the Coulomb zone eventually reaches a limiting value given by the geometry of the system. Then the rest of the material will fall in. If the material does not fulfill equation (2.13), failure is governed by the total collapse criterion.

The experimental work of Bratli and Risness [31] indicated that the arching behaviour was always the same. The flow rate could be increased steadily until a small amount of sand was produced suddenly. Then the flow rate could be increased further without incident until a new amount of sand broke loose. This repeated itself several times until the sand pack broke down completely and came pouring out of the opening. It is important to mention that the sand production was qualitatively reproducible. The spread in the results was typical of sand arching experiments.

The arch radius, R_1, was calculated assuming a spherical cavity around the orifice:

(2.14) $$W_s = \frac{4}{3}\pi R_1^3 (1-\phi)\rho_s$$

where: Ws = the mass of sand produced
ρ_S = the sand density
ϕ = porosity

The authors [31] considered that the arches formed were stable if the flow rate could be reduced to zero and increased to its former value several times without sand production. This later effect was probably caused by using well-sorted sand.

From the theoretical analysis it was observed that the fluid drag forces appear through the term:

(2.15) $$\frac{\mu q}{4k\pi R_1}$$

Critical conditions could be reached when this flow term attains a certain maximum value given by the strength parameters S_{co}, α and σ_T for the sand.

The authors emphasized the spread in the experimental results and the uncertainties in the parameters involved made it impossible to discuss each experiment and the difference between them in detail. To test their theories they took average values of the calculated radius and flow rates.

2.3.2 Effect of grain morphology, grain size distribution and opening diameter

Hall and Harrisberger [29] studied the stability of sand arches and their relation to the maximum sand free petroleum production rate. They found that arch stability may be rate sensitive at low confining stress but independent of flow rate at high confining stress levels. The difference between strong-grain round sands and weak grain angular sands in regard to the stress level for grain crushing was shown. Arch failure under load occurred at lower stresses for angular sands.

The apparatus used by Hall and Harrisberger [29] consisted of a cylindrical chamber 3.75 in (9.53 cm) in diameter, fitted with a piston loaded vertically by a hydraulic jack. In order to observe arch formation a removable trap door of 7/16 in (1.11 cm) was placed in the centre of the vessel floor. The experiments consisted of removing the trap door and observing the formation of an arch or the production of sand. To evaluate the stability of the arch load was increased or fluids were injected in or out of the cell.

They compared the arch stability for round sands to angular sands. They observed that angular sand without compaction did not form an arch. When a moderate compaction was applied it could lead to a slightly stable arch, easily destroyed by tapping the apparatus. A higher load of 500 psi (3.4 MPa) helped to stabilize the arch. A better interlocking of the surface grains was the explanation for this result. A slow outward flow of air did not disrupt the arch, although a higher flow rate did. When a 2000 psi load (13.8 MPa) was applied, and the trap door was open, the arch failed. They observed that this failure was different and that the grain crushing was audible for several seconds.

For the round sand, they found that it would not arch for a loose or dense pack at low loads. Even at 500 psi (3.4 MPa) it seems that the grains did not interlock enough to stabilize the structure. The only way they could form arches with this sand was to inject air in counter current flow, in this way they could even go to higher loads without grain crushing. However as soon as the air flow decreased the arch failed.

Yim et al's work was cited by Charlez [4]. In this work it was established that besides the flow rate, the arch stability is strongly dependent on the granulometry of the porous material and the size of the perforation. Larger perforations required larger grains to form stable arches. Selecting perforation diameter is also used as a sand production control design strategy.

McCormack [32] conducted experimental work with spherical particles to determine the arching/bridging mechanism that influences the performance of wire-wrapped sand screens. He cited Coberly's work, who also studied the arching/bridging of steel balls and

sands using an adjustable gap opening size. McCormack's summarized of Coberly's findings is as follows:

For both well rounded sands and steel balls of a uniform size, stable arches were observed when the gap opening or slot size was less than 2 times the diameter of the particles. Unstable arches were observed when the slot width to particle diameter ratio was 2.5.

Particle mixtures of two sizes produce results that are intermediate between those of the individual sizes. When the difference in particle size is small, the mixture behaves like the larger of the two particles except at very low concentration of the large particles. When the size difference is greater, the smaller particles have a greater influence on the performance of the mixture.

Two types of arches were observed in the cell, a low three particle type and a high, four or five particle type. The lower type of arch tended to re-establish more quickly when the cell was disturbed.

A test with oil flowing through the cell had nearly identical results to a test with dry sand when other conditions were held constant. However, when oil wet sand with no fluid flow was tested, wider stable arches could be formed.

Numerous experiments showed that the stable gap opening size was generally 2 times the 10 % percentile size, D_{10}, of the sand. Vertical and horizontal slots gave similar results when sufficient particles covered the openings and oil is flowing. Gap openings with parallel sides were plugged. However, if an undercut, or keystone of 6^{o} was used then no plugging occurred. Arch stability was affected by the spacing between adjacent gap openings.

McCormack [32] also mentioned that even though there are several selection criteria for gap size opening cited in the literature, there is limited evidence that supports the selection of these criteria.

McCormack [32] recognized two types of packing using wire-wrapped screen. The first one is multiple particle arches; in this type of packing, breaking and re-establishment of the arches is observed which allows some resistance to fines plugging. This type of packing was called "partial sand retainment". The second type of packing is total sand retainment, which is usually employed with gravel packs. In this type of sand control an opening is chosen that is smaller than the size of the smallest particles. Therefore no sand is produced but plugging with fines may occur.

In the study by McCormack [32] the particles were assumed to be spherical and the arrangements were restricted to 2-dimensions. He assumed that the arches were formed by three particles. This assumption was confirmed by 3D experiments performed later. He established rules of particle stability which depend on the relative angle of contact between the particles and the base plane as shown in Figure 2.4. For particles of the same size and a slot width to particle size diameter ratio of 2, a wide range of stability was predicted as shown in Figure 2.5. A stable arch is defined as having at least one particle resting flat on the base plane. While a quasi-stable arch has both side particles positioned on the edge of the gap opening.

The same stability criteria were applied for other combinations of three particles of non-uniform size. The main difference between the stability of the arches formed by these particles with respect to the arches formed by uniform particles is that the stability range is reduced (see Figure 2.6).

McCormack [32] applied statistics to determine the probability of arching of a sand field. The statistic analysis was based on the particle size distribution of the sand and the width of the opening. He divided the size distribution in four ranges:

- Zone1: Highest percentiles (>18 to 80 mesh)
- Zone 2: Percentiles between 80 to 120 mesh
- Zone 3: Percentiles between 120 to 170 mesh

- Zone 4: Percentiles below 170 mesh.

The average diameter of each range was calculated. The probability of each 3 particle combination was calculated along with the appropriate sum of the nominal particle diameters (Figure 2.7). He predicted that a small percentage of the combination, less than 25%, was able to form a 3 particle arch. In the case study, the key arrangement was the range2-range2-range3. It was also shown that 10 to 20 % of the possible 3 particle arches for a given sand must be large enough to bridge across the selected gap opening in order to form an arch. This is a procedure that can be used for a wide variety of sand types particularly poorly sorted sands.

Mc Cormack [32] also studied the effect of the particles adjacent to the arching particles. The study was performed for arches of 4 spherical particles instead of three. The arches formed with 4 particles were more common than those formed by three particles according to experimental studies.

The 2D experiments were carried out with glass beads in a visual model where the packing structure could be seen. The glass beads were uniform in size and no fluids were used in the tests. He defined arch stability as the amount of force that has to be applied in order to disturb the arch and he observed this in a qualitative way. He defined the arch formation rate as the rate at which the arch re-establishes itself once disturbed. The average diameter of the glass beads used was 14.2 mm. Gaps opening twice and 1.5 times the percentile diameter were used.

The most important results were:

- The arches formed by 3, 4 or 5 particles arrengement.
- The location of the side particles of the arch could drastically affect arch stability and formation. He observed that side arch particles that were not firmly supported by the end walls greatly reduced arch stability.
- Secondary arches can occur under certain arrangements of the test cell.

- The opening that was 1.5 times the diameter of the uniform particles had the tendency to form faster and more stables arches.

In the 3D experiments, glass beads of 15.4 mm diameter were used. The major results were:

- Stable arches were observed when the opening was 1.8 times the particle diameter. However, for size openings around twice the particle diameter, stable arches would not form after the arch was even slightly disturbed. More glass beads went through the opening when the bed height was low or/and when the size opening was increased

- As the gap opening size increased, the arches tended to be composed of more particles.

The previous author [32] tested arch stability to different inclination angles of the bottom plate of the model. Slight differences in the stability of the arch were observed.

Arch stability and formation was quantified by disturbing the arch, applying force until the whole pack was produced. This was done for different positions of the bottom plate. When the opening was decreased to approximately 1.67 times the particle diameter, a substantial improvement in arch stability was observed. The 3D experiments showed that for a flat base wire arrangement, stable arches could be achieved when the gap opening size was up to 1.8 times the particle diameter.

Some of the limitations of the study were mentioned. Glass beads of uniform size were used. Different results may be found with particles of different shape and with a sand with different size distribution. Fluid flow was not considered, therefore the effect of fines and porosity changes in the pack was not taken into account. The applied stress field was due to gravity only. In real systems, the stress field would be multi-dimensional with localized stress concentrations.

McCormack concluded that:

1) For multiple particle, (2 to 6), arching occurs when the partial sand retainment criteria is used.

2) When 10-20 % of the arches are of the 3 particle type, the overall arch structure should be stable. This may be estimated by calculating the average diameter of all three particle combinations from a seoaration of the sand size distribution curve into four fractions.

3) Significant force concentrations can be expected on the arch particles. Breakage of particle is a probable source of arch failure and sand production. A controlled amount of breakage can serve to clean the arch of fines and scale plugging.

2.3.3 Effect of confining stress

Selby and Farouq Ali [33] performed sand production experiments in a cylindrical model 17.7 cm in height by 20.0 cm in diameter. A perforated tubing 1.3 cm in diameter was fitted into a hole drilled in the centre of the cell bottom. Radial flow was simulated by lining the inner walls of the cell with a sintered sheet. Two injection ports were located at the outer walls of the cell. They varied the overburden pressure, the flow rate, the sand grain size and shape, and the size and shape of the tubing perforations

They [33] performed tests to evaluate the effect of grain size on sand production both with and without and overburden load. Ottawa Sand (70 to 140 mesh) and Silica sand (40 to 70 mesh) were used in the experiments. In the case where overburden pressure was applied, no arching was observed when the smaller grain sand size diameter was used and unstable arches were observed for the larger grain size diameters. In the other case, without overburden pressure, both sands formed stable arches around the perforation. They reported that sand production was higher for the smaller diameter sand.

No arches were formed when glass beads were used under the same conditions used in the Ottawa sand and Silica sand experiments. Therefore, more sand was produced for the glass beads than for the angular sand.

Selby and Farouq Ali [33] also studied the effect of the perforation shape and size. They observed that all wells (slotted and round perforations) produced glass beads. The slotted tubing allowed more beads production than angular sand. Increasing the perforation size from 0.08 to 0.11 cm lead to a slight decrease in the amount of sand produced. Similar runs were performed with Ottawa Sand of the same size. No sand production was observed when the wells with the round perforations were used whereas substantial sand was produced when the slotted well was used.

The sand arches formed very slowly at low flow rates in the tests using the slotted tubing. Arching occurred rapidly at higher flow rates when no overburden was applied. However, sand arches were formed instantaneously when tubings with round holes were used, even though the tests were conducted under moderate overburden loads.

Hall and Harrisberger [29] examined the load that would cause an arch to fail by sand crushing. They formed the arch with a load of 500 psi (3.4 MPa) and then they increased the load. They found that the arch formed by the rounded sand support the total load that the equipment could stand (3450 psi or 23.8 MPa). The angular sand crush at 1950 psi (13.4 MPa). When they wet the angular sand a slightly higher crushing pressure was obtained (2100 psi or 14.5 MPa).

They concluded that the two conditions required for stability of an arch of sand are:

1) Dilatancy and

2) Cohesiveness or some other grain restraint.

Toma et al [17] mentioned that sand arching is directly related to the high confining stress. The failure of arches leads to massive sand inflow. For a given sand and cohesive force, the size of the arch depends on the pressure drop across it. With increasing fluid production rate, an increase in the arch radius is required to maintain the integrity of the arch. At a critical flow rate the arch will collapse. Furthermore, the maximum arch radius and critical flow rate do not depend directly on slot size.

Bratli and Risness [31,34] stated that a comprehensive study of the stability of sand arches must include a study of the stress distribution in the sand. These stresses will depend on the stress at the boundaries, the fluid pressure and flow rate, the geometry of the arch and on the stress strain relations of the material. They also studied the effect of overburden pressure and surface tension on the stability and formation of arches.

Cleary et al. [35] reported an experimental study of the sand behaviour across casing perforations. Bottom hole production conditions with overburden stresses of 250 psi (1.7 MPa), 750 psi (5.2 MPa), 1500 psi (10.3 MPa), 2250 psi (15.5 MPa) and 3000 psi (20.7 MPa) were used. The sand stabilization mechanism around the wellbore was by the formation of sand arches across the perforations.

They observed that the structure of an arch depends on the stress distribution in a sand pack. They also observed that the shape of the sand arch depended on the direction of the principal stresses with arch size decreasing with increasing confining pressure. It was also found that arch stability increased with increasing horizontal and vertical stresses. More stable arches were formed when the horizontal stress was maximum and the vertical stress minimum. The cohesive force as shown to have an important role in arch stability when different hydrocarbons liquids were used.

Cleary et al [35] pointed out that sand flow into the wellbore is generally associated with one or more of the following factors:

- Fluid drag associated with high oil viscosities.
- Fluid drag due to high oil velocities.
- Skin build up around the wellbore
- Rate surges
- Changing loading conditions around the wellbore due to pore pressure changes.

- The destruction of cohesive forces between the sand grains due to phase changes or changing saturations around the wellbore.

They used coarse sand (20-40 mesh). The arch size decreased with increased overburden pressure. The distinction between an arch and a cavity was explained. An Arch was defined as the sand structure that supports the sand behind it. A cavity was defined as the void space created in front of the arch as a consequence of the removed of the unstressed sand.

They visualized cavities in all tests after the overburden was applied. The cavities were ellipsoidal with the major axis in the vertical direction. They extended over the perforation. The cavity was observed to grow in the vertical direction when the flow rate was increased.

They stated that the mechanism that governs cavity growth is a combination of fluid effects and stress at the arch. They investigated the influence of cohesive force through the use of two different hydrocarbon liquids: mineral spirit and kerosene. The mineral spirit/water system did not exhibit as much cohesion as did the kerosene/water system. As a result, the arches did not exhibit the same level of stability as observed with the kerosene/water system.

When discussing restructuring of the sand arches, the viscosity of the fluids becomes important. Thus, mineral spirit having a lower viscosity than kerosene, has a higher initial arch restructuring flow rate.

Flow rates through the arch were increased until sand failure occurred. The arch failure was marked by a decrease in inlet and outlet pressures and a corresponding drop in sand stress.

In their test with mineral spirit they observed that the stress dropped at initial arch failure at lower stress levels. The stress drop at arch failure decreased as the initial stress increased.

Fines migration during oil flow results in an increase in the skin factor around the perforation. The pressure drop due to skin damage causes a rate surge at arch failure, which results in greater sand production. The increase in sand production results in an increase in stress drop at arch failure. The first test for each sand pack indicated a general decrease in vertical stress drop at arch failure as the initial vertical stress was increased. Likewise, a general decrease in horizontal stress drop at arch failure was observed as the initial horizontal stress was increased.

The authors [35] concluded that:

Sand free producing rates occurred through stable sand arches formed by sand stress around the perforation. The arch size was found to be a function of the confining stress level. Arch size decreased with increasing confining stress. A more stable arch occurred when the horizontal stress was maximum and the vertical stress was minimum. Arch restabilization under reloading conditions was found to occur at the upper confining stress level. Two modes of arch instability were indicated: initial arch restructuring and final arch failure. Only in highly cohesive sand packs did arches exhibit both modes of instability.

Melvan and Cleary et al. [37,35] mentioned that the arch which forms around a perforation, is oriented so that its minimum cross-sectional area faces the direction of maximum principal stress. They concluded that the orientation of the principal stress axes would govern the shape of the initial arch which forms upon the application of the overburden load.

Melvan [37] found that arch stability increases with increasing stress. He also observed that additional tests with the same sand pack resulted in less stable arches as a result of sand movement around the perforation which implied a decrease in the cohesive force. The water injection prior to each test would increase the cohesive force enough to allow an arch to form but not enough to obtain the same cohesion force as existed during the first test. It can be concluded that the cohesive forces between sand grains, which are necessary for arch formation, are very sensitive to sand movement. The previous author

observed that confining stress (horizontal) is more conducive to forming stable arches than vertical stress.

The stress drop during arch failure was studied. For any given sand pack, as the initial horizontal stress increased, the horizontal stress drop at arch failure increased. The increase in sand production resulted in an increase in stress drop at arch failure.

Miller [36] studied the flow of sand into and through well-casing perforations. The effect of sand particle size, casing perforation diameter, shape and roughness of perforation opening, sand porosity, sand confining stress, flow conditions through perforations and capillary cohesion between two fluids in a sand were examined experimentally.

He found that heavy oil formation sand, with only one fluid present, would not arch over or plug field size perforation openings. However, increased confining stress resulted in decreased sand flow rates. The presence of a high enough confining stress was able to prevent sand flow. Capillary cohesion between two fluids in a sand, such as gas and water, gas and oil or oil and water resulted in the formation of sand arches over perforation. The other variables investigated (i.e. sand particle size, casing perforation diameter, shape and roughness of perforation opening, sand porosity) had no or little effects on sand arching compared to the effect of capillary cohesion and confining stress.

2.3.4 Effect of flow rate and other parameters

Melvan [37] observed in his experimental work that the flow rate could be increased until sand failure occurred. The arch failure was marked by a decrease in inlet and outlet pressure with a corresponding rate surge. Flow rate surge was controlled in the experiment using a flow control valve located downstream from the perforation. He also observed that sand flow would occur with a corresponding drop in effective stress.

Hall and Harrisberger [29] investigated the effect of wettability and surface tension on the formation of arches with rounded sand. They observed that a wetting fluid like water can give cohesion to the sand and allow it to form stable arches; an opposite result was obtained when kerosene was used.

Melvan [37] observed that in addition to the application of stress, cohesive force is also needed to form an arch. He showed that sand production at arch failure disturbed the two phase saturation around the perforation enough to reduce the cohesive forces. Because of this, a new arch could not be formed upon the application of the overburden load as indicated by the drop in sand stress following a small amount of sand production. To prove the importance of cohesive forces in the formation of arches he injected water through the perforation prior to the start of each subsequent test where mineral oil or kerosene were used as a flowing fluid. The water injection increased the cohesive force sufficiently to allow the formation of a new arch.

Durrett et al. [38] studied: 1) the static forces holding sand in place 2) the dynamic and static forces tending to counteract these static holding forces; 3) the sand transport phenomenon.

He mentioned that the presence of two fluids in the matrix helped to avoid sand production due to an increase in cohesive strength. This was shown in experiments with either a mixture of oil and water or with just one fluid. In the first case flow rates up to 7 BOPD per perforation were reached before sand production occurred through the perforation at the downstream end of the cell. When the test was repeated with only one fluid, sand production occurred at a flow rate of 0.5 BOPD per perforation.

These tests indicated that interfacial tension forces could be significant in controlling sand production. The findings of these tests are in agreement with field observations where an increase in the water cut leads to increase in sand production. Due to an increase in the water saturation, there is a decrease in the cohesive strength.

Sand grains will be transported to the wellbore when the drag forces of the produced fluid exceeds the body forces holding the sand in place.

Stein et al [39] considered that it is possible to produce oil or gas at high flow rates from a friable formation, with potential problems of sand production, without any sand control measures. They considered that stable arches can form around the perforation. They

determined the maximum flow rate that can be achieved without sand production using sonic and density log data.

These authors [39] concluded that when the stress at the arch face exceeds the strength of the sand, particle movement will begin. The stress at the arch face is directly related to the fluid pressure gradient, which is a critical factor in maintaining formation stability. Moreover, the maximum stress that may be applied without causing a sand production problem should be proportional to the strength of the sand.

They applied Darcy's Law for spherical flow for the situation shown in Figure 2.8. The pressure drop across dr is:

(2.16) $$\frac{dp}{dr} = \frac{QB\mu}{1.127 * 10^{-3} kA}$$

where: B = formation volume factor
A = surface area of the hemispherical arch
k = permeability of the formation
μ = reservoir fluid viscosity
Q = fluid production rate

They assumed that adjacent perforation arches do not overlap and that the production rate from the well can be divided equally between the numbers of perforation N. Therefore, for one perforation q = Q/N

(2.17) $$\frac{dp}{dr} = \frac{qB\mu}{1.127 * 10^{-3} kAN}$$

They defined the factor R as the ratio of the pressure gradient at a well which is producing sand free (T) to the pressure gradient at a well with sand production (Z).

(2.18) $$R = \frac{\left(\frac{dp}{dr}\right)_T}{\left(\frac{dp}{dr}\right)_Z}$$

They related the factor R to the shear modulus, E_s, values in the same way. After mathematical calculations they came up with the following expression:

$$q_z = \frac{0.025x10^{-6} k_z N_z (E_s)_z A_z}{B_z \mu A_T} \tag{2.19}$$

The value of $(E_s)_T$ can be obtained from log data. Specifically they estimated the shear modulus from log data obtained with an 11-lb/gal mud. They recommended the application of the above equation to wells where $(E_s)_T$ can be obtained in a similar way.

Vaziri [27] showed theoretically that sand production causes changes in permeability and formation properties, which develop around the wellbore. He concluded that the exsolution of gases is responsible for most of the fluid flow under primary conditions. The model provides means of testing the influence of various recovery schemes, which can be employed in controlling the sand cuts.

The time dependent response of oil sands subject to the boundary conditions imposed by drilling a wellbore was calculated using a finite element program. Vaziri concluded that the major factor responsible for fluid production under primary conditions is the increase in compressibility of the pore fluid due to gas exsolution. Large movements in the soil mass around the unsupported region resulted in an enlarged cavity surrounded by a plastic zone when the well was on production. The flow rate was shown to be the main parameter that governs the instability around the wellbore. The transient flow rate is in turn a function of soil strength properties, permeability, fluid compressibility, and the pressure gradient near the well. He showed that a critical flow rate for the instability of the system may exist, leading to the development or extension of a liquid and plastic zone.

More recently Vaziri et al [40] reported an experimental study conducted to evaluate the effect of sand production on the oil flow rate from unconsolidated heavy oil reservoirs. They considered that the high production rate observed in the fields is a combination of sand production-induced wellbore cavitation and solution gas drive mechanisms. They stated that the most favourable geotechnical characteristics for improving flow rate are

low strength properties and strong permeability-porosity relationship. Within the shear – failed zone, permeability increases due to dilation and a net reduction in the mean effective stress state.

Tippie and Kohlhaas [30] described an investigation of flow rate effects on arch formation and stability. They used a semi-cylindrical cell which had a semi-cylindrical casing attached to its flat side. They performed experiments where the initial flow rate was gradually increased until sand production occurred. Their results showed that arch size increased with increasing fluid velocity at a control flow rate. Small arches were found to be more stable than larges arches. When an arch was re-established after an increase in flow rate the new arch was larger than the previous one. A gradual increase in flow rate to a certain value during a test yielded a stable arch. Starting the test at this flow rate resulted in sand failure. They determined that flow rate is a factor determining arch size and stability and that adjusting the flow rate can have marked effects on the producing characteristics of unconsolidated-sand reservoirs.

Selby and Farouq Ali [33] also investigated the effect of flow rate on sand production. In their experiments, the flow rate was varied from 2 ml/min to 13.3 ml/min with an intermediate flow rate of 8 ml/min. No overburden pressure was applied. The results were compared to when an overburden pressure was applied. In the absence of an overburden load, the sand formed arches regardless of the flow rate employed. The sand arched more rapidly at higher flow rates; however, the initial sand flux values were higher at higher rates. When overburden pressure is applied, arching occurred at a flow rate of 2 ml/min, but not at higher flow rates.

2.4 Stress Field Around a Slotted Liner

One issue that arises in the investigation of the flow of sand through slots is the effect of the stress field on the production of sand. The collapse of a heavy oil formation around a slotted liner by rapid depressurizing of a horizontal well was modelled numerically by Boone et al. [41]. The numerical calculations showed that the initial gap between the borehole and liner could be filled with oil sand, thereby preventing the flow of steam along the length of the well. These simulations were extended by Yuan [42] in order to

calculate the stress field around a slotted liner under typical field pressure and stress conditions given in appendix A.

The simulator (ABAQUS) used in the calculations by Yuan assumes single phase fluid flow with constant compressibility. The oil and gas in the porous media was assumed to flow as a single fluid with a compressibility given by:

(2.20) $$c_F = S_g / p$$

where c_F = compressibility of the fluid
Sg = gas saturation
p= pressure

The live oil compressibility was neglected. The simulations were run at two compressibilities $2x10^{-8}$ Pa^{-1} and $1x10^{-7}$ Pa^{-1} corresponding to a gas saturation of approximately 1 % and 5% respectively at a pressure of 500 kPa.

The latter compressibility ($1x10^{-7}$ Pa^{-1}) is most likely higher than in the field since gas does not come immediately out of solution from heavy oil as is assumed in the calculations.

The simulations showed that the stress field around a typical liner is quite low under low gas saturations conditions (1%) but increases with increasing gas saturation. For example, the radial, tangential and axial effective stress distribution around a 140 mm diameter liner due to the sudden collapse of a 219 mm wellbore, three hours after a 4 min wellbore pressure decline from 3 to 0.5 MPa, are shown in Figures 2.9, 2.10 and 2.11 respectively. At the higher compressibility of $1x10^{-7}$ Pa^{-1} the radial, tangential and axial effective stress at the wellbore were: 1000 kPa, 284.45 kPa and 554.88 kPa respectively.

These simulations showed that the magnitude of the stresses at the outer surface of a typical horizontal well (slotted liner) are comparable in magnitude to the maximum stress calculated at the bottom of the pressure vessel used in this thesis (Section 4.1.2.4, Table 4.8).

The radial distribution of the porosity around the well is shown in Figure 2.12. The porosity at the outer surface of the slotted liner was quite high (58 %). This curve shows that the porosity around a slot in a liner is higher than the formation porosity. Only at a distance of 0.3 m from the axis of the 140 mm diameter slotted liner was the porosity the same as in the field. Therefore, in order to model physically the flow of sand into a slot using a sand pack with a slot at the bottom the porosity of the sand pack should be higher than the formation porosity.

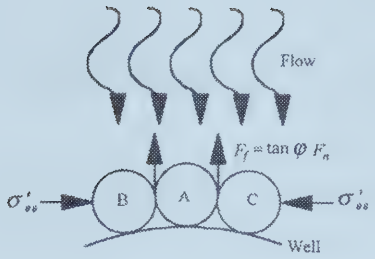

Figure 2.1: Micromechanical forces exerted on a grain lying on the borehole wall. After A. Charlez [4]

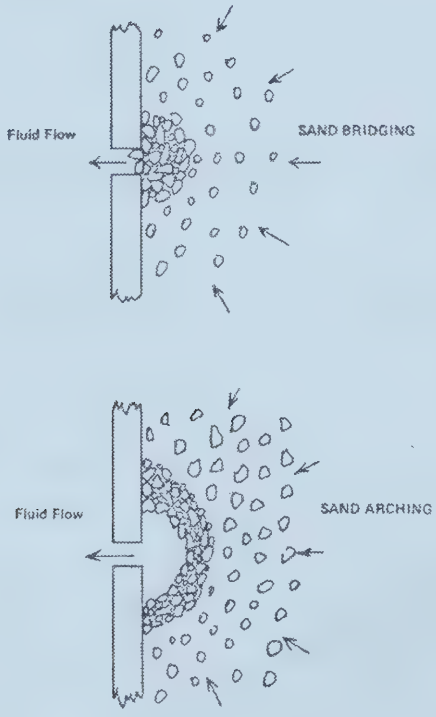

Figure 2.2: Difference between sand bridging and sand arching. After Tippie et al. [26]

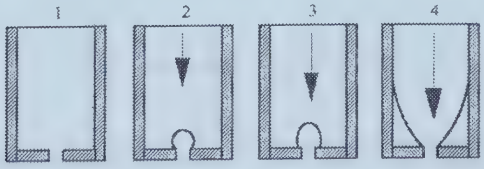

Figure 2.3: Sand arching experiment. After A. Charlez [4]

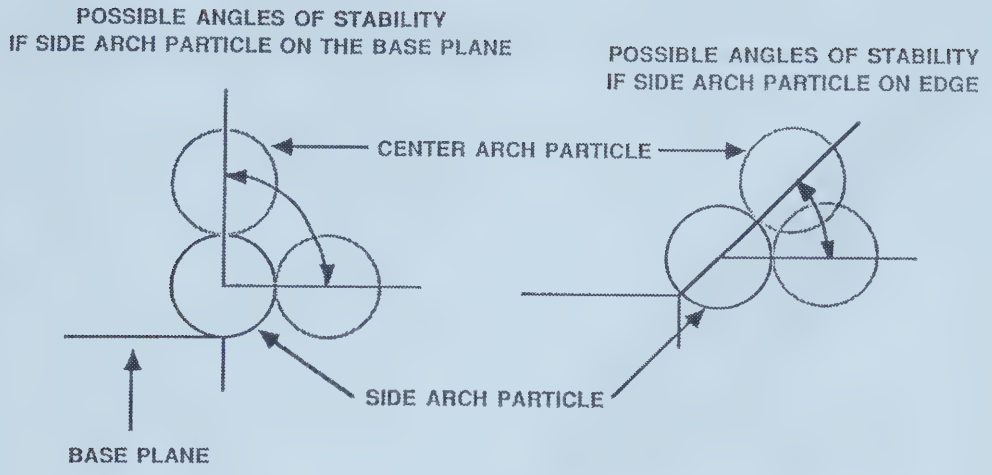

Figure 2.4: Rules of particle stability. After McCormack [28]

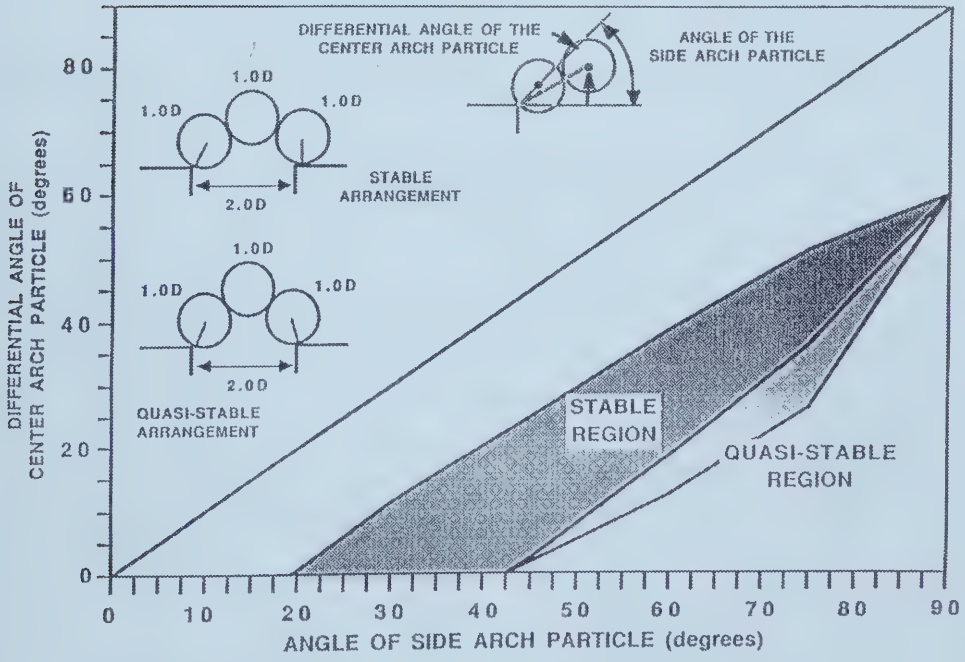

Figure 2.5: Stability diagram for 3-particle arches when the gap opening is 2 x the particle diameter. After McCormack [28]

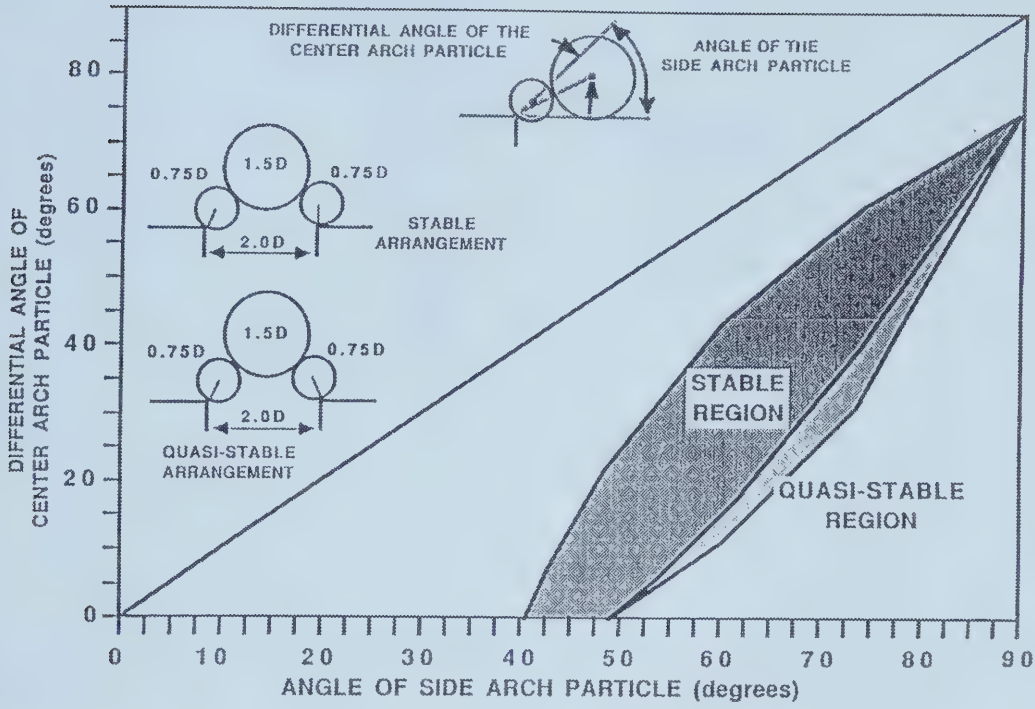

Figure 2.6: Stability diagram for 3-particle of different particle sizes. After McCormack [28]

US mesh size	wt%	Fraction	Fraction wt%	Average size (mm)
> 18	0.00			
18–25	0.01			
25–35	0.06	1	1.33	0.444
35–45	0.00			
45–60	0.04			
60–80	1.13			
80–120	36.75	2	36.75	0.150
120–170	37.88	3	37.33	0.106
170–230	13.27			
230–325	6.11	4	24.57	0.063
325–400	1.79			
< 400	3.4			

- From laboratory experiments the gap opening size was determined to be 0.254 mm
- In order to anchor a stable arch the width of three particles must be

$$\frac{3.0}{1.8} = \frac{X}{0.254}$$

$$X = 0.423$$

- Determined from experimental work
- Denotes combinations large enough to bridge
- Denotes combination with some bridging possibility

Group			Freq	Prob	Size
1	1	1	1	0.0002	1.332
1	1	2	3	0.0195	1.038
1	1	3	3	0.0198	0.994
1	1	4	3	0.0129	0.951
1	2	2	3	0.5388	0.744
1	2	3	6	1.0950	0.700
1	2	4	6	0.7206	0.657
1	3	3	3	0.5559	0.656
1	3	4	6	0.7320	0.613
1	4	4	3	0.2409	0.570
2	2	2	1	4.9633	0.450
2	2	3	3	15.1248	0.406
2	2	4	3	9.9549	0.363
2	3	4	6	20.2242	0.319
3	3	3	1	5.2020	0.318
3	3	2	3	15.3636	0.362
3	3	4	3	10.2717	0.275
4	4	4	1	1.4833	0.189
4	4	2	3	6.6555	0.276
4	4	3	3	6.7608	0.232

Figure 2.7: Calculation of gap opening size from sand fraction arrangement probability. After McCormack [28]

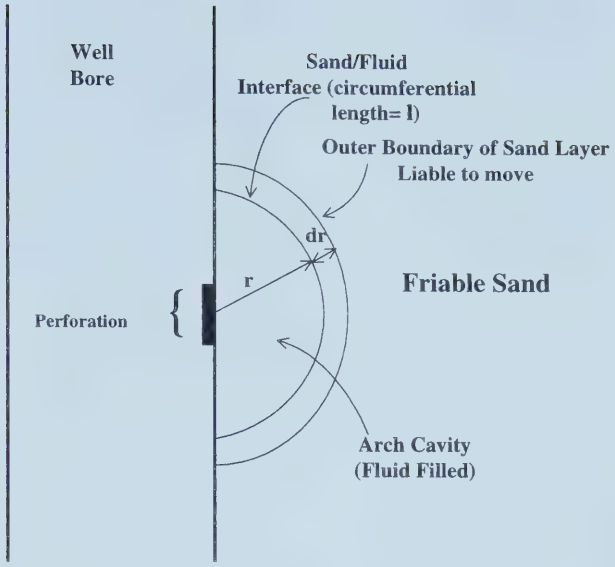

Figure 2.8: System of an arch that can stabilize a friable sand. After Stein et al. [36]

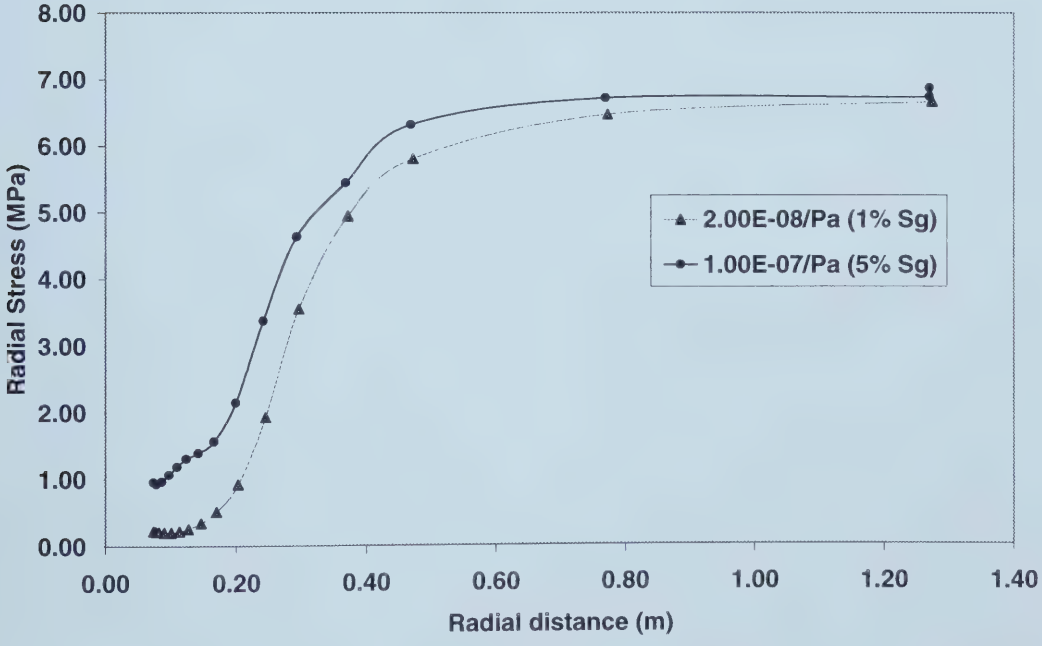

Figure 2.9: Radial stress versus distance at different compressibilities and gas saturation. After Yuan [44]

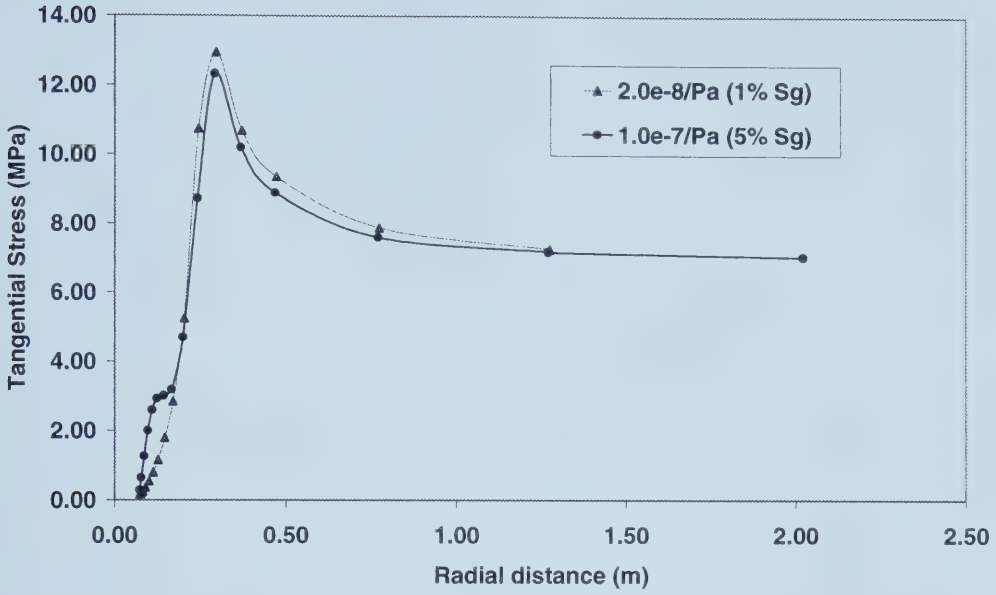

Figure 2.10: Tangential stress versus distance at different compressibilities and gas saturation. After Yuan [44].

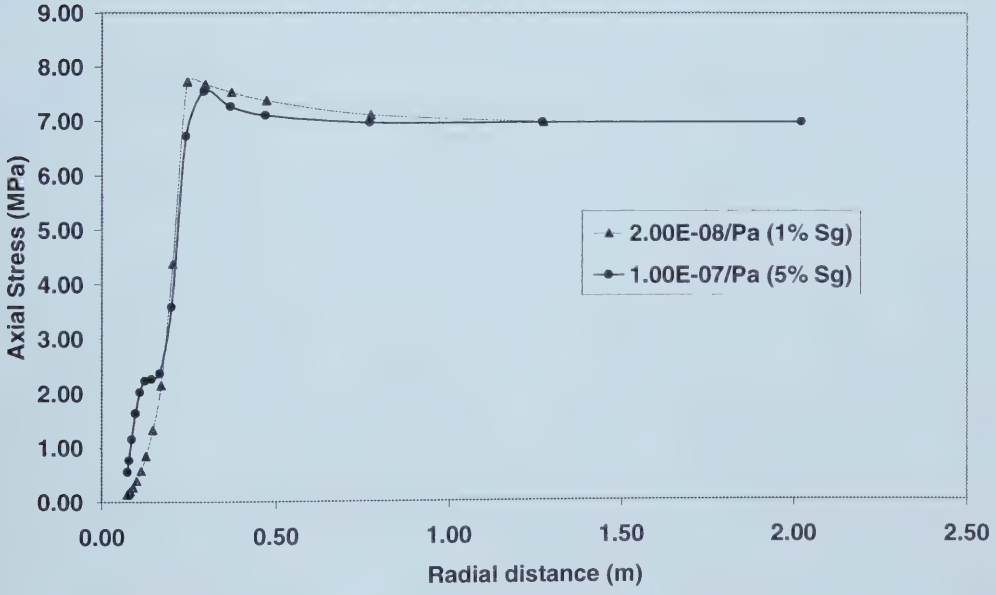

Figure 2.11: Axial stress versus distance at different compressibilities and gas saturation. After Yuan [44]

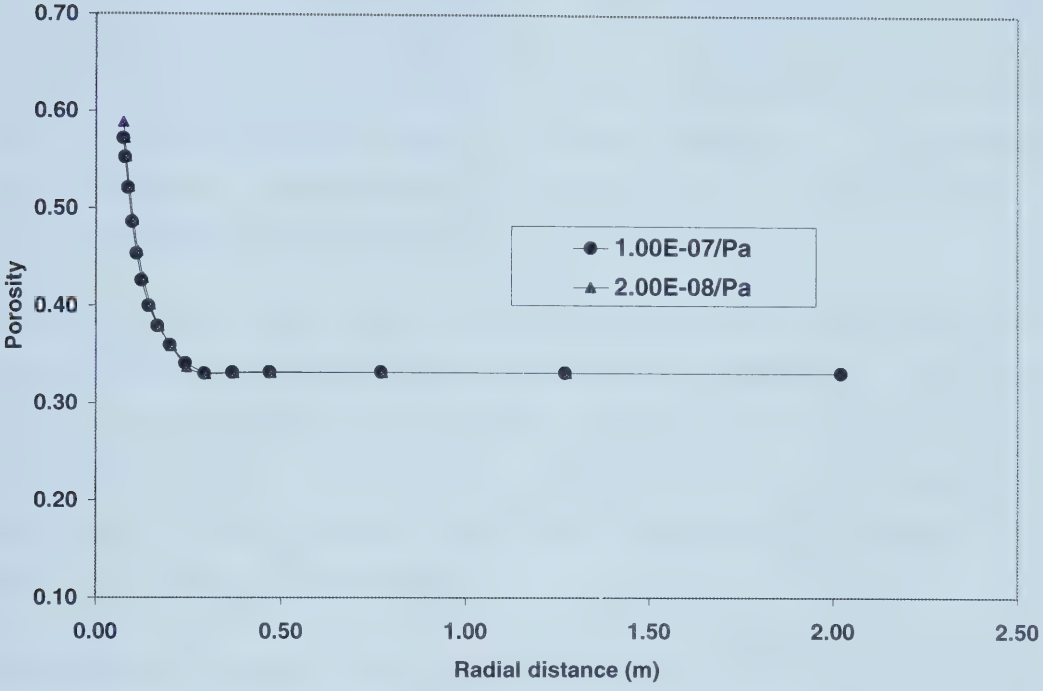

Figure 2.12: Porosity versus distance at different compressibilities. After Yuan [44]

3 Statement of the Problem

Oil producers in Alberta and Saskatchewan have reported high oil recovery for heavy oil reservoirs under cold production using vertical wells, with large volumes of sand being produced along with the oil. For horizontal wells, cold production to some extent has not been as successful, due mainly to sand cleanout cost. Therefore, reducing sand cleanout cost by controlling sand production into horizontal wells is an important aspect in optimizing production from these reservoirs.

This study focuses on the experimental investigation of the flow of oil and sand in the vicinity of a heavy oil horizontal well under cold production. Specifically, in terms of the formation of structures due to sand grain re-arrangement under different conditions of slot size, sand type, fluid and flow rate. An experimental apparatus was designed and assembled at the Alberta Research Council. Four different types of experiments were planned and carried out. They include:

Sand production experiments with air as the flowing fluid. These experiments allowed a rapid scoping of the factors affecting sand production.

Experiments of sand production with liquid (Silicone oil) as the flowing fluid. These experiments, were designed to investigate the effects of slot size, sand type and distribution and oil flow rate on sand production. In addition, analytical models were utilized to provide an estimation of the change in reservoir rock properties (i.e. porosity and permeability) due to sand production.

Thin-section visualizations. The influence of the variables listed above (including slot size, sand type and distribution and oil flow rate) on the rearrangement of the sand grains in the vicinity of the slot was investigated in these tests.

CT scans of the sand packs before and after sand production through slots. In these tests, the variation of the structure in the vicinity of the slot was surmised from CT scans of the sand pack.

Other important objective of this study was, besides gaining a better understanding of the reservoir behavior during sand production, to quantify the changes to reservoir properties such as porosity and permeability due to sand production. For this aspect of the investigation, models developed for flow through porous media were considered and used to calculate the magnitude of the property changes in the vicinity and at certain distance(s) away from the slot.

4 Experimental Equipment, Materials and Procedure

The flow behaviour of sand and oil in the vicinity of a slot in a horizontal well was studied under different experimental conditions. In the following sections, the description of the materials used, as well as the types of tests performed in this study are described.

4.1 Materials Used and their Properties

4.1.1 Fluids

Three fluids were used in the testing program carried out in this research: Epoxy, synthetic oil and air. Epoxy resin was used to solidify the cores for thin section tests while air and dead oil were used in the sand production experiments. Single-phase flow was chosen to simplify the problem.

Compressed air was supplied at 80 ± 5 psi (551.58 ± 34.47 kPa) from the ARC central plant. The synthetic oil was a polydimethylsiloxane (Viscasil® 12M). Typical product data are listed in Table 4.1. The viscosity of the oil was measured at ARC laboratories at different temperatures (22 to 28 °C) [43]. The viscosity data was fitted to the following equation:

(4.1) $$\mu = 38788*(T^{-0.342})$$

where μ = viscosity (cP)
T = temperature (°C)

EPO-THIN® resin and EPO-THIN® hardener were used for the thin sections (see Section 2.2.3).

4.1.2 Sands

Three different sands were used:

- Reservoir sand: Husky sand, obtained from cold production surface collection tanks in the Lloydmister area.

- Synthetic sand: Sil-1 (crystalline silica) sand provided by Sil Industrial Minerals Inc.

- Synthetic sand: Glass (soda lime) beads provided by Sil Industrial Minerals Inc. They are formulated from chemically inert soda lime glass.

The glass beads were supplied in bags with nominal size ranges of 20 to 40 mesh, 40 to 60 mesh, 50 to 80 mesh, 60 to 100 mesh, 70 to 120 mesh, 80 to 140 mesh, 170 to 200 mesh, 325 to 400 mesh. Two different sands were prepared from these sizes. One which will be called glass beads like Husky (GBLH) simulated the size distribution of the Husky sand. The other sand called glass beads less fines (GBLF) had the same particle size distribution as the Husky sand except for the diameters below 170 U.S. mesh.

All the sands mentioned above were characterized as follows:

4.1.2.1 Grain Size Analysis

The purpose of this analysis was to determine the average grain size and particle size distribution (grain sorting) of the different sands. These two parameters influence significantly sand production through slots, as was pointed out in the literature [4,29, 32,33,44].

The particle-size distribution of a sand is defined as the distribution of the percentage of the total weight of the different fractions within a given size range. Grain size is usually defined, for grains larger than 0.1 mm, as equivalent to the width of that circular or square aperture which allows the grain to just pass through [44,45].

The size distribution or grain sorting is used also to classify the sands in two categories. Sand containing a wide range of grain sizes is said to be poorly sorted. A sand is well sorted when the range is narrow [18].

The sands were sieved according to the ASTM Standard Test Method for Particles: ASTM # D 422-63 [46].

In this method, particles are separated into various grain-size groups or fractions. This is achieved by sieving a sample using a set of standard sieves and weighing the material retained at each sieve screen. The percentage by weight of each fraction is then calculated.

The results of this analysis can be presented either as a distribution of the weight of each fraction or as a cumulative plot of the percentage, by weight, of grains finer than the diameter denoted by the abscissa [44]. Since the grain size may vary significantly, a logarithmic scale is commonly used for the abscissa.

The slope of the sieve analysis curves indicates the sand's uniformity, the more vertical the slope; the more uniform the sand [20]. The uniformity coefficient (C_u) is representative of the uniformity of the sand [20,47]:

(4.2) $$C_u = \frac{D_{60}}{D_{10}}$$

where D_{10} and D_{60}, also called effective diameters. These diameters are equal to the size of the sieve which allows a certain percentage by weight, given by the values of the subscript, to pass through.

Other percentiles that are considered important for sand production through slots are the D_{90} and D_{50} equivalent diameters. The importance of the $D_{99.9}$ will be discussed in a later section. However, the best number to look for in sand control strategies for oil wells has not yet been established.

In this work, dry samples of each sand were accurately weighed and sieved through a stacked set of sieves with the following sizes in US mesh: 18, 25, 35, 45, 60, 80, 120, 170, 230, 325, 400. When it was decided to match the size distribution of the glass beads to that of the Husky sand the following sieves were added: 40,50,70,100 mesh. In this

manner, a more accurate size distribution of the biggest fractions by weight of the Husky sand was obtained leading to a better match. Table 4.2 shows the sieve opening sizes in mm and inches.

The particle size distribution curves of the sands used in this study are shown in Figure 4.1 while the equivalent diameter of the grains at different percentiles as well as the uniformity coefficient are reported in Table 4.3. The sieve analysis data for Figure 4.1 is presented in Table 4.4. An example of the reproducibility of the sieve analysis is shown in Figure 4.2 and Table 4.5 where the data for the Sil-1 sand is presented. The reproducibility measurements for the other sands are given in appendix B.1.

A good match was obtained between the particle size distribution of the Husky sand and the glass beads since all the percentiles and the C_u show similar values, (the maximum difference between Husky sand and the glass beads was 16 % in the $D_{99.9}$).

4.1.2.2 Solids Density Measurement

The density values of the sands used were measured based on ASTM method designation: D1817-96 [48].

In this method, a Weld's specific gravity bottle (picnometer) was used. The sand is first weighed into the clean and dry picnometer to the calibrated volume of the bottle. Solvent is then added. The picnometer is then placed in a vacuum dessicator for a certain period of time to remove all the air bubbles. The picnometer is then "toped" up and placed in a water bath for 15 minutes at the desired temperature, then capped and reweighed [48]. The measurements are used in equations (4.3) and (4.4). More details regarding the test are given in the ASTM method D1817-96 [48].

The major change made to this method was the use of 1-Butanol as the filling solvent instead of water when the sand densities were calculated. The use of 1-butanol reduces air trapped in the sample. To determine the density of the 1-butanol, the ASTM method D1817-96 [48] was followed without any change.

The sand density was calculated using the following equations:

(4.3) $$S = \frac{(K - m_P) * \rho_{H_2O}}{m_{1-butanol+P} - m_P}$$

(4.4) $$\rho_{sand} = \frac{P * S}{K - (G - P)}$$

where: m_P = mass of picnometer

$m_{1\text{-}butanol+P}$ = mass of 1-butanol + mass of picnometer

m_{S+P}= mass of sand + mass of picnometer

P= mass of sand = m_{S+P} - m_P

S= butanol density

K= $mass_{picnometer + butanol} - m_P$

G= $mass_{picnometer + sand + butanol}$

Three densities were measured per sand. The average of the three measurements was taken as the density of the material. The results of these tests are summarized in Table 4.6, while table B.4 in appendix B.2 provided the details of the measurements.

Sand densities were used in the porosity calculations as well as in the calculations of the volume of the sand produced.

4.1.2.3 Morphology Analysis

Since the effect of the grain shape on sand production was investigated it was necessary to determine the morphology of the sands.

The traditional morphology analysis includes the concepts of: 1) form, 2) sphericity, 3) roundness and 4) surface features [49]. Among the four factors that characterize the grain shape, the sphericity and roundness are the ones that have been cited in the literature as having an influence on sand production [4,29, 50].

Sphericity is a property that states quantitatively how close the shape of an object is to that of a sphere. Wadell [49,51] introduced the following definition of sphericity:

(4.5) $$\psi_w = \sqrt[3]{\frac{V_p}{V_{cs}}}$$

where: V_p = volume of the particle (measured by immersion in water)
V_{cs} = volume of the circumscribed sphere (smallest sphere that will just enclose the particle)

Numerous attempts have been made to calculate sphericity based on estimating surface area. However, the most widely used method of determining sphericity is through the visual comparator. This allows a large number of grains to be classified at the same time. A comparator can be built by simply collecting a series of grains and mounting them on slides and /or photographing them. Grains to be classified are then compared with the standards. Powers [52] constructed such a comparator, shown in Figure 4.3. Powers' widely used chart presents two classes of sphericity (high sphericity and low sphericity), in combination with six classes of grain roundness.

Grain *roundness* is defined as the relative sharpness of the grain corners, or in other words, as the grain surface curvature [51]. The different roundness categories as well as the definition for each of them are presented in Table 4.7. This classification, jointly with a visual silhouette comparator, can be used for sand grain classification [51].

Scanning electron microscope (SEM) photographs of the three sands used in the experiments are shown in Figure 4.4 to 4.10. Figure 4.4 is an overall picture of the Sil-1 grains taken at a magnification of X50 while Figure 4.5 shows a Sil-1 single grain. The scale is given in the upper right hand corner of the photomicrograph. Comparing the photomicrograph of the sand grain with those in Power's chart and taking into account the sieve analysis results, allowed Sil-1 to be classified as a well sorted subrounded sand with low sphericity.

Similarly, the Husky sand can be classified as a poorly sorted, subangular sand with low sphericity (Figure 4.6–4.8) while the glass beads are poorly sorted, well rounded sand (Figure 4.9 and Figure 4.10).

4.1.2.4 Shear Strength: Shear box test

The shear box test is used for measuring the angle of internal friction, also called the angle of shear resistance of the sand. In this test, sand is placing in a square rigid metal box, comprised of two halves. The lower part of the box is pushed (or pulled) by a motorized drive unit whereas the upper part of the box, which does not move, is connected to a load cell which records the resistance load, F [53]. The lower half of the sample is then forced to slide along the top half.

A normal load N is applied to the sand throughout the test. The vertical stress σ_n, is equal to N/L^2, where L is the length of sides of the square box. The bottom half of the shear box is pushed at a constant rate by a motor drive. Since the top and bottom halves move relative to one another a shearing plane is created where the sand is deformed. The shear stress is equal to F/L^2. A maximum shear stress is eventually reached where sand grains start to slide completely past one another. This point is known as the 'peak' of the shear stress /displacement curve. After the peak, the shear resistance falls off, and eventually reaches a plateau which is called the residual shear stress [53].

A failure envelope can be constructed by measuring the peak stress for samples of the same soil under different normal stresses. The general relationship between maximum shearing resistance τ_f, and normal stress, σ_n, for granular materials, can be represented by the Mohr-Coulomb equation:

(4.6) $$\tau_f = c_u + \sigma_n \tan\varphi$$

where: c_u = cohesive strength
φ = friction angle

This relationship represents the most widely used failure criterion. The curve represented by this equation is known as the 'failure envelope' [53].

The shearing resistance is composed of two components [53]:

1) A friction force between particles ($\sigma_n \tan \varphi$), which is due to the interlocking and friction between particles when sheared under a normal stress.

2) A cohesion force (denoted by c_u), which is due to the internal forces holding sand particles together in a solid mass.

Direct shear tests under dry conditions were performed to determine the friction angle of the sands used in the testing program. The ASTM method D 3080-90 was followed [54]. The applied normal stress on the sand in the shear box covered the range of effective stress estimated within the sand pack in the liquid experiments.

The effective stress within the sand pack was estimated using the following equation derived previously by Tremblay et al. [2] based on the analysis of Johanson and Jenike [55]:

$$\sigma_{eff}(x) = \left(p_{inj} - p_{prod}\right)\left[\frac{(1-\upsilon)D}{4Lc_f\nu}\right]\left(1 - e^{-\left[4c_f\left(\frac{\nu}{(1-\nu)}\right)\right]\left(\frac{x}{D}\right)}\right) \tag{4.7}$$

where: p_{inj} = pressure at inlet
p_{prod} = pressure at outlet (atmospheric pressure in this case)
υ= poisson ratio (0.3, a typical value for oil sand [2])
D= diameter of the cell
c_f= coefficient of friction at the wall = $\tan\varphi$
L= length of the pack
x= distance where the effective stress is calculated, in this case x =L, the outlet.
φ = friction angle

In deriving this equation, the friction force at the wall of the vessel was assumed to be given by the product of the normal stress times the friction coefficient. The vessel was assumed to be cylindrical throughout its length.

Table 4.8 summarizes the effective stress at the bottom of the sand pack (x=L) calculated from equation (4.7) while Table 4.9 presents the actual normal loads applied and the

shear stress at failure in the shear box tests performed. The details of the effective stress calculations are presented in appendix B.3.

Figure 4.11 gives an example of the shear stress/displacement graphs for the Husky Sand (Raw data is shown in appendix B.4). The presence of the maximum or 'peak' strength is clear. The shear stress reaches a constant called the residual stress. Figure 4.12 to 4.14 show the failure envelopes for each sand. The measured friction angles for the sands tested are presented in Table 4.9.

The glass beads (round grains) had a smaller friction angle than the more angular grain sands at the same porosity. The poorly sorted sand (Husky sand) and the well sorted sand (sil-1) had approximately the same friction angles.

4.2 Description of the apparatus and experimental procedure

4.2.1 Air Tests

The air tests were performed in order to rapidly scope the influence of the particle size distribution, morphology of the small grains, pressure gradient and slot size on sand production through slots. These measurements were helpful in selecting the experimental conditions for the liquid tests. The weight of the sand produced and the pressure drop along the pack were recorded throughout the experiment using a data acquisition system.

A schematic diagram of the equipment is shown in Figure 4.15. The dimensions are shown in Figure 4.16. The capacity of the cell was 9.1litres. The physical model consisted of a stainless steel vessel with a cylindrical upper part and a converging section at the bottom. A circular slotted stainless steel plate, 11.37 cm in diameter and 0.996 cm in thickness shown in Figure 4.17, was bolted to the bottom of the converging section.

The slot was 7.57 cm in length. Plates with three different slot widths were used: 0.018 in (0.46 mm), 0.028 in (0.71 mm) and 0.040 in (1.02 mm). These slot sizes are within the

range of those machined in slotted liners for horizontal wells. The cell is rated to pressures up to 350 psi (2413 kPa) and 100 °C.

A regulator (number 2 in Figure 4.15) was connected to the ARC air line. A constant injection pressure was maintained. A capillary tube (3) was used to measure the flow rate knowing the pressure drop (4) across the tube and the pressure at the end (5) of the capillary. Pressure transducers were located at the top of the cell (6), in the middle (7) and near the bottom of the vessel (8). A thermocouple was connected to one of the ports to measure the temperature of the cell. A container placed on a Mettler scale was used to collect and measure the instantaneous sand production rate.

The tests were performed at four different air injection pressures shown in Table 4.10 (see appendix B.5 for the corresponding air flow rate calculations). Two sands were evaluated: Sil-1 and Husky sand.

The experimental procedure consisted of the following steps:

1. The slotted bottom plate was first cleaned with an air jet and closed with a plug. The plate was inserted at the bottom of the cell.

2. The cell was packed with dry sand, which was in the oven at 90 °C for at least 6-h before the test. Two different sand pack preparation techniques were used by: a) pluviating (pouring) the sand into the container (high porosity packs), b) vibrating the cell while pluviating the sand into the vessel (lower porosity packs). The mass of the sand used was recorded.

3. The height of the sand within the cell was measured in order to calculate the porosity of the pack. A sample porosity calculation is shown in appendix B.7

4. Air was delivered at the desired pressure through the inlet port of the cell.

5. The slot was unplugged.

6. The weight of sand produced and pressure drop along the core were recorded with the data acquisition system.

7. After sand production stopped, a delay of one hour was allowed before increasing the air flow rate.

8. Step 7 was repeated until the last flow rate was reached.

Steps 1 to 8 were repeated with the same sand starting at a higher flow rate in order to evaluate the influence of the initial flow rate on sand production.

4.2.2 Liquid Tests

The liquid tests were performed in order to investigate slurry production (oil/sand) through a slot at pressure gradients comparable to those at the surface of slotted liners in a horizontal well. The influence on sand production of sand grain morphology (Sil-1, Husky sand and glass beads), particle size distribution, slot width (0.022 in (0.559mm), 0.028 in (0.711mm) and 0.040 in (1.016 mm)) and pressure gradient (flow rates: 50, 100 and 150 cc/h) was investigated.

The equipment used in these tests was similar to that used in the air tests with some modifications. An extension was added to the cylindrical body of the cell increasing its capacity by 42%. The new dimensions of the cell as well as the position of the pressure transducers along the cell can be seen in Figure 4.18. The capacity of the cell was 15.8 litres.

The slotted plates were similar (in some cases the same) as those used in the air tests except that three pressure ports were added (see Figure 4.19). In addition, a fourth port was added to serve as an outlet port during the saturation process.

A vibrator, attached to the cell with two metals bands, was used when the cell was packed with dry sand. A DB Robinson Jeffrey positive displacement pump with dual cylinders was used to displace the silicone oil from an accumulator into the cell. Each pump cylinder was calibrated before the liquid tests started. An accuracy of $\pm$ 1 % was obtained.

The calibration charts as well as the procedure and the measurements obtained are presented in appendix B.6.

The experimental procedure consisted of the following steps:

1 The slotted bottom plate was first cleaned with an air jet and then closed with a plug. The plate was inserted at the bottom of the cell.

2 The cell was packed using an automatic vibrator for the dry sand or by manual vibration with a metal plunger when wet sand was used.

3 The porosity of the pack was calculated. A sample calculation is presented in appendix B.7. The porosity values for each sand pack used are shown in Table 4.11.

4 The core was saturated with one and half pore volume (PV) of silicone oil, which was shown in compressibility tests to evacuate at least 99 % of the air initially in the pack

5 A compressibility test was performed (see appendix B.8). If the air saturation was greater than 1% step 4 was repeated.

6 The permeability was measured (see appendix B.9 and Table 4.11)

7 The transducer off-set was taken when the pressure vessel was depressurized initially and finally to correct the pressure.

8 A video camera was used to record the produced sand and oil during the experiment.

9 The pressure transducers were connected to the data acquisition system

10 The plug was removed from the slot.

11 The pumps were activated at the desired flow rate.

12 The flow rate was maintained either until sand production stopped or for 48 h.

13 The flow rate sequence was: 50 cc/h, 100 cc/h and 150 cc/h. If the injection pressure reached the pressure rating (approximately 300 psi –2068.4 kPa-) at the vessel, the pump was stopped.

The slurry produced out of the slot was collected in containers placed on a Mettler balance. The slurry weight and pressure along the cell were recorded on-line using a data acquisition system. The apparatus is shown in Figure 4.20.

4.2.2.1 Scaling flow rates to field conditions

In order to scale the volumetric flow rates to field conditions, a horizontal well producing a 10,000 cP heavy oil at a rate of 100 m^3/day was assumed (typical field data). Other typical values assumed in this calculation were:

- Length of the horizontal well (L_w): 500 m
- Outer Diameter of the pipe (D_w): 5.5 in (13.97 cm)
- Open area of the slots: 1 % of the pipe surface
- Dimensions of the slot: 0.028 in (0.071 cm) width (W_s) and 7.7 cm length (L_s)

The volumetric flow rate for a single slot was calculated as followed:

(4.8) $$Q_{Slot} = Q_{well} \frac{S_s}{S_T}$$

where: Q_{slot} is the slot volumetric flow
Q_{well} is the well volumetric flow rate
S_s is the slot surface area
S_T is the total open area of the slots

While the surface area of the slot and the total surface area are given by:

(4.9) $$S_s = W_s L_s$$

(4.10) $$S_T = 0.01\pi D_w L_w$$

Applying equations (4.8) to (4.10) with the assumed values, yielded a volumetric flow rate of 104 cc/h for a single slot. Therefore, flow rates of 50, 100 and 150 cc/h were chosen to perform the liquid tests.

4.2.2.2 Absolute Permeability of the Pack

The absolute permeability of the core was calculated by flowing silicone oil for approximately 12 h at the highest flow rate possible in order to increase the accuracy of the pressure measurements. The pressure drop along the sand pack was recorded and Darcy's linear flow equation was then used to calculate the absolute permeability. A sample calculation and a typical table of data are shown in appendix B.9.

The permeability values for each of the packs are presented in Table 4.11.

4.2.2.3 Measurement of the produced sand

Two methods were used to determine the quantity of produced sand. The first method consisted in extracting the sand from the collected slurry. The second method was based on a material balance knowing the slurry production rate, the injection flow rate and the densities of the sand and oil.

4.2.2.3.1 Extraction process

The slurry was extracted every time the container was changed. The steps followed in the separation process were:

1. Toluene was added to the mixture and left soaking for 2 days, stirring occasionally.
2. After the two days, the solvent was changed and again the sample was left to soak.
3. Steps 1 and 2 were repeated until oil was completed removed from the sand.
4. The sample was put into the oven to evaporate the toluene used in the extraction process.

5. The weight of the clean sand produced was recorded.

4.2.2.3.2 Material Balance

In order to calculate the sand production rate, the mass balance equation was derived. The incremental produced slurry, was equated to the corresponding incremental changes inside the cell and the incremental mass of oil injected at the same time.

In this equation any injected quantity is positive (+), any produced quantity is negative (-). Thus the mass balance can be written as:

- For the oil

(4.11) $$dm_{oi} + dm_{ot} + dm_{op} = 0$$

- For the sand

(4.12) $$dm_{st} + dm_{sp} = 0$$

where the changes during a time interval Δt are:

dm_{oi}: differential mass injected
dm_{ot}: differential mass of oil in the cell
dm_{st}: differential mass of sand in the cell
dm_{sp}: differential mass of sand produced
dm_{op}: differential mass of oil produced

From the conservation of mass for the sand:

(4.13) $$dm_{st} + dm_{sp} = 0 \Rightarrow dm_{st} = -dm_{sp}$$

Similarly, from the conservation of mass for the oil:

(4.14) $$dm_{oi} + dm_{ot} + dm_{op} = 0 \Rightarrow dm_{ot} = -dm_{op} - dm_{oi}$$

In addition, the volume of the cell is fixed and equal to the sum of the volumes of oil and sand within the cell:

(4.15) $$V_s + V_o = V_{cell}$$

Since the volume of the cell does not change, the sum of the changes inside the cell in sand volume and oil volume must equal zero.

(4.16) $$dV_{st} + dV_{ot} = 0 \Rightarrow -dV_{ot} = dV_{st}$$

The differential mass can be converted to the differential volume from the definition of density:

(4.17) $$\rho = \frac{dm}{dV}$$

Therefore equation (4.13) becomes:

(4.18) $$dV_{st} = -dV_{sp}$$

Substituting (4.16) into (4.18):

(4.19) $$dV_{ot} = dV_{sp}$$

Again, using the density equation and replacing dV_{ot} by expression (4.14) yields an expression relating the volume of oil injected to the produced oil and sand.

(4.20) $$dV_{oi} = -\left(dV_{sp} + dV_{op}\right)$$

On the other hand:

(4.21) $$dm_{slurry} = dm_{op} + dm_{sp}$$

(4.22) $$dm_{slurry} = dV_{op}\rho_o + dV_{sp}\rho_s$$

where dm_{slurry} is the differential mass of slurry produced at time t.

Expressions (4.20) and (4.22) form a system of two equations with two unknown dV_{op} and dV_{sp}. From equation (4.20), dV_{op}, is substituted into expression (4.22):

(4.23) $$dm_{slurry} = \left(-dV_{sp} - dV_{oi}\right)\rho_o + dV_{sp}\rho_s$$

From expression (4.23):

(4.24) $$dV_{sp} = \frac{dm_{slurry} - dV_{oi}\rho_o}{\rho_s - \rho_o}$$

Since the flow rate was constant, the volume of oil injected was given by:

(4.25) $$dV_{oi} = Q_i dt$$

where Q_i is the volumetric flow rate and dt is the time increment.

Therefore:

(4.26) $$dV_{sp} = \frac{dm_{slurry} - Q_i dt\rho_o}{\rho_s - \rho_o}$$

The mass increment of produced sand can be obtained from equation (4.1) as follow:

(4.27) $$dm_{sp} = \frac{\left(dm_{slurry} - Q_i dt\rho_o\right)\rho_s}{\rho_s - \rho_o}$$

The calculated cumulative mass of sand produced at the end of each test by this method was compared with the mass measured using the extraction process (see section 5, Table 5.21). In general, the two methods differed by 10%. It is important to note that the method is less accurate when small amounts of sand are produced (less than 50 g for example). This is because sand, in this case, is produced mainly during the first minutes of the run when the system has not reached a stable flow rate. In certain tests where little sand was produced the error in the cumulative sand was 37 %.

The advantage of using equation (4.26) is that sand production can be measured instantaneously and can be related to the on-line measurements of the pressure within the cell.

4.2.3 Sand Arch Visualization Using Thin Sections

Qualitative experiments were performed to visually investigate the structure of the arches formed around slots when sand production stops. The sands evaluated were Sil-1, Husky and glass bead less fines (GBLF). Two slot sizes (0.022 in or 0.56 mm and 0.028 in or 0.71 mm), were used with the Sil-1 sand. One slot size (0.028 in or 0.56 mm) was used with Husky sand and GBLF.

The main objective of these experiments was to immobilize the sand grain within the sand pack after sand production. These tests were performed under dry conditions and gravity flow. Then, the epoxied sand core was sliced and thin sections were mounted on slides. The slides were cut perpendicularly to the length of the slot and were observed under a microscope to detect sand structures that may have formed in or around the slot. Thin sections from the central part of the core were also cut in order to observe the formation of possible preferential channels along the core after sand production.

The tests were conducted in a split cylindrical aluminium cell. The experimental set up for these experiments is shown in Figure 4.21 where the dimensions of the cell can be observed.

The cell was equipped with two aluminium leads one of which had a circular incision where a PVC slot plate could be fixed. The PVC plates were 82.01 mm in diameter and 8.93 mm in thickness, the slot width was either 0.022 in (0.558 mm) or 0.028 in (0.711 mm). The slotted plates were scaled such that the ratio of the slot length to the diameter of the aluminium cell was the same as the slotted plates used in the liquid tests. Therefore, a slot length of 5.40 cm was chosen. The thickness of the slot was the same as that of the plate.

The interior surface of the cell was lined with a rubber membrane to prevent the epoxy from sticking to the walls of the cell. A vacuum was applied to eliminate the air between the membrane and the walls of the cell and to keep the rubber membrane against the inner surface of the cell.

The fluid used to immobilize the sand pack was a mixture of the EPO-THIN® resin and EPO-THIN® hardener mixed according to the supplier.

The experimental procedure was as follows:

1. A rubber membrane was placed into the cell such that the rubber membrane was squeezed to the end face of the cell.
2. The slotted plate was bolted onto the cell.
3. A vacuum was applied between the inner surface of the cell and the rubber liner until epoxy was injected.
4. Sand, previously dried in the oven at 90 °C for 12 h, was poured into the cell. The sand pack was vibrated with a hammer for 1 min.
5. The height and weight of the sand within the cell was recorded in order to calculate the porosity of the sand pack (see Table 4.12). Sufficient space was left at the top of the pack to pour in epoxy as described further on.
6. The plug within the slot was removed.
7. After sand production stopped, approximately two pore volumes (PV) of epoxy were poured into the cell which was half filled with sand.
8. The upper end cap was closed and either air or silicone oil was injected to push the epoxy through the sand pack. Oil was used in latter tests to prevent fingering into the sand pack. Care was taken not to exceed a pressure of 60 psi (cell pressure limit).
9. When only sand free epoxy resin was produced from the slot, the injection was stopped. The PVC slotted plate was plugged when the injection was stopped to prevent air from entering the slot.
10. A resin cure time of 18 h was allowed before opening the split cell and removing the epoxied core.

The epoxied cores obtained are shown in Figure 4.22. An overview of some of the thin sections is presented in Figure 4.23. The thin sections were cut perpendicularly to the slot

length. They were grounded down to a thickness of 30 μ in order to obtain a better definition of the sand grains. Thin sections were prepared by the Earth Sciences Department (geological laboratory) at the University of Alberta.

4.2.4 X-ray Computed Tomography

Computed tomography (CT) is a procedure by which a series of x-ray slices of a sample, scanned at different angles of rotation, are assembled to obtain a cross-sectional image. As an X-ray beam passes through a sample, it is absorbed according to the density of the different structures found in the sample. Each cross-sectional image is subdivided into pixels. The average attenuation in each pixel can be converted to a porosity provided baseline scans of the different phases are taken before the tests.

The X-ray scanner was used in two modes. The first mode was a chest X-ray type of scan. The sample is simply moved at different locations in the plane perpendicular to the X-ray beam without any rotation around its axis. The second mode is a computed tomography type of scan.

1) **Full 2D Radiographic Imaging:** The X-ray source was set at 300kV, 10mA, with a 4mm focal spot. Radiographic imaging of the entire sand pack required sixteen (16) separate 630 X 630 pixel images. Each image was collected as five (5) exposures at 400msec. This gave an overview of the changes along the whole sample.

2) **Computed Tomography (CT):** The X-ray source was set at 300kV, 10mA, with a 4mm focal spot. CT slices were reconstructed from scans of ten (10) pixel thickness (or height) along the length of the cylinder and 180 views (2 degree steps). Each view was collected as ten (10) exposures at 400msec. CT slices 1 mm, 10 mm and 50 mm from the slot were taken.

In order to investigate the effect of sand production on the porosity distribution in a sand pack, a set of CT scanner experiments were performed. Dry samples and epoxied sand cores were scanned.

The CT Scanner used at ARC is a Smartscan Model 100-111 built by Scientific Measurement Systems (SMS), Austin, Texas. The scanner is a self-contained facility, with the X-ray source, positioning system and detector housed within a lead enclosure. The x-ray source is a dual focal spot (4 and 1.5mm) tube with a maximum output of 320kV at 13mA [56].

4.2.4.1 Dry Sand Tests

Sand packs were prepared by pouring dry sand into a cylinder with a plugged slotted plate (0.028 in or 0.71 mm width) at the bottom. The slot was unplugged and the sand pack was scanned after the sand production stopped. The original X-ray scan of the pack was compared to the X-ray scan after the test.

Three sands were evaluated: Sil-1, Husky and GBLF. The packing procedure was the same for the three sands (see Table 4.12).

The CT scanning and preparation procedure was as follows:

1) Sand was dried in an oven for 12 h approximately at 90 °C.
2) The slotted plate was cleaned with an air jet and was then plugged. The plate was inserted at the bottom of the cylindrical cell.
3) A scan of the empty cylinder served as a baseline.
4) Sand was poured into the cylinder. The mass and height of the sand in the cylinder were recorded for porosity calculations (see Table 4.12).
5) The sand-filled cylinder was then scanned.
6) The slot was unplugged.
7) After sand production stopped, the cylinder was scanned again.

4.2.4.2 Epoxied Cores

The preparation procedure for these samples was explained in section 4.2.3. The idea was to scan the epoxied cores before they were cut in thin sections. The CT images combined with the thin section observations allowed a better understanding of the sand production mechanisms through slots.

The X-ray source was set at 300kV, 10mA, with a 4mm focal spot. The CT slices were reconstructed from scans of 280 pixels thickness (or height) along the length of the entire epoxy cores at 180 views of 2° each. Ten (10) exposures at 400 msec were collected per image (view). Entire core scans required 4 or 5 scans along the length of the cores. Each scan was reconstructed into 28 slices.

The epoxied cores were not scanned initially before injecting the epoxy. In order to convert the attenuation numbers measured within the epoxied core to porosity values, it was necessary to also scan the top of the cores which contained only hardened epoxy.

Table 4.1: Typical Data for Viscasil 12M

Property	Data
Nominal Viscosity cstks @25 °C (77 °F)	12,500
Approximate Molecular Weight	67,700
Specific Gravity 25/25 °C(77/77 °F)	0.975
Surface Tension dynes/cm @ 25 °C(77 °F)	21.3
Maximum Volatility, % Wt Loss, 24 hrs at 150°C (302 °F)	2

Table 4.2: Sieve opening sizes [20]

Sieve # U.S.mesh	Size (mm)	Size (in)
18	1.000	0.0394
20	0.850	0.0331
25	0.710	0.0278
35	0.500	0.0197
40	0.425	0.0165
45	0.355	0.0139
50	0.300	0.0117
60	0.250	0.0098
70	0.212	0.0083
80	0.180	0.0070
100	0.150	0.0059
120	0.125	0.0049
170	0.090	0.0035
230	0.063	0.0025
325	0.045	0.0017
400	0.038	0.0015
BP	< 0.038	<0.0015

Table 4.3: Sand equivalent diameters and uniformity coefficients

Sand	$D_{99.9}$ (mm)	D_{90} (mm)	D_{60} (mm)	D_{50} (mm)	D_{10} (mm)	C_u (mm)
Sil-1	0.50	0.34	0.29	0.28	0.19	1.57
Husky	0.85	0.20	0.16	0.15	0.08	2.00
GBLH	0.71	0.21	0.17	0.16	0.08	2.06
GBLF	0.71	0.21	0.16	0.15	0.10	1.60

Table 4.4: Sieve analysis data

Sieve #	Size (mm)	Finer than (%)			
		Sil-1	Husky	Beads like Husky	Beads with Less Fines
#18	1.000	100.00	100.00	100.00	100.00
#20	0.850		99.93	99.99	100.00
#25	0.710	100.00	99.76	99.84	99.95
#35	0.500	99.95	99.43	99.17	99.50
#40	0.425		99.25	99.15	99.48
#45	0.355	98.92	99.04	98.83	99.19
#50	0.300		98.69	98.32	98.78
#60	0.250	35.64	97.82	96.51	97.47
#70	0.212		94.94	90.60	91.24
#80	0.180	8.47	80.45	77.03	80.25
#100	0.150		49.08	45.18	48.46
#120	0.125	1.05	32.72	31.58	35.09
#170	0.090	0.13	13.37	14.04	1.54
#230	0.063	0.00	5.45	4.04	0.37
#325	0.045	0.00	2.55	1.05	0.13
#400	0.038	0.00	2.18	0.89	0.10

Table 4.5: Sieve analysis for two different samples of the Sil-1 Sand

U.S. Mesh		Finer than (%)	
	Size (mm)	Sample 1	Sample 2
#18	1.000	100.00	100.00
#25	0.710	100.00	100.00
#35	0.500	99.95	99.90
#45	0.355	98.92	98.52
#60	0.250	35.64	32.89
#80	0.180	8.47	7.81
#120	0.125	1.05	0.80
#170	0.090	0.13	0.03
#230	0.063	0.00	0.01
#325	0.045	0.00	0.00
#400	0.038	0.00	0.00

Table 4.6: Butanol and Solid Densities

Material	ρ (g/ml)
1-Butanol	0.8075 ± 0.0001
Sil-1	2.6175 ± 0.0135
Husky	2.6280 ± 0.0029
Glass Beads	2.4733 ± 0.0044

Table 4.7: Roundness classes (after Schneiderhöhn, 1954) [51]

Classes	Definition
Angular	Strongly developed faces with sharp corners. Sharply defined, large reentrants (indentations) with numerous small reentrants.
Subangular	Strongly developed flat faces with incipient rounding corners. Small reentrants (indentations) subdued and large reentrants preserved.
Subrounded	Poorly developed flat faces with corners well rounded. Few small and gently rounded reentrants (indentations), and large reentrants weakly.
Rounded	Flat faces nearly absent with corners all gently rounded. Small reentrants absent and large reentrants only suggested.
Well Rounded	No flat faces, corners, or reentrants discernible, and a uniform convex grain outline.

Table 4.8: Effective stress at the bottom of the pressure vessel found in the liquid experiments

Sand	q (cm^3/h)	$\sigma_{eff(x)}$ (kPa)		
		0.022 in	0.028 in	0.040 in
Sil-1	50	12.52	8.14	7.90
	100	24.40	17.25	5.22
	150	35.40	27.58	20.83
Husky	50	---	67.68	65.40
	100	---	157.62	137.07
	150	---	---	200.76
GBZF	50	---	52.94	---
	100	---	107.39	---

Table 4.9: Normal stresses applied during the shear box tests. Rate of displacement: 0.10 mm/min.

Sand	Porosity (ϕ)	σ_n (kPa)	τ (kPa)	Friction angle φ (Degree)
Sil-1	35.46	40.56	45.61	49.06
	35.30	20.29	25.29	
	35.86	4.49	6.94	
Husky	33.82	40.56	49.33	47.63
	34.53	122.18	136.10	
	34.59	162.98	168.57	
	34.64	176.59	180.72	
	35.10	211.95	248.65	
GBZF	33.78	40.56	25.53	28.10
	32.85	67.77	35.20	
	35.45	122.18	59.25	
	34.08	176.69	97.92	

Table 4.10: Injection pressure and average flow rates for Husky and Sil-1 sand used in the air experiments

Air delivery Pressure psi (kPa)	Q_A (l/min)
Atmospheric	Gravity flow
10 (68.95)	5.66
20 (137.90)	9.53
40 (275.79)	13.68
60 (413.69)	14.08
80 (551.58)	14.73

Table 4.11: Porosity and permeability of the sand packs used in the liquid tests

Sand	Run	k (darcy)	ϕ	PV (cm^3)
Silica Sand	2*	37.81	42.96	6658.51
	3*	39.92	41.80	6443.30
	4*	27.76	39.18	5743.83
	5	50.70	42.07	6618.89
Husky Sand	6	4.43	38.81	6041.04
	7	4.87	39.60	6137.46
GBLH	8	5.29	30.93	4866.71
GBLF	9	8.95	33.78	5325.18

*Wet sand packing with manual vibration

Table 4.12: Porosity of the sand packs used for the thin sections and dry sand CT scanner tests

Sand	Slot Size (in)	ϕ Thin section packs	ϕ Dry CT scanner Tests
Sil-1	0.022	36.17	---
	0.028	37.16	43.77
Husky	0.028	39.87	47.87
	0.028	38.53	---
GBLF	0.028	34.31	37.85

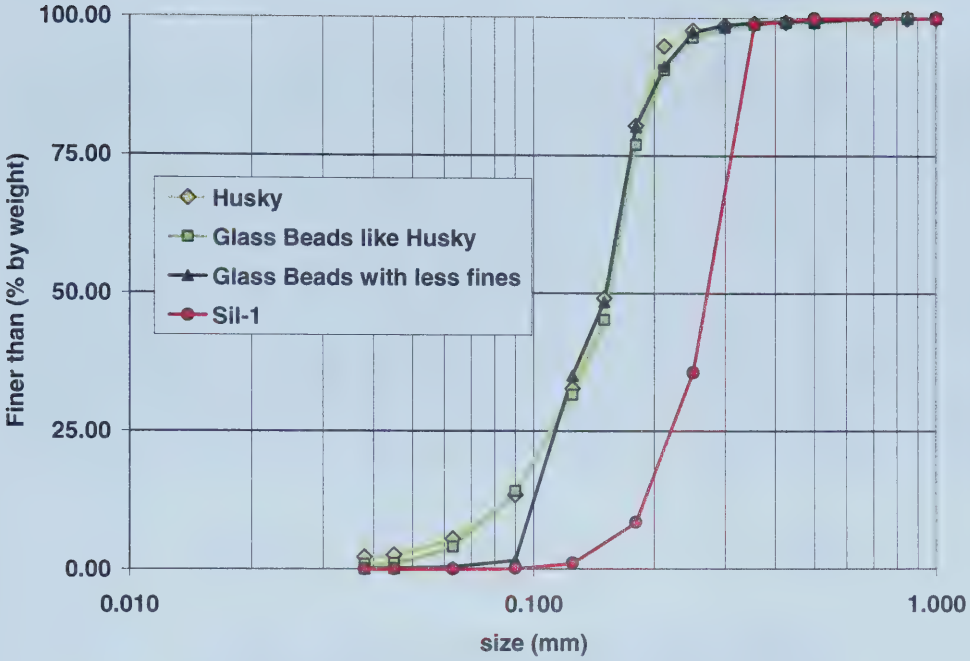

Figure 4.1: Particle size distribution curves

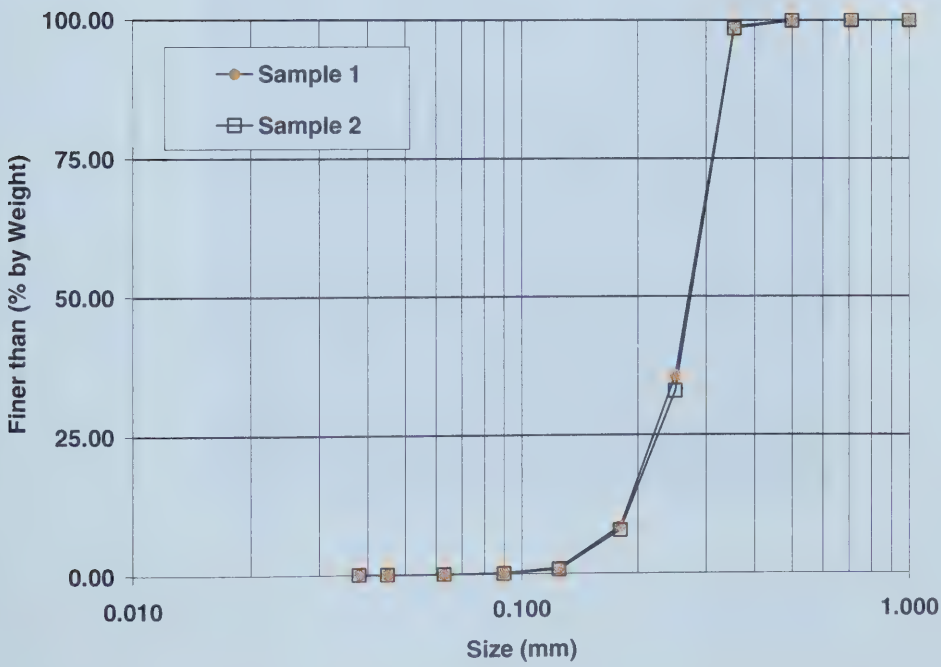

Figure 4.2: Reproducibility of the sieve analysis. Sil-1 sand, two different samples

Figure 4.3: Roundness scale of Maurice Powers [52]

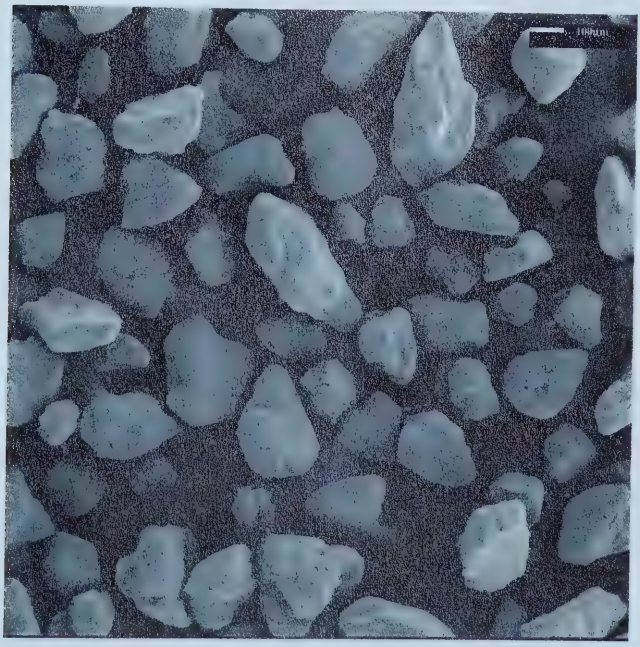

Figure 4.4: SEM photomicrograph of the Sil-1 sand. MAG: X50.

Figure 4.5: SEM photomicrograph of a Sil-1 grain. MAG X500

Figure 4.6: SEM photomicrograph of the Husky sand. MAG: X50.

Figure 4.7: SEM photomicrograph of the Husky sand showing the difference between the grain sizes. MAG:X50

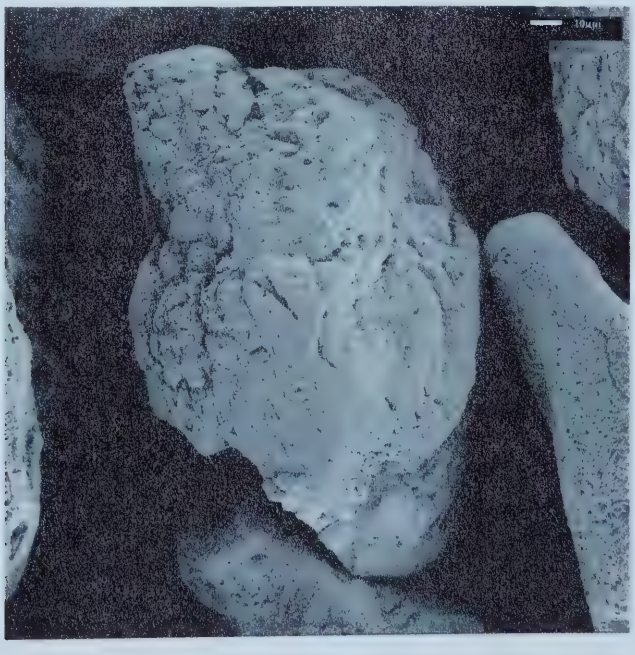

Figure 4.8: SEM photomicrograph of a Husky grain. MAG X450

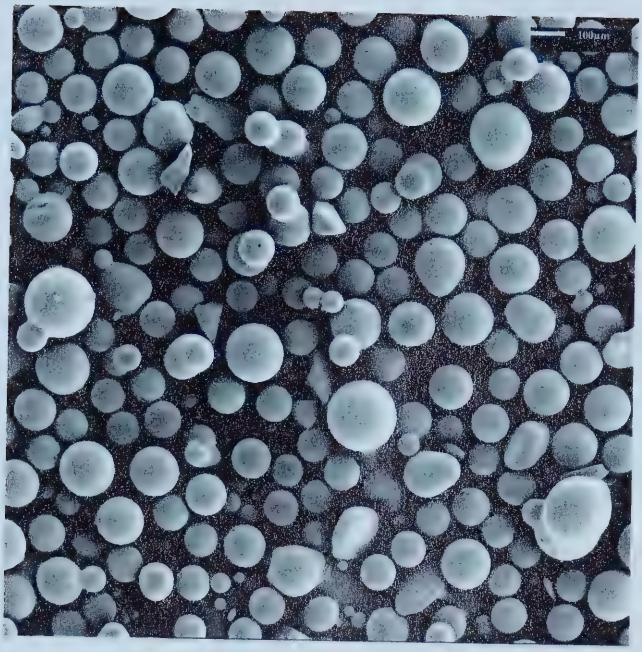

Figure 4.9: SEM photomicrograph of the glass beads. MAG: X50.

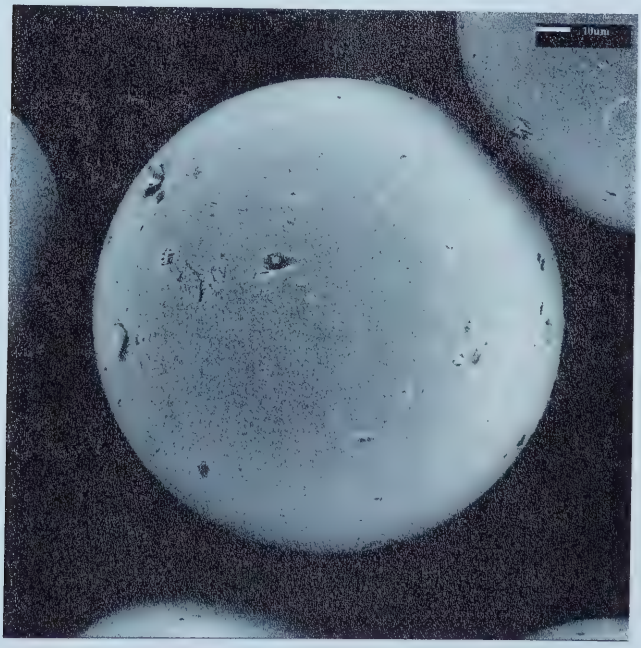

Figure 4.10: SEM photomicrograph of a glass bead. MAG X500.

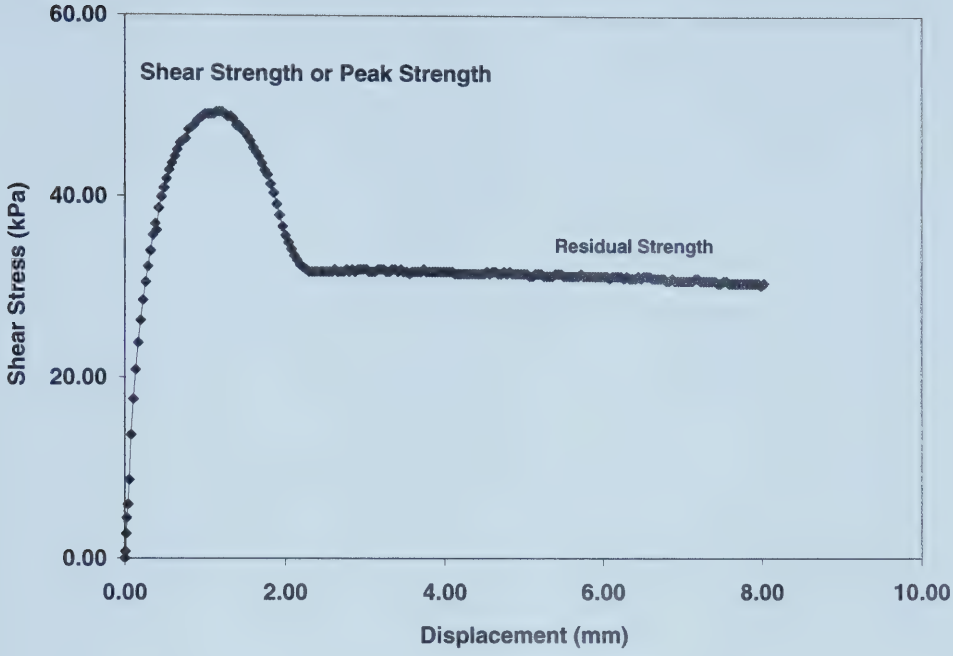

Figure 4.11: Shear stress displacement curve for Husky sand. σ_n=40.56 kPa

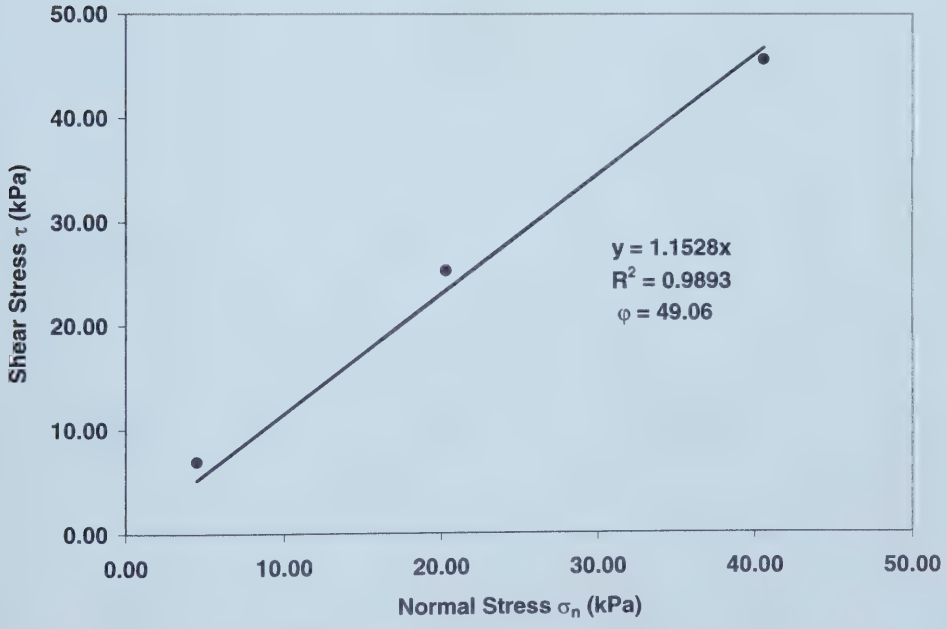

Figure 4.12: Mohr-Coulomb failure envelope Sil-1 sand

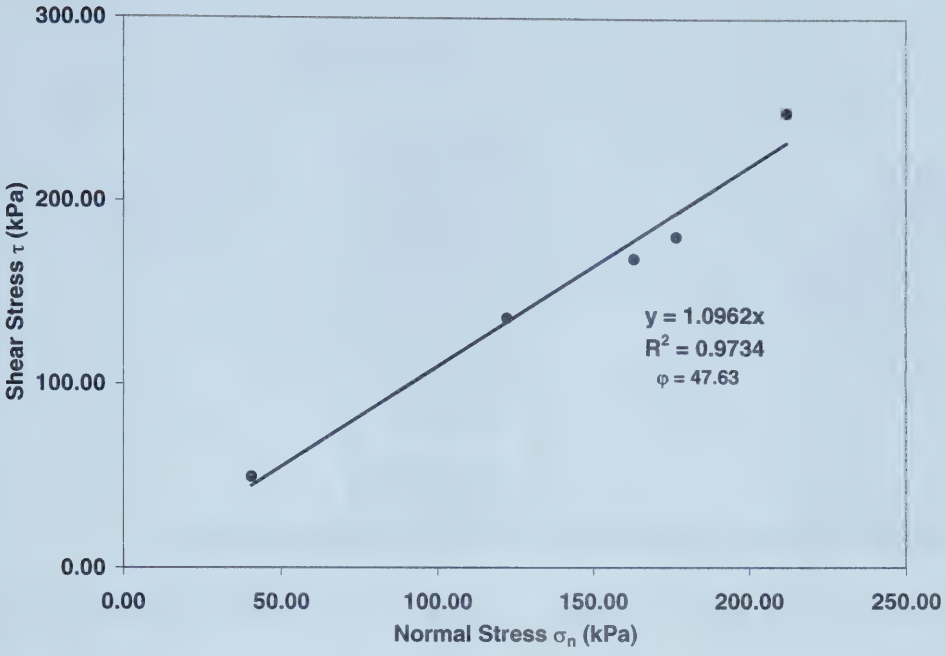

Figure 4.13: Mohr-Coulomb failure envelope Husky sand

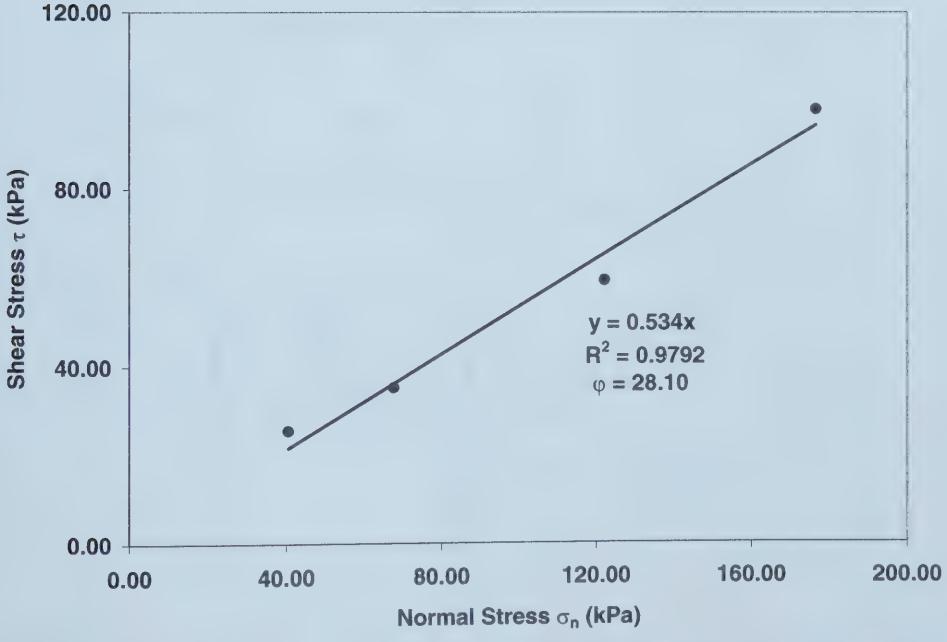

Figure 4.14: Mohr-Coulomb failure envelope glass beads with less fines

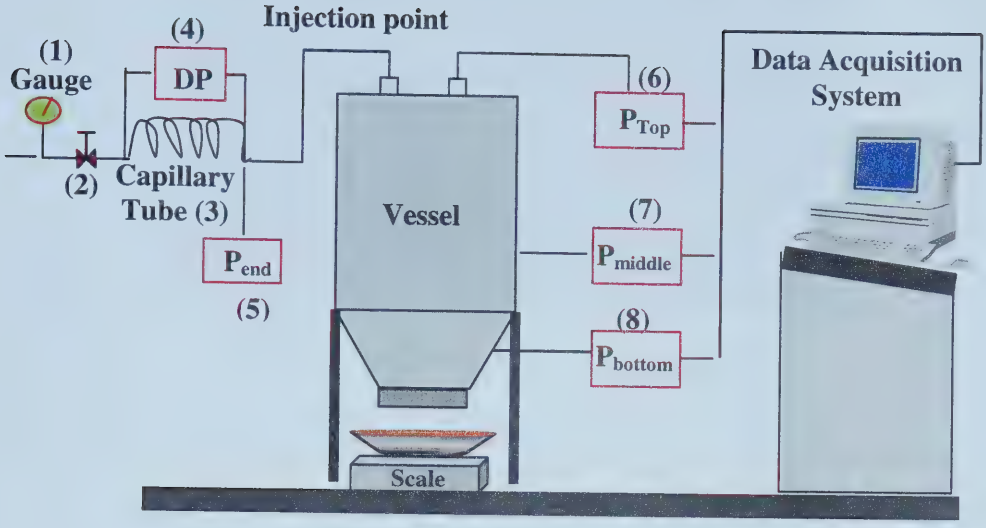

Figure 4.15: Schematic of sand production apparatus for the air tests (not to scale)

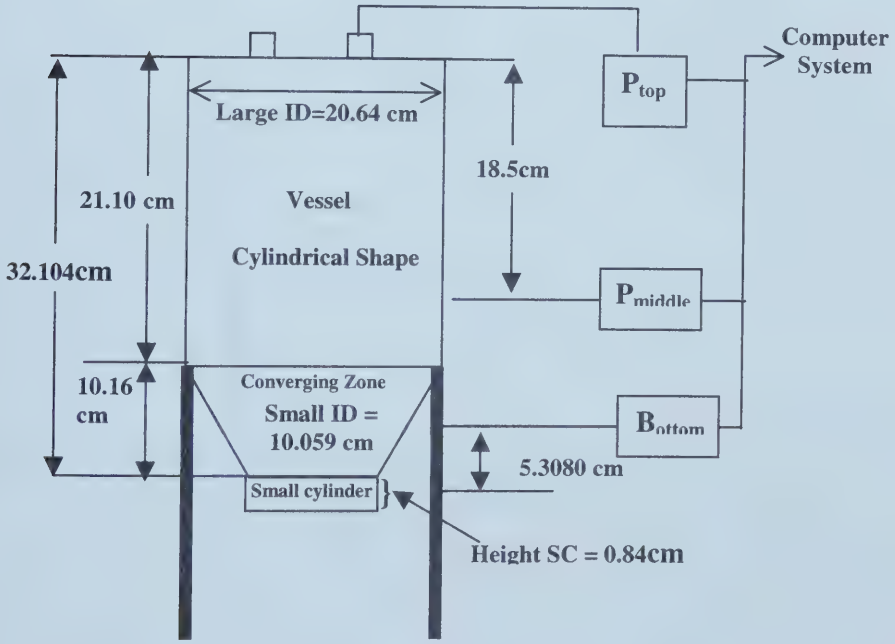

Figure 4.16: Dimensions of the vessel used in the air experiments (not to scale)

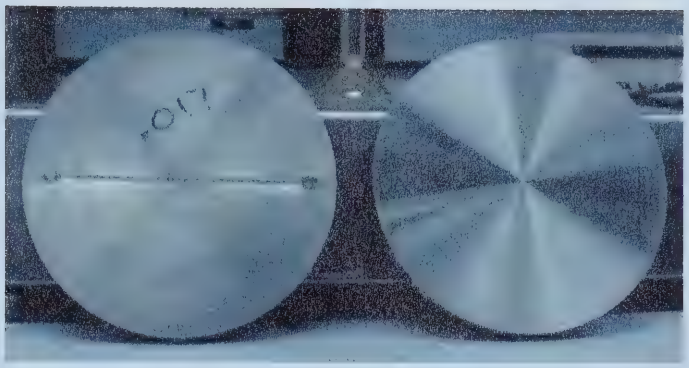

Figure 4.17: Slot plates used in the air experiments

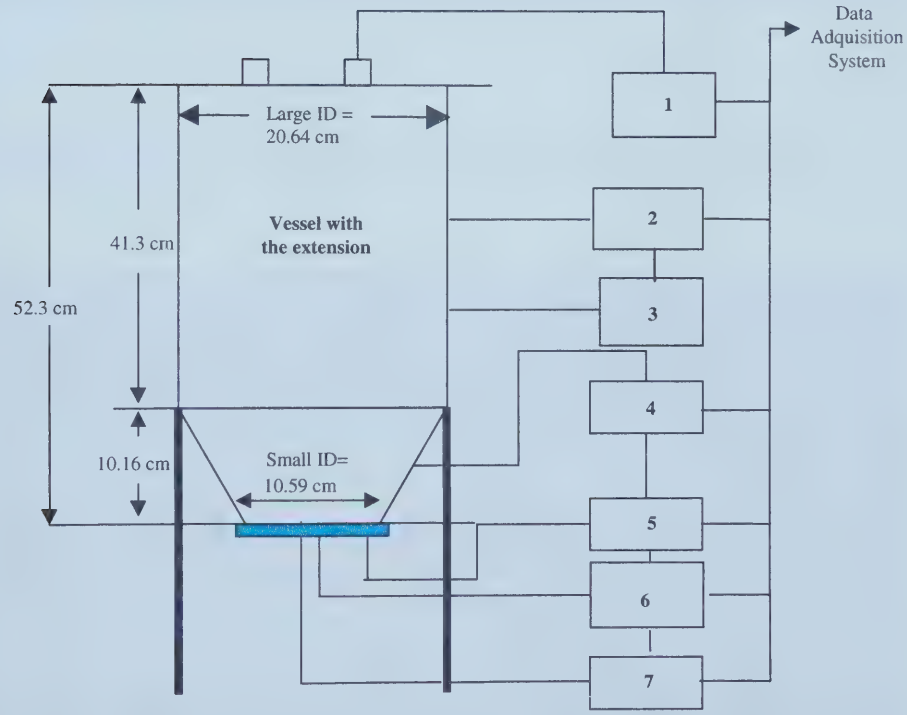

Legend:

1: $\mathbf{P_1}$= Absolute transducer, measures P at the top of the cell.
2: $\mathbf{P_2}$= Absolute transducer, measures P at the first lateral port.
3: $\Delta\mathbf{P_1}$=Measures differential pressure between points (2) and (3).
4: $\Delta\mathbf{P_2}$= Measures differential pressure between points (4) and (5).
5: $\mathbf{P_3}$= Absolute transducer, measures P at the first port in the slot.
6: $\Delta\mathbf{P_3}$=Measures differential pressure between points (5) and (6).
7: $\Delta\mathbf{P_4}$ =Measures differential pressure between points (6) and (7).

Figure 4.18: Schematic of sand production apparatus for liquids tests (not to scale)

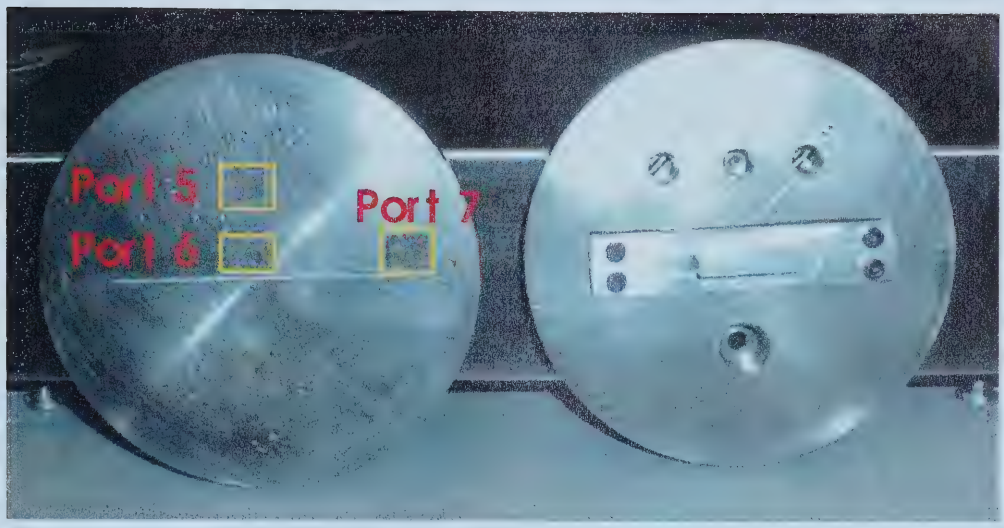

Figure 4.19: Slot plates used in the sand production liquid experiments

Figure 4.20: Equipment for the liquid experiments

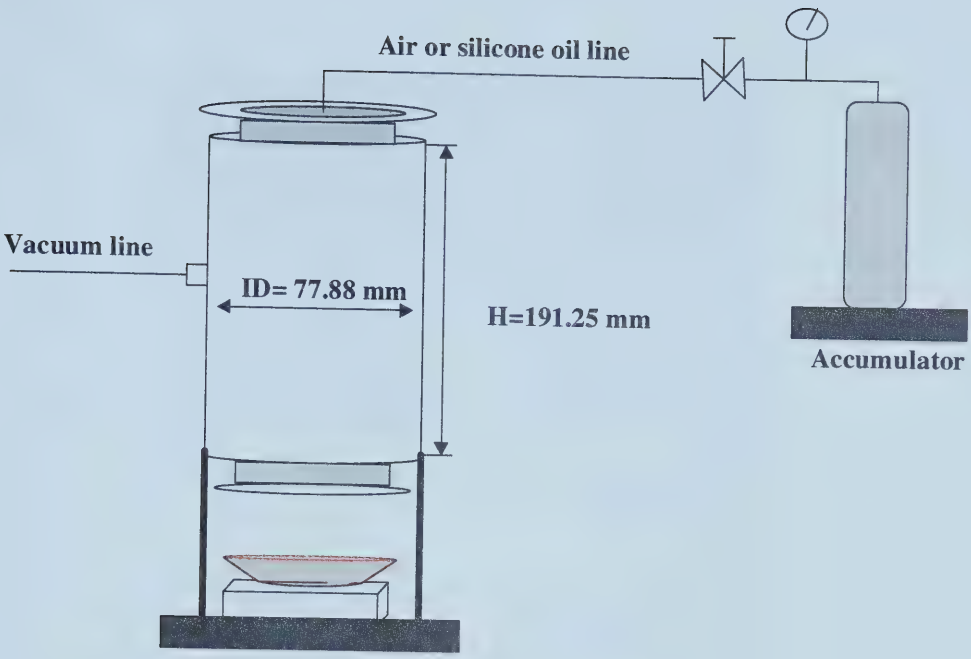

Figure 4.21: Experimental apparatus to prepare the epoxied core for the thin sections

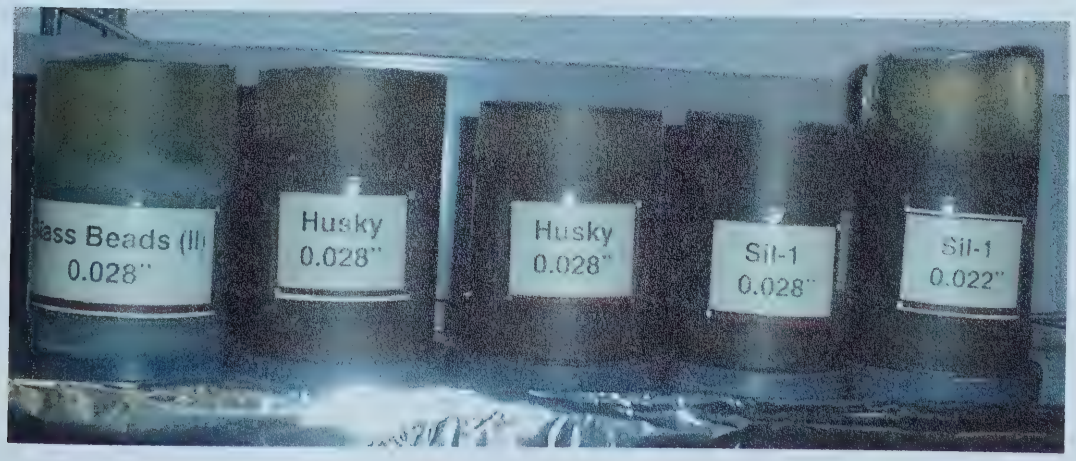

Figure 4.22: Pictures of epoxied core obtained for the thin sections

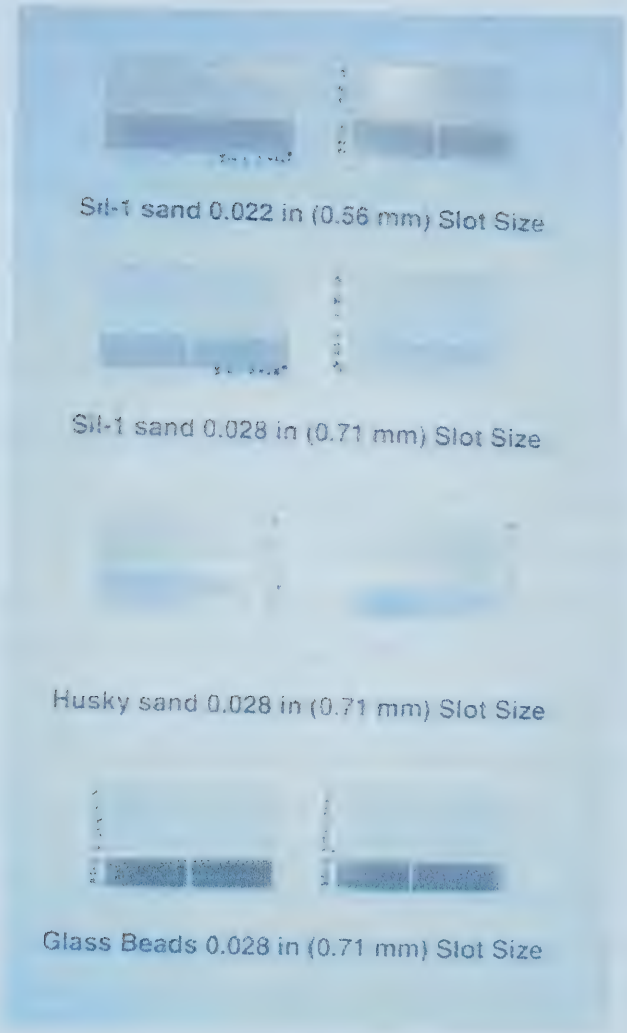

Figure 4.23: Overview of the thin sections

5 Discussion of the Experimental Results

The presentation of the results was divided into four main sections: air experiments, liquid experiments, CT scanner tests and core thin section analysis. The CT scanner and thin section tests were performed in order to observe in more detail the porosity distribution and packing of the sand in the sand pack.

The experimental results are discussed in the following sections.

5.1 Air Test Experiments

Thirty-two runs were performed to investigate the influence of sand morphology and size distribution, slot size and initial flow rates on sand production. Two different sands were used: a commercial silica sand called Sil-1 sand and a sand obtained from cold production collection tanks called Husky sand. The flow through three different slots with widths of: 0.018 in (0.46mm), 0.028 in (0.71 mm) and 0.04 in (1.02 mm) was investigated. The effect of the initial porosity on sand production was also examined. In order to determine if the size distribution of the produced sand was the same as that of the sand in the pack, samples were taken in one test (Run 39) at different time intervals.

The first 5 runs were used to define the procedure and test the experimental apparatus. Data was not collected from these runs, and therefore they will not be discussed. Runs 6-7 and 9-10 were performed to evaluate the effect of the initial flow rate on the production of silica sand through a 0.028 in (0.711 mm) slot. The same tests were carried out with Husky sand (runs 16-17, 19 and 23). The flow rate was varied by adjusting a pressure regulator. The corresponding flow rates were calculated. The pressure range was from atmospheric to 60 psi (414 kPa) equivalent to air flow rates from 0 to 14.08 l/min. The procedure followed during the air tests was described in Section 4.2.1

The effect of the slot width on sand production was investigated in runs 6 (0.028 in or 0.71 mm), 11 (0.018 in or 0.56 mm) and 13 (0.040 in or 1.02 mm) for the Sil-1 sand and runs 16 (0.028 in or 0.71 mm), 14 (0.018 in or 0.56 mm) and 26 (0.040 in or 1.02 mm)

for the Husky sand. In addition, the influence of the initial porosity on sand production was studied in runs 6, 37 and 40 for Sil-1 sand and runs 16 and 41 for Husky sand using a 0.028 in (0.71 mm) slot.

Several runs were repeated to determine the reproducibility of the results.

Two different runs (6 and 16) will be described in detail in order to show the methodology used in the experiments. The results from the other tests will be presented in tabular form.

5.1.1 History of a Typical Air Test

5.1.1.1 Sil-1 Sand

Figure 5.1 presents the cumulative production of Sil-1 sand as a function of time for run 6. Run 16, also shown in the Figure 5.1, will be discussed in the next section. The initial porosity of the sand pack was 43.87%. The test was performed at atmospheric pressure under gravity flow. The plot shows that the sand is produced at the beginning of the test and quickly reaches a constant value indicating that sand production stopped. This behaviour was observed in all the tests performed with Sil-1 sand.

The corresponding sand production rate vs time was plotted in Figure 5.2. The sand production rate increased rapidly until a maximum value was reached. The sand production rate then decayed to zero after a certain time. The quantity of sand produced in this test was 784.06 g, which represents 6.50 % of the sand within the vessel. Sand was produced during the first 15 minutes of the test.

The sand production stopped most likely due to the formation of arches and/or bridges at the entrance and within the slot as described earlier in the literature [36]. The stability of the arches/bridges to changes in oil production rate is an important question with practical implications in cold production using horizontal wells.

The delivery pressure was increased to 10 psi (69 kPa), equivalent to an air flow rate (Q_A) of 5.66 l/min, 30 minutes after the start of run # 6 (Figure 5.2). Again, sand was produced but this time the quantity was less than in the preceeding step. The quantity of sand produced was 260.02 g, which represented 2.16 % of the original sand within the cell. Another difference was the sand production time. In this case, sand production stopped after (1.25 min) compared to 15 min in the preceding step under gravity flow.

No sand production was observed when the pressure was increased in steps to: 20 psi (138 kPa), 40 psi (276 kPa) and 60 psi (414 kPa).

5.1.1.2 Husky Sand

Husky sand was tested as for Sil-1 sand. The production of Husky sand under gravity flow, through a 0.028 in (0.71 mm) slot, is shown in Figure 5.1 (Run 16). The corresponding sand flow rate is shown in Figure 5.3. As in the Sil-1 sand test, sand started to be produced after the slot was unplugged. In this case, the quantity of sand produced was 89.81 g, which represents approximately 1 % of the sand in the pack. Sand production stopped after 94 s. The injection pressure was increased to 10 psi (69 kPa) yielding an air flow rate of 5.66 l/min at that pressure. A small quantity of sand (15.44 g) was produced. The sand production only lasted for 26 sec. The air delivery pressure was increased to 20, 40 and 60 psi, without further sand production.

Now that two typical sand production experiments were described, the results for all sand production experiments will be grouped in terms of the main parameters affecting sand production.

5.1.2 Effect of the Slot Size

The influence of slot size on sand production was investigated. Three slot width sizes were used: 0.018 in (0.457 mm), 0.028 in (0.711 mm) and 0.048 in (1.02 mm). These dimensions are within the typical range of slot widths for horizontal well liners. An important parameter in the investigation of sand production through the slots is the ratio

of the slot width to the grain diameter. Since the sands investigated are not uniform in size, different definitions of the diameter of the sand grains will be used. The different diameters shown in Table 5.1 correspond to the dimensions of the sieve mesh which allows a certain percentile (in subscript) by weight of sand to pass through. It is important to note in comparing the Sil-1 and Husky sands, that the ratio of the slot width to grain diameter is smaller for the Sil-1 sand for all diameters except the $D_{99.9}$ diameter.

5.1.2.1 Sil-1 Sand

The effect of the slot width on sand production is observed in Table 5.2 by comparing the total weight percentage of sand produced for the different slot sizes (Runs 6, 11, and 13). The abbreviation SPT stands for "sand production time", i.e. the time during which sand was produced for the corresponding step in the test.

Run 6 was described in the former section. The results of Run 11 (Table 5.2) shows that Sil-1 sand could not be produced through the 0.018 in (0.46 mm) slot at all injection pressures. The lack of sand production is likely due to arching/bridging at the entrance and within the slot since the slot width to D_{50} grain diameter for example was small (1.7).

Almost all of the sand in the pack was produced in Run 13 for the 0.04 in (1.02 mm) wide slot. This test was repeated twice (Runs 32 and 33) with the same results. Figure 5.4 shows the sand flow rate versus time for Runs 13, 32 and 33. The reproducibility of the tests will be discussed in a latter section.

The results obtained indicate that, more sand is produced when the slot width increased.

5.1.2.2 Husky Sand

An increase in sand production with increasing slot width was also observed for Husky sand as shown in Table 5.3.

The results of run 14 (Table 5.3) show that very little Husky sand was produced through the 0.018in (0.46mm) wide slot. The test was repeated (Run 14a) with some

modifications. The pressure was increased directly from atmospheric to 40 psi (276 kPa) to find out if a sudden increase in the injection pressure would encourage sand production. A small quantity of sand, 3.5 g (0.04 %), was produced at 40 psi and approximately 2 g (0.02 %) were produced at 60 psi. (414 kPa). Significantly more Husky sand was produced through the wider slots (Runs 16 and 26)

The greater sand production of the Sil-1 sand compared to the Husky sand for all slot widths can be explained by the larger slot width to $D_{99.9}$ ratio for the former sand (Table 5.1). This larger ratio implies that more sand grains are required to form an arch at the entrance or within a slot for the Sil-1 sand. It is interesting to note that in test 26 the arch/bridge did not stabilize and the complete pack was produced.

Since the Husky sand was more angular than the Sil-1 sand, it was thought that the angularity of the Husky sand would lead to more stable arches. In order to investigate the influence of angularity on sand production, glass beads with approximately the same size distribution as the Husky sand but very different sphericity were used in sand production experiments. These experiments were described in a further describing the liquid tests.

Miller [36] also investigated the influence of the slot width to sand diameter ratio on sand production. He concluded that sand in a dry state, without confining stress and under gravity flow, will not exhibit arching until the slot width is less than approximately four times the D_{50} sand grain diameter. As explained earlier, it appears that the D_{50} may not be the best diameter to use in determining the production of sand through a slot, although we examined only two types of sands.

5.1.3 Effect of the Initial Flow Rate

In the previous experiments, the injection pressure was increased in steps from atmospheric pressure to 60 psi (414 kPa). As will be shown in the following section, sand production is not the same if the pressure is initially increased in steps from atmospheric pressure to 60 psi (414 kPa) or directly to 60 psi for example. In order to investigate the influence of the initial air flow rate on sand production, a series of tests

were performed at different initial pressures: atmospheric pressure or gravity flow, 20 psi (138 kPa) Q_A= 9.53 l/min, 40 psi (276 kPa) Q_A=13.68 l/min, and 60 psi (414 kPa) Q_A=14.09 l/min. The flow rates are given at the corresponding injection pressure. The flow of Sil-1 and Husky sand through a 0.028 in (0.71 mm) slot was investigated in these tests.

5.1.3.1 Sil-1 Sand

The tests investigating the effect of the initial pressure on the production of Sil-1 sand through a 0.028 in (0.71 mm) slot are listed in table 5.4. These results show that, within experimental error, more sand is produced at a given injection pressure if the pressure is increased directly to that pressure rather than in steps.

Figure 5.6 and 5.7 summarize the sand production rate versus time and cumulative sand production for Runs 6, 8, 9 and 10. It is interesting to note in Figure 5.7 that sand production took significantly more time to decrease to zero under gravity flow. The time at which sand production stopped for the other runs was approximately the same. The sand production rate and cumulative sand seem to increase when the initial injection pressure increases. The average sand production rate increased with increasing initial injection pressure:

Atm	20psi (137.9 kPa)	40psi (275.8 kPa)	60psi (413.7 kPa)
50.91 g/min	361.16 g/min	680.12 g/min	777.87 g/min

The average sand production rate was calculated as follows:

(5.1) $$q_{ST} = \frac{m_{TSP}}{t_{TSP}}$$

where: q_{ST}: total sand flow rate
m_{TSP}: total mass of sand produced
t_{TSP}: elapsed time during which sand was produced

Sand production likely stopped due to the formation of arches/bridges. These arches/bridges are stable to air flow rate changes.

5.1.3.2 Husky Sand

The tests investigating the effect of the initial pressure on the production of Husky sand through a 0.028 in (0.71 mm) are listed in Table 5.5. These results show that more sand is produced at a given injection pressure if the pressure is increased directly to that pressure rather than in steps (see figures 5.8 and 5.9).

The influence of the initial flow rate on sand production through a 0.040 in (1.02 mm) slot was performed at two different initial flow rates for Husky sand (Runs 26 and 27) as shown in Table 5.6

Figure 5.10 shows the effect of initial air flow rate on sand production for Runs 26 and 27. As observed for the flow of the Sil-1 and Husky sands through the 0.028 in (0.71 mm) slot (Figure 5.8 and 5.9), the sand took a significantly longer time to stabilize under gravity flow than at an initial flow rate of 5.66 l/min @ 10 psi (69 kPa). After sand production stabilized during the initial flow rate, further increase in the flow rate yielded two types of failure. In one type, partial failure of the arches/bridges occurred, sand is produced but stops in a short time. In the second type the arches/bridges break and the total sand within the container is produced. Thus, starting at atmosphere pressure (Run 26) the threshold air flow rate (Q_T) for sand production was 13.68 l/min. In the test which started directly with an initial flow rate of 5.66 l/min (Run 27) the threshold flow rate was14.73 l/min.

The effect of the injection flow rate is shown in Figure 5.11 for Run 27. The sand production rate changed sharply at each increase in injection rate and declined sharply there after. In the first step (5.66 l/min @ 10 psi/68.95 kPa) arches/bridges likely formed stopping sand production. Increases in air pressure flow rate to 20, 40 and 60 psi lead to negligible sand production if at all. Therefore, the arches/bridges formed were stable to flow rate changes in this interval. A further increase of the air flow rate to 14.73 l/min at

80 psi (551.58 kPa) caused the production of the entire sand pack. The highest sand flow rate was found at the highest injection rate.

Intermittent sand production was also observed by Miller [36] in his experiments performed in a visualization model with dry coarse sand without confining stress. In his experiments, Miller [36] vibrated the pack manually with a rubber hammer throughout the test. Although the procedure and other factors like the opening width to equivalent size diameter ratio were different in Miller's experiments, his results further indicate that sand arching over a perforation can be destroyed and re-established by applying an external disturbance.

Total amounts of sand produced in experiments 26 and 27 were 93.02% and 97.4% respectively. Therefore, sand production stopped at the end of the tests simply because there was no more sand available in the pressure vessel. Figure 5.12 provides graphs of sand production rate versus time for the threshold flow rate (Q_T) for each test. The maximum sand production rate was highest for test 27 possibly due to the higher threshold flow rate for that test.

5.1.4 Size Distribution of the produced sand

Test 39 was performed in order to determine potential changes in the size distribution of the produced sand. It was expected that certain fractions of the sand might be preferentially produced through a slot. The test was performed starting at atmospheric pressure (under gravity flow) with the Sil-1 sand using a 0.028 in (0.71 mm) slot. Samples were taken at the following times after the start of the test (0.5, 1, 1.5, 2, 3, 4, 5, 6, 8, 10, 15, 20 min).

The results are shown in Figure 5.13 to 5.15 and Table 5.7and 5.8 where the particle size distribution curves of the different samples and the mass of sand produced are presented. For the first step of the test, the size distribution of the samples was approximately the same as that of the original sample in the pack as seen in Figure 5.13 where representative

size distribution curves are shown. For the second step, a good match was also obtained between the samples and the original size distribution of the sand (Figure 5.14).

A similar result was obtained for the last step where sand was produced, Q_A= 13.68 l/min, the sieve analysis yielded a size distribution curve very similar to that of the original sand (Figure 5.15).

The results imply that the bulk of the Sil-1 sand was produced through a 0.028 in (0.71 mm) slot. A similar behaviour is expected for the 0.040 in (1.02 mm) wide slot since the flow of sand through this slot is less restrictive.

5.1.5 Effect of Initial Porosity on sand production

The objective of tests 6,34, 37, 40 and 41 was to determine the effect of initial porosity on sand production. All these experiments were performed using a 0.028 in (0.71 mm) slot. In tests 6 and 34 the sand was pluviated into the pressure vessel which explains the higher porosities than for tests 37, 40 and 41 where the sand was vibrated.

There did not appear to be any correlation between initial porosity and the total sand produced as observed in Table 5.9 and Figure 5.16. As will be discussed in a latter section, sand production is a random process. A comparison of the total sand production in Runs 37 and 40 (Table 5.9) gives an indication of this randomness. In both runs, the sand pack was vibrated to almost the same initial porosity. It appears that more tests would be required to investigate the influence of initial porosity on sand production.

5.1.6 Reproducibility of the Tests

Several tests were repeated to evaluate the reproducibility of the experiments. The results are shown in Table 5.10 and 5.11 for Sil-1 and Husky sand respectively. The original mass of sand in the pack is indicated as the symbol m_S. The blank sections in the table indicate that the test were not performed for the corresponding step.

The sand production results for Sil-1 sand under gravity flow are shown in Figure 5.17 (Cumulative sand) and Figure 5.18 (Flow rate).

In spite of the large scatter in the data, there appears to be an average trend in the production behaviour. It is more difficult to observe a general trend in Figure 5.19 and 5.20 for Sil-1 sand and in Figure 5.21 and 5.22 for Husky sand. More tests would likely be required to observe a trend in these latter figures. These tests show the inherent randomness in sand production experiments. As will be shown in a later section, the production of sand through a slot is very sensitive to the size of the grains. A single sand grain can have a significant impact on sand production.

5.1.7 Comparison Between Sands

In spite of the randomness of the tests, a definite difference was observed between the average production of Sil-1 and Husky sands as shown in Figure 5.23 for a 0.028 in (0.71 mm) slot. It appears that Husky sand can arch/bridge more easily than Sil-1 sand since less Husky sand was produced than Sil-1 sand (Figure 5.23). Significantly more Sil-1 sand than Husky sand was also produced from the 0.040 in (1.02 mm) slot. As will be discussed in a further section, the Husky sand had larger sand grains within the highest sand fraction. The grains could arch more easily due to their larger size.

5.1.8 Summary of the section

- No sand was produced with the slot size 0.018 in (0.457 mm) (both Husky and Sil-1). Therefore a new slot width of 0.022 in (0.56 mm) was chosen to perform the liquid tests.
- The ratio of the slot width to D_{50} diameter may not be a reliable criterion for sand control. Significantly more Sil-1 sand than Husky sand was produced through a 0.028 in (0.71 mm) slot even though the later ratio was 2.6 for the Sil-1 sand compared to 4.6 for the Husky sand.

- Husky sand had the tendency to arch/bridge more easily than Sil-1 sand. This was inferred from the higher sand production for the Sil-1 sand for the 0.028 in (0.711 mm) and 0.040 in (1.016 mm) wide slots.
- For both sands a higher initial flow rate meant a greater sand production rate. There is also a tendency to produced more sand when the air flow rate is further increased.
- Sand production likely stopped due to arch/bridge formation. These arches/bridges are apparently stable to increases in air flow rate. However, threshold flow rates exist above which sand may be produced again.

Sand production appears to be a random process as observed in the scatter of the sand production results.

Table 5.1: Slot width to equivalent diameter ratio for different percentiles

Percentile less than	Sil-1			Husky		
	0.018 in (0.457 mm)	0.028 in (0.711 mm)	0.040 in (1.016 mm)	0.018 in (0.457 mm)	0.028 in (0.711 mm)	0.040 in (1.016 mm)
$D_{99.9}$	0.9	1.4	2.0	0.5	0.8	1.2
D_{90}	1.3	2.1	3.0	2.3	3.6	5.1
D_{60}	1.6	2.5	3.5	2.9	4.4	6.4
D_{50}	1.7	2.6	3.7	3.0	4.6	6.6
D_{10}	2.5	3.8	5.5	5.7	8.9	12.7

Table 5.2: Effect of slot width: Sil-1 sand (runs 6, 11, and 12)

Run #	Slot width (in)	ϕ_i (%)	Mass of Sand Produced (wt % with respect to the original sand pack)										Total Sand Produced (wt %)
			p_{inj} Atm	SPT (min)	p_{inj} 10 (psi)	SPT (min)	p_{inj} 20 (psi)	SPT (min)	p_{inj} 40 (psi)	SPT (min)	p_{inj} 60 (psi)	SPT (min)	
11	0.018	41.93	0.00	0.00	0.00	0.00	0.00	0.00	0.00	0.00	0.00	0.00	0.00
6	0.028	43.87	6.50	15.4	2.16	1.3	0.00	0.00	0.00	0.00	0.00	0.00	8.66
13	0.040	44.78	97.74	53	—	—	—	—	—	—	—	—	97.74

ϕ_i = Initial porosity
SPT = Sand production time
p_{inj} = Injection pressure

Table 5.3: Effect of slot width: Husky sand (runs 14, 16, and 26)

Run #	Slot width (in)	ϕ_i (%)	Mass of Sand Produced (wt % with respect to the original sand pack)										Total Sand Produced (wt %)
			p_{inj} Atm	SPT (min)	p_{inj} 10 (psi)	SPT (min)	p_{inj} 20 (psi)	SPT (min)	p_{inj} 40 (psi)	SPT (min)	p_{inj} 60 (psi)	SPT (min)	
14	0.018	45.95	0.00	0.00	0.00	0.00	0.00	0.00	0.02	28.00	0.04	25.00	0.06
16	0.028	47.78	0.99	1.5	0.20	0.43	0.00	0.00	0.00	0.00	—	—	1.15
26	0.040	47.60	35.07	31.00	5.57	3.80	0.00	0.00	52.38	4.60	—	—	93.02

ϕ_i = Initial porosity
SPT = Sand production time
p_{inj} = Injection pressure

Table 5.4: Effect of initial air delivery pressure (p_{inj}): Summary of results with Sil-1 sand for runs 6, 8, 9 and 10. Slot size 0.028 in (0.711 mm)

Run #	p_{inj} (psi)	ϕ_i (%)	Mass of Sand Produced (wt % with respect to the original sand pack)								Total Sand Produced (wt %)
			Atm	SPT (min)	p_{inj} 20 (psi)	SPT (min)	p_{inj} 40 (psi)	SPT (min)	p_{inj} 60 (psi)	SPT (min)	
6	Atm	43.87	6.50	15.4	0.00	0.00	0.00	0.00	0.00	0.00	6.50
8	20	43.47	—	—	5.70	1.77	0.00	0.00	0.12	33.77	5.82
9	40	45.06	—	—	—	—	7.36	1.20	0.00	0.00	7.36
10	60	44.21	—	—	—	—	—	—	13.27	1.43	13.27

ϕ_i = Initial porosity
SPT = Sand production time
p_{inj} = Injection pressure

Table 5.5: Effect of initial air delivery pressure: Summary of results with Husky sand for runs 16, 17, 19 and 23. Slot size 0.028 in (0.711 mm)

Run #	p_{inj} (psi)	ϕ_i (%)	Mass of Sand Produced (wt % with respect to the original sand pack)								Total Sand Produced (wt %)
			Atm	SPT (min)	p_{inj} 20 (psi)	SPT (min)	p_{inj} 40 (psi)	SPT (min)	p_{inj} 60 (psi)	SPT (min)	
16	Atm	47.78	0.99	1.57	0.00	0.00	0.00	0.00	---	---	0.99
17	20	47.02	---	---	2.09	1.20	0.00	0.00	0.17	1.20	2.27
19	40	45.06	---	---	---	---	4.08	0.33	0.00	0.00	4.08
23	60	46.57	---	---	---	---	---	---	6.61	1.00	6.61

ϕ_i = Initial porosity
SPT = Sand production time
p_{inj} = Injection pressure

Table 5.6: Summary of results with Husky sand for runs 26 and 27. Slot size 0.04 in (1.02 mm)

Run #	Q_{Ai} (l/min) @ p_{inj}	ϕ_{Ii} (%)	Mass of Sand Produced (% with respect to the original sand pack)												Total Sand Produced (%)
			Atm	SPT (min)	p_{inj} 10	SPT (min)	p_{inj} 20	SPT (min)	p_{inj} 40	SPT (min)	p_{inj} 60	SPT (min)	p_{inj} 80	SPT (min)	
26	Gravity flow	47.60	35.07	31.0	5.57	3.8	0.00	0.00	52.38	4.6	---	---	---	---	93.02
27	5.66	46.27	---	---	52.37	3.3	0.00	0.00	2.17	25	0.79	16.23	42.07	20.4	97.40

ϕ_i = Initial porosity
SPT = Sand production time
p_{inj} = Injection pressure
Q_{Ai} =Initial injection flow rate

Table 5.7: Mass of sand produced (test 39). Sil-1 sand. Slot size 0.028 in (0.71 mm).

Flow rate (l/min)	Sample #	Time at sampling (s)	Sand produced (g)
Gravity Flow	1	30	59.60
	2	60	51.42
	3	90	46.70
	4	120	50.45
	5	180	91.52
	6	240	90.25
	7	300	88.86
	8	360	79.06
	9	480	134.31
	10	600	118.71
	11	900	181.13
	12	1170	56.82
5.66	1	30	96.93
	2	60	65.05
	3	80	14.93
13.68	1	40	54.00

Table 5.8: Size distribution of the sand produced. Sieve analysis data. Test 39

U.S. Sieve #	Size mm	Finer than (%)											
		Gravity Flow								5.66 l/min @ 10 psi (68.9 kPa)			13.68 l/min @ 40 psi (413kPa)
		Original	1	3	4	8	10	11	12	1	2	3	1
18	1.000	100.00	100.00	100.00	100.00	100.00	100.00	100.00	100.00	100.00	100.00	100.00	100.00
25	0.710	100.00	100.00	100.00	100.00	100.00	100.00	100.00	100.00	100.00	100.00	100.00	100.00
35	0.500	99.95	100.00	99.91	99.94	99.95	99.94	99.94	99.89	99.90	99.94	99.87	99.92
45	0.355	98.92	98.93	98.82	99.07	99.05	99.00	99.23	98.99	98.94	98.79	98.93	98.90
60	0.250	35.64	36.40	44.86	45.94	40.81	32.06	19.36	39.25	30.59	34.32	58.67	40.35
80	0.180	8.47	8.46	10.79	11.05	10.10	8.22	4.70	9.58	8.58	8.46	13.60	9.99
120	0.125	1.05	1.02	1.16	1.07	1.10	0.96	0.61	1.01	1.34	1.00	1.34	1.23
170	0.090	0.13	0.08	0.09	0.04	0.09	0.06	0.05	0.05	0.15	0.05	0.13	0.13
230	0.063	0.00	0.00	0.00	0.00	0.00	0.00	0.00	0.00	0.00	0.00	0.00	0.00
325	0.045	0.00	0.00	0.00	0.00	0.00	0.00	0.00	0.00	0.00	0.00	0.00	0.00
400	0.038	0.00	0.00	0.00	0.00	0.00	0.00	0.00	0.00	0.00	0.00	0.00	0.00

Table 5.9: Effect of porosity in sand production behaviour. Summary of results for runs 6, 37, 40, 34 and 41. Slot size: 0.028 in (0.711 mm).

Sand	Test #	Initial Porosity ϕ	% Sand Produced (with respect to the original pack) @ different Q_A												Total sand produced	
			Pack way	Original m_s (g)	Gravity flow	SPT (min)	Q_A = 5.66 (l/min)	SPT (min)	Q_A = 9.53 (l/min)	SPT (min)	Q_A = 13.68 (l/min)	SPT (min)	Q_A = 14.08 (l/min)	SPT (min)	(g)	(%)
Sil-1	6	43.87	Pluviated	12058.00	6.50	15.4	2.16	1.3	0.00	0.0	0.00	0.0	0.00	0.0	1044.08	8.66
Sil-1	37	36.75	Vibrated	12480.00	11.55	23.6	0.69	0.6	0.00	0.0	0.00	0.0	0.00	0.0	1526.94	12.24
Sil-1	40	35.49	Vibrated	13858.00	4.77	12.3	0.27	0.3	0.00	0.0	0.00	0.0	0.09	0.2	711.07	5.13
Husky	34	47.39	Pluviated	8550.00	3.68	4.0	3.43	3.2	0.00	0.0	0.00	0.0	0.00	0.0	608.01	7.11
Husky	41	31.60	Vibrated	8435.54	0.00	0.0	5.45	0.7	0.00	0.0	0.55	33.4	1.78	7.9	657.06	7.79

SPT: sand production time

Table 5.10: Summary of the reproducibility tests for the Sil-1 sand

Test #	Slot Size (in)	ϕ	Original m_s (g)	% Sand Produced (respect to the original m_s) @ different Q_A					
				Gravity flow	SPT (min)	9.53 (l/min) 20 psi	SPT (min)	13.68 (l/min) 40 psi	SPT (min)
11	0.018	41.93	11866.00	0.00	0.00	---	---	---	---
11a	0.018	42.50	11750.00	0.00	0.00	---	---	---	---
6	0.028	43.87	12058.00	6.50	15.4	---	---	---	---
21	0.028	43.00	11498.00	4.92	19.0	---	---	---	---
22	0.028	43.14	11468.00	1.27	16.7	---	---	---	---
24	0.028	43.54	11438.00	9.67	34.0	---	---	---	---
30	0.028	43.79	12814.00	5.14	9.1	---	---	---	---
38	0.028	44.18	12480.00	3.92	8.4	---	---	---	---
7	0.028	43.48	11500.00	---	---	11.85	9.97	---	---
8	0.028	43.47	11250.00	---	---	5.70	1.77	---	---
28	0.028	42.05	12449.00	---	---	3.52	1.03	---	---
9	0.028	45.06	11082.00	---	---	---	---	7.39	1.93
29	0.028	43.23	12444.00	---	---	---	---	11.74	3.27
13	0.040	44.78	11572.00	97.74	53.0	---	---	---	---
32	0.040	42.50	12605.00	97.66	83.6	---	---	---	---
33	0.040	42.87	12524.00	97.76	44.3	---	---	---	---

SPT: sand production time

Table 5.11: Summary of the reproducibility tests for the Husky sand

Test #	Slot Size (in)	ϕ	% Sand Produced (respect to the original m_s) @ different Q_A				
			Original m_s (g)	Gravity flow	SPT (min)	9.53 (l/min) 20 psi	SPT (min)
14	0.018	45.95	8784.00	0.00	0.00	---	---
14a	0.018	46.27	8732.00	0.00	0.00	---	---
16	0.028	47.78	9082.00	0.99	1.6	---	---
25	0.028	47.55	8754.00	0.70	1.3	---	---
31	0.028	47.16	8588.00	4.01	8.7	---	---
34	0.028	47.39	8550.00	3.68	4.0	---	---
17	0.028	47.02	9074.00	---	---	2.09	1.20
18	0.028	44.92	8952.00	---	---	0.71	0.47
35	0.028	47.48	8536.00	---	---	1.93	0.77

SPT: sand production time

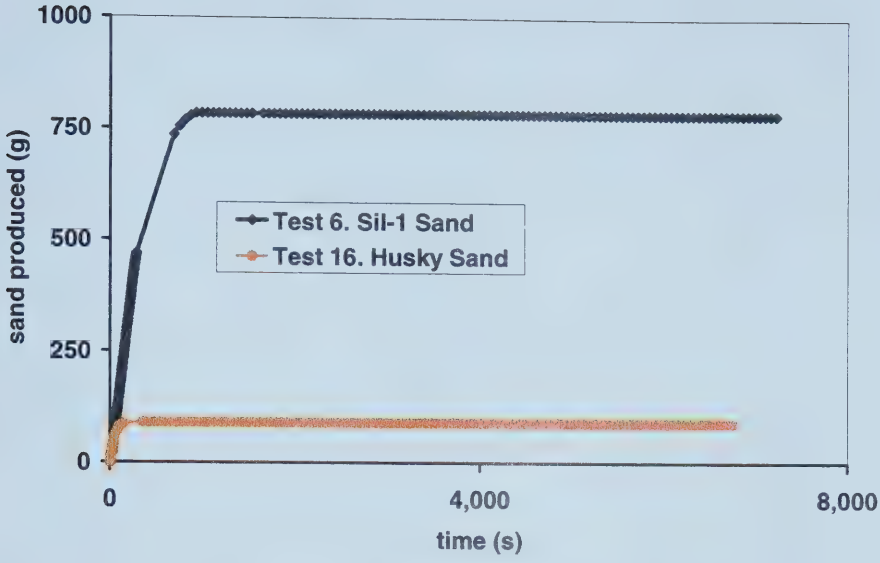

Figure 5.1: Cumulative sand production versus time. Sand: Sil-1 and Husky. Gravity flow. Slot size: 0.028 in (0.71 mm). Runs 6 and 16.

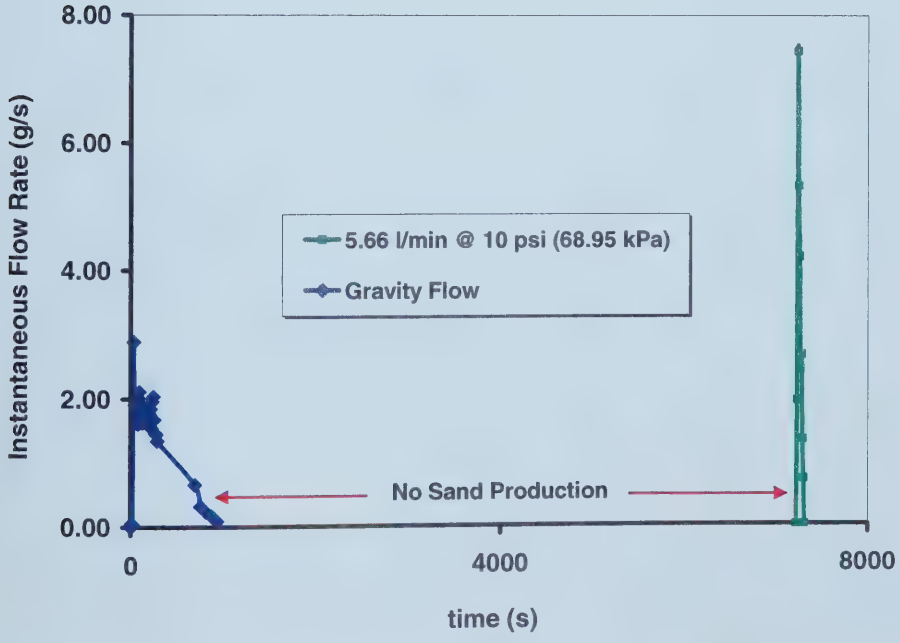

Figure 5.2: Sand production rate versus time. Gravity flow and 10 psi (69 kPa) injection pressure. Sand: Sil-1. Slot size: 0.028 in (0.711 mm). Run 6.

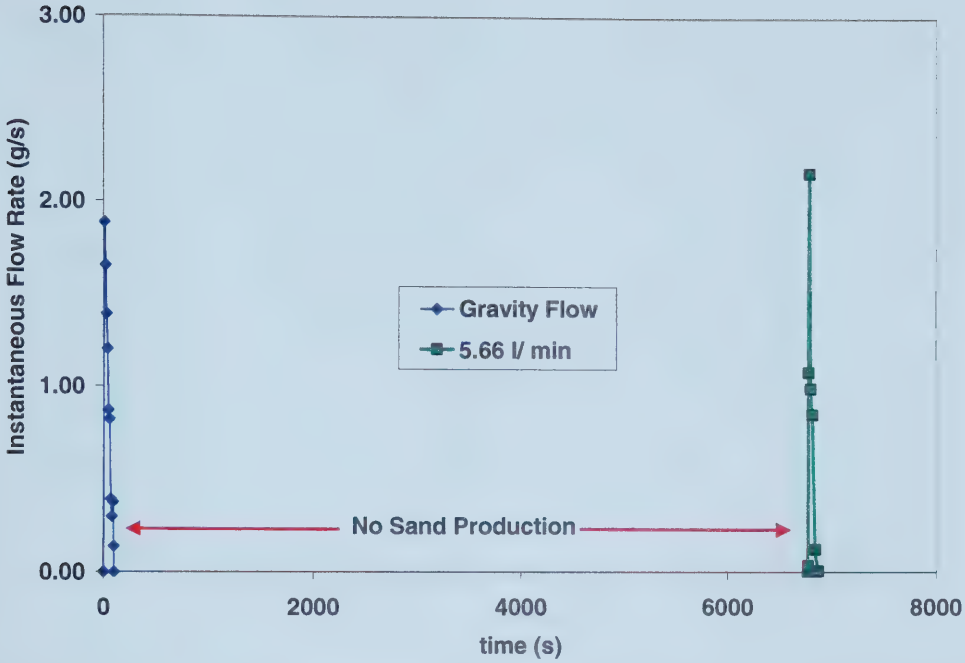

Figure 5.3: Sand production rate versus time. Gravity flow and 10 psi (69 kPa) injection pressure. Sand: Husky. Slot size: 0.028 in (0.711 mm). Run16.

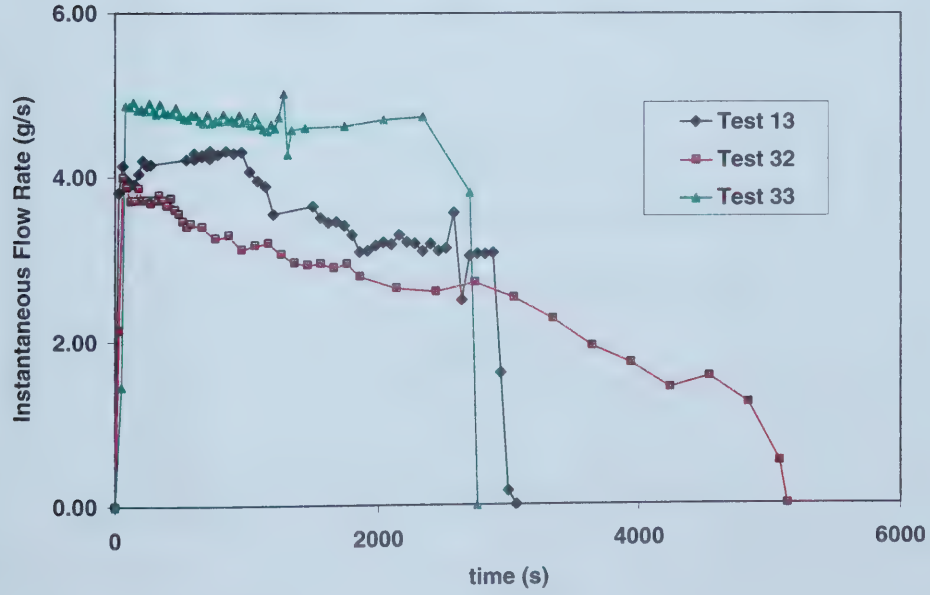

Figure 5.4: Sand flow rate versus time. Sil-1 sand. Slot width: 0.040 in (1.02 mm). Run 13

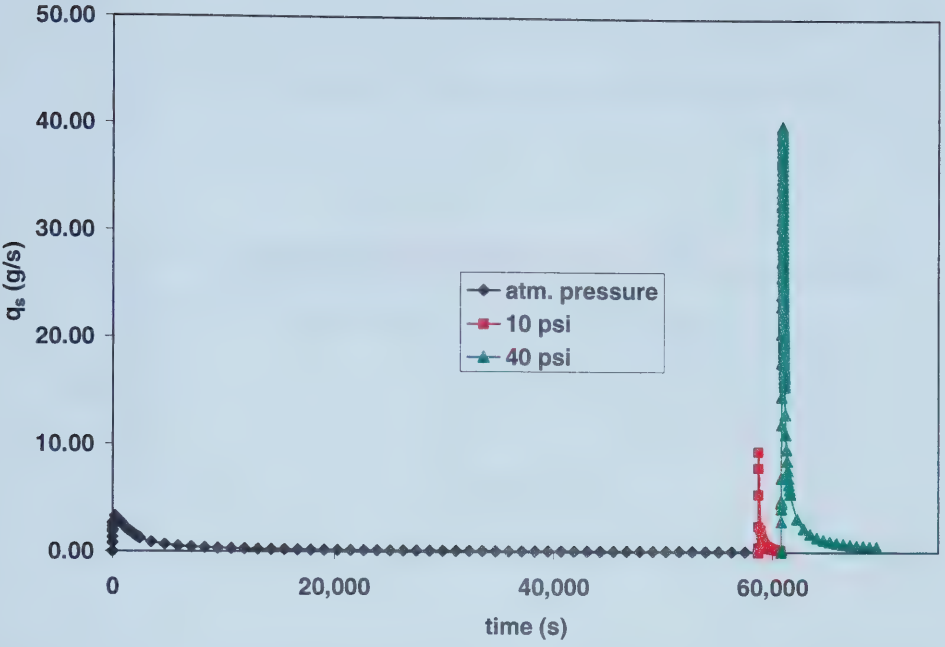

Figure 5.5: Sand flow rate Vs time. Husky sand. Slot width: 0.040 in (1.02 mm). Run 26

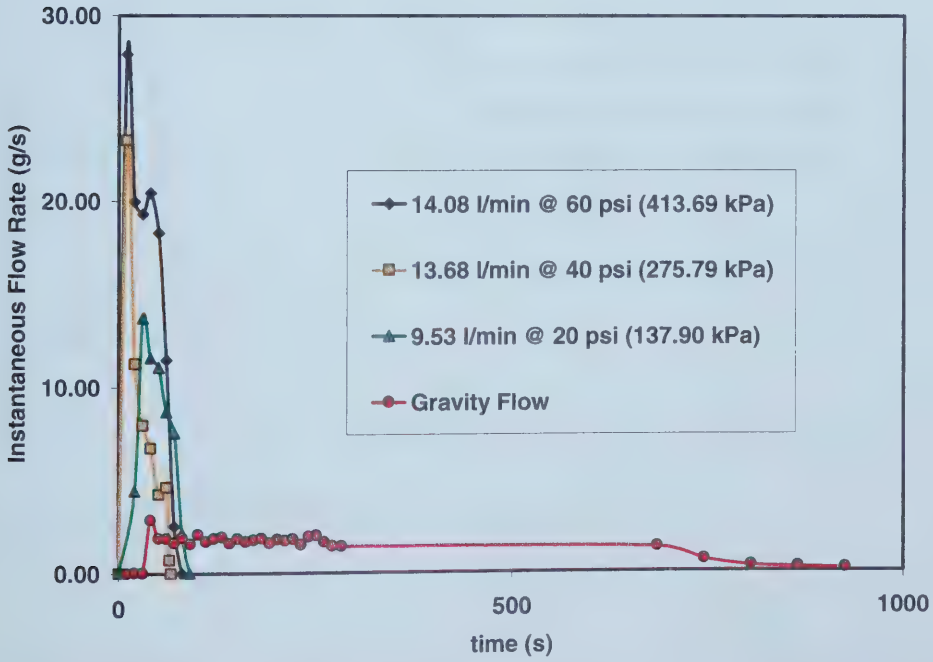

Figure 5.6: Effect of initial air delivery pressure. Sand production rate versus time. Sil-1 sand. Slot size: 0.028 in (0.71 mm). Different flow rates.

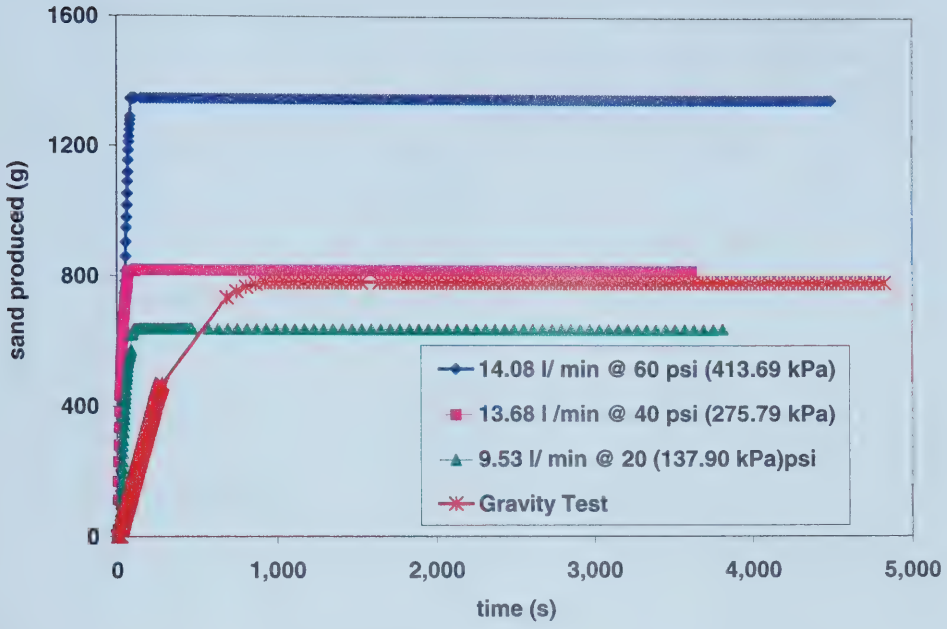

Figure 5.7: Effect of initial air delivery pressure. Sand production versus time Sil-1 sand. Slot size: 0.028 in (0.71 mm). Different flow rates.

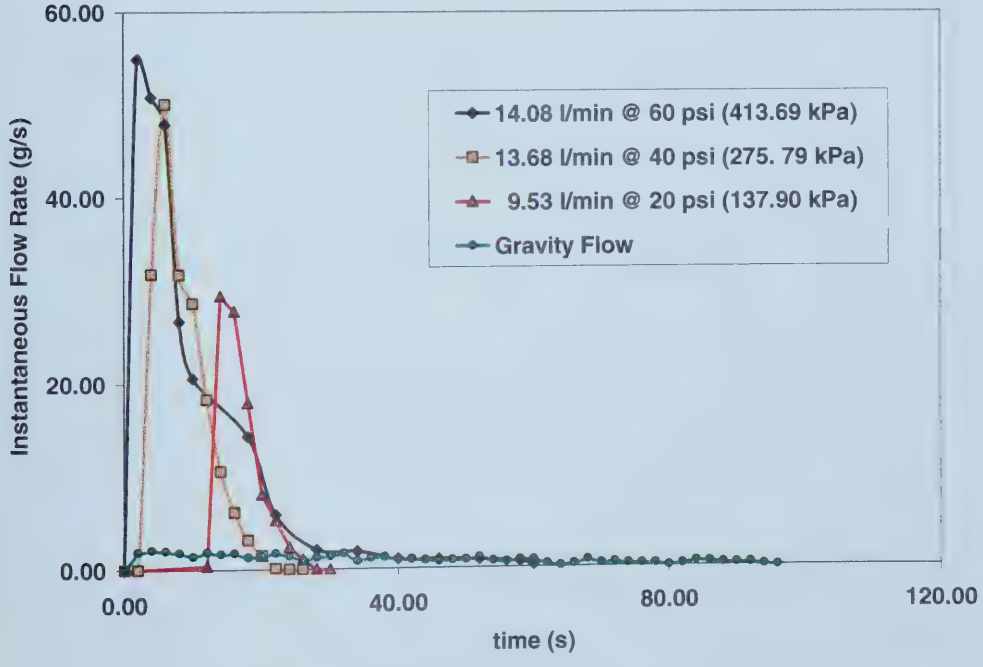

Figure 5.8: Effect of initial air delivery pressure. Sand production rate versus time. Husky sand. Slot size: 0.028 in (0.71 mm). Different flow rates.

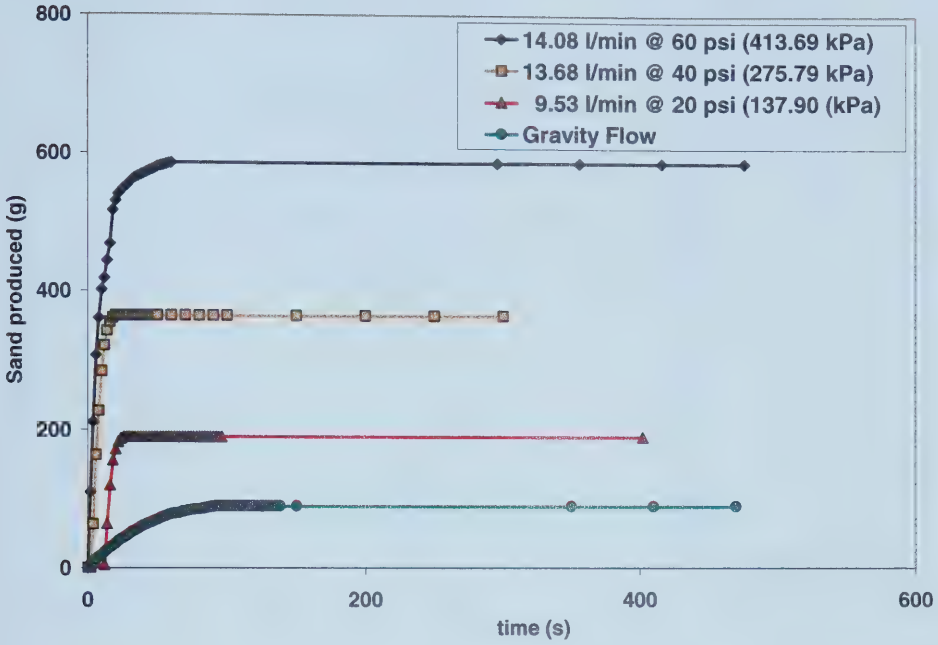

Figure 5.9: Effect of initial air delivery pressure. Sand production versus time Husky sand. Slot size: 0.028 in (0.71 mm). Different flow rates.

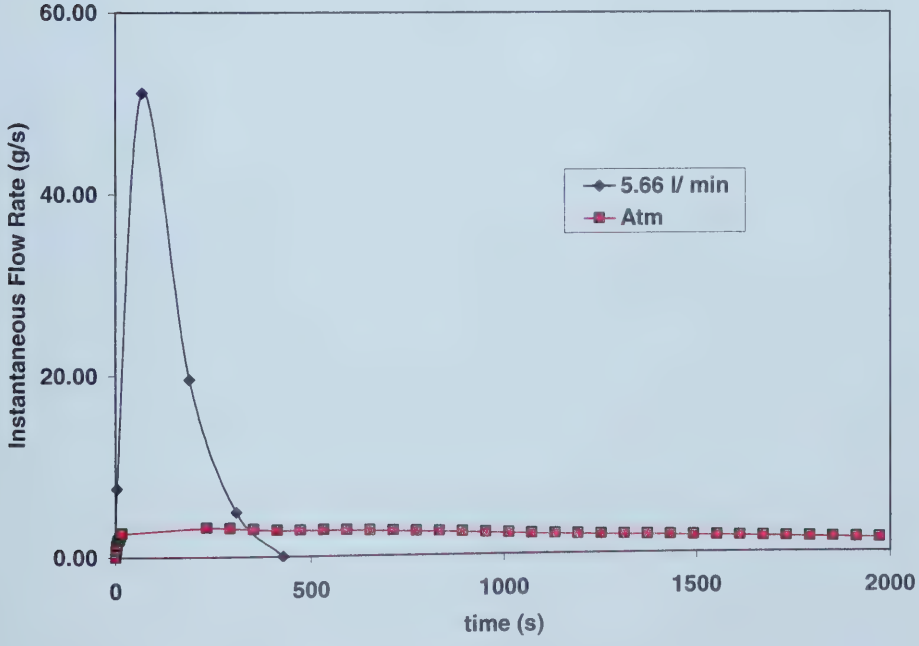

Figure 5.10: Effect of initial flow rate: Sand production rate versus time at initial conditions for runs 26 and 27. Husky sand. Slot size: 0.040 in (1.02 mm).

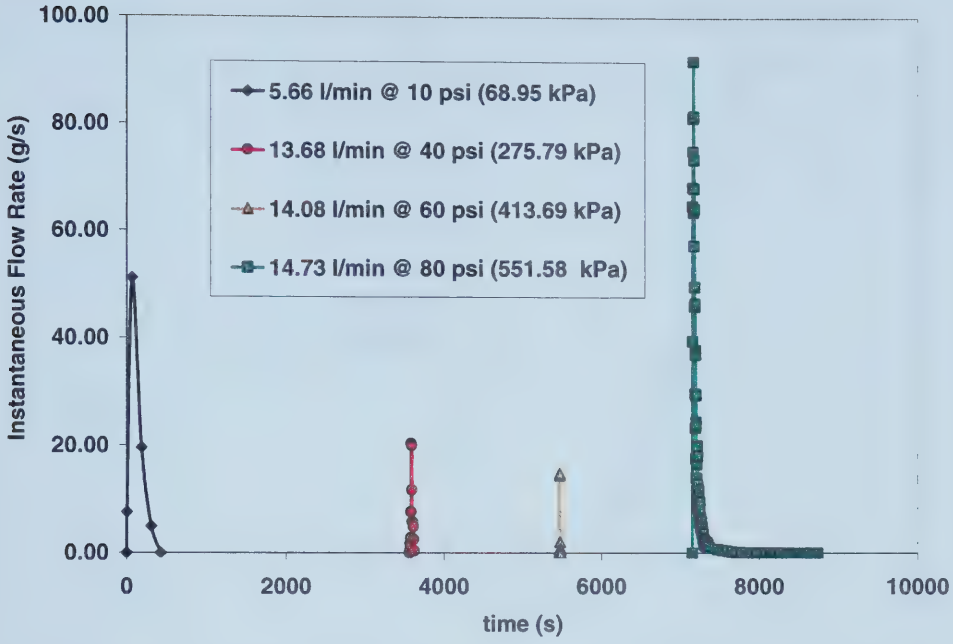

Figure 5.11: Effect of flow rate: Sand production rate versus time. Husky sand. Slot size: 0.040 in (1.02 mm). Run 27. Initial flow rate 5.66 l/min

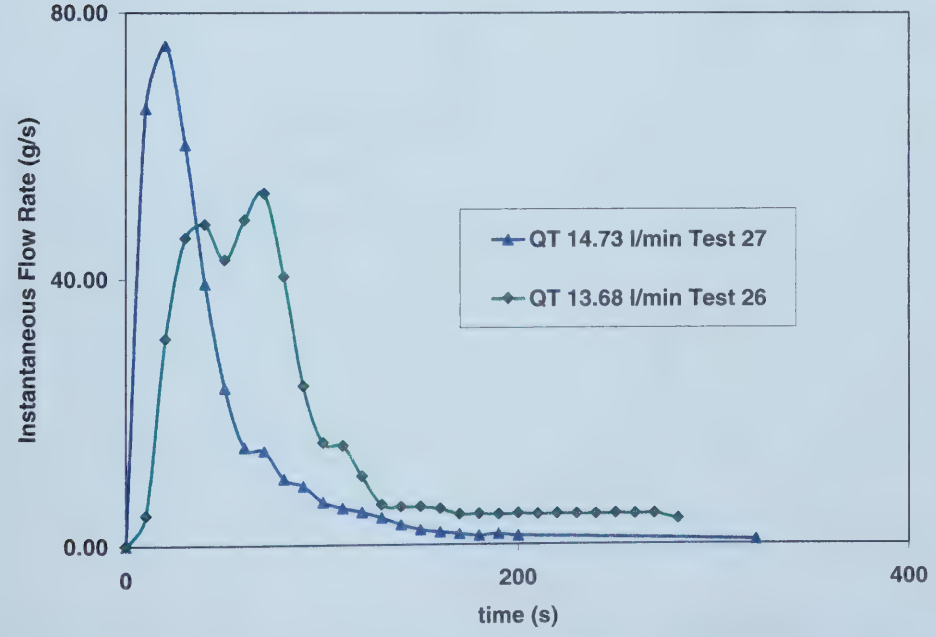

Figure 5.12: Sand production rate versus time at the air threshold flow rate for runs 26 and 27. Husky sand. Slot size: 0.040 in (1.02 mm).

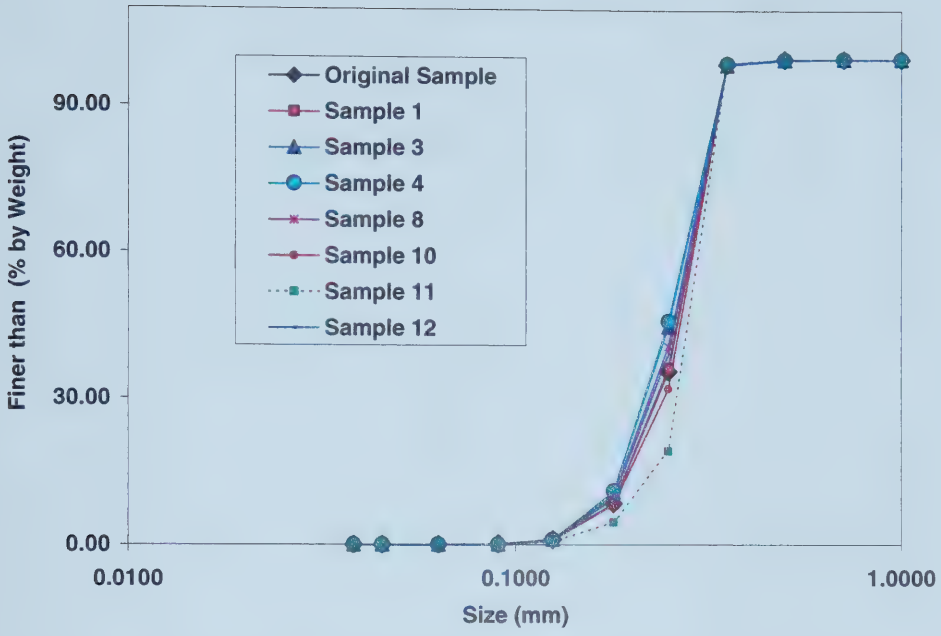

Figure 5.13: Particle size distribution curves for the sand produced by gravity flow test 39. Sand: Sil-1. Slot size: 0.028 in (0.711 mm).

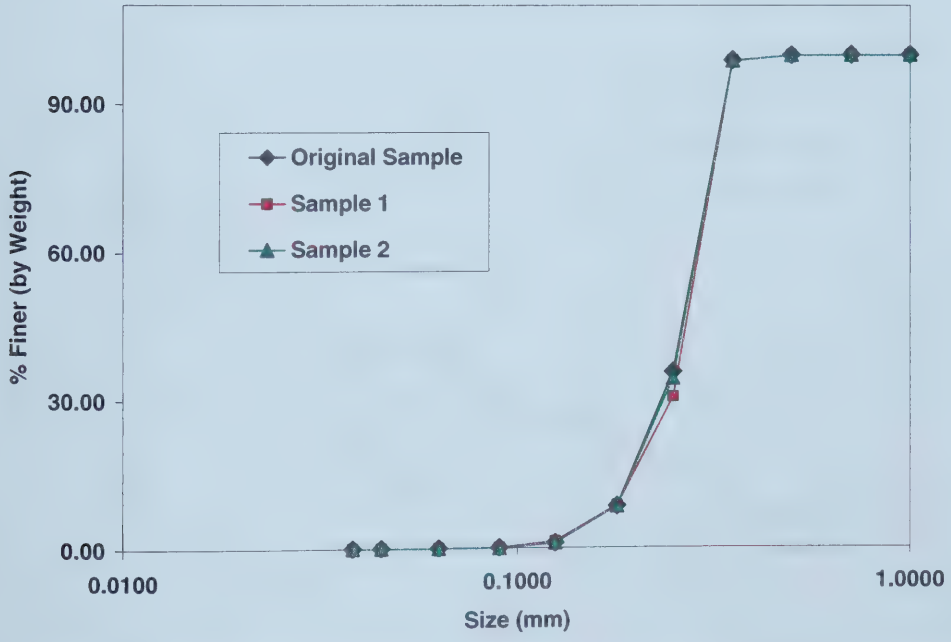

Figure 5.14: Particle size distribution curves for the sand produced at flow rate of 5.66 l/min @10 psi (68.90 kPa). Sand: Sil-1. Slot size: 0.028 in (0.711 mm).

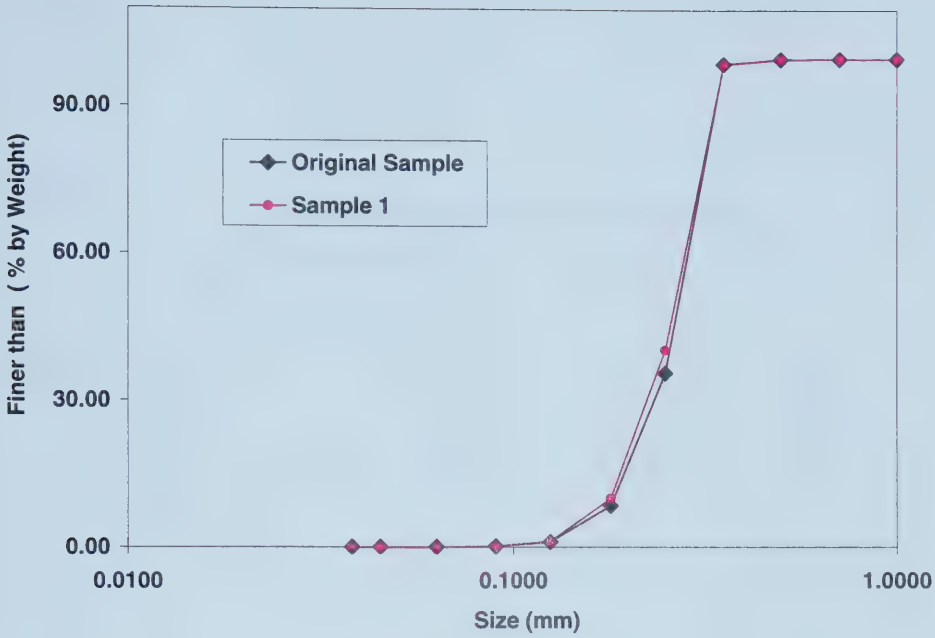

Figure 5.15: Particle size distribution curves for the sand produced with a flow rate of 13.68 l/min @ 40 psi (275.79 kPa). Sand: Sil-1. Slot size: 0.028 in (0.711 mm).

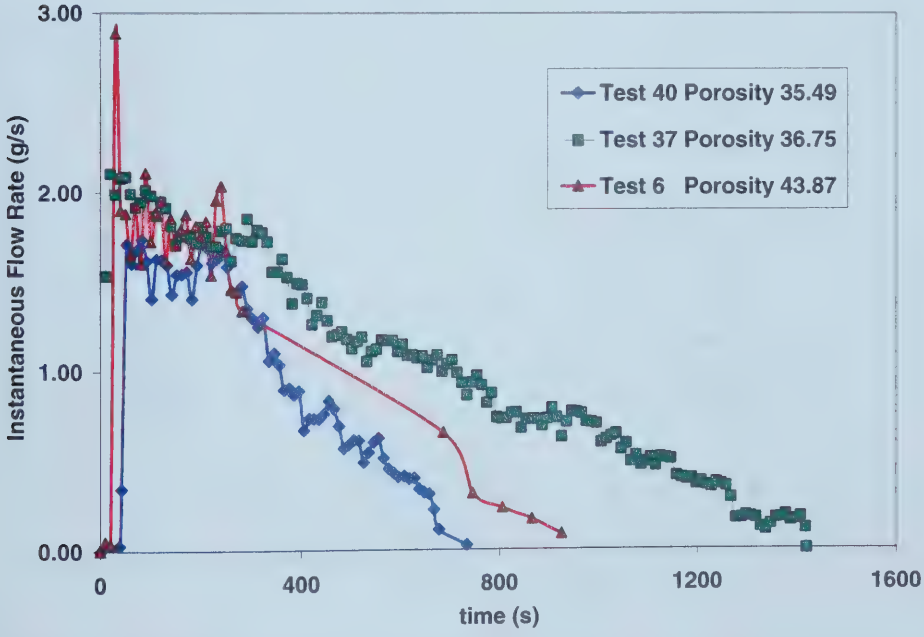

Figure 5.16: Effect of porosity in the sand production rate. Tests 6, 37 and 40. Sand: Sil-1. Slot size: 0.028 in (0.711 mm).

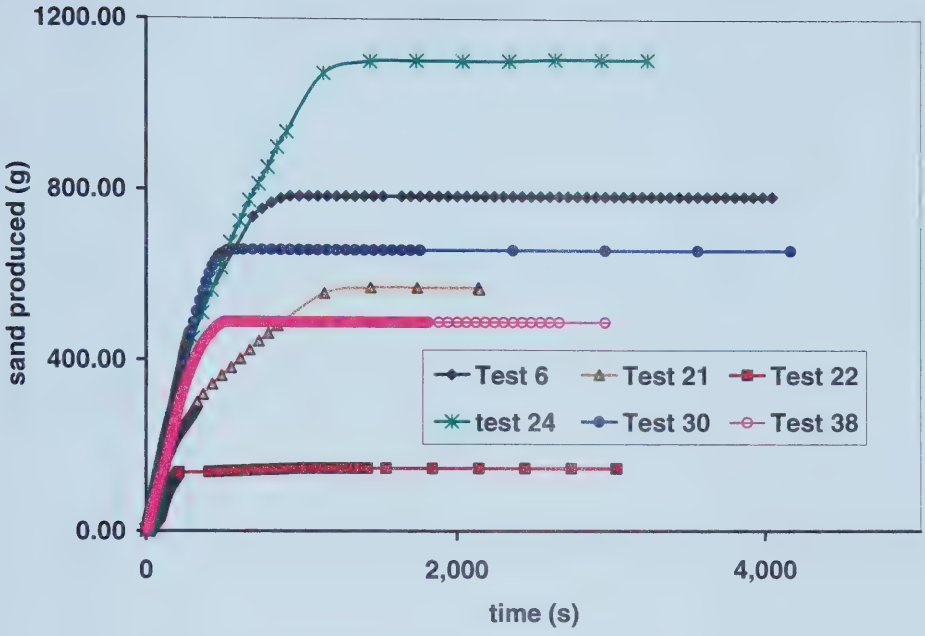

Figure 5.17: Sand produced versus time. Tests: 6, 21, 22, 24, 30, and 38. Sil-1 Sand. Gravity flow. Slot size: 0.028 in (0.711 mm).

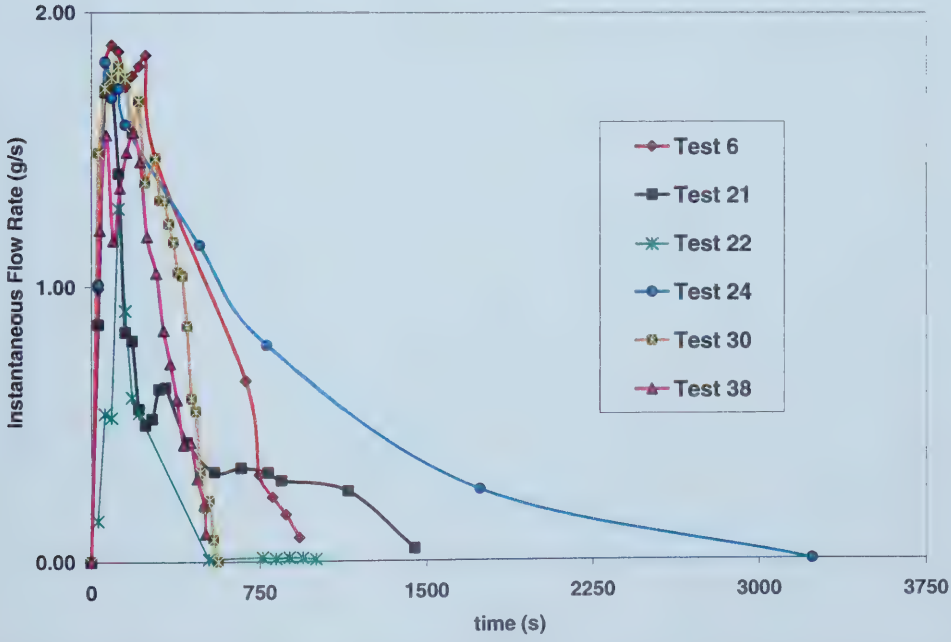

Figure 5.18: Sand flow rate versus time. Tests: 6, 21, 22, 24, 30, and 38. Gravity flow. Sil Sand. Slot size: 0.028 in (0.711 mm).

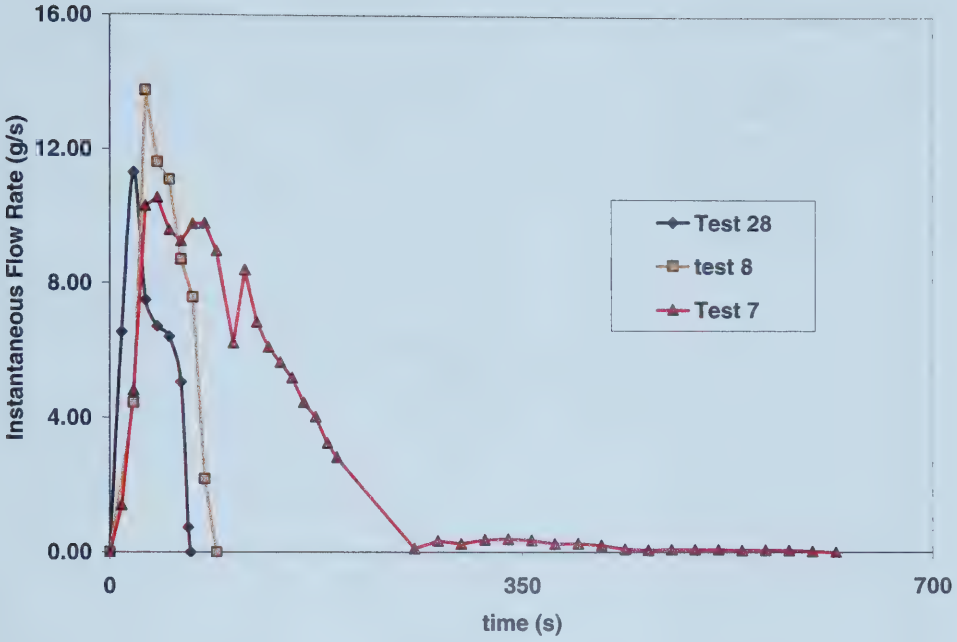

Figure 5.19: Sand Production rate versus time. Tests: 7, 8 and 28. Air flow rate: 9.53 l/min @ 20 psi (137.90 kPa). Sil-1 Sand. Slot size: 0.028 in (0.711 mm).

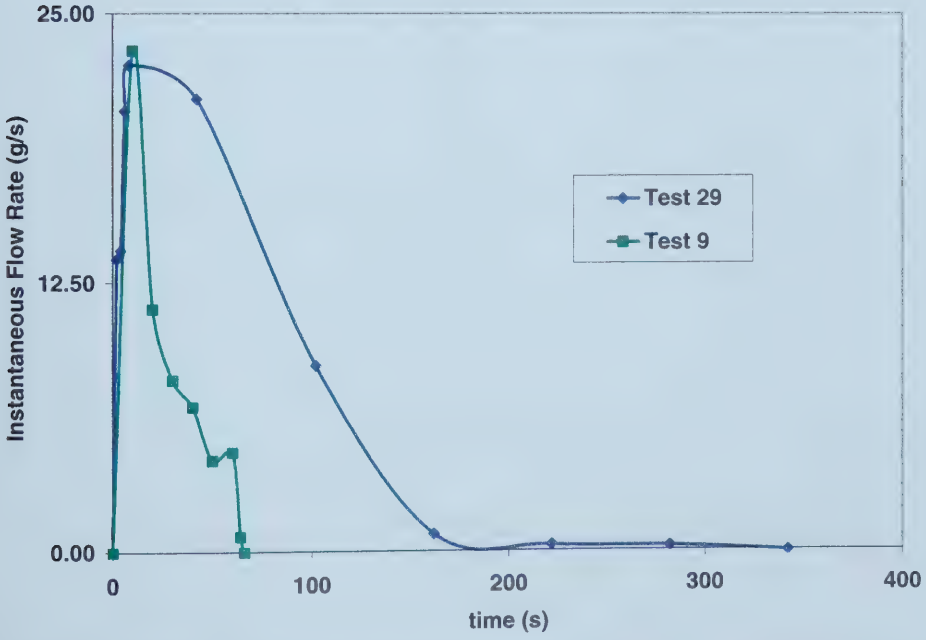

Figure 5.20: Sand Production rate versus time. Tests: 9 and 29. Air flow rate: 13.68 l/min @ 40 psi (275.79 kPa) Sil-1 Sand. Slot size: 0.028 in (0.711 mm).

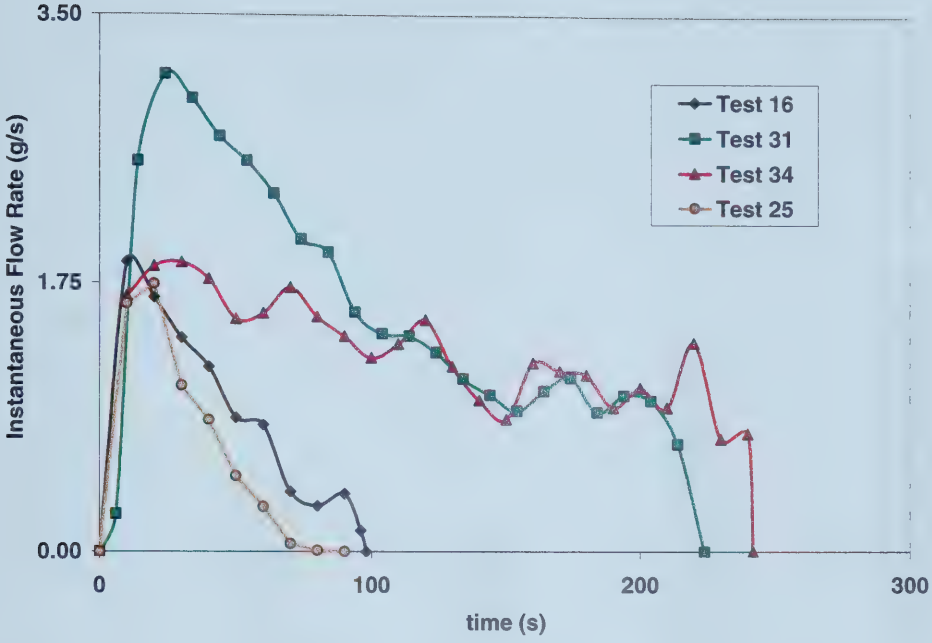

Figure 5.21: Sand Production rate versus time. Tests: 16, 25, 31 and 34. Gravity flow. Husky Sand. Slot size: 0.028 in (0.711 mm).

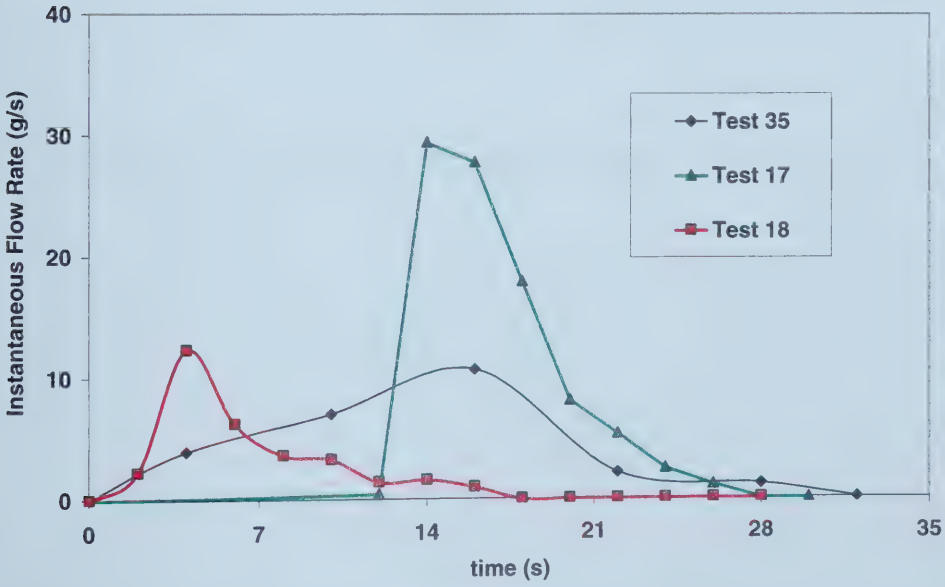

Figure 5.22: Sand Production rate versus time. Tests: 17, 18 and 35. Air flow rate: 9.53 l/min @ 20 psi (137.90 kPa). Husky Sand. Slot size: 0.028 in (0.711 mm).

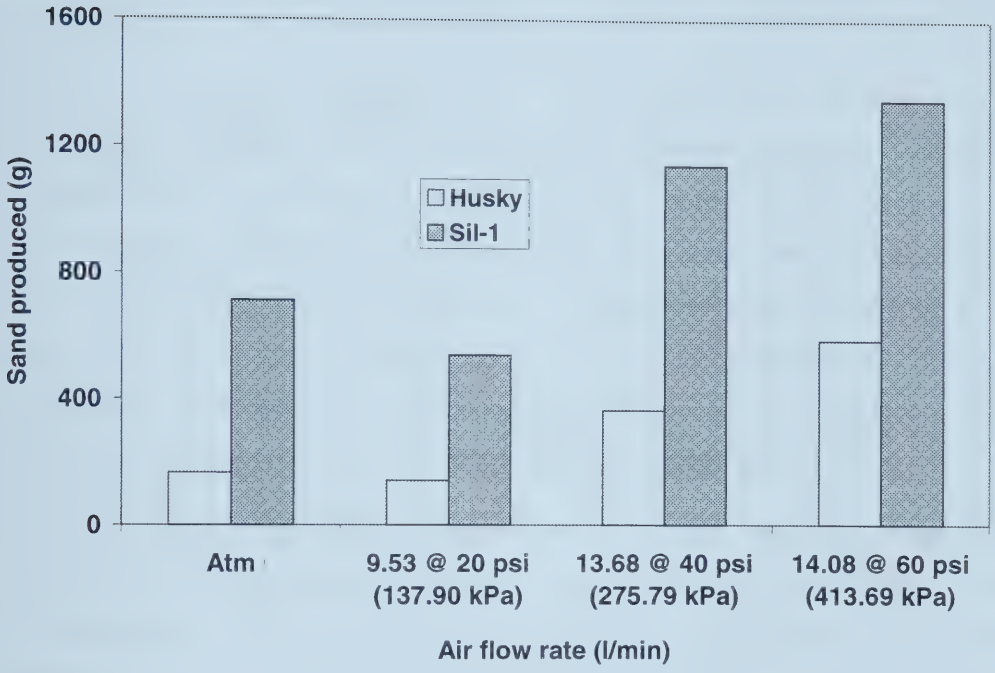

Figure 5.23: Average sand produced versus time at different air flow rates. Slot size: 0.028 in (0.711 mm).

5.2 Liquid Experiments

Nine sand production experiments were performed with a high viscosity silicone oil to analyze the effect of slot size, fluid flow rate, sand morphology, pressure gradient and size distribution on sand production behaviour.

In order to evaluate the influence of slot size on sand production five runs were performed with three slot sizes: 0.022 in (0.56 mm), 0.028 (0.71 mm) and 0.040 in (1.02 mm). Runs 2 to 4 were carried out with Sil-1 sand, while Runs 6 and 7 were performed with Husky sand. The effect of sand morphology was investigated by comparing the production of Husky sand (run 6) to the production of glass beads (run 8) with approximately the same size distribution. The effect of the size distribution was investigated by comparing the production of the previous glass beads (run 8) to the production of glass beads with the same distribution except for a lower fines content (Run 9).

Run 5 was carried out using Sil-1 sand and a 0.028 in (0.71 mm) slot, as was Run 3, however a different test procedure was used. A portion of Run 5 was performed to check the reproducibility of Run 3 at the lowest flow rate. The procedure and experimental apparatus were tested in Run 1. No data was collected for this run.

In each experiment, the flow rate was varied in steps from 50 cm^3/h to 100 cm^3/h and to 150 cm^3/h. The experimental procedure employed in these runs was described in detail in Section 4.2.2. Production of sand and oil out of the slot was filmed on video. An analysis of the results obtained from the runs is presented in the following sections.

5.2.1 Data Analysis Procedure

5.2.1.1 Slot width to equivalent diameter ratio

The ratio of the slot width to sand grain diameter is an important parameter in controlling sand production through a slot. Since the sands used in the liquid tests are not uniform in size, different definitions of the equivalent diameter of the sand grains will be used. The

slot width to equivalent diameter ratio for different percentiles of these sands was calculated and tabulated in Table 5.13. The different diameters shown in the first column to the left of Table 5.13 correspond to the dimensions of the sieve mesh, which allows a certain percentile by weight of sand to pass through. It is important to note, in comparing the Sil-1 sand to other sands, that the ratio of the slot width to grain diameter is smaller for the Sil-1 sand for all diameters except at the $D_{99.9}$ diameter. The glass bead with less fines (GBLF) had a smaller slot width to grain diameter ratio at the D_{10} diameter compared to the Husky and the glass beads like Husky fines (GBLH).

5.2.1.2 Pressure Gradient Calculations

The pressure data obtained in each test was used to estimate the pressure gradients (*dp/dL*) along the cell and in the vicinity of the slot. The distances between the pressure ports are shown in Table 5.14, along with the designation of the pressure gradients. The pressure gradient $(dp/dL)_{6,slot}$ between port 6 and the entrance of the slot was also calculated.

The pressure at the entrance of the slot (p_{slot}) must be calculated in order to calculated $(dp/dL)_{6,slot}$. If the flow through the slot is assumed to be the same as the flow between two infinite parallel planes a distance W apart, then the Hagen-Poiseuille equation for the slot can be used to estimate p_{slot} as follows [57]:

(5.2) $$Q = \frac{2}{3}\frac{(p_{slot} - p_B)W^3 L_s}{\mu b}$$

where: p_B = pressure at the end of the slot, atmospheric pressure
W = width of the slot
L_s = length of the slot
b = depth of the slot = thickness of the plate
μ=viscosity of the slurry or oil flowing out of the slot
Q = the slurry or oil flow rate

All pressure measurements in this thesis are given in terms of the gauge pressure, therefore, p_B=0, and p_{slot} is obtained from Equation (5.2)

(5.3) $$p_{slot} = \frac{3}{2}\frac{bQ\mu}{W^3 L_s}$$

The pressure gradient $(dp/dL)_{6,slot}$ is calculated simply as the ratio of the pressure drop (p_6-p_{slot}) to the distance, $\Delta L_{6,slot}$, between pressure port 6 and the centre of the slot. The viscosity of the produced slurry varied since the sand cut also varied. Therefore the viscosity of the slurry should be calculated and used in Equation (5.3) when sand was produced. This approach is approximate since the sand and oil do not exactly flow as a continuum through the slot.

The viscosity of the sand-oil slurry can be calculated as follows:

(5.4) $$\mu_{Slurry} = \mu_r \mu_o$$

where μ_r is the relative viscosity of the slurry and μ_o is the oil viscosity.

The relative viscosity of Husky sand slurries was measured previously [58] at ARC and was fitted to the following equation:

(5.5) $$\mu_r = e^{\frac{5c_s}{2(1-1.48c_s)}}$$

where c_s is the sand concentration.

The Thomas equation [59] below is commonly used for the relative viscosity of uniform spherical sand slurries :

(5.6) $$\mu_r = 1 + 2.5c_s + 10.05c_s^2 + 0.00273e^{16.6c_s}$$

Equation (5.6) was used to calculate the relative viscosity of the glass beads slurry since the beads are approximately spherical in shape, although not uniform in size, as described in section 4.1. The relative viscosity of a Unimin (Ottawa) sand was measured at the

Saskatchewan Research Council (SRC). This type of sand is sub-rounded but not spherical. The measurements were fitted with the following equation [58]:

$$\mu_r = 1 + 2.5c_s + 10c_s^2 + 0.0019e^{20c_s} \tag{5.7}$$

This equation was used to calculate the relative viscosity of the Sil-1 sand, which is also sub-rounded with low sphericity.

5.2.1.3 Determination of the variations in the properties of the sand pack

Sand production is usually associated with improvement in primary recovery in Alberta and Saskatchewan heavy oil reservoirs [7-9]. One postulated mechanism for this field based observation is the creation of a zone of enhanced permeability and high porosity around the wellbore, which allows the viscous oil to flow more easily to the perforations. Another mechanism explaining the higher oil recoveries during cold production is the formation of high permeability channels (wormholes). In either case the overall effect of sand production is to increase the permeability of the formation. It was therefore important to determine the permeability enhancement within the pack during sand production

The calculated porosity and permeability of the sand pack were compared to the corresponding initial values. These two parameters were calculated in the cylindrical section of the pack (Ports 2 and 3) and around the slot (Ports 5 and 6).

Darcy's linear flow equation was used to estimate the sand pack permeability based on pressure measurements obtained at different points along the cylindrical section of the pack. For example, the permeability between pressure ports 2 and 3 was calculated using Equation (5.8):

$$k = -\frac{Q_o \mu}{A(dp/dL)_{3,2}} \tag{5.8}$$

It was assumed in this calculation that the area perpendicular to the flow was constant with time. Furthermore, the fluid viscosity was also constant.

Permeability was also calculated around the slot. The flow close to the slot was assumed to be radial. This assumption will be further discussed in the next section. The slot was assumed to act as a horizontal well just penetrating, along its axis, a semi-infinite porous medium. Therefore, the equation for radial flow into a well was modified as shown below since only half of the fluid entered into the slot.

(5.9) $$Q_o = \frac{\pi h k \Delta p_{5,6}}{\mu \ln(r_5 / r_6)}$$

Permeability around the slot was obtained as follows:

(5.10) $$k = \frac{Q_o \mu \ln(r_5 / r_6)}{\pi h \Delta p_{5,6}}$$

where: h is the length of the slot
r_6 the distance from port 6 to the centre of the slot and
r_5 the distance from port 5 to the centre of the slot

The porosity was then calculated using the Carman-Kozeny equation [60]:

(5.11) $$k = \frac{1}{c} \frac{\phi^3}{(1-\phi)^2}$$

which was rearranged to give,

(5.12) $$\phi^3 - ck\phi^2 + 2ck\phi - ck = 0$$

where c is the "Kozeny constant", which depends on the inverse square of the average particle diameter [60].

The constant c was calculated from the initial values for the permeability and porosity by applying equation 5.11. Values of c for each test, shown in Table 5.15, followed the expected tendency of decreasing values when the sand particle diameter was smaller.

Once the constant c was calculated, the porosity between either ports 2 and 3 or between ports 5 and 6, was calculated from equation (5.12) by substituting the permeability calculated in equations (5.8) or (5.10) respectively. The pressure gradient when only oil was produced at the end of the test, usually at the last flow rate evaluated was used in the calculations. Any variation in the range of + 1 % was considered within experimental error.

Table 5.12: Summary of the changes in permeability and porosity for the liquid runs.

Property	Run							
	2	3	4	5	6	7	8	9
Δk_p	0.31	4.40	62.85	-0.47	0.01	0.05	0.11	-0.04
Δk_s	8.94	26.82	35.14	20.50	6.85	3.98	5.31	4.75
$\Delta\phi_p$	0.08	1.00	11.43	-0.10	-0.08	0.02	0.06	-0.08
$\Delta\phi s$	2.04	4.98	7.80	3.26	8.92	5.60	5.85	3.72

p = property calculated in the pack
s = property calculated in the vicinity of the slot.

The changes in the sand pack porosity and permeability for all runs were much more significant in the vicinity of the slot, than away from it. Detailed discussion of these results is given in the following sections.

5.2.2 History of a Typical Liquid Test

5.2.2.1 Sil-1 Sand

Table 5.16 summarizes the results for Run 2 performed with Sil-1 sand using a 0.022 in (0.56 mm) slot. Figure 5.24-5.30 show sand production rate, cumulative sand production and sand concentration versus time, pressure versus time and pressure gradient versus time for each flow rate evaluated.

The run was started with the pack at atmospheric pressure. The plug was removed from the slot and the flow rate was increased to 50 cm^3/h. Sand started to be produced from one end of the slot approximately 5 minutes after oil injection began (Figure 5.31a). Sand

production then continued to the centre and finally reached the other end of the slot (Figure 5.31b). One minute after the start of sand production, sand was produced throughout the slot. Twenty minutes after the start of the Run sand production decreased gradually, starting from both corners of the slot. One hour later, only oil was produced from the slot. The flow rate was maintained for 26 hours. The arches/bridges around and within the slot appeared to be stable during the remainder of this period since no sand was produced. No further sand production was observed in the following second and third steps of the run when the flow rate was increased to 100 cm^3/h and 150 cm^3/h respectively. In both steps, the flow rate was maintained for approximately 24 hours.

- First step: flow rate of 50 cm^3/h

The sand production rate followed the trend observed before in the air tests, i.e., sand production rate reached quickly a maximum and then slowly declined (Figure 5.24). Since the oil injection rate was constant, the sand cut of the produced slurry also followed the same trend.

The pressure data at this flow rate is presented in Figure 5.25. The ports at which the pressure was measured are shown in Section 4.2.2, Figure 4.18. The pressure within the sand pack began to increase from atmospheric pressure when oil injection began. The pressures continued to build up even during the period of sand production, probably due to the limited flow of sand through the slot. The relative velocity between the oil and the sand is higher when the sand is not moving. Therefore, from Darcy's law, the pressure gradient will be higher than when the sand is moving. The constriction to sand flow then leads to higher pressures (Figure 5.25) and pressure gradients (Figure 5.26) throughout the sand pack. The pressures and pressure gradients seem to level off, when sand production stopped.

The magnitude of the pressure gradients in Figure 5.26 becomes higher as the slot is approached except for the pressure gradient $(dP/dL)_{6,7}$ which is measured along the length of the slot. Note that pressure gradients $(dp/dL)_{1,2}$ and $(dp/dL)_{2,3}$ are very similar since they are measured in the cylindrical part of the sand pack where linear flow predominates.

The pressure gradient $(dp/dL)_{3,4,}$, on the other hand, is measured within the conical section of the sand pack where converging flow predominates. This pressure gradient is therefore higher. As the slot is further approached the flux of oil increases which explains the higher pressure gradients $(dp/dL)_{5,6}$ and $(dp/dL)_{6,slot}$.

The magnitude of the pressure gradient $(dp/dL)_{6,7}$ was much smaller than at other locations within the sand pack. This result is evidence of little or no fluid flow along the horizontal plane next to and parallel to the slot. The lower pressure gradients (i.e., lower driving force) along that direction meant that little flow was occurring in the transverse direction, even in the region near the slot. There could be cases in the field where horizontal permeability could be much larger that the vertical permeability. As such, flow in the horizontal plane parallel to the slot could be significant. In such a case, the pressure gradient in the transverse direction might behave slightly differently from what was observed in the experiments. The irregular shape of the $(dp/dL)_{6,7}$ pressure gradient in Figure 5.26 is indicative of uneven sand production along and within the slot.

The termination of sand production resulted in the stabilization of the sand pack, i.e., stopping the redistribution of the sand grains in the sand pack as indicated by the stable pressures and hence pressure gradients.

- Second and third flow rates: 100 cm3/h and 150 cm^3/h

The pressure and pressure gradient versus time for these flow rates can be seen in Figure 5.27 to 5.30. The pressure behaviour was the same in both cases; p increased due to the flow rate changes, as more oil was injected. After some time (i.e. the time needed to reach a steady flow rate and to compress the fluid up to the new pressure condition), the pressure reached a value that remained constant during the step. Consequently, the same tendency was observed for the pressure gradients (Figure 5.28 and 5.30).

The fact that no sand was produced during these stages implies that the sand arches/bridges formed over the slot were stable enough to resist changes in the flow rate

up to three times the initial flow rate. The stability of arches/bridges will be discussed in a further section.

The permeability and porosity of the pack were calculated for the third stage (flow rate of 150 cm^3/h). The results are presented in Table 5.16. No difference, within experimental error, was found in the permeability of the pack; which was not surprising since only approximately 16 g of sand (0.07 %) was produced.

Greater changes in ϕ and k were estimated around the slot. This tendency was observed in all tests performed. The change in the permeability near the slot for this test was approximately 24 % (see Table 5.16) while the porosity change was found to be approximately 5 %. Once sand production stopped there likely was a redistribution of the sand grains in the vicinity of the slot.

The permeability increase estimates around the slot are supported by thin sections observations in the vicinity of the slot. In these sections, sand free regions at the inlet to the slot could be detected (see Section 5.3).

5.2.2.2 Husky Sand

Table 5.17 summarizes the results of Run 7 performed with Husky sand and a 0.040 in (1.02 mm) slot. Figure 5.33 to 5.41 show sand production rate, cumulative sand production and sand concentration versus time, pressure versus time and pressure gradient versus time for each flow rate evaluated.

The run was started with the pack at atmospheric pressure. The plug was removed from the slot and the flow rate was set at 50 cm^3/h. Sand started to be produced approximately 3 minutes after oil injection began. The sand was initially produced at the corners of the slot (Figure 5.32) with sand production continuing to the centre. After another 2 minutes, sand was produced throughout the entire slot. The details of the sand production for the entire test are given in Table 5.18

Intermittent sand production was observed in the experiment (see Table 5.18) with no external disturbance applied to the system. Arches/bridges appear to form and break randomly. Interestingly, some grains could be seen inside the slot by the time the slot was producing only oil. Some of these grains were stationary while others moved slowly through. Some bridging of sand grains could be observed in thin sections

The flow rate was maintained for 24 hours and then increased to 100 cm^3/h. The sand arches/bridges were very sensitive to external disturbances (the refilling of the pumps and the oil cylinder). During the refilling the flow rate might be momentarily stopped. Surprisingly, sand started to be produced. This observation may be tentatively explained by a dynamic bridging of sand grains within the slot.

Figure 5.42 illustrates the bridging of two sand grains within a slot, which was observed in a thin section of sands within a slot (Figure 5.76). The arrows in the schematic illustrate the forces exerted on the grain to the right. Since the oil velocity in the slot is highest at the centre of the slot, a net torque will be exerted in the counter clockwise direction on the grain to the right. The right sand grain will be pressed against the left sand grain. The friction force between the sand grains and the walls required to slide the grains along the wall is equal to the friction coefficient times the normal stress. If the angle θ is small enough, the friction force required to slide the grain will be larger than the sum of the weight of the sand grain and the drag force exerted on the grain. The sand grain will not move. If the flow rate is suddenly stopped the normal force between the sand grains will be zero. The sand grains will simply fall by gravity.

In stage 3 of the experiment (Figure 5.39 to 5.41), the fluid flow rate was increased to 150 cm^3/h. The sand arches/bridges were likely unstable: sand production occurred within a very short time after the flow rate was changed as shown in Table 5.18. As was seen in Figure 5.33 to 5.38 for the first two stages (flow rate of 50 cm^3/h and 100 cm^3/h, respectively), sand production was periodic, i.e. a period of sand production was followed by a period without sand production. Moreover, the amount of sand produced from the vessel decreased in subsequent sand production periods. As noted in Table 5.18 the periodic sand production at 100 cm^3/h injection rate was externally induced when the

flow rates was stopped. This behavior is probably no different from field observations of sand production occurring after changes are made to operational procedure and/or equipment.

The sequence of sand production followed by a period of no sand production in Run 7 seems to indicate the existence of a dynamic process of re-arrangement of the granular materials in the reservoir. As fluid flows through the unconsolidated porous medium, it transports some of the sand grains constituting the porous medium. The amount of solid materials transported by the fluid is dependent on many factors, including the pressure gradient and fluid properties (such as viscosity, density), properties of the solid materials (including size, size distribution, angularity, density), the cohesion of the granular materials, as well as the interaction between the fluid and the solid materials (including the effects of boundary conditions). Generally, it is reasonable to expect that for a given fluid flow rate more solid production from a poorly consolidated or unconsolidated reservoir than from a reservoir made up of cemented sand grains. During sand production through an opening, some of the sand grains could (first) stop and (then) lodge at the opening, with the net effect of reducing the effective size of the opening. Over time, more sand grains stop due to the ever-decreasing size of the opening; they begin to bridge with one another, first across and then around the opening, to form a "temporary" structure (bridge or arch). The stability of such structures is strongly influenced by its cohesive strength, the nature and arrangement of the sand grains, especially how the different grains of different sizes interlock with one another, the stress distribution around the slot, and the pressure gradient across it. During this period, little or no sand production is commonly observed, as the sand grains are stopped by the structure. It is possible that with time such structures could reach a "critical" scale whereby the pressure differential across it become too great, causing the structure to break. A sudden, large slug of sand production is commonly associated with the collapse of the structure. It is then followed by a continuous stream of sand production, albeit at a much lower sand rate (i.e. lower sand cut), until sand grains again begin to accumulate around the opening and reduce its size. The cycle described above could then repeat itself. It is possible that the sand structure (for example, arch) could remain stable for a long time, due to its cohesive

strength to bridging stress between sand grains and/or depleted pressure state in the reservoir (thus lowering the pressure differentials across the structure). In such a case, fluid production could be significantly reduced.

- First stage of Run 7, flow rate of 50 cm^3/h

The produced sand cut in Figure 5.33 follows a "pulsating" profile corresponding to the dynamic sequence of formation and destruction of sand arches, in the vicinity of the slot (as described above). The sand cut (concentration) also decreased in later pulses (approximately 52 % in the first pulse, 34 % in the second pulse, and 6 % in the last pulse. Also, the duration of the pulse became shorter in later pulses (roughly 2 hours for the first pulse, and 1 h for the third and final pulse). It is believed that as more and more sand was produced from the vessel the stability of the sand arch/bridges became more stable. As observed in thin sections of the sand distribution around the slot section, larger sand grains appear to plug either the slot entrance or the slot itself. Since the sand investigated contains relatively few large grains, the time for larger sand grains to block the slot depends on the size distribution. The formation of the bridge requires certain arrangements between sand grains to occur. Therefore a certain time is required before these combinations of particles occur. The profile for instantaneous sand flow rate followed closely that of the sand cut. As expected, the cumulative sand production profile had a "step" profile, with each of the steps corresponding with each of the pulses. This profile reached a plateau and stayed level thereafter, when sand production stopped. In total, 460 g (or 1.9 % of the reservoir solid mass) of sand were produced during this stage (Stage 1) of Run 7.

Figure 5.34 and 5.35 show the pressure profiles, as measured at different locations inside the sand pack, and the pressure gradients between these locations, respectively. The pressure profiles tracked one another closely. As expected, the pressure became progressively smaller (i.e., closer to atmospheric pressure) as the slot was approached. Generally, pressures inside the cell started to build up immediately after oil injection. This pressure buildup period was rather brief, however, and pressures began to fall (throughout the reservoir) when oil and sand started to be produced. The relatively steep

pressure increase occurring at approximately 6-7 hours of elapsed time was probably due to the beginning of the formation of sand arches/bridges around the slot. This arch-formation process was transient (in nature) in the early period, as seen quite clearly by fluctuations in both the sand cut and instantaneous sand flow rate graphs (Figure 5.33). This transient period was quite short (lasting approximately 1-2 hours), and then followed by a (pseudo) steady-state behaviour period during which the pressures were constant, and both the produced sand cut and instantaneous sand flow rate (mostly) declined. The pressures increased sharply when sand production stopped (after 7.34 hours, approximately, had elapsed). The same observation held true for the second pulse of sand production. The pressures built up quickly following the end of the third (final) pulse, as expected since only a small amount of sand was produced during this pulse.

Pressure gradients were also plotted versus time, as shown in Figure 5.35. This profile agrees quite closely with the pressure profiles (Figure 5.34). As in the case of the Sil-1 sand, the magnitude of the pressure gradients are seen to become higher near the slot and smaller at positions further away from the slot. In general, the pressure gradients increased from the top to the bottom of the sand pack as observed previously.

The pressure decline behaviour with time can be explained by referring to the analytical model of Geilikman et al.[61] or the flow of oil and sand into a vertical well as described in the book by Charlez [4]. In this model, as sand is produced massively with the oil a remolded zone of higher porosity, ϕ_y, is created. The difference in velocity between the oil, v_o, and the sand, v_s is given from Darcy's law by:

$$v_o - v_s = -\frac{k_y}{\mu_o}\frac{\partial p}{\partial r} \tag{5.13}$$

Therefore the pressure gradient in the yielded zone will be given by:

$$\frac{\partial p}{\partial r} = -\mu_o \frac{(v_o - v_s)}{k_y} \tag{5.14}$$

where k_y is the permeability of the yielded region. The pressure gradient decreases with time due to the decrease in the relative velocity between the oil and the sand and to an increase in the permeability of the dilated region. The velocities v_o, and v_s, are related to the oil and sand flow rates Q_o and Q_s respectively by [61]:

(5.15) $$Q_o = 2\pi r L_s \phi_y v_o$$

(5.16) $$Q_s = 2\pi r L_s (1-\phi_y) v_s$$

where ϕ_y is the porosity of the yielded region and Ls is the length of the slot.

At the very start of the experiment considerable changes in the porosity can occur. If the porosity within the sand pack stabilizes then the sand flow rate in the yielded region will be the same as the sand flow rate produced out of the slot. Therefore:

(5.17) $$Q_o = \phi_{slurry} Q_i$$

(5.18) $$Q_s = (1-\phi_{slurry}) Q_i$$

where: ϕ_{slurry} = porosity of produced slurry
Q_i = injection flow rate

The pressure gradient can then be written as:

(5.19) $$\frac{\partial p}{\partial r} = \frac{\mu_o}{k_y}\left[\frac{\phi_{Slurry} Q_i}{2\pi r L_s \phi_y} - \frac{(1-\phi_{Slurry}) Q_i}{2\pi r L_s (1-\phi_y)}\right]$$

Rearranging Equation (5.19) leads to:

(5.20) $$\frac{dp}{dr} = -\frac{\mu_o}{k_y}\frac{Q_i}{2\pi r L_s}\left[\frac{\phi_{slurry} - \phi_y}{\phi_y (1-\phi_y)}\right]$$

This equation shows that the pressure gradient decreases when the difference ϕ_{slurry}-ϕ_y decreases and/or when the porosity ϕ_y and permeability k_y increases.

When the porosity of the produced slurry is the same as that of the yielded sand, the oil and sand will flow as a slurry. In this case the flow of the slurry into the slit can be solved using the Hamel flow equation [62].

Since the value of the pressure gradient $(dp/dL)_{6,7}$, along the length of the slot, is considerably smaller than the pressure gradient $(dp/dL)_{5,6}$, perpendicular to the slot, the flow along the length of the slot is likely significantly smaller than the flow perpendicular to the slot.

- Second and third stages: 100 cm^3/h and 150 cm^3/h

Sand concentration, flow rate and cumulative sand production versus time are shown in Figure 5.36 and 5.39 for both 100 cm^3/h and 150 cm^3/h flow rates. When bursts of sand were observed at the outlet of the slot, isolated peaks of sand concentration and sand flow rate were observed at both flow rates (Figure 5.36 and 5.39).

The pressure and pressure gradient versus time for the second and third stages can be seen in Figure 5.37-5.38 and Figure 5.40 –5.41 respectively. It is important to note that the pressures reached at 150 cm^3/h are out of range for part of the test, which explains the lack of data points in the graphs. The transducers were changed in the last part of the test.

The pressure behaviour was similar to that observed at the first flow rate; p increased when the flow rate was increased, and decreased as soon as sand was produced to increase again to a plateau value once sand production stopped. This cycle was repeated each time sand production occurred either when the flow rate was stopped or because the flow rate was increased. The same tendency was observed for the pressure gradients (Figure 5.38 and 5.41).

The permeability and porosity at different points of the pack (in the straight section of the vessel –ports 2 and 3- and near the slot –ports 5 and 6-) were calculated in the third step at a flow rate of 150 cm^3/h, when no sand was produced. The results are presented in Table 5.17. No difference was calculated (within the experimental error) in the permeability and porosity of the pack. The permeability (k_s) and porosity (ϕ_s) in the

vicinity of the slot increased significantly, 80 and 14 % respectively, with respect to the initial values.

This suggests that sand production caused a redistribution of the sand grains in the vicinity of the slot leading to an increase in porosity and permeability. However the sand production was not enough to modify the permeability and porosity far away from the opening.

5.2.2.3 Glass Beads

Table 5.19 summarizes the results for Run 9 performed using glass beads with a size distribution similar to that of the Husky sand and a 0.028 in (0.71 mm) wide slot. Figure 5.44 to 5.50 show sand production rate, cumulative sand production and sand concentration versus time, pressure versus time and pressure gradient versus time for each flow rate evaluated (50 cm^3/h, 100 cm^3/h and 150 cm^3/h).

The run was started with the pack at atmospheric pressure. The plug was removed from the slot and the pump was started at 50 cm^3/h. Sand started to be produced approximately 5 minutes after oil injection began. The sand was initially produced at one corner of the slot (Figure 5.43), seconds after sand production was observed in an isolated spot in the centre of the slot. After 5 minutes, sand was produced throughout the slot. The details of the sand production behaviour in run 9 are shown in Table 5.20,

The sand was mainly produced (96 %) at 50 cm^3/h. Sporadic bursts of sand production were observed in isolated parts of the slot after the main sand production period. After the first five hours of the test no more sand was produced during the reminder of the first step which lasted 45 hours.

Oil flow rate was successively increased from 50 cm^3/h to 100 cm^3/h and to 150 cm^3/h in order to investigate the influence of flow rate (pressure gradient) on sand production, Small quantities of sand were produced (0.9 g) and for a very short time (2 min) when the flow rate was changed to 100 cm^3/h. This occurred shortly after the flow rate was

changed (see Table 5.20). From this time on no more sand production was observed even when the flow rate was increased to 150 cm^3/h.

As explained previously the rearrangement of sand grains around and in the slot reached a stable arches/bridges structure.

- First stage: flow rate @ 50 cm^3/h

The sand concentration in the slurry at the beginning of the sand production period reached an average maximum of approximately 55 % (Figure 5.44). The sand concentration remained approximately constant for approximately two hours until it declined sharply.

The sand flow rate showed the same trend as the sand concentration, i.e. a sharp increase at the beginning of the test, a stabilization period during the sand production and rapidly decreasing sand production. The cumulative sand production versus time plot showed the different stages in the sand production process.

The pressure profiles (Figure 5.45) reflected the sand production changes occurring during the test. At the beginning, pressure built up suddenly as the oil was compressed. When sand started to be produced the slope of pressure build up curve decreased due to the decrease in the relative velocity between the oil and the sand and to the increase in permeability around the slot. More details regarding the pressure decline curves was given in section 5.2.2.2. When sand production decreased and finally stopped, a sharp increase in the pressure was observed and the pressures seemed to level off.

Pressure gradients were also plotted versus time, as shown in Figure 5.46. In this case the time scale was cut in the "steady state" phase, when the pressure was constant and no changes were observed, in order to better appreciate the changes occurring at the beginning of the test. This profile agrees with the description given previously related to the changes that the sand production generates in the pressure response. The pressure gradient increased as the slot was approached as observed with the other two sands.

- Second and third steps: 100 and 150 cm^3/h

A small quantity of sand was produced (1.47 g) for a short time (2 min) shortly after the flow rate was increased to 100 cm^3/h. The production of sand coincided with the spikes in the pressure and pressure gradient curves in Figure 5.47 and 5.48. The pressure/pressure gradient behaviour was fairly constant for the remainder of the test, except for a slight disturbance when the pumps/cylinders were refilled. At the last flow rate, i.e. 150 cm^3/h, a similar behaviour was observed; pressure values increased sharply at the beginning and then stabilized rapidly. However, a steady state was not reached due to operational problems (accumulator leakage).

Table 5.19 presents the variation in percentage of the pack properties. Again, the permeability and porosity seemed to increase in the vicinity of the slot but not inside the pack.

5.2.3 Effect of the Slot Size

The influence of slot size on sand production was investigated. Three slot sizes were used: 0.022 in (0.56 mm), 0.028 in (0.71 mm) and 0.048 in (1.02 mm). These dimensions are within the range of the slot widths for horizontal well liners [63].

5.2.3.1 Sil-1 Sand

The effect of the slot width on sand production is observed in Table 5.21 where the total sand production for each stage is presented. Both the estimated weight of sand produced, based on the method described in section 4.2.2.3.2, and the actual weight obtained by extraction are presented.

As mentioned previously, the method used to calculate the produced sand based on a material balance was more accurate when more sand was produced. One factor contributing to this discrepancy is that the flow rate exiting the slot is not constant at the beginning of the test due to the compressibility of the oil inside the vessel. Although

sand is produced, the quantity during the first minutes cannot be calculated. However, the accuracy is considered good enough and allows a measurement of the history of the sand production, sand cut and sand flow rate in most cases (Figure 5.33 for example).

It is important to note that for a given test, the flow rate was changed, either when sand production stopped or after 48 h. This means that in certain cases (Run 3 and 4) sand production did not stop before the flow rate was changed.

More Sil-1 sand was produced with increasing slot width (Table 5.21) for a given flow rate. More time is needed for sand production to stop when slot size increases. It is important to note that the sand cut declined more quickly in the case of the 0.022 in (0.56 mm) and 0.028 in (0.71 mm) slots than in the case of the 0.040 in (1.02 mm) slot at the flow rate of 50 cm^3/h as shown in Figure 5.51. Furthermore, when the oil flow rate was increased to 100 cm^3/h, sand production eventually stopped in the run performed with the 0.028 in (0.71 mm) slot. The sand cut decreased very slow for Run 4 performed with the 0.040 in (1.02 mm) slot (Figure 5.52). Surprisingly, the sand cut declined to zero for the 0.040in (1.02 mm) slot when the flow rate was 150 cm^3/h almost at the end of the run time (Figure 5.53).

The total sand production through the 0.04 in (1.02 mm) slot was 49.53 % of the sand in the pack. Therefore, there was enough sand in the pack for production to continue if the slot had not been blocked with sand.

No production of the Sil-1 sand was observed in the run with the 0.022 in (0.56 mm) slot size when the flow rate was changed from 50 cm^3/h to 100 cm^3/h and then to 150 cm^3/h. This indicates that the arches/bridges formed were stable to an increase in flow rate. Sand was not produced also for the 0.028 in (0.71 mm) wide slot when the flow rate was increase from 100 to 150 cm^3/h.

The sand cut has the tendency to be higher at the start of the first step at 50 cm^3/h and then to decline with time until no more sand was produced. The initial sand cut was approximately the same (52 %) for both slot sizes 0.028 (0.71mm) and 0.040 in (1.02 mm). In the case of the 0.028 in (0.71mm) slot, the sand cut started to decline almost

immediately. In the case of the 0.040 in (1.02 mm) slot the sand cut declined more slowly until flow rate was changed to 150 cm^3/h.

The trends observed in the sand cut may be due to constrictions to sand flow at the slot Moreover, it is highly possible that only sand arching, as seen in thin sections, is the mechanism acting to stop sand production when the 0.040 in (1.02 mm) slot was used. Bridging at the inlet and within the slot would occur at the smaller slot widths. More time might be needed to form arches when a bigger slot size is used since arches require more sand grains to form whereas bridges can form only with one or two grains as shown in the thin sections. The same arguments explain why the sand production stops quicker when the 0.022 in (0.56 mm) slot size was used.

The pressure gradients between ports 2 and 3, located in the middle of the cell, were plotted as a function of time for each slot size and each flow rate evaluated (Figure 5.54). Similar treatment was applied to the data collected from ports 5 and 6, located in the vicinity of the slot (Figure 5.55).

The pressure gradient between ports 2 and 3 are considerably smaller than between ports 5 and 6 for any of the slot sizes at any flow rate (Figure 5.54-5.55). This difference comes from the different flow regimes that prevail in the different sections of the model. Linear flow occurs between ports 2 and 3 while converging flow is likely where ports 5 and 6 close to the slot. As the slot is approached the flux of oil increases which explains the higher pressure gradients $(dp/dL)_{5,6}$.

The pressure gradients were lower in magnitude when slot size was larger when sand was produced. Higher slot sizes implied less restriction to the flow of sand. The difference between pressure gradients measured at the same ports, at a given flow rate, decreased when sand production stopped since the relative velocity between the oil and the sand was closer for the different slots. The pressure gradients seemed to level off when sand production stopped.

Note that the pressure gradient dropped (Figure 5.54-5.55) towards the end of run 4 @150 cm^3/h due to an interruption in the flow rate. This event encouraged sand production as

shown by the increase in the sand cut between 135-140 hours (Figure 5.56). Shortly after, sand production stopped, and consequently the pressure gradient increased and reached similar values as observed in Run 3 for the 0.028 in (0.71 mm) slot size. This phenomenon will be discussed in more detail in a latter section jointly with the Husky results.

The permeability and porosity were calculated using the pressure data recorded from the experiments. Equation (5.10) and (5.11) were used for that purpose. The permeability and porosity estimated at initial conditions and after sand production are presented in Table 5.22. The results indicate that when sand is produced changes in porosity and permeability in the vicinity of the slot occur. The magnitude of these changes increases with the quantity of sand produced. The properties in the cylindrical part of the cell for example, were also affected by sand production. However, the magnitude of the changes is less than in the vicinity of the slot.

Properties of the sand pack between ports 2 and 3 for run 4 after sand production were estimated. However, they are not reported since the values obtained (more than 200 %) might be affected by the large volume (50 %) of sand produced from the vessel. It is believed that port # 2 was above the sand level since the pressure values for port 1 and 2 were practically the same.

The enhancement in the properties of the pack (permeability and porosity) far away from the slot is an encouraging result from the oil recovery point of view. However, it seems that this effect might be temporary, as it will be shown in the next sections.

As described in section 5.1.2.2, the pressure gradient in the region around the slot is proportional to the difference, ϕ_{slurry}-ϕ_y, between the porosity of the slurry produced out of the slot and the porosity of the yielded zone around the slot. The porosity difference, ϕ_{slurry}-ϕ_y, was smallest for the flow through the 0.040 in (1.02 mm) slot since more sand is produced which explains why the corresponding pressure gradient was the lowest in Figure 5.55. The pressure gradient around the 0.028 in (0.71 mm) slot at 50 cm^3/h and

around the 0.040 in (1.02 mm) at 150 cm^3/h increased gradually as the porosity difference, $\phi_{slurry}-\phi_y$, also increased.

5.2.3.2 Husky Sand

In order to investigate the effect of the slot width on the production of the Husky sand, two slot sizes were used: 0.028 in and 0.040 in (0.71 and 1.02 mm respectively). Run 6 was performed at two different flow rates: 50 cm^3/h and 100 cm^3/h. Run 7 was performed at 50 cm^3/h, 100 cm^3/h and 150 cm^3/h.

The sand production results for the two runs are shown in Table 5.21. Negligible sand was produced from the 0.028 in (0.71 mm) slot (Run 6) compared to the production from the 0.040 in (1.02 mm) slot (Run 7).

In Run 6, the sand was produced during the first 30 minutes. After this time, no more sand production was observed, either when the oil flow rate was changed or when the system was disturbed by changes in the pumping rate. Stable arches/bridges likely formed and stopped sand production.

Since the production occurred for a short time at the beginning of Run 6, when the flow rate was not stabilized, the history of the sand production could not be estimated through material balance calculations.

The behavior of the Husky sand using the 0.040 in (1.02 mm) slot was explained in detail in section 5.1.2.2. It is important to emphasize that the mechanisms acting to prevent sand production are less stable than for the 0.028 in (0.71 mm) slot. This lower stability is likely due to the higher slot width to equivalent diameter ratio at any of the percentiles measured with the 0.040 in (1.02 mm) slot (Table 5.13). This implies that the formation of arch(es) is the predominant mechanism preventing sand production for the latter slot size since bridges are normally more stable.

The lack of stability of the arches is likely due to the wider structures needed to block the slot. Charlez [4] cited Yim et al's work in which the authors note that the arch stability is strongly dependent on the granulometry of the porous material and the size of the perforation (slot in this thesis). For larger perforations, larger sand grains are needed to form a stable arches. These results agree with the results presented in this thesis since sand production increased with increasing slot size. One issue, however, concerns the definition of the grain size for typical sands. As mention previously, on average, Sil-1 sand had larger particles (90 % of the grains have diameters between 0.18 - 0.25 mm) than the Husky sand (84 % of the Husky grains have diameters between 0.09 - 0.18 mm). However, Sil-1 sand was produced in larger quantities. This apparent discrepancy was explained at first by the difference in the morphology of the sands.

The influence of angularity and roundness (morphology) of the different sands on sand production was investigated by comparing the production of Husky sand, which is angular, to the production of spherical-well rounded particles (glass beads) for the same slot width, flow rate and particle size distribution. The production results detailed in a latter section showed that the angularity of the sand did not have a significant effect on sand production, considering the random nature of the phenomenon shown in the reproducibility tests for the air Runs.

For both the Sil-1 sand and the Husky sand more sand was produced when the slot size was larger, as expected, and more sand was produced in the air Runs than in the oil Runs. This difference in sand production with different fluids was noticeable for the Husky sand (35 % for the air test by gravity flow vs 4% at different oil flow rates with the 0.040 in plate). Although the drag force is higher in the case of the liquid experiments significantly less sand was produced than in the case of the air tests. A possible explanation could be found in the difference in viscosity for the two fluids. The flow of the sand grains in the air tests is much more rapid. Therefore any potentially stable arrangement of sand grains can be disrupted more easily when air is used than when oil is used.

The pressure gradients between ports 2,3 and 5,6 are shown for both slot sizes in Figure 5.57 and 5.58. The pressure gradients tended to be similar in magnitude for both slot sizes when sand was not produced. This is particularly true for $(dp/dL)_{5,6}$. The sudden pressure and pressure gradient declines and subsequent buildups corresponded to sand production episodes. Moreover, it seems that the pressure gradient between ports 5 and 6 had the tendency to be slightly higher with the 0.040 in (1.02 mm) slot at 50 cm^3/h and 100 cm^3/h. It appears that pressure port 6 was far enough from the slot for the pressure gradient between ports 5 and 6 not to be affected by the flow at the entrance of the slot.

A similar situation was observed with the Sil-1 sand in the last stage (150 cm^3/h) (Figure 5.55). The pressure gradient 5,6 seemed to stabilize to the same value for both 0.028 in and 0.040 in (0.71 and 1.02 mm respectively) slots. The pressure gradient reached for the 0.022 in (0.56 mm) slot was approximately 40 % higher than for the other two slots. A possible explanation is that more fines migration occurred for the smaller slot sizes since the larger sand grains did not move. Eventually the fines blocked the pore throats of the larger sand grains, leading to higher pressure gradients. Fines production was seen for Husky sand when sand production stopped.

The values of porosity and permeability estimated at initial conditions and after sand production occurred are presented in Table 5.23 along with the results for the glass beads. The results indicate that when sand is produced, changes in porosity and permeability in the vicinity of the slot occur. However, these changes are not static and the conditions found for a given flow rate seem to decrease more when a higher flow rate is applied (Table 5.23) possibly due to a compaction of the sand due to the corresponding higher pressures gradients.

The changes estimated in the vicinity of the slot appear to be high in magnitude (up to 150 % increase in one case) The higher values may be due to the assumptions of isotropic initial permeability in the sand pack and pure radial flow around the slots. Both assumptions involve some errors. The second assumption is partly supported by a comparison of the pressure gradients along and perpendicular to the slot. The ratio of

these pressures gradients was plotted in Figure 5.59. This ratio indicates to what extend the flow is non radial. Ratio values of zero should be obtained from a purely radial flow. The values obtained in this work were close to zero but not equal to zero which indicated some deviation for purely radial flow. As mentioned previously and in a subsequent section on computed tomography imaging of sand production through slots, sand is often produced unevenly along the slot leading to further non radial flow.

The permeability and porosity away from the slot, k_p and ϕ_p respectively, were also calculated (Table 5.23). Some changes in k_p and ϕ_p were found when the properties were calculated @ 100 cm^3/h but practically no changes were estimated when the flow rate was 150 cm^3/h regardless of the quantity of sand produced. The same trend was observed in the permeability, k_s, and porosity, ϕ_s, calculated near the slot.

5.2.4 Effect of Morphology and Size Distribution

5.2.4.1 Shape

At first the larger amount of Sil-1 sand produced compared to Husky sand, for a given slot size was thought to be due to the greater angularity of the Husky sand. Therefore, a test with glass beads, having the same size distribution as the Husky sand (GBLH), was prepared to investigate the effect of roundness and angularity on sand production. Size distribution curves for both sands were shown in Section 4.1.2.1 and Figure 4.1.

As was described in the experimental section, the Husky sand can be classified as a poorly sorted, subangular sand with low sphericity while the glass bead sand is classified as a poorly sorted, well rounded sand with high sphericity.

Table 5.21summarized the production of glass beads sand (Run 8) and Husky sand (Run 6) through a 0.028 in (0.71 mm) slot. More glass beads than Husky sand (82 g vs 8 g) was produced. Given the random nature of these tests, shown previously in the air tests, this difference in sand production is not considered significant. It had been expected to obtain

a more definitive result in the production behavior of the glass beads, based on previous work reported in the literature [29,33]. Although their experiments were performed with different conditions (larger opening diameter, some overburden pressure and different fluids) than those used in this thesis, these investigators suggested that the absence of sand arching with the glass beads was due to the angularity of the sand. Hall and Harrisberg concluded that angular sands formed stable arches, while round grain sand failed to arch due to a lack of surface restraint. The results found in this experimental study do not support the above conclusions. Moreover, the thin section tests quite clearly indicate that glass beads are able to arch (see Figure 5.82, Section 4.3). It is possible that Hall and Harrisberg's conclusion could be valid when a larger slot width to equivalent diameter ratio is used.

Some glass bead sand was produced after the initial sand production period. At 50 cm^3/h, sand was produced for 4 min, after the initial sand production period and after a period of only oil production (3 ½ h). At 100 cm^3/h, sand was produced for 8 minutes the first time and for 3 minutes the second time. Since the production periods were short and the quantity of sand produced was small (see Table 5.21), it is considered that the arches/bridges were stable.

Values of porosity and permeability were estimated after the tests and are presented in Table 5.23. The results indicate changes in k and ϕ in the vicinity of the slot. Although more glass bead sand was produced, the variation in the permeability and porosity in the vicinity of the slot was higher for the Husky sand. This can be explained by the morphology of the sand. When sand is sheared, the displacement in the direction perpendicular to the shearing plane, defines as dilation, is greater for an angular sand than for a round sand as observed in shear box tests using Husky sand and Glass Beads (GBLH). Therefore, the change in porosity and permeability of the Husky sand was greater. No noticeable changes in permeability and porosity were found inside the pack, away from the slot.

Pressure gradients, $(dp/dL)_{2,3}$ and $(dp/dL)_{5,6}$, were plotted versus time for both sands (Figure 5.60 and 5.61) for the flow rates evaluated. The $(dp/dL)_{2,3}$ gradient was greater for the Husky sand than for the glass beads reflecting the higher permeability of the glass bead pack. The contrary tendency was obtained for the $(dp/dL)_{5,6}$ gradient reflecting the lower permeability of the glass bead pack around the slot. The pressure gradients increase sharply after the flow rate was changed but stabilized after a short time.

5.2.4.2 Size distribution

Since the angularity effect experiment yielded similar results for both sands (Husky and glass beads), taking into account the randomness of the process, the difference in sand production behavior between the Sil-1 sand and Husky sands was thought to be due to differences in the different grain size distribution. The hypothesis was that either the fine particles or the largest particles were responsible for the difference in sand production between the Husky and Sil-1 sands. Another glass bead sand (GBLF) with the same size distribution as the glass bead like Husky sand (GBLH), except for a lower fines content, was prepared (see Table 4.4, chapter 4).

The production of the glass beads with lesser fines (GBLF) sand through a 0.028 in (0.71 mm) slot is presented in Table 5.21. Unexpectedly, more sand was produced with the GBLF than with the Husky and GBLH sands. A greater production of GBLF sand compared with Husky and GBLH sands would be expected if the fines were the key to explaining arching/bridging behaviour. The results indicated that the particles with greater average diameter have a stronger influence on the formation of the arches/bridges although they represent a small percentage of the total size distribution. The combination of different grain sizes could explain the lower sand production in the Husky sand case.

The sand production results with the GBLF sand were explained in detail in a previous section (5.2.2.3). As for the case of GBLH sand the arches/bridges formed were considered to be stable to flow rate changes, within the range of flow rates evaluated.

The initial permeability of the new sand (GBLF) was higher than for the Husky and GBLH sands. This can be explained by the lower fine particle content of the GBLF sand. The higher permeability of this sand explains the lower pressure gradients compared to the Husky or GBLH sands (Figure 5.60-5.61).

The permeability and porosity changes estimated after sand production are presented in Table 5.23. The most important changes seemed to occur in the vicinity of the slot. No significant changes occurred inside the pack far away from the slot.

As mentioned in section 5.2.2.3 a steady state was not reach in the last stage (flow rate = 150 cm^3/h) for the GBLF sand due to leak in the accumulator. Although a steady state was not reached the permeability and porosity were calculated with the available data (last hours of 150 cm^3/h step) to compare with the values obtained for the preceeding step (100 cm^3/h). Different values of permeability and porosity were calculated at different flow rates (100 and 150 cm^3/h) as in the Husky sand case (see Table 5.23 Runs 7 and 9). This behaviour seems to indicate that a subsequent rearrangement of the porous medium occurred with an increasing pore pressure.

The results found with glass beads sand, suggest that the morphology of the sand itself, taking into account the randomness of the process, did not have a significant effect on sand production. The presence of fines (finer than 170 mesh U.S. or 90 μm) in the size distribution of the sand did not affect sand production significantly. It is likely that the largest fractions of the sand (< 20 mesh U.S. or 500 μm) have an important role in the arches/bridges formation. The lower production of the Husky sand compared to the Sil-1 sand can be explained by the broader size distribution, particularly in the largest fractions, of the Husky sand which may increase the probability of forming sand arches/bridges.

5.2.5 Reproducibility Test: Sil-1 sand

Run 5 was performed with Sil-1 sand flowing through a 0.028 in (0.71 mm) slot. The difference between this run and Run 3 is in the duration of the flow rate steps. A comparative summary of these two runs is presented in Table 5.24.

Sand production, sand cut and pressure gradient data for Runs 3 and 5 for the first 48 h of stage 1 at 50 cm^3/h will be compared to estimate the reproducibility of the tests. It is important to point out that a higher permeability was observed for Run 5. The higher permeability is possibly due to a non uniform vibration applied to the model during the packing stage.

Figure 5.62 to 5.68 show the sand cut, pressure and pressure gradient data for the different stages of Run 5. Approximately 74 % of the total sand production was produced in the first stage. The sand cut behavior is similar to that observed with the other sands, i.e. high sand cut at the beginning of each stage decreasing with time until no more sand production is observed. The arches/bridges formed were metastable since changes in the flow rate due to the operative procedure encouraged sand production in parts of the slot that were previously sand free. Additional sand was produced at 100 cm^3/h but in smaller quantity and in a shorter time. The maximum sand cut was also lower (36 % in stage 1 versus 27 % in stage 2) as shown in Figure 5.62. An increase in flow rate to 150 cm^3/h, provoked additional sand production but in smaller quantity and for a shorter time (Table 5.24 and Figure 5.62).

The pressure profiles for the Sil-1 sand test are show in Figure 5.63, 5.65 and 5.67. In this run, the pressure was recorded every 5 minutes compared to every 20 minutes in previous runs. The shorter recording time allowed a finer resolution of the pressure fluctuations, which occurred when sand is intermittently produced. Any changes in the sand pack are captured in the pressure recordings. The pressure dropped when the sand started to be produced and increased when sand production decreased. The changes in sand production were also observed at the slot outlet. A dramatic drop in pressure was observed in Figure

5.65 when the flow rate stopped. A possible explanation was given in Section 5.1.1.2 for the corresponding sudden increase in sand production

The estimated permeability and porosity at 150 cm^3/h show (Table 5.24) that changes in the vicinity of the slot occurred while practically no changes were found in the sand pack far away from the slot

The corresponding pressure gradients shown in Figure 5.64, 5.66 and 5.68 follow closely the pressure profiles. Again, it seems that the flow parallel to the slot is very small as it is indicated by the small value of pressure gradient $(dp/dL)_{6,7}$ compared to the pressure gradient $(dp/dL)_{5,6}$ perpendicular to the slot length.

As shown in Section 5.2.2.2, the pressure gradient, in radial flow, is proportional to the difference between the produced porosity and the fluidized porosity around the slot. Therefore, any changes in the sand cuts in Figure 5.62 will be reflected in the pressure gradients in Figure 5.64, 5.66 and 5.68.

Figure 5.69 shows the sand cut versus time for Runs 3 and 5 over 48 h approximately. The sand cuts were similar during the first 25 h, but after 48 h, 25 % more sand was produced in Run 5 than in Run 3. The random nature of sand production tests was shown in the air tests. The difference in sand production for Runs 3 and 5 reflects this randomness.

Figure 5.70 compares the pressure gradients between Runs 3 and 5. In the first stage, sand was produced in considerable quantity. Pressures gradients started to increase for Run 3 once sand production stopped. Some of the differences in the pressure gradients $(dp/dL)_{5,6}$ was probably due to the difference in the permeabilities of the packs as indicated by the difference in pressure gradients $(dp/dL)_{2,3}$ measured away from the slot

The changes in the properties of the pack between Runs 3 and 5 (shown in Table 5.24) are difficult to compare since the duration of the tests was completely different (5 days for Run 3 versus 11 days for Run 5). It was shown in a previous section that a rearrangement

of the sand grains might occur inside the porous medium with time after sand production finished. This could cause a decrease in the magnitude of the permeability and porosity changes found previously in the vicinity of the slot or even yield zero changes in the properties of the pack far away from the slot (Table 5.23, Runs 7 and 9).

In summary, the similarity in the sand production, pressure gradient and Kozeny constant (Table 5.15) results between runs 3 and 5 for the first 48 hof the first stage (at 50 cm^3/h) indicates that the liquid tests are relatively reproducible.

5.2.6 Summary of the section

- More sand was produced with increasing slot width at a given flow rate. More time was required for sand production to stop and consequently arching/bridging to form for wider slots.
- The sand cut had a tendency to be higher at the beginning of the sand production period and to decline with time. In certain tests, the decline in sand cuts continued until no more sand was produced.
- Husky sand had a tendency to arch/bridge more easily than the Sil-1 sand as indicated by the higher sand production for the latter sand when both a 0.028 in (0.71 mm) slot and a 0.040 in (1.016 mm) slot were used.
- The porosity and permeability was calculated at the start of the experiment and after sand production stopped. The results indicate that, when sand is produced, changes in porosity and permeability in the vicinity of the slot occur. In general, no significant changes were found for the sand pack away from the slot, i.e in the cylindrical part of the cell.
- The morphology of the sand itself, taking in account the random nature of the sand production process, could not explain the sand production behaviour of the Husky sand.

- The presence of fines (finer than 170 mesh U.S. – 90 μm) in the size distribution did not influence significantly the production of sand.
- It is likely that the largest fractions of the sand (< 20 mesh U.S. - 500 μm) have an important role in the arches/bridges formation.

Table 5.13: Slot width to Equivalent diameter ratio for different percentiles of different sands

Percentile less than	Sil-1			Husky			Glass Beads like Husky			Glass Beads with less fines		
	0.022 in (0.56 mm)	0.028 in (0.711 mm)	0.040 in (1.016 mm)	0.022 in (0.56 mm)	0.028 in (0.711 mm)	0.040 in (1.016 mm)	0.022 in (0.56 mm)	0.028 in (0.711 mm)	0.040 in (1.016 mm)	0.022 in (0.56 mm)	0.028 in (0.711 mm)	0.040 in (1.016 mm)
$D_{99.9}$	1.12	1.42	2.03	0.66	0.84	1.20	0.79	1.00	1.40	0.79	1.00	1.43
D_{90}	1.65	2.09	2.99	2.80	3.56	5.08	2.70	3.38	4.80	2.7	3.40	4.80
D_{60}	1.93	2.45	3.50	3.50	4.44	6.35	3.40	4.30	6.20	3.50	4.40	6.4
D_{50}	2.04	2.59	3.69	3.67	4.66	6.66	3.60	4.58	6.60	3.70	4.70	6.70
D_{10}	3.03	3.84	5.49	7.00	8.89	12.70	7.00	8.88	12.70	5.60	7.10	10.2

Table 5.14: Distance between pressure ports and identification of the estimated pressure gradients

Distance Location	Distance (cm)	Pressure gradient identification
Port 1 to 2 ($D_{1,2}$)	29.50	$(dp/dL)_{1,2}$
Port 2 to 3 ($D_{2,3}$)	9.50	$(dp/dL)_{2,3}$
Port 3 to 4 ($D_{3,4}$)	9.50	$(dp/dL)_{3,4}$
Port 4 to 5 ($D_{4,5}$)	5.31	$(dp/dL)_{4,5}$
Port 5 to 6 ($D_{5,6}$)	1.91	$(dp/dL)_{5,6}$
Port 6 to 7 ($D_{6,7}$)	4.01	$(dp/dL)_{6,7}$
Port 6 to centre of the slot ($D_{6,slot}$)	0.54	$(dp/dL)_{6,slot}$

Table 5.15: Calculated values for the Kozeny constant "*c*"

Sand	Test #	C_{avg} (m^{-2})	% Difference
Silica Sand	2	6.45E+09	-16.5
	3	5.45E+09	1.6
	4	4.38E+09	20.9
	5	5.86E+09	-5.9
	Average	5.53E+09	
Husky Sand	6	3.53E+10	-1.4
	7	3.43E+10	1.4
	Average	3.48E+10	
Glass Beads	8	1.17E+10	-8.8
	9	9.82E+09	8.8
	Average	1.08E+10	

Table 5.16: Results of Run 2 (Sil-1 Sand)

k_i	37.81
k_{fp}	38.12
k_{fs}	46.75
Change in k_p (%)	0.82
Change in k_s (%)	23.63
ϕ_i	42.96
ϕ_{fp}	43.04
ϕ_{fs}	45.01
Change in ϕ_p (%)	0.18
Change in ϕ_s (%)	4.75
m_{sp} (g)	16.40
% of m_{sp}	0.07

Subindices meaning: i = initial, f= final, p = pack, s=slot

Table 5.17: Results of Run 7 (Husky Sand)

k_i	4.96
k_{fp}	5.01
k_{fs}	8.94
Change in k_p (%)	0.91
Change in k_s (%)	80.2
ϕ_i	39.60
ϕ_{fp}	45.20
ϕ_{fs}	39.70
Change in ϕ_p (%)	0.21
Change in ϕ_s (%)	14.08
m_{sp} (g)	1040.92
% of m_{sp}	4.20

Subindices meaning: i = initial, f= final, p = pack, s=slot

Table 5.18: Sand produced in Run 7 (Husky sand)

Q_o (l/min)	Run Time (h)	m_{sp} (g)	Comments
50	0.0 - 7.0	359.70	Sand was produced for 7 h
	7.0 - 14.0	0.00	No sand production
	14.0 - 16.0	85.06	Sand was produced for 2 h
	16.0 - 24.0	0.00	No sand production
	24.0 - 24.3	16.00	Sand was produced for 20 min
	24.3 - 48.0	0.00	No sand production
Sub-Total (1)		460.76	
100	0.0 - 18.8	0.00	No sand production
	18.8 - 19.2	64.3	Sand production for 25 min due to changes in the equipment
	19.2 - 22.6	0.00	No sand production
	22.6 - 22.7	36.7	Sand production for 6 min due to changes in the equipment
	22.7 - 58.0	0.00	No sand production
Sub-Total (2)		101.0	
150	0.0 – 0.8	0.00	No sand production
	0.8 - 2.3	324.1	Sand was produced for 2h20min
	2.3 – 8.1	0.00	No sand production
	8.1 - 8.7	226.2	Sand was produced for 35 min
	8.7 - 30.0	0.00	No sand production
Sub-Total (3)		444.5	
Total theoretical[(1)+(2)+(3)]		1006.26	
Total sand extracted		1040.90	
% Difference		3.33	

Table 5.19: Results of Run 9 (Glass Beads Less Fines)

k_i	8.95
k_{fp}	8.91
k_{fs}	14.38
Change in k_p (%)	0.00
Change in k_s (%)	52.9
ϕ_i	33.78
ϕ_{fp}	33.74
ϕ_{fs}	38.11
Change in ϕ_p (%)	0.00
Change in ϕ_s (%)	12.83
m_{sp} (g)	190.70
% of m_{sp}	0.74

Subindices meaning: i = initial, f= final, p = pack, s=slot

Table 5.20: Sand produced in run 9 (Glass Beads Less Fines)

Q_o (l/min)	Run Time (h)	m_{sp} (g)	Comments
	0.00 – 3.54	160.48	Sand was produced for 2 h 35 min
50	3.54 – 4.04	0.00	No sand production
	4.04 – 4.24	4.17	Sand was produced for 13 min
	4.24 – 4.7	0.00	No sand production
	4.70 – 4.75	0.91	Sand was produced for 4 min
	4.75 – 45.00	0.00	No sand production
Sub-Total (1)		165.56	
	0.0 – 1.97	0.00	No sand production
100	1.97 – 2.00	1.47	Sand production for 2 min
	2.00 – 37.00	0.00	No sand production
Sub-Total (2)		1.47	
150	0.0 – 31.00	0.00	No sand production
Sub-Total (3)		0.00	
Total theoretical[(1)+(2)+(3)]		167.00	
Total sand extracted		190.70	
% Difference		12.41	

Table 5.21: Sand produced in the liquid experiments

Sand	Run	Slot Size (in)	k_i (darcy)	Initial Mass of sand in the Pack (g)	Sand Produced (g)					Error (%)	Total Mass produced (%)
					Q_o (cm^3/h)			Total			
					50	100	150				
					Actual	Actual	Actual	Actual	Estimated		
Sil-1	2	0.022	37.81	23137.23	16.40	0.00	0.00	16.40	11.99	26.89	0.07
	3	0.028	39.92	23481.70	1362.01	71.98	0.00	1433.99	1456.56	-1.57	6.11
	4	0.040	27.76	23343.01	2500.31	4808.23	4253.54	11562.08	11697.89	-1.17	49.53
Husky	6	0.028	4.43	24960.00	8.20	0.00	---	8.20	---	---	0.03
	7	0.040	4.87	24532.00	435.52	99.69	505.71	1040.92	1111.84	3.35	4.24
GLH	8	0.028	5.29	26873.12	68.27	0.00	---	68.27	42.71	37.43	0.25
GBLF	9	0.028	8.95	25821.89	190.70	0.00	0.00	190.70	164.67	13.65	0.74

Table 5.22: Changes in the properties of the pack. Sil-1 sand. Different slot sizes

Run #	Slot Size in (mm)	ki (darcy)	k_{VS} (darcy)	k_{pack} (darcy)	% Increase		ϕ_i	ϕ_{VS}	ϕ_{pack}	% Increase	
					Vicinity slot	Pack				Vicinity slot	Pack
2	0.022 (0.56)	37.81	46.75	38.12	23.63	0.82	42.96	45.01	43.04	4.75	0.18
3	0.028 (0.71)	39.92	68.70	45.43	72.10	20.14	41.80	47.45	43.65	13.52	4.41
4	0.040 (1.02)	27.76	62.90	---	126.56	---	39.18	46.97	---	19.91	---

VS: vicinity of the slot

Table 5.23: Changes in the properties of the pack. Husky and Glass Beads sands. Different slot sizes

Sand	Run #	Slot Size in (mm)	ki (darcy)	k_{VS} (darcy)	k_{pack} (darcy)	% Change		ϕ_i	ϕ_{VS}	ϕ_{pack}	% Change	
						VS	Pack				VS	Pack
Husky	6	0.028 (0.71) @100 cm^3/h	4.43	11.28	4.44	153.53	0.18	38.81	47.74	38.73	22.99	-0.22
	7	0.040 (1.02) @100 cm^3/h	4.96	9.63	5.16	94.23	4.06	39.60	46.44	40.18	17.28	1.46
		@150 cm^3/h	4.96	8.94	5.01	80.24	0.95	39.60	45.2	39.62	14.14	0.05
GBLH	8	0.028 (0.71) @100 cm^3/h	5.29	10.60	5.40	100.42	0.28	30.93	36.78	30.99	18.90	0.18
GBLF	9	0.028 (0.71) @100 cm^3/h	8.95	15.16	9.16	69.36	2.35	33.78	38.01	33.65	12.52	0.39
		@150 cm^3/h	8.95	13.70	8.91	53.12	-0.43	33.78	37.50	33.70	11.01	0.24

VS: vicinity of the slot

Table 5.24: Summary of results for Runs 3 and 5. Sil-1 sand. Slot size: 0.028 in (0.71 mm).

	Run 3	Run 5
k_i	39.59	50.70
k_{fp}	43.99	50.23
k_{fs}	66.41	71.20
Change in k_p (%)	11.11	-0.94
Change in k_s (%)	67.74	40.43
ϕ_i	41.80	42.07
ϕ_{fp}	42.80	41.97
ϕ_{fs}	46.78	45.33
Change in ϕ_p (%)	2.39	-0.25
Change in ϕ_s (%)	11.91	7.75
m_{sp} @ 50 cm^3/h (g) (48 h)	1362.01	1832.50
m_{sp} @ 50 cm^3/h (g) for total stage time	1362.01	4259.40
m_{sp} @ 100 cm^3/h (g)	71.98	1440.60
m_{sp} @ 150 cm^3/h (g)	0.00	61.70
Total m_{sp} (g)	1433.99	5761.70
% of mass produced	6.11	24.15

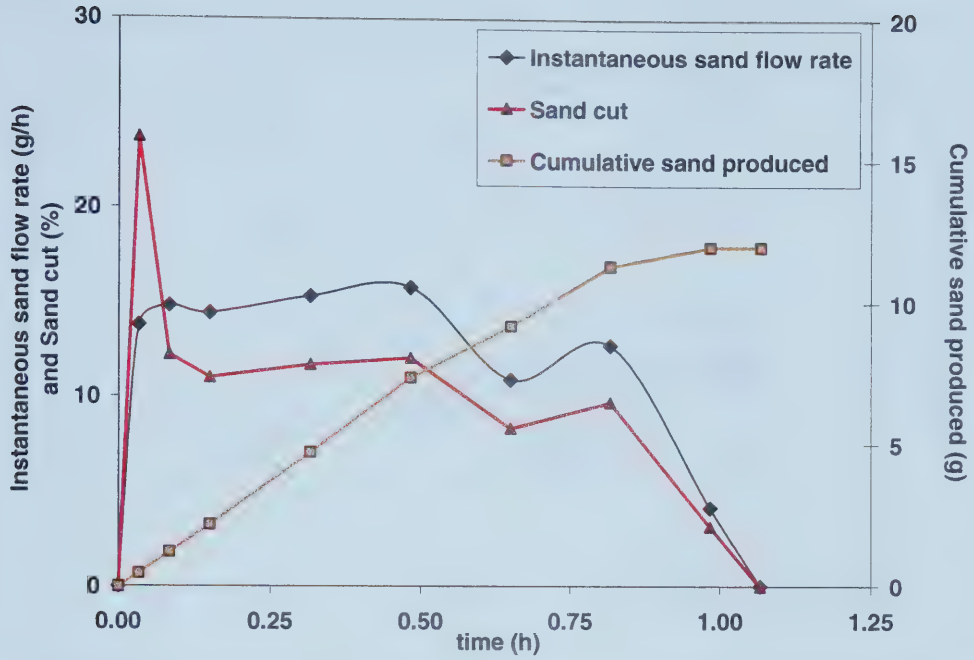

Figure 5.24: Sand flow rate, cumulative sand production and sand concentration versus time for test # 2. Sil-1 sand, slot size: 0.022 in (0.56 mm). Flow rate: 50 cm^3/h

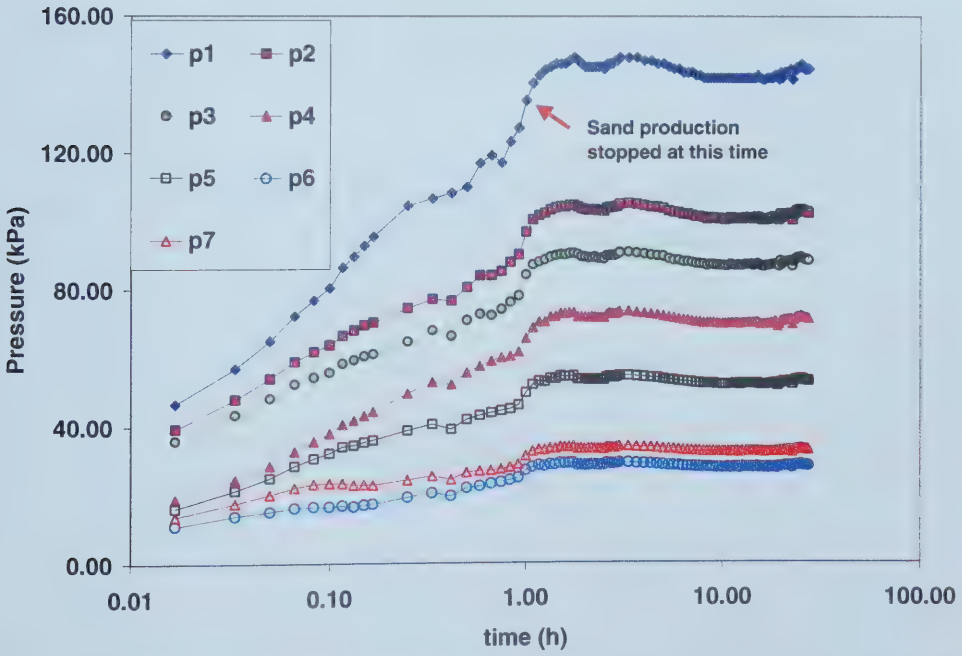

Figure 5.25: Pressure versus time for test # 2. Sil-1 sand, slot size: 0.022 in (0.56 mm). Flow rate: 50 cm^3/h.

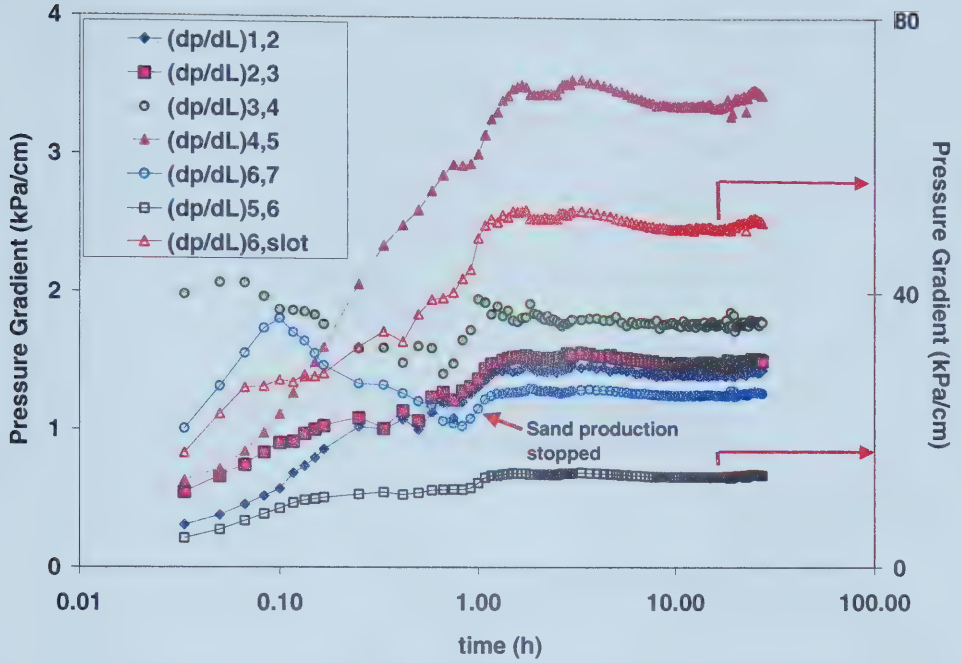

Figure 5.26: Pressure gradients versus time for test # 2. Sil-1 sand, slot size: 0.022 in (0.56 mm). Flow rate: 50 cm3/h

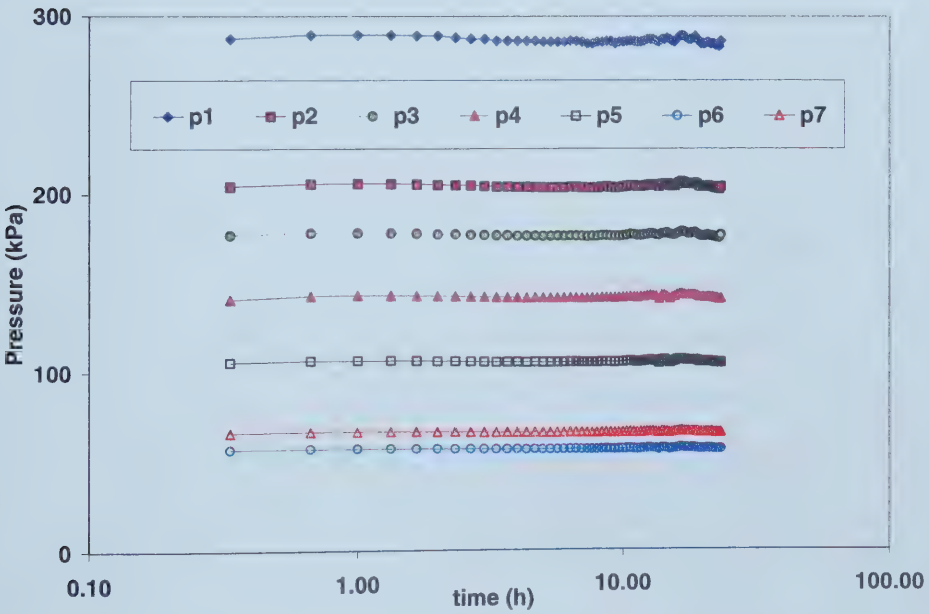

Figure 5.27: Pressure versus time for test # 2. Sil-1 sand, slot size: 0.022 in (0.56 mm). Flow rate: 100 cm^3/h.

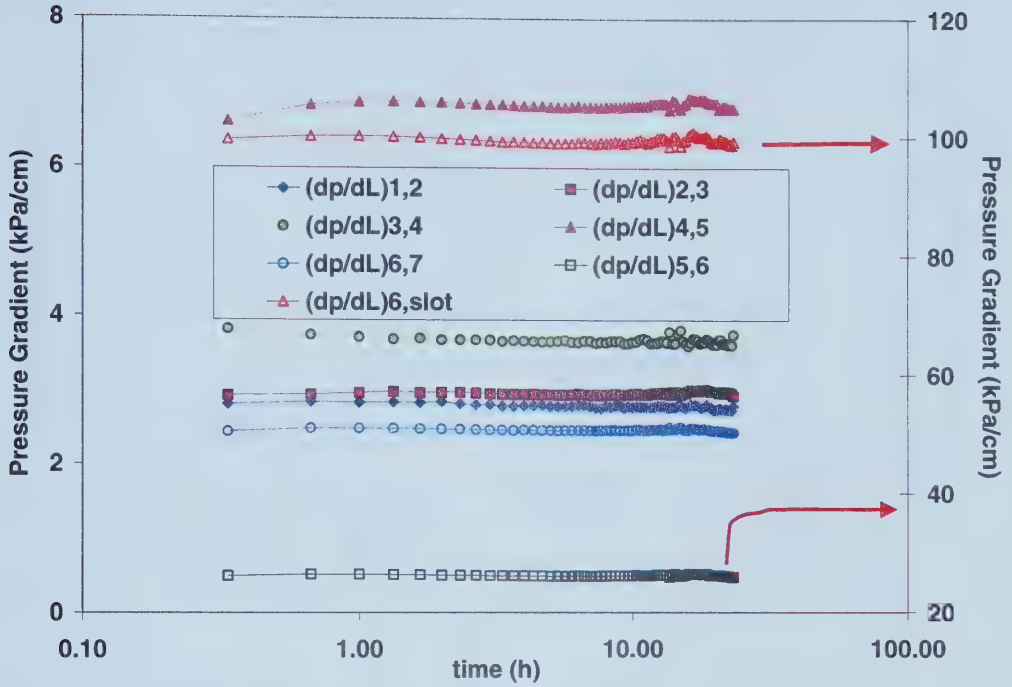

Figure 5.28: Pressure gradients versus time for test # 2. Sil-1 sand, slot size: 0.022 in (0.56 mm). Flow rate: 100 cm3/h

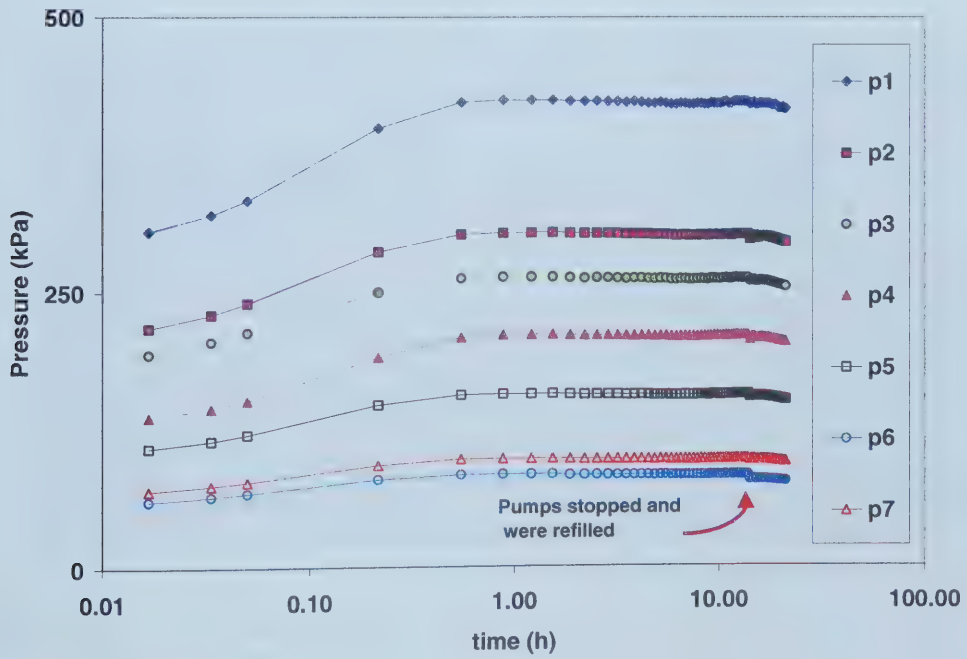

Figure 5.29: Pressure versus time for test # 2. Sil-1 sand, slot size: 0.022 in (0.56 mm). Flow rate: 150 cm3/h.

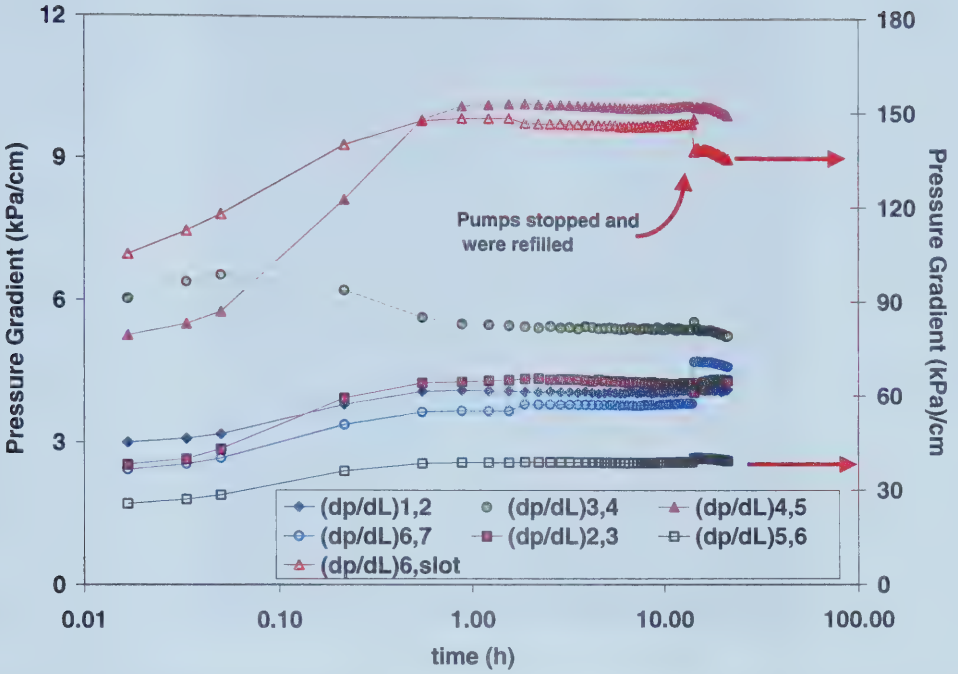

Figure 5.30: Pressure gradients versus time for test # 2. Sil-1 sand, slot size: 0.022 in (0.56 mm). Flow rate: 150 cm^3/h.

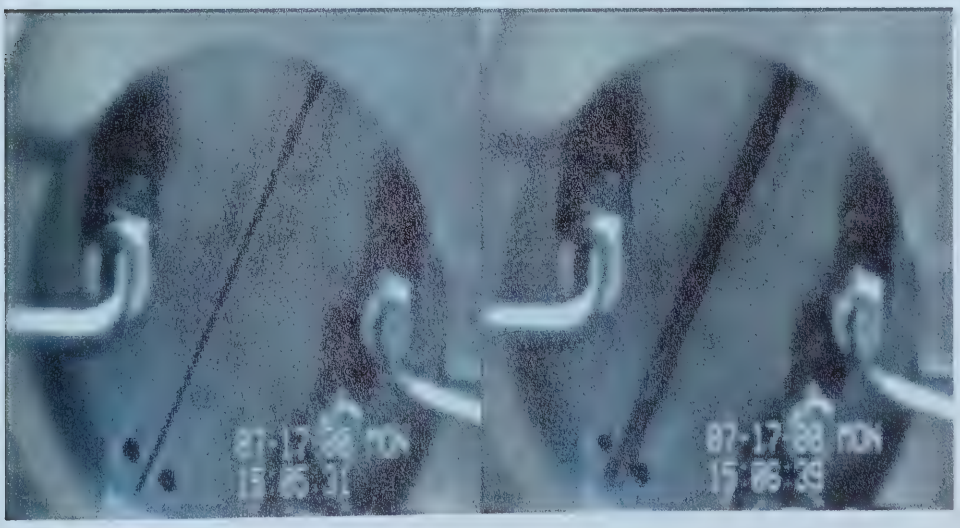

a) At the beginning of the Run

b) One minute after Run started

Figure 5.31: View of the slot producing Sil-1 sand. Run 2. Slot size 0.022 in (0.56 mm). Flow rate: 50 cm^3/h

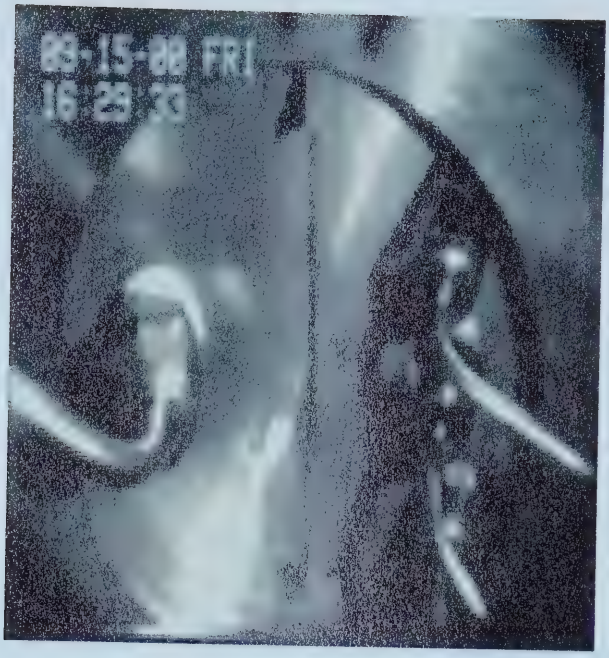

a) At the beginning of the Run

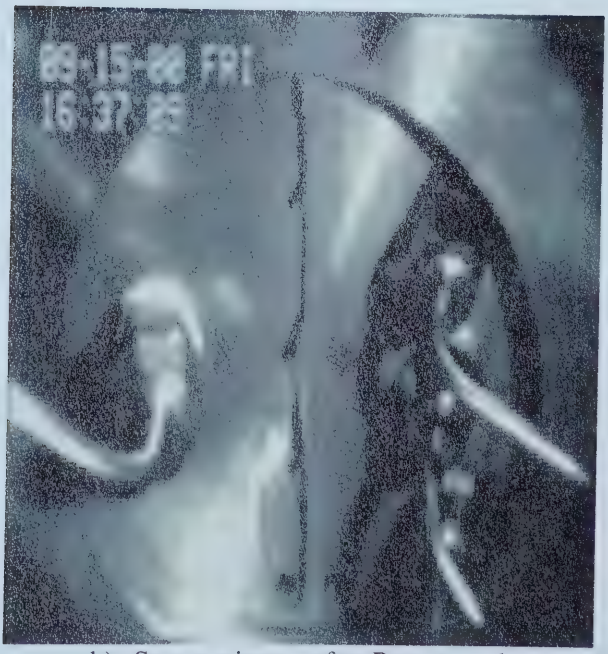

b) Seven minutes after Run started

Figure 5.32: View of the slot producing Husky sand. Run 7. Slot size: 0.040 in (1.02 mm). Flow rate 50 cm^3/h.

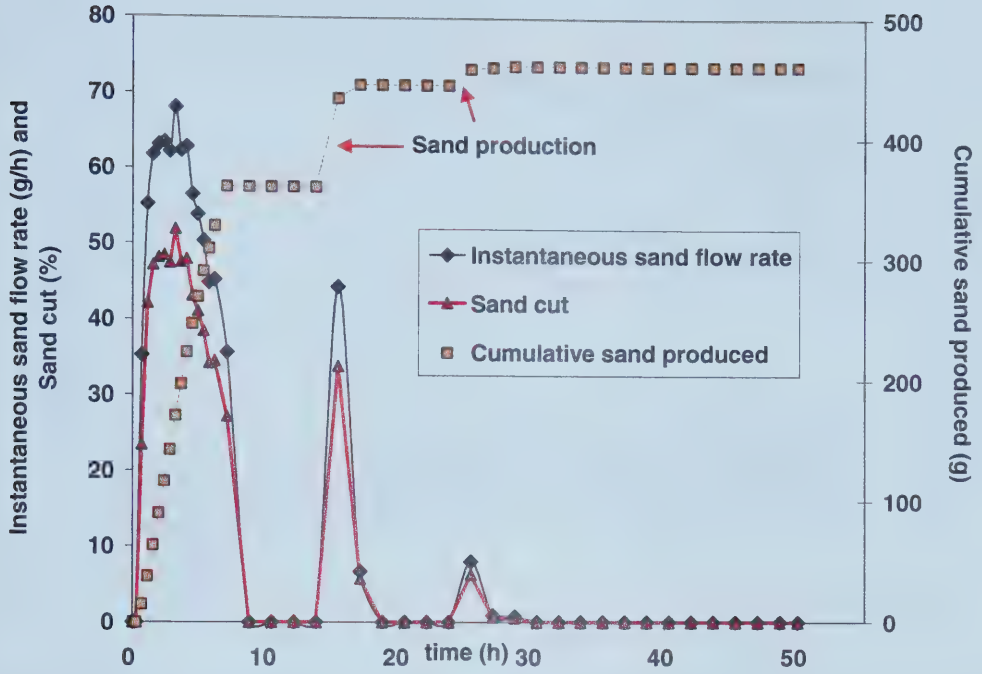

Figure 5.33: Sand flow rate, cumulative sand production and sand concentration versus time for run 7. Husky sand, slot size: 0.040 in (1.02 mm). Flow rate: 50 cm^3/h

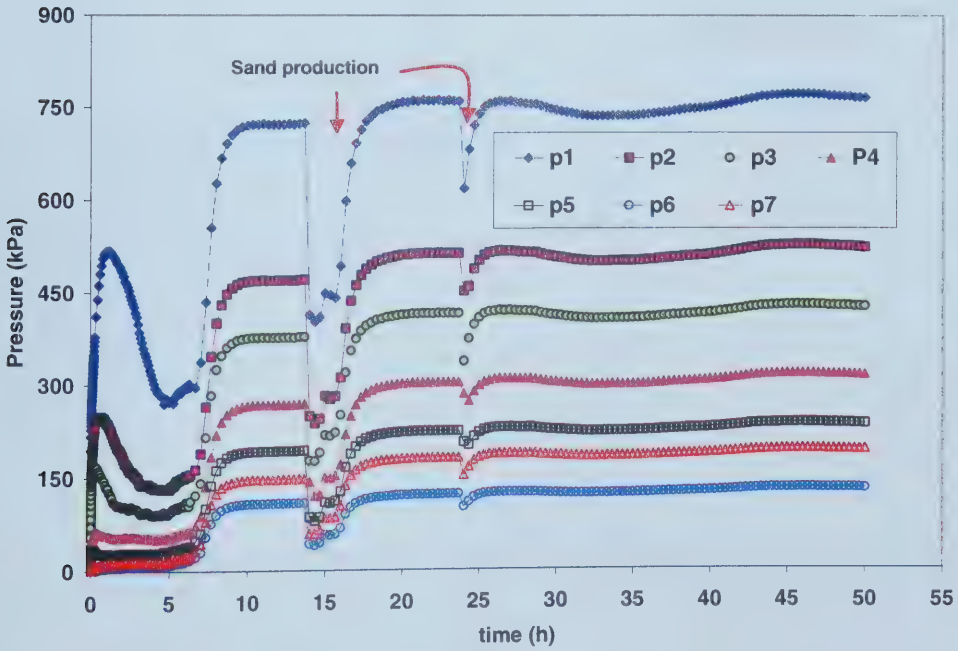

Figure 5.34: Pressure versus time for run 7. Husky sand, slot size: 0.040 in (1.02 mm). Flow rate: 50 cm^3/h.

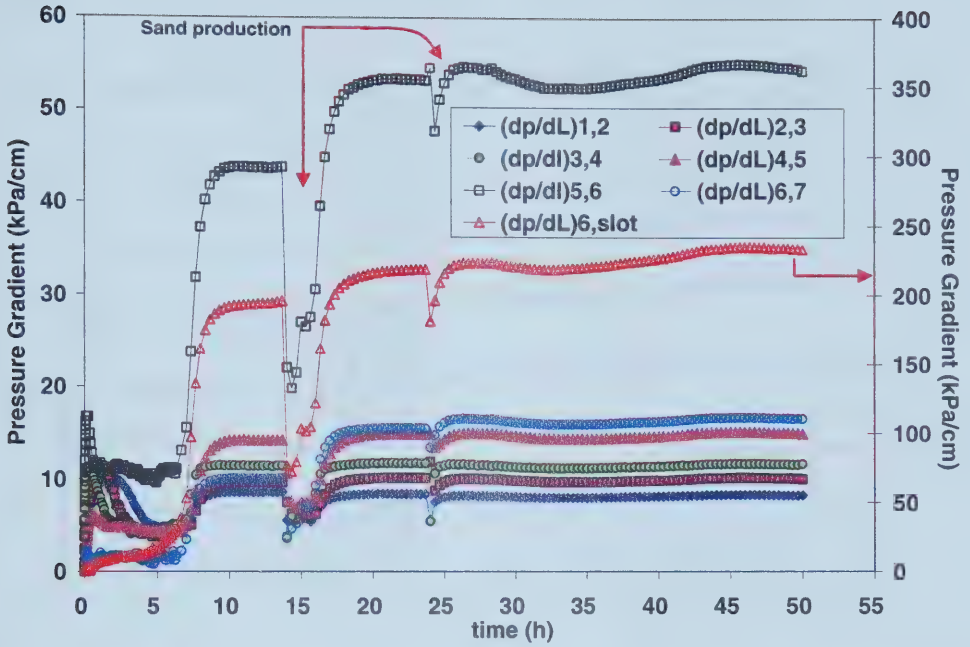

Figure 5.35: Pressure gradients versus time for run 7. Husky sand, slot size: 0.040 in (1.02 mm). Flow rate: 50 cm^3/h.

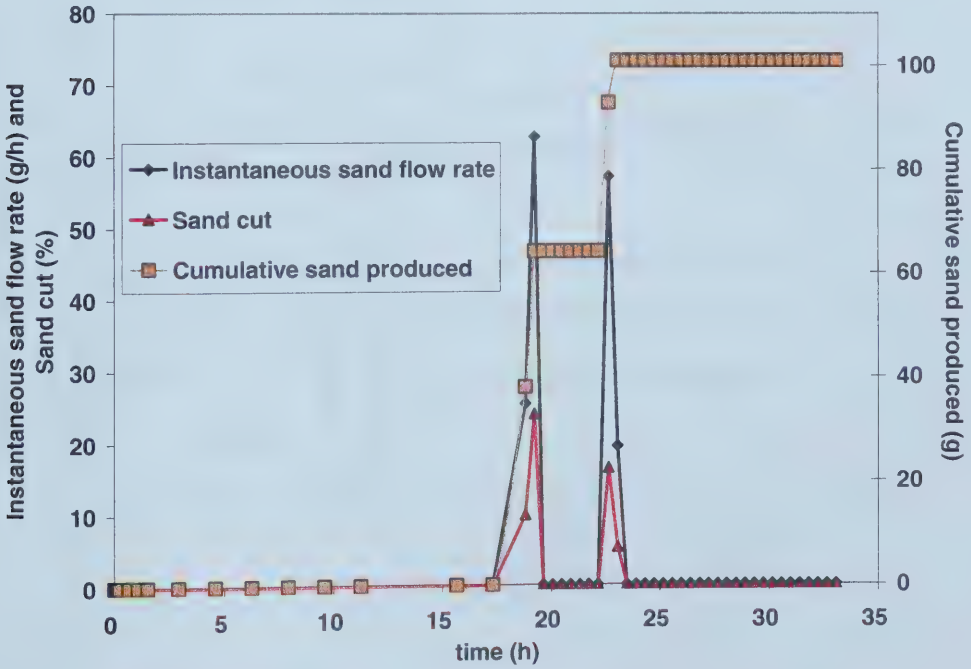

Figure 5.36: Sand flow rate, cumulative sand production and sand concentration versus time for run 7. Husky sand, slot size: 0.040 in (1.02 mm). Flow rate: 100 cm^3/h

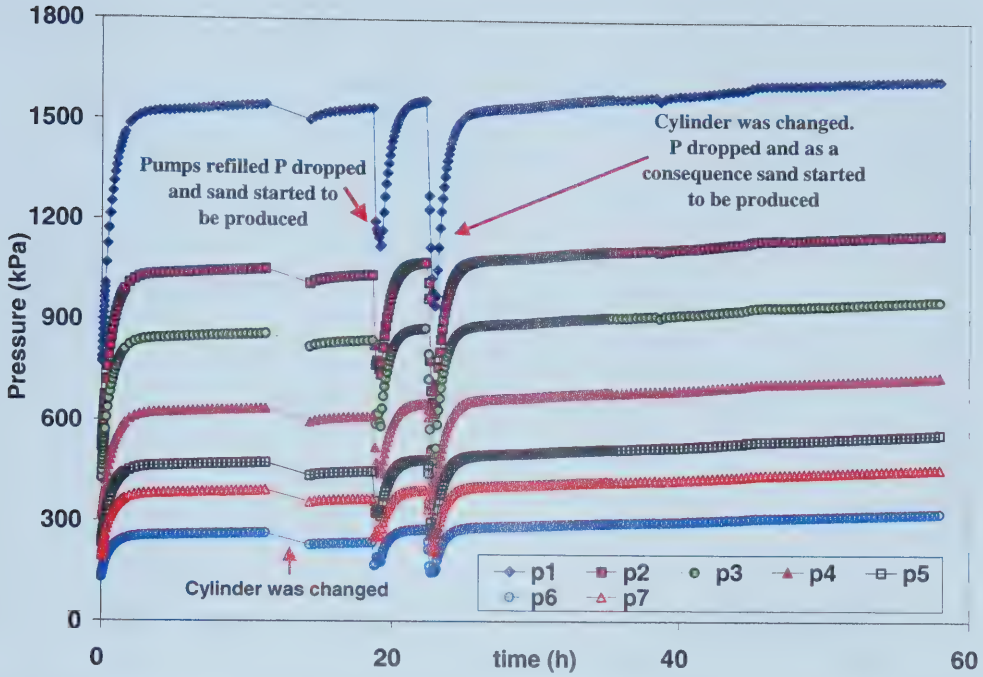

Figure 5.37: Pressure versus time for run 7. Husky sand, slot size: 0.040 in (1.02 mm). Flow rate: 100 cm^3/h.

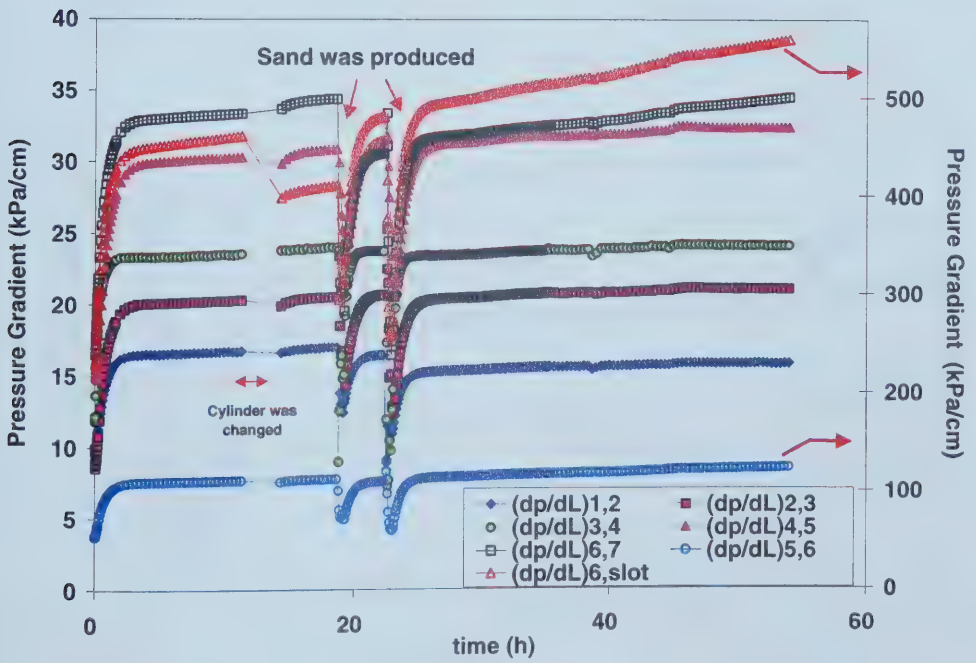

Figure 5.38: Pressure gradients versus time for run 7. Husky sand, slot size: 0.040 in (1.02 mm). Flow rate: 100 cm^3/h.

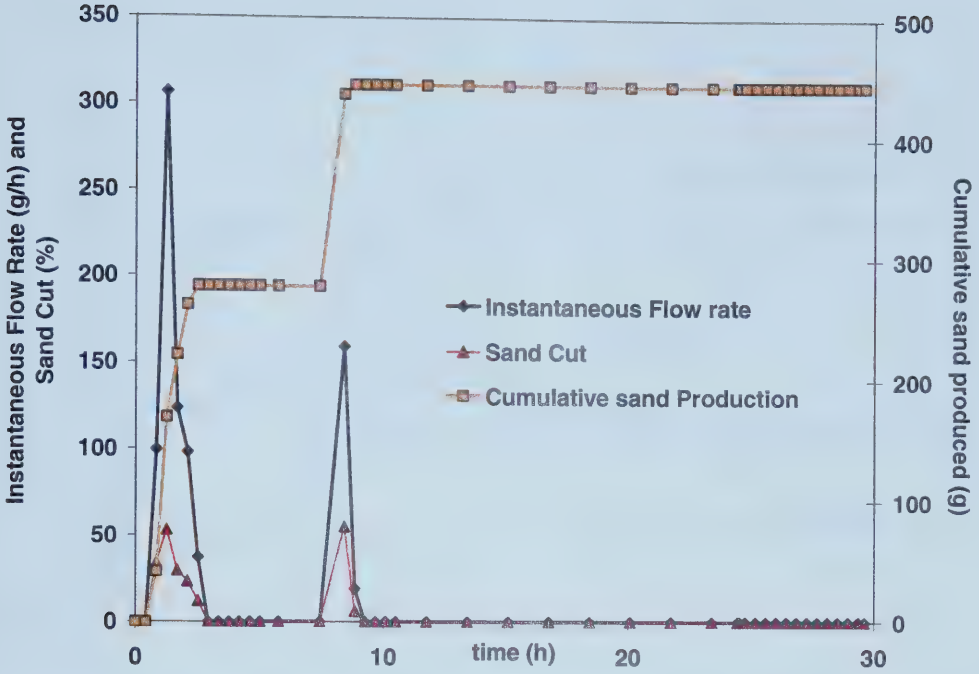

Figure 5.39: Sand flow rate, cumulative sand production and sand concentration versus time for run 7. Husky sand, slot size: 0.040 in (1.02 mm). Flow rate: 150 cm^3/h

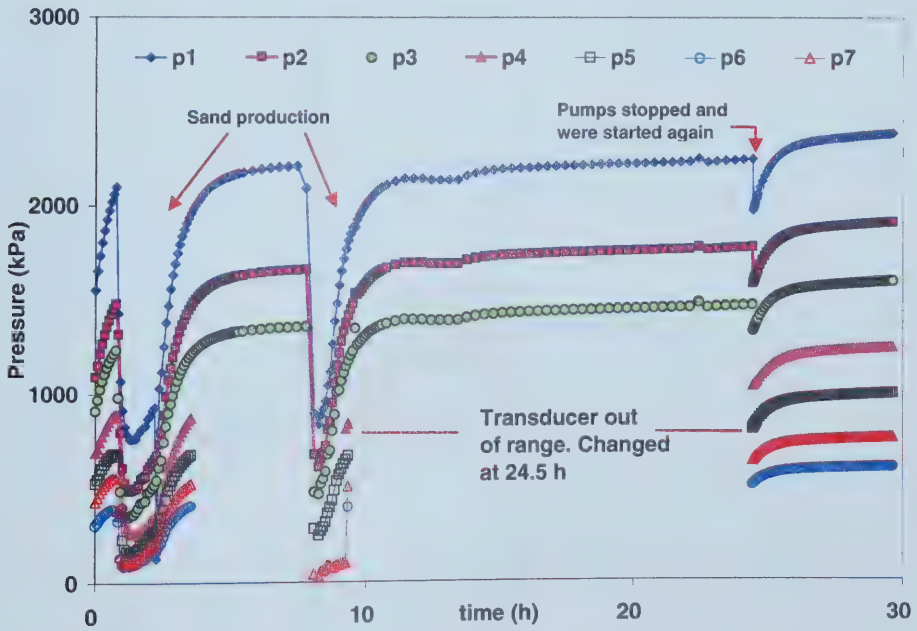

Figure 5.40: Pressure versus time for run 7. Husky sand, slot size: 0.040 in (1.02 mm). Flow rate: 150 cm^3/h.

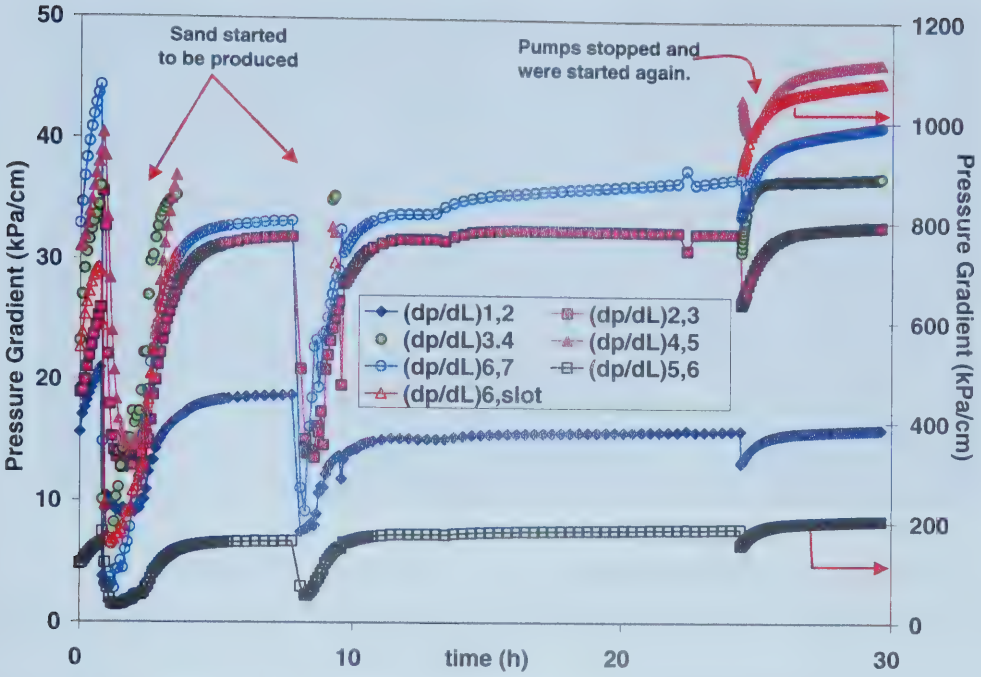

Figure 5.41: Pressure gradients versus time for run 7. Husky sand, slot size: 0.040 in (1.02 mm). Flow rate: 150 cm^3/h.

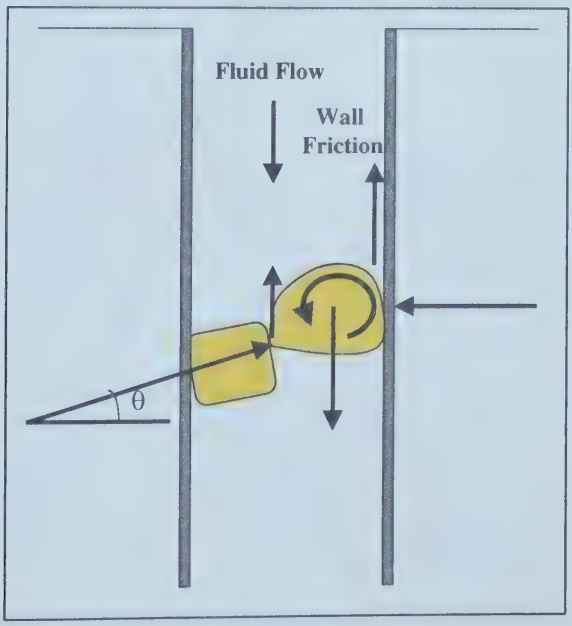

Figure 5.42: Bridging of two sand grains within a slot. Arrows indicate forces acting on right hand sand grain.

a) At the beginning of the Run b) Three minutes after the Run started

Figure 5.43: View of the slot producing Glass Beads sand. Run 9. Slot size 0.028 in (0.71 mm). Flow rate: 50 cm^3/h.

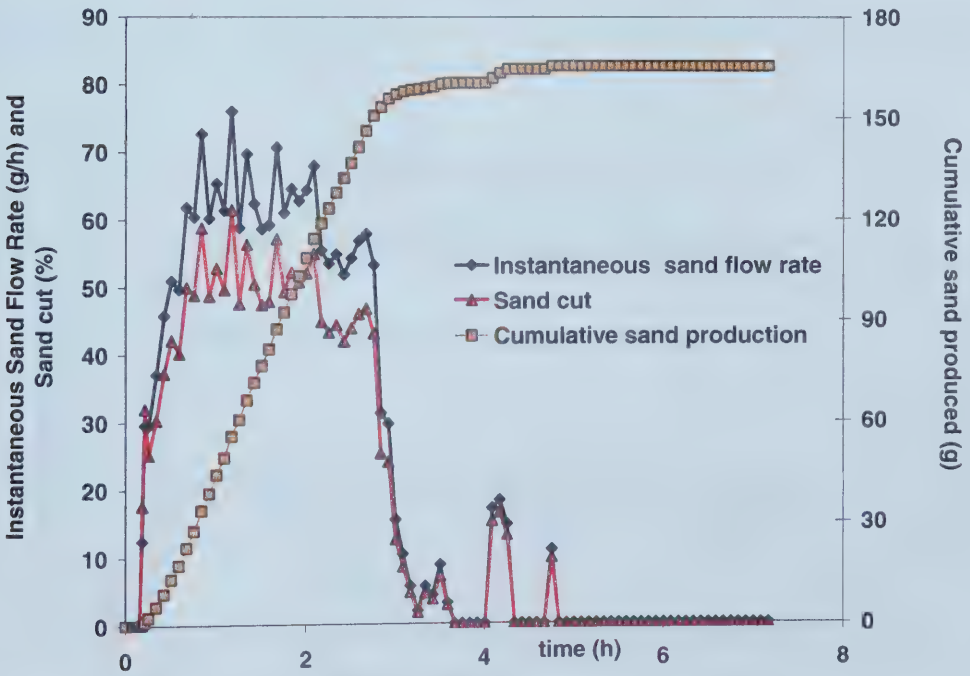

Figure 5.44: Sand flow rate, cumulative sand production and sand concentration versus time for run 9. Glass Beads with less fines, slot size: 0.028 in (0.71 mm). Flow rate: 50 cm^3/h

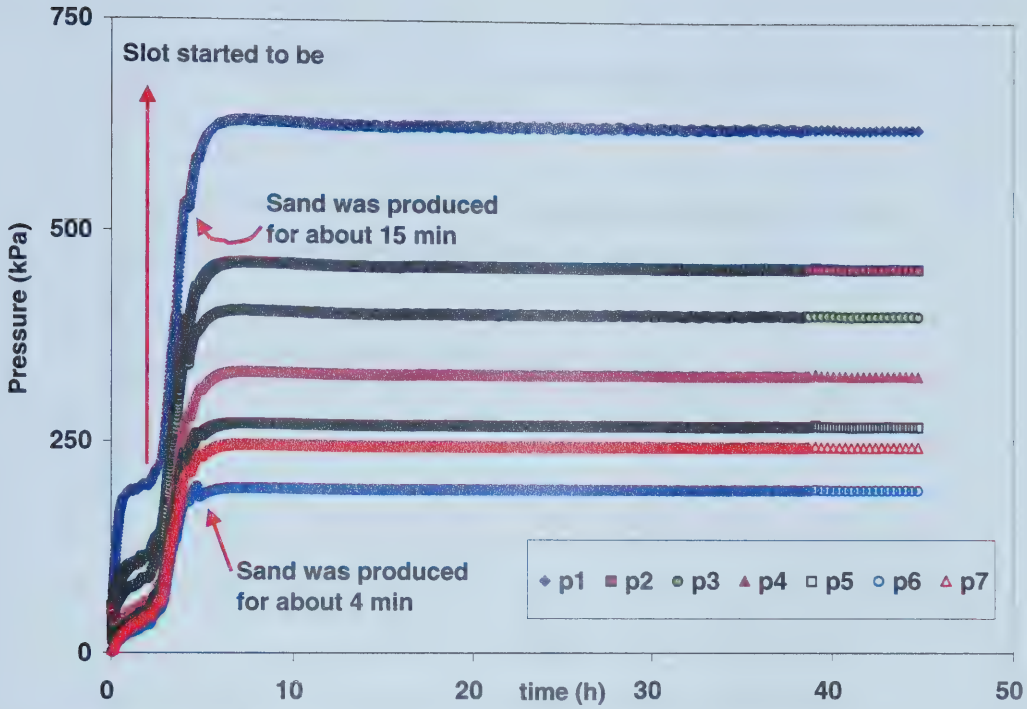

Figure 5.45: Pressure versus time for run 9. Glass Beads less fines, slot size: 0.028 in (0.71 mm). Flow rate: 50 cm^3/h.

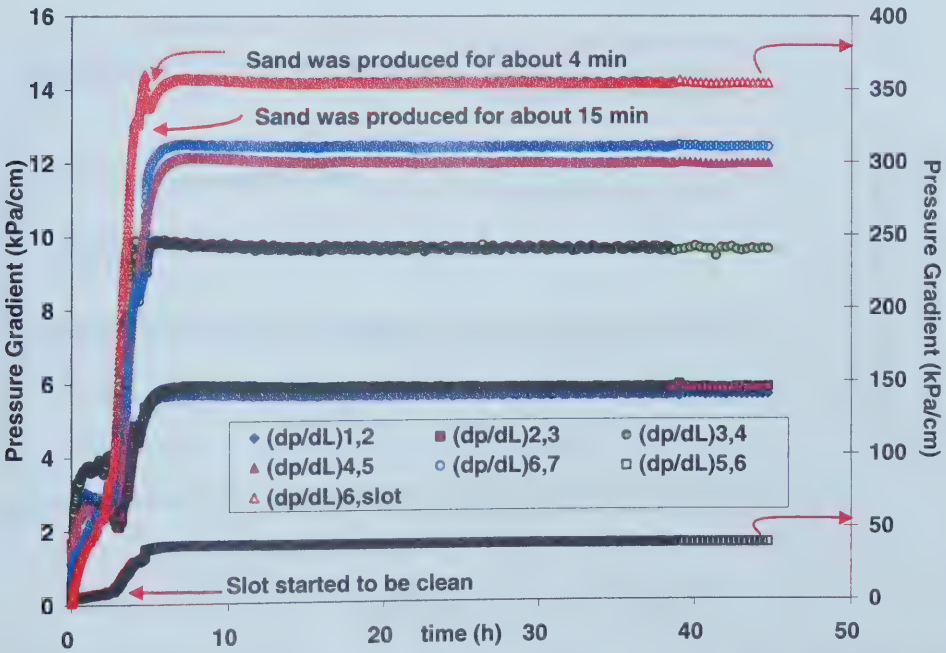

Figure 5.46: Pressure gradients versus time for run 9. Glass Beads with less fines, slot size: 0.028 in (0.71 mm). Flow rate: 50 cm3/h.

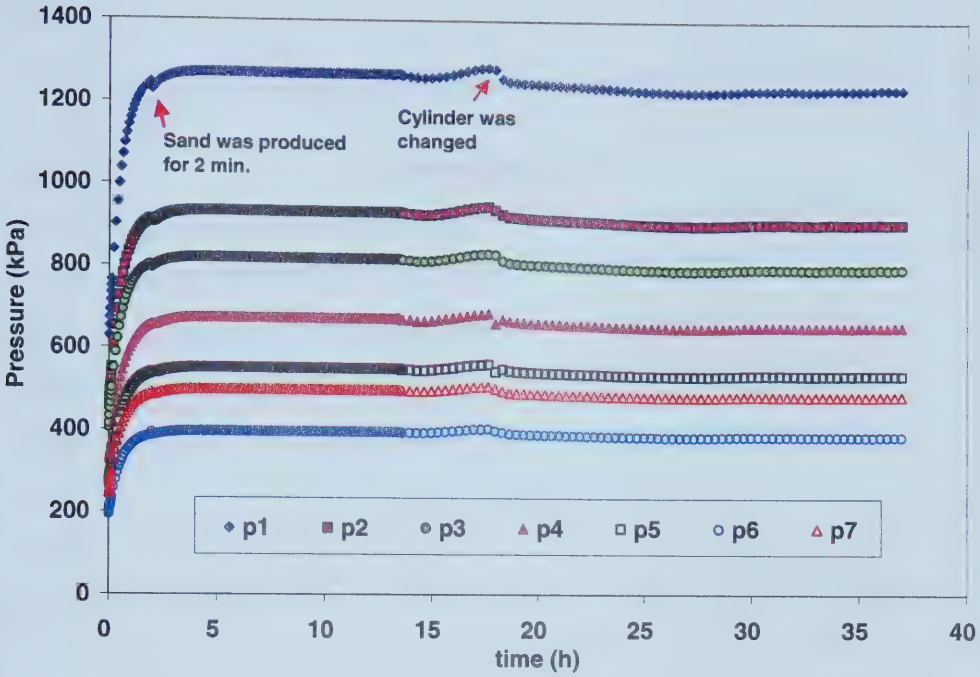

Figure 5.47: Pressure versus time for run 9. Glass Beads less fines, slot size: 0.028 in (0.71 mm). Flow rate: 100 cm^3/h.

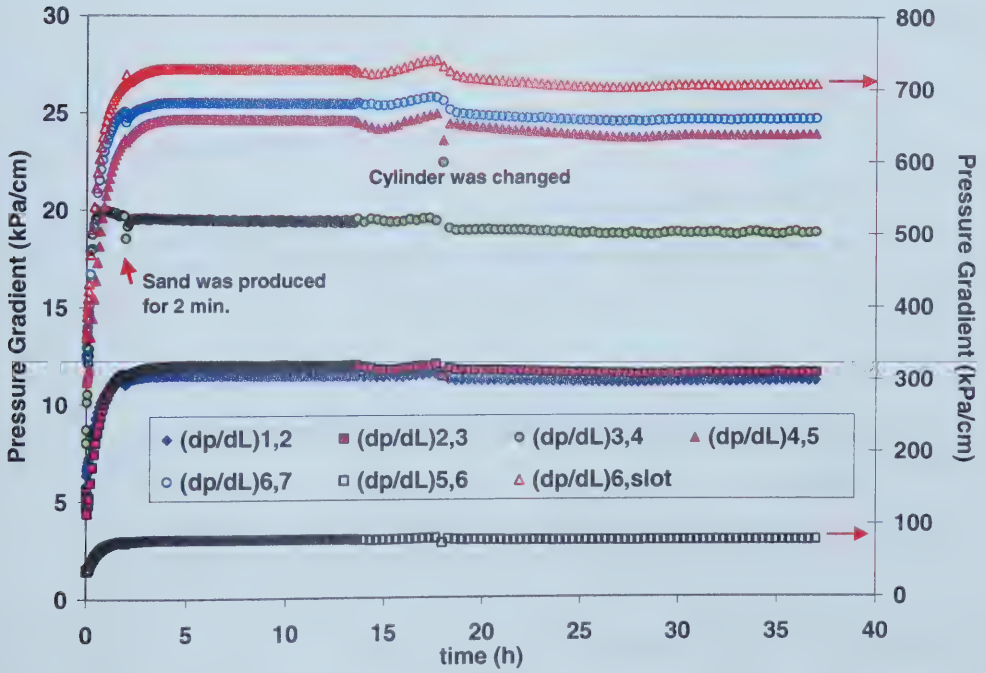

Figure 5.48: Pressure gradients versus time for run 9. Glass Beads with less fines, slot size: 0.028 in (0.71 mm). Flow rate: 100 cm3/h.

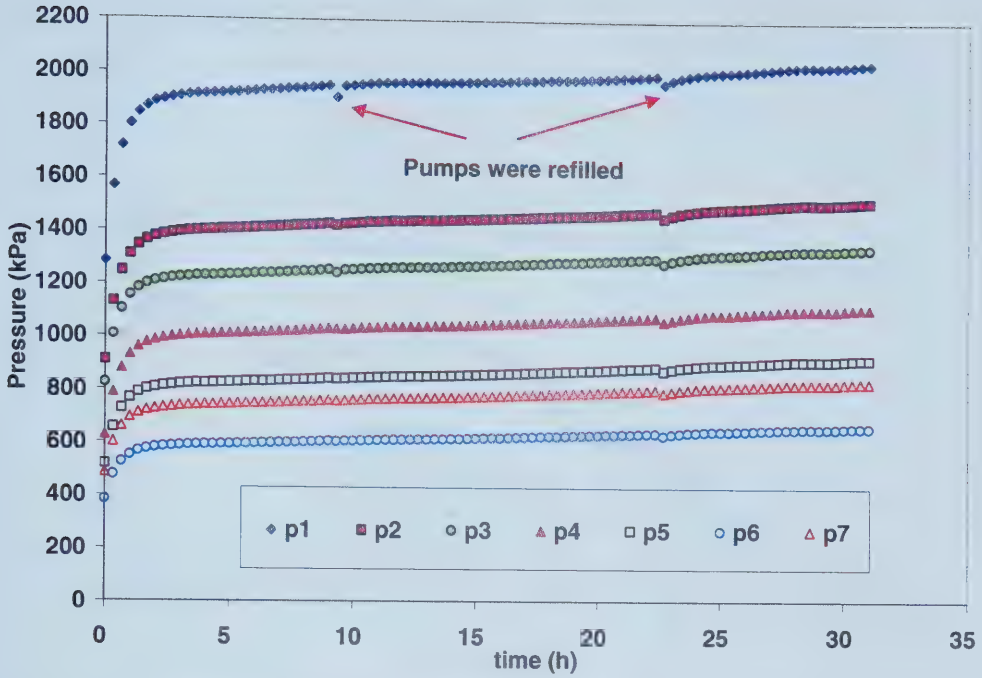

Figure 5.49: Pressure versus time for run 9. Glass Beads with less fines, slot size: 0.028 in (0.71 mm). Flow rate: 150 cm3/h.

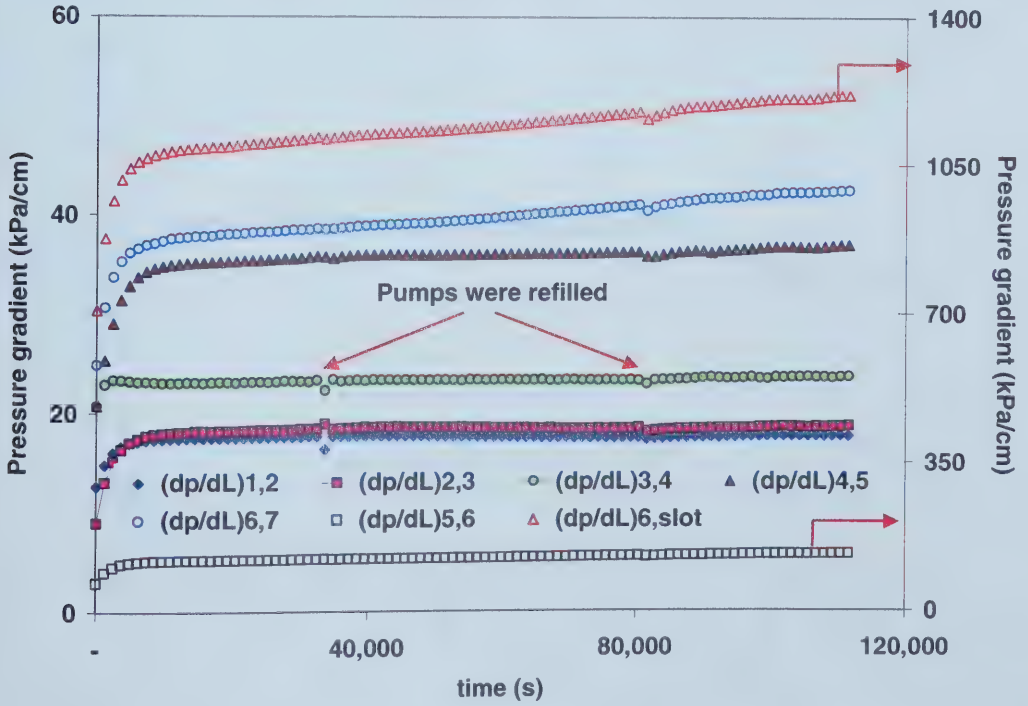

Figure 5.50: Pressure gradients versus time for run 9. Glass Beads with less fines, slot size: 0.028 in (0.71 mm). Flow rate: 150 cm3/h.

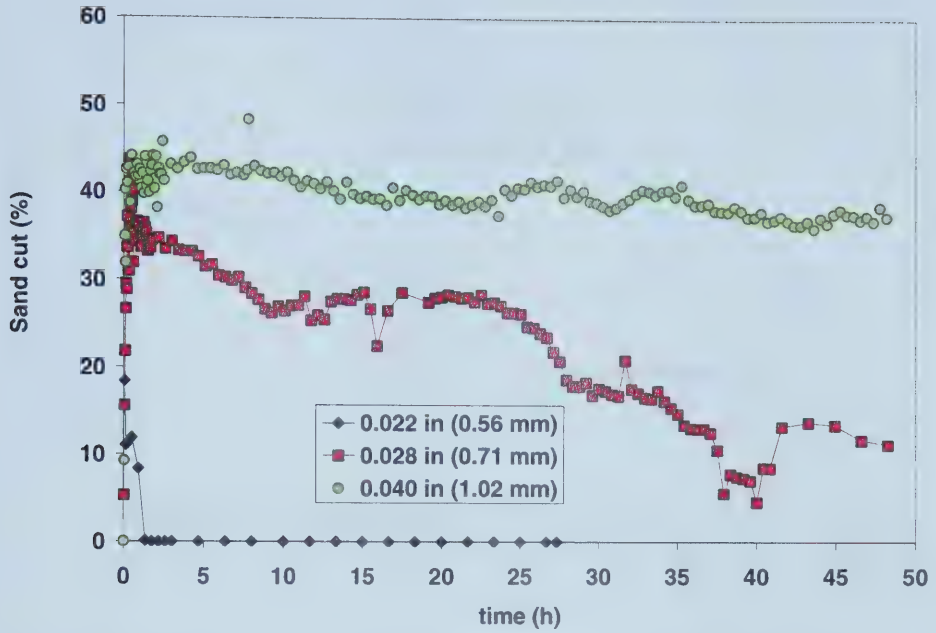

Figure 5.51: Sand cut versus time for different slot sizes. Sil-1 sand. Flow rate: 50 cm^3/h.

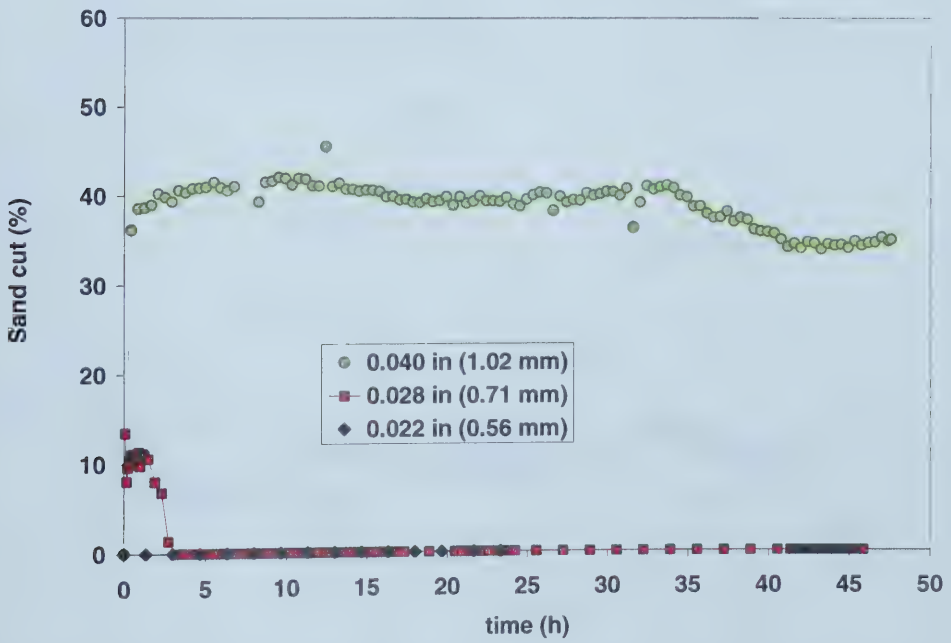

Figure 5.52: Sand cut versus time for different slot sizes. Sil-1 sand. Flow rate: 100 cm^3/h.

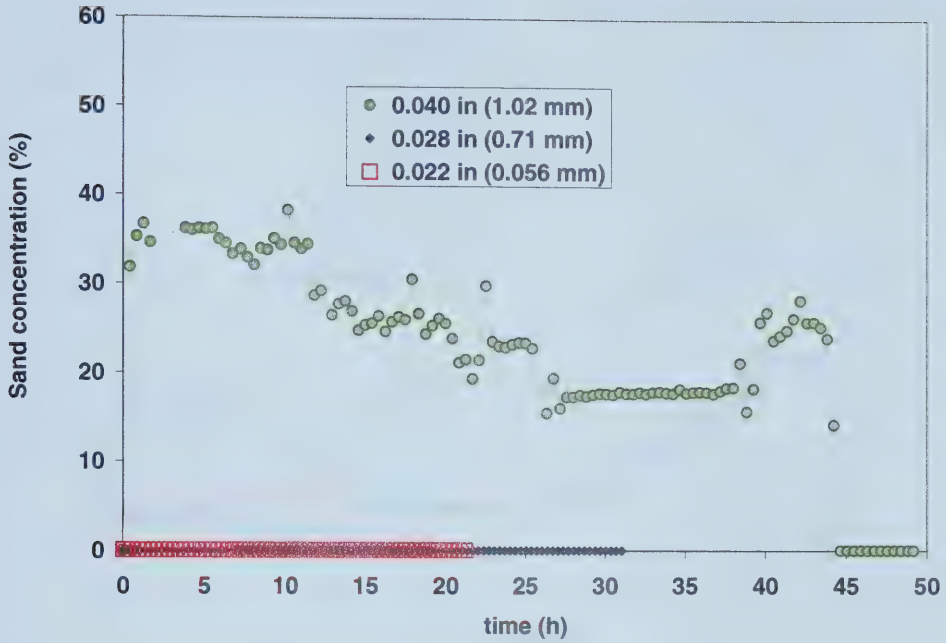

Figure 5.53: Sand cut versus time for different slot sizes. Sil-1 sand. Flow rate: 150 cm^3/h.

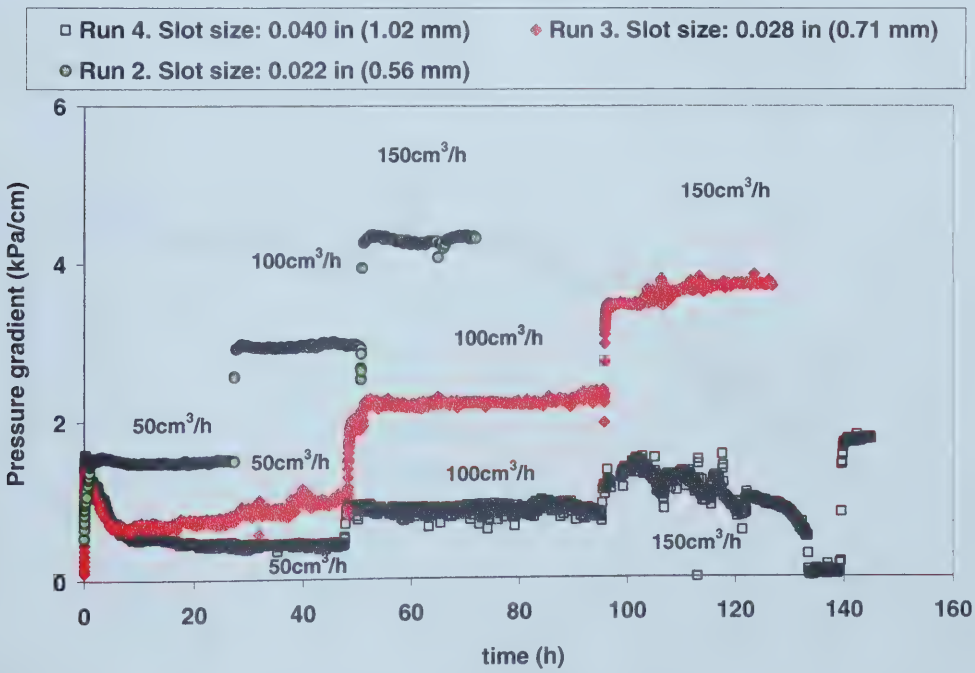

Figure 5.54: Pressure gradient $(dp/dL)_{2,3}$ between ports 2 and 3 versus time for different slot sizes and flow rates. Sil-1 sand.

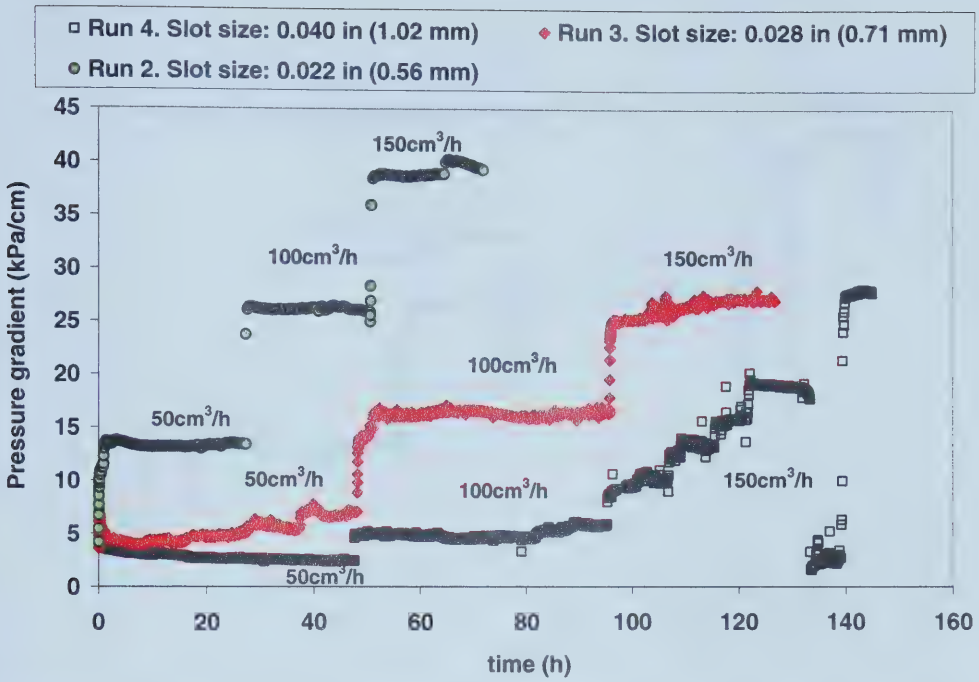

Figure 5.55: Pressure gradient $(dp/dL)_{5,6}$ between ports 5 and 6 versus time for different slot sizes and flow rates. Sil-1 sand.

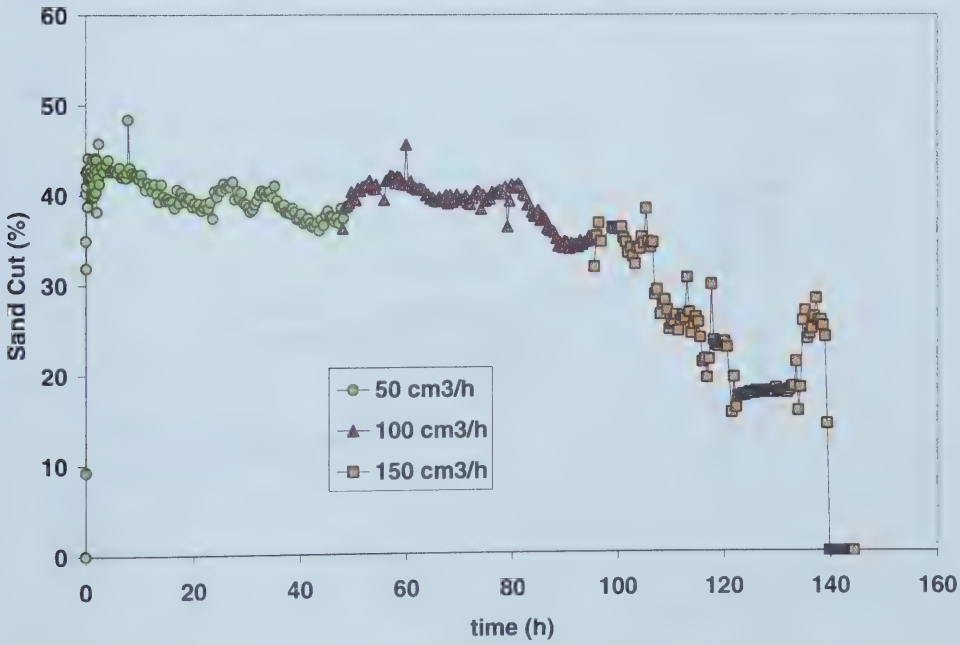

Figure 5.56: Sand cut versus time for different flow rates. Run 4. Sil-1 sand and slotted plate 0.040 in (1.02 mm).

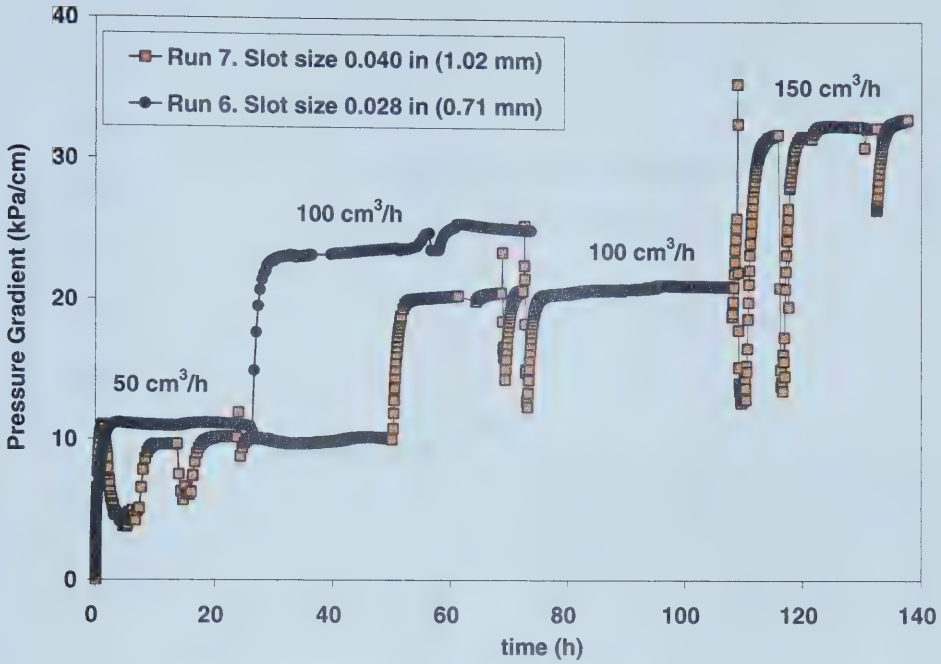

Figure 5.57: Pressure gradient $(dp/dL)_{2,3}$ between ports 2 and 3 versus time for different slot sizes and flow rates. Husky sand.

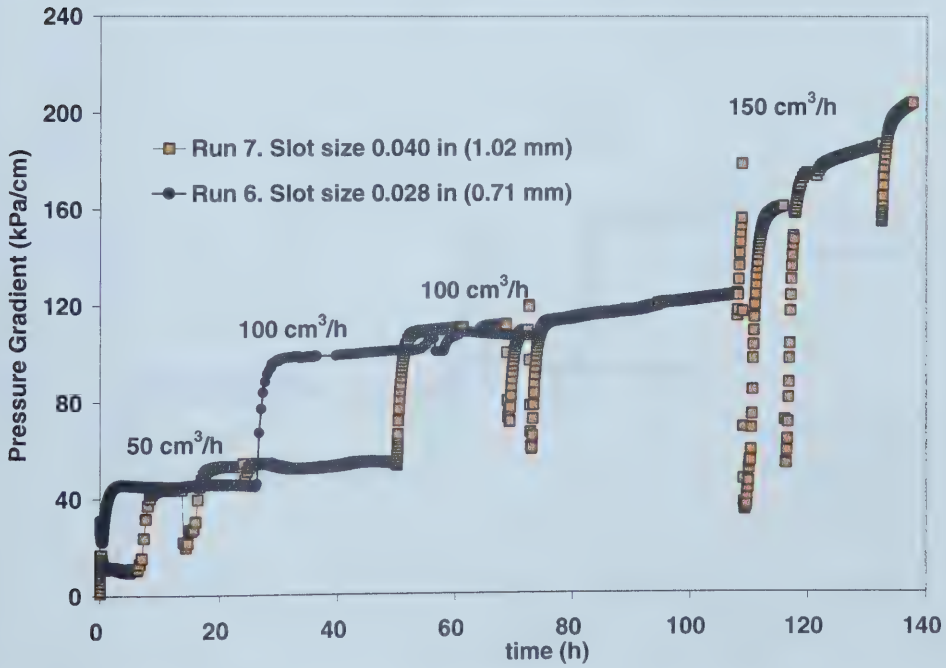

Figure 5.58: Pressure gradient $(dp/dL)_{5,6}$ between ports 5 and 6 versus time for different slot sizes and flow rates. Husky sand.

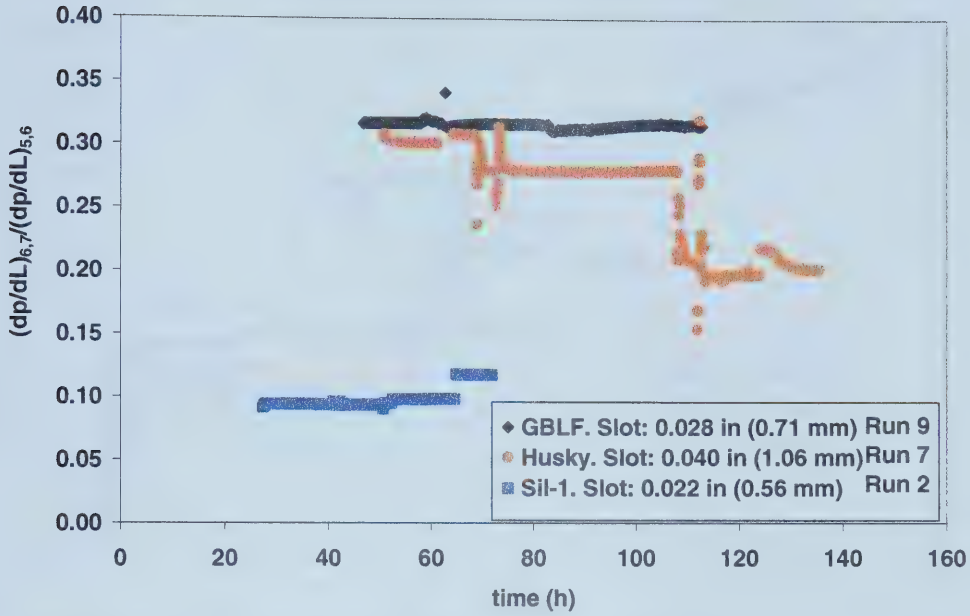

Figure 5.59: Pressure gradient ratio versus time for different sands and slot sizes

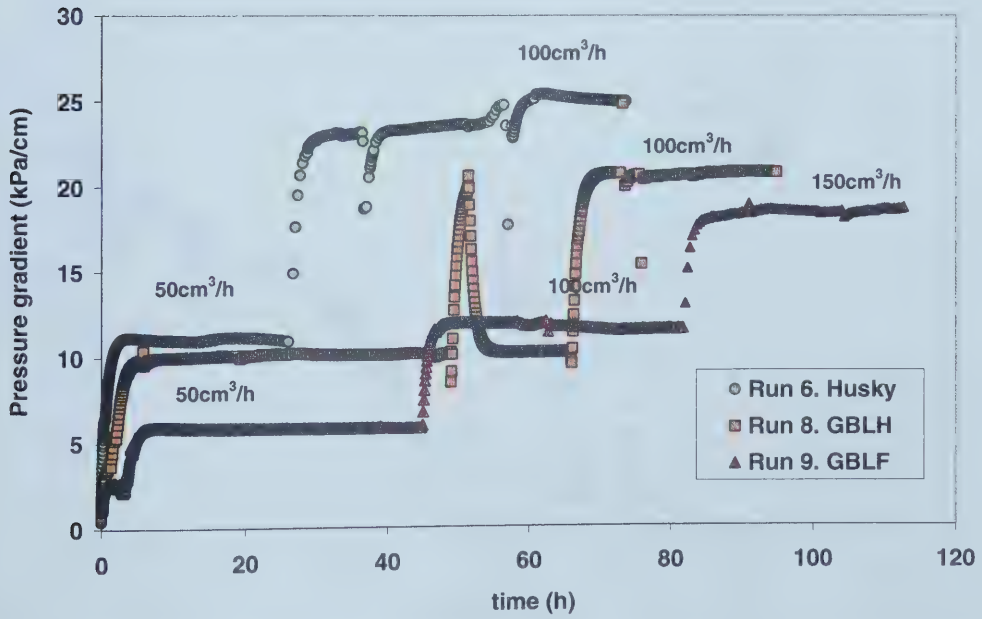

Figure 5.60: Pressure gradient $(dp/dL)_{2,3}$ between ports 2 and 3 versus time for different sands and flow rates. Slot size: 0.028 in (0.71 mm).

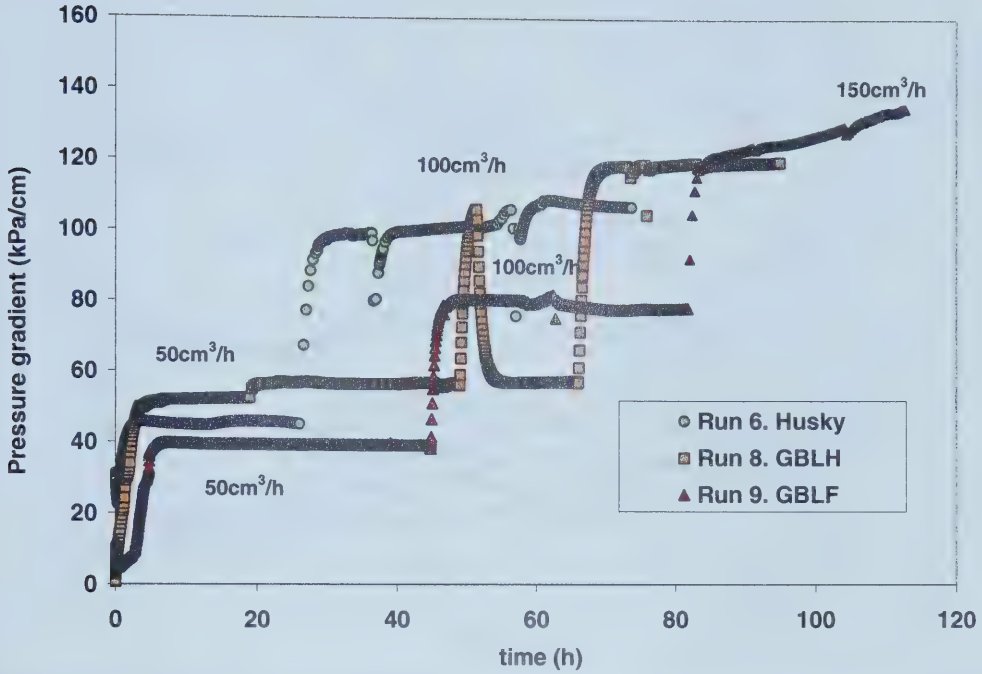

Figure 5.61: Pressure gradient between ports 5 and 6 versus time for different sands and flow rates. Slot size: 0.028 in (0.71 mm).

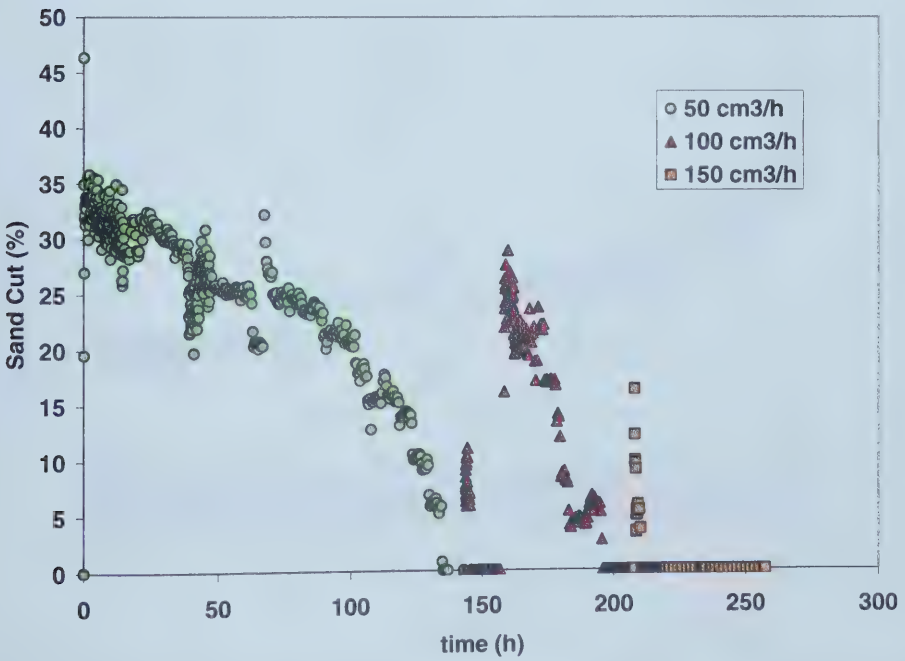

Figure 5.62: Sand cut versus time. Run 5. Sil-1 sand. Slot size 0.028 in (0.71 mm). Different Flow rates.

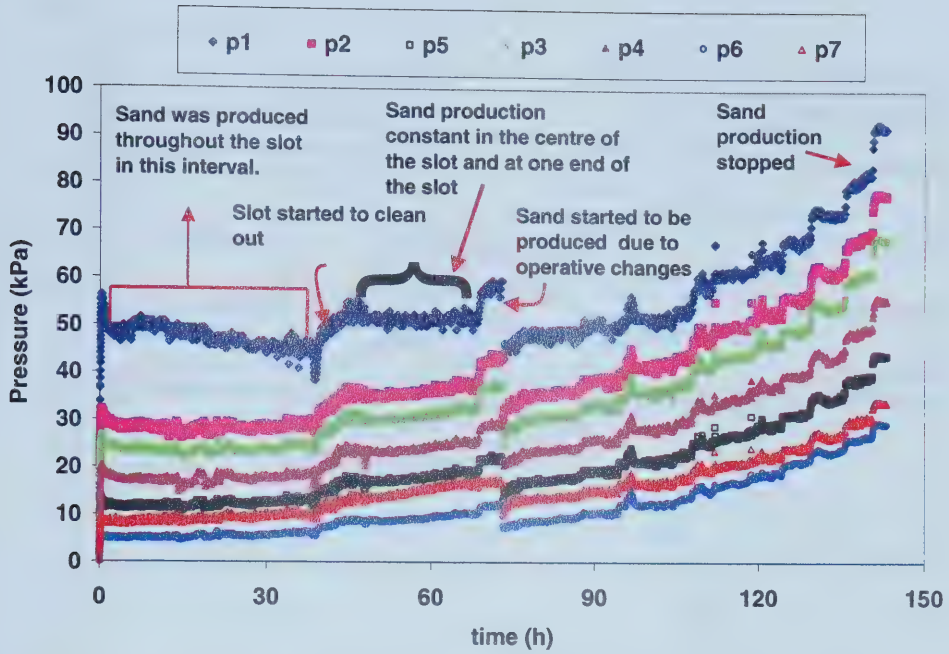

Figure 5.63: Pressure versus time for run 5. Sil-1 sand, slot size: 0.028 in (0.71 mm). Flow rate: 50 cm^3/h.

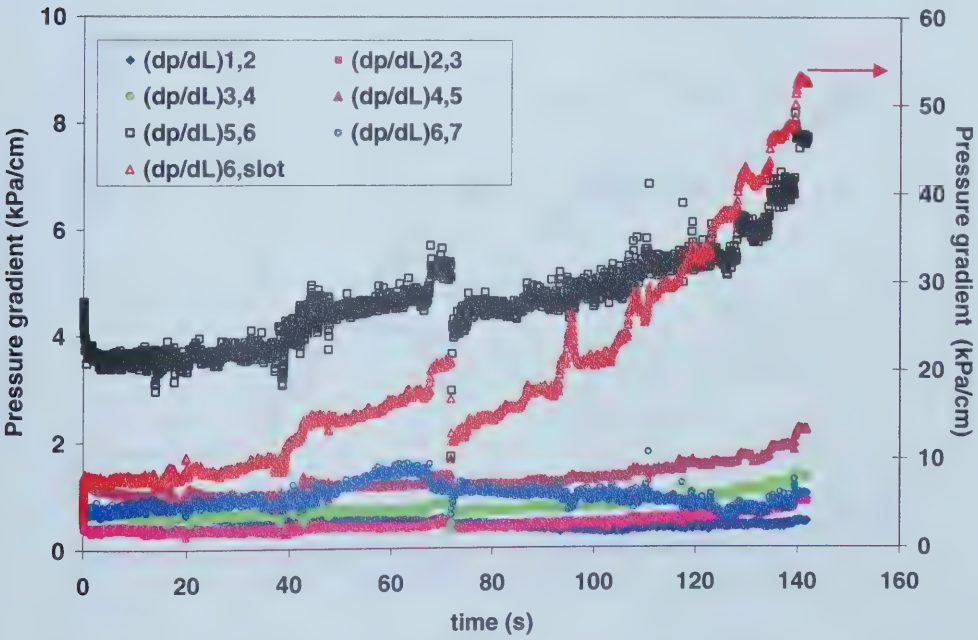

Figure 5.64: Pressure gradients versus time for run 5. Sil-1 sand, slot size: 0.028 in (0.71 mm). Flow rate: 50 cm^3/h.

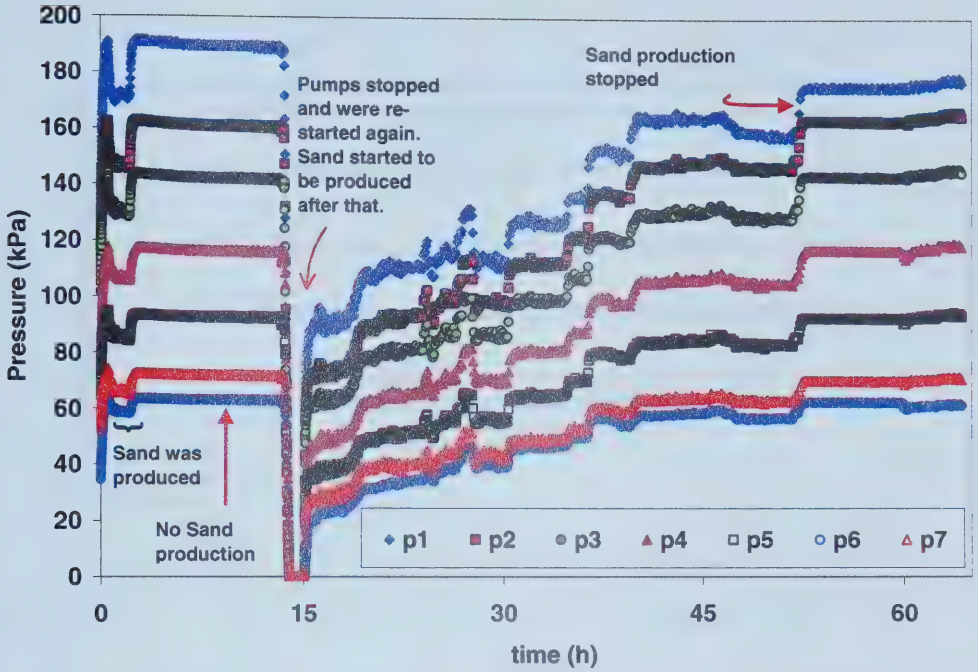

Figure 5.65: Pressure versus time for run 5. Sil-1 sand, slot size: 0.028 in (0.71 mm). Flow rate: 100 cm^3/h.

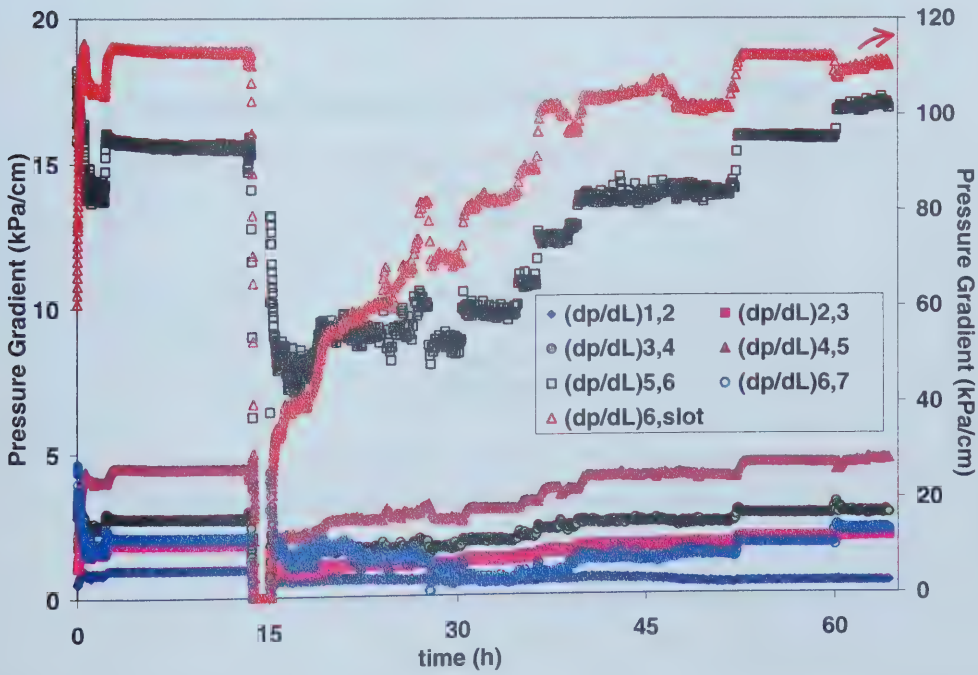

Figure 5.66: Pressure gradients versus time for run 5. Sil-1 sand, slot size: 0.028 in (0.71 mm). Flow rate: 100 cm^3/h.

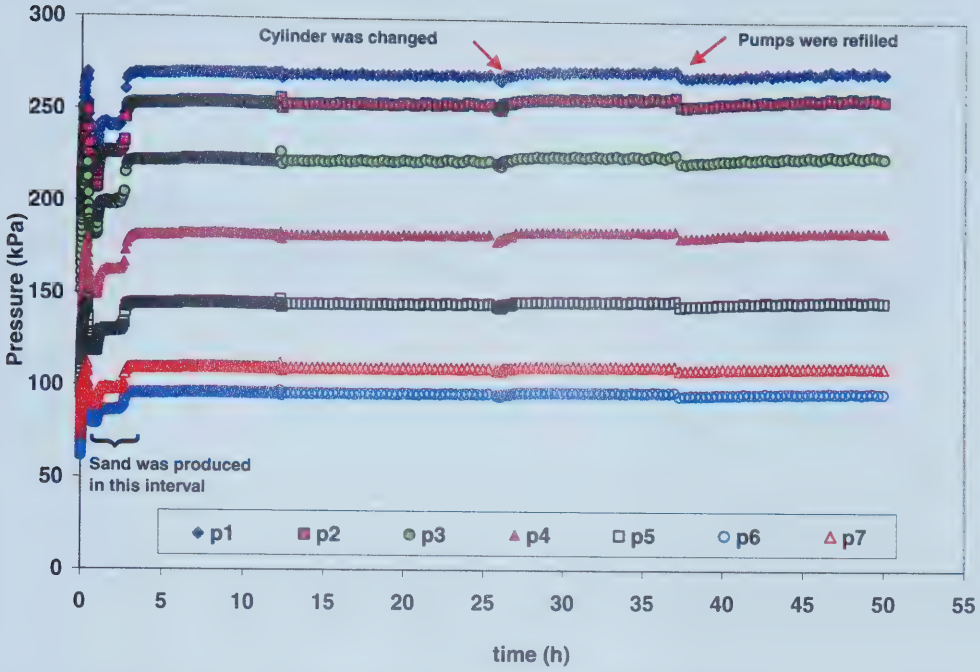

Figure 5.67: Pressure versus time for run 5. Sil-1 sand, slot size: 0.028 in (0.71 mm). Flow rate: 150 cm^3/h.

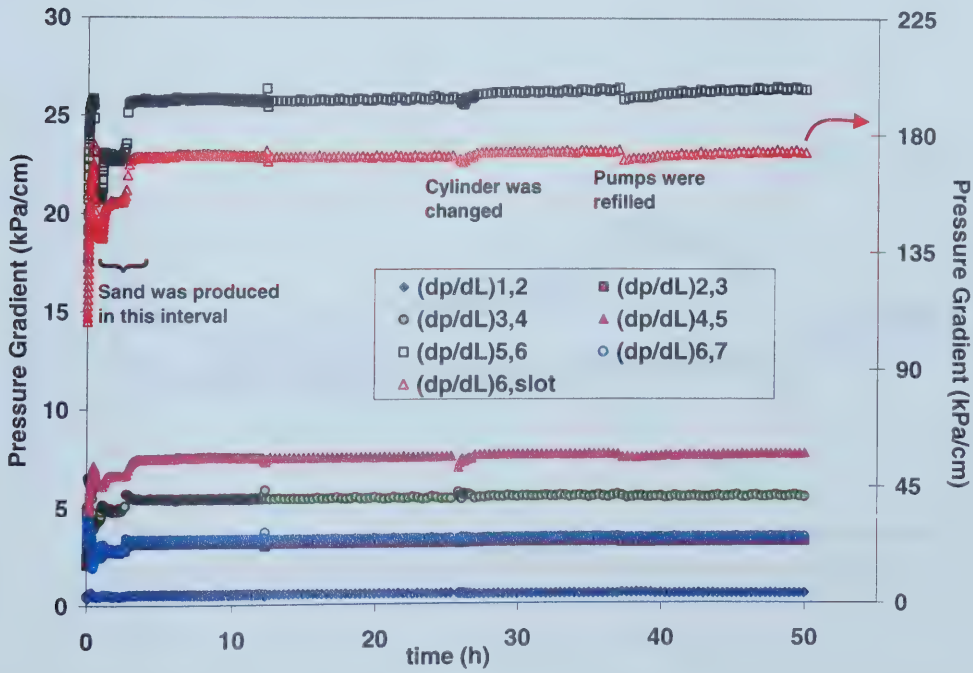

Figure 5.68: Pressure gradient versus time for run 5. Sil-1 sand, slot size: 0.028 in (0.71 mm). Flow rate: 150 cm^3/h.

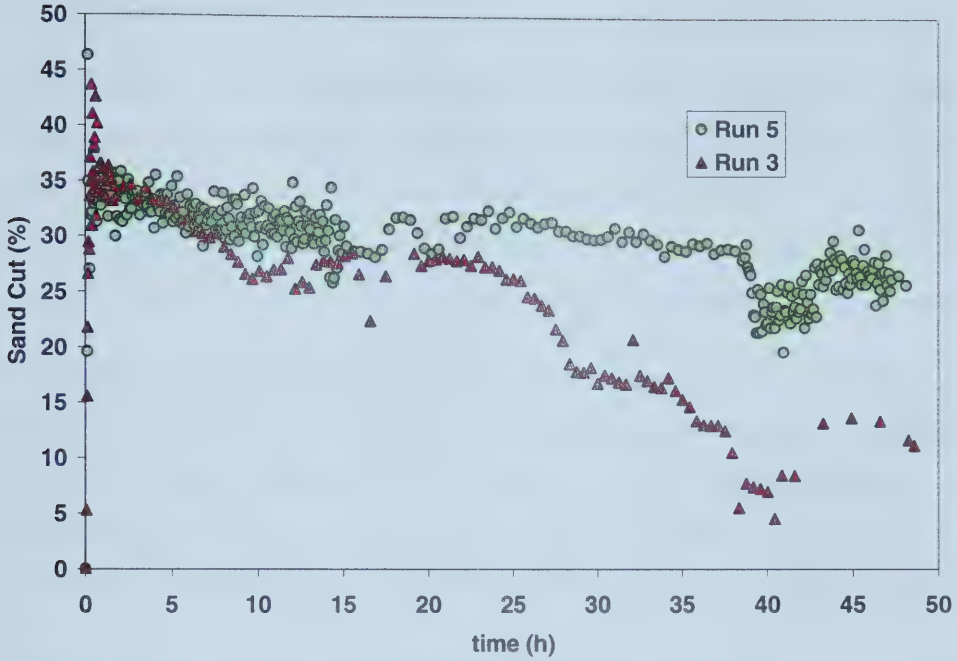

Figure 5.69: Sand cut versus time. Runs 3 and 5. Sil-1 sand. Slot size: 0.028 in (0.71 mm). Flow rate 50 cm^3/h.

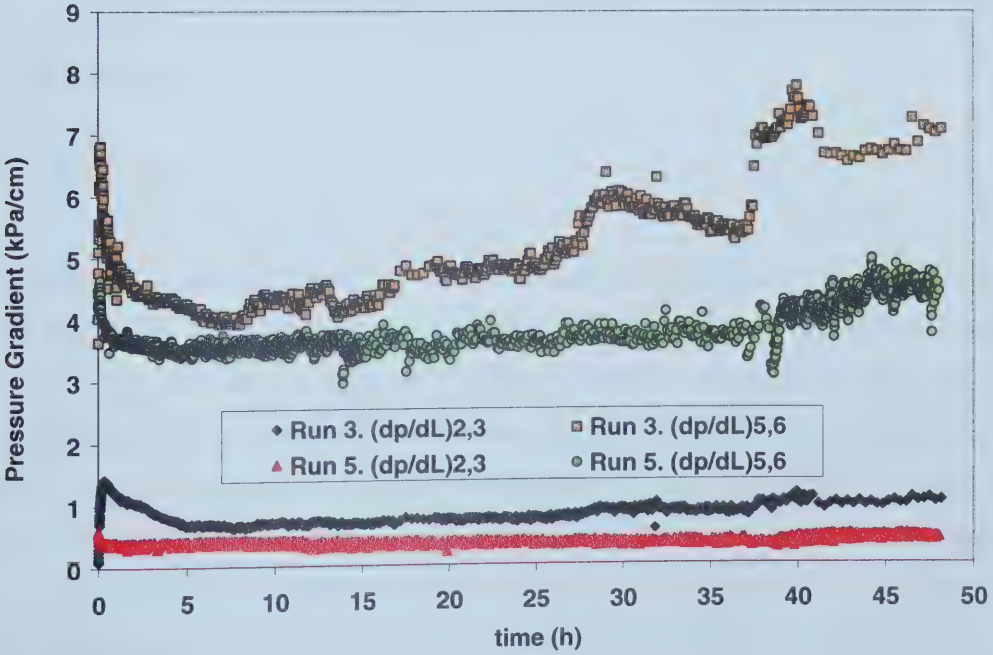

Figure 5.70: Pressure gradients versus time. Sil-1 sand. Slot size: 0.028 in (0.71 mm). Flow rate 50 cm^3/h.

5.3 Thin Sections

These qualitative experiments were designed to visually investigate the structure that might form in and around the slot when sand production stops. Sand packs were prepared using the following sands: Sil-1 sand, Husky sand and glass beads with less fines. Two slot sizes: 0.022 in(0.56 mm) and 0.028 in (0.71 mm), where used with the Sil-1 sand. One slot size, 0.028 in (0.71 mm), was used with Husky and glass beads sand packs.

First, gravity tests were performed under dry conditions with the sands and slot sizes mentioned above. Then, the sand packs were impregnated with epoxy to reveal porosity changes after sand production. Thin sections of the solidified sand packs were cut perpendicular to the slot lengtht. The prepared thin sections were examined using a petrographic microscope to observe porosity changes in the proximity of the slot.

A detailed description of the procedure used in these tests can be found in section 4.2.3. The characteristics of the sand packs used are presented in table 5.25. The thin section photomicrographs are presented in Figure 5.71-5.83. The photomicrographs are framed with a scale from A to R in the horizontal direction and a scale from 1 to 12 in the vertical direction.

5.3.1 Sil-1 sand

The photomicrographs of the thin sections in Figure 5.71-5.74 show the arches/bridges along the 0.022 in (0.56 mm) slot. Two different arches are shown in these views (Figure 5.71 and 5.72). The arch in Figure 5.71 is approximately 3 times wider and 3.5 times higher than the one in Figure 5.72. The photomicrographs in Figure 5.73 shows the same arch as in Figure 5.71 but at a lower magnification to capture the complete arch, the surrounding area and the slot. The dark circles in Figures 5.71 and 5.73 within the spherical arch are due to gas bubbles migration from the exit of the slot when the flow of epoxy was stopped. The migration of bubbles from the outlet would not likely disturb the arches.

The arch presented in Figure 5.71 is approximately 1.6 mm high and 2.2 mm wide. The arrangement of the grains above the arch seems to be similar to that observed further away from the slot (Figure 5.74).

Based on the above observations, it appears that different arch structures can be formed along the slot. These structures might have different stabilities as reported in the literature. The arches with larger radii are less stable [31]. This may explain why after sand production has stopped, burst of sand are sometimes observed only in certain parts of the slot.

Figures 5.75-5.77 show photomicrographs of the thin sections from the Sil-1 sand pack with the 0.028 in (0.71 mm) slot. Two important observations can be made from these photomicrographs. The first is that higher porosity paths (I 4-5 in figure 5.75 for example) are observed in the vicinity of the slot (Figure 5.75, F-M 1,7) compared with the bulk of the sand (Figure 5.75, A-B 1,7 and P-R 1,7). The second important observation is that grain bridging is observed inside the slot (Figure 5.76, I-J 4,6). Consequently, it might be also possible that sand production stopped due to sand bridging. Figure 5.77 shows the early stage of arch forming.

5.3.2 Husky sand

Two sand packs were prepared with Husky sand using a 0.028 in (0.71 mm) slot in order to verify the reproducibility of this type of test. Sand arches were observed in all thin sections prepared from the Husky sand packs (Figures 5.78, sand pack II and 5.79, sand pack I). They were usually of similar size and composed of multiple grains of different size and morphology. Enhanced intersticial spaces between grains around the slot can be clearly observed in Figure 5.78 (A-C 4,8 for example) in comparison with the sand bulk (Figure 5.80, O-R 6-10, for example). The slot might be plugged by the biggest grains as shown in Figure 5.81 (I-K 7,11). This means that besides sand arching or bridging, slot plugging might contribute to stop sand production. Again, higher porosity is observed in the vicinity of the slot, which is plugged by a larger grain than the slot width.

The importance of slot plugging in decreasing sand production will depend, naturally, on the percentage of large grains in the sand (D_{90} and higher), how they are distributed in the sand pack and when they reach the slot.

These observations indicates that the presence of the larger sand grains should be taken into account during the selection of the slot.

All these considerations (sand arching, bridging and plugging) contribute to the randomness of the sand production process.

5.3.3 Glass beads less fines (GBLF)

Wide arches were observed in the thin sections cut from the glass bead less fines sand pack. An example of these arches is presented in Figures 5.82 and 5.83.

It is interesting to observe the symmetry of the arch and the combination of different size particles in the arch. Furthermore, a large particle is resting at the top of the sand structure. There is no evidence of higher porosity around the arch structure as was observed with the previous sand packs.

Summarizing, for a given sand, different mechanisms affect the termination of sand production: arch formation, grain bridging or grain(s) plugging. A high porosity region might be located in the vicinity of the slot.

Table 5.25: Epoxied cores characteristics

	Sil-1		Husky		GBLF
Slot size: in (mm)	0.022 (0.56)	0.028 (0.071)	0.028 (0.071)	0.028 (0.071)	0.028 (0.071)
$V_{epoxy\ injected}$ (cm^3)	308.0	321.8	247.3	261.8	316
Pore Volume (cm^3)	125.1	134.59	125.00	108.3	95.01
ϕ	36.2	37.2	39.87	38.5	34.3

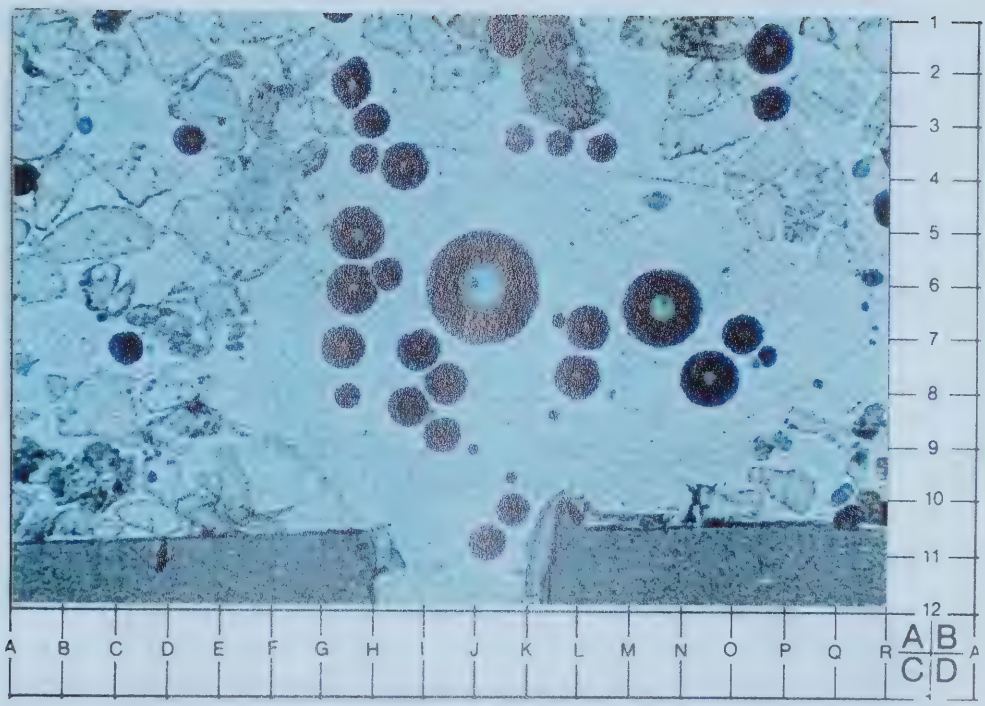

Figure 5.71: Microphotograph of the Sil-1 sand thin section showing a wide arch structure. Slot size 0.022 in (0.56 mm). Magnification: 32x

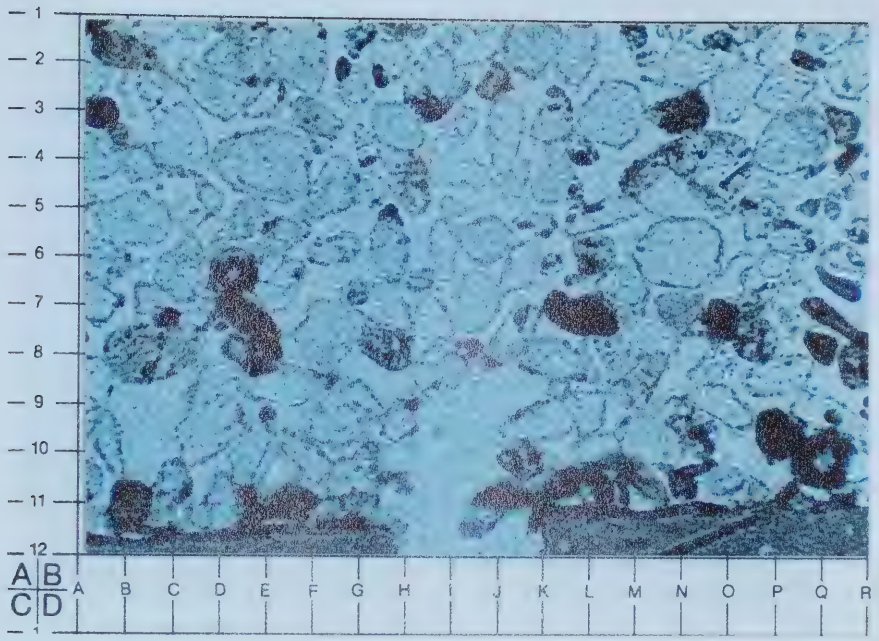

Figure 5.72: Microphotograph of the Sil-1 sand thin section showing a narrow arch structure. Slot size 0.022 in (0.56 mm). Magnification: 32x

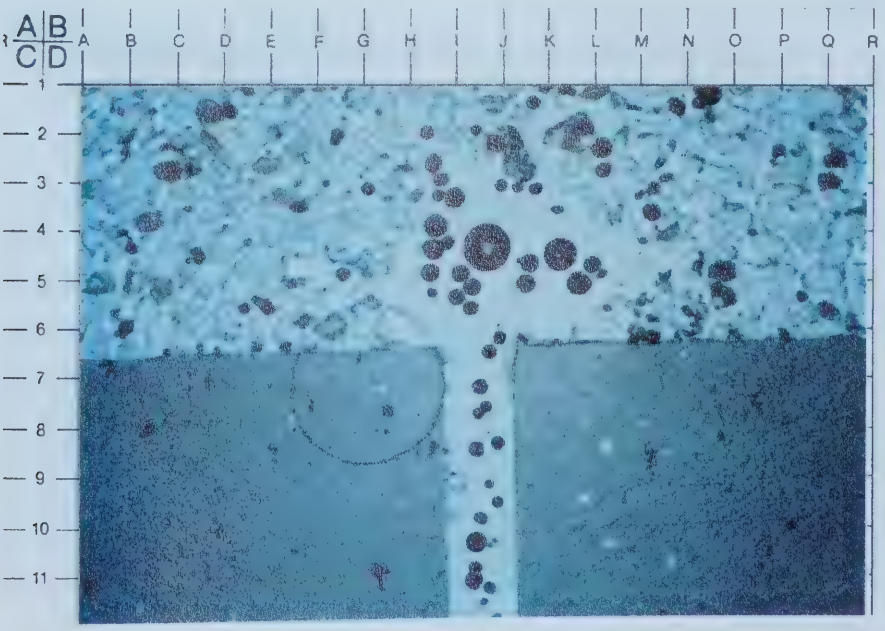

Figure 5.73: Microphotograph of the Sil-1 sand thin section showing the arch and surrounding area. Slot size 0.022 in (0.56 mm). Magnification: 16x

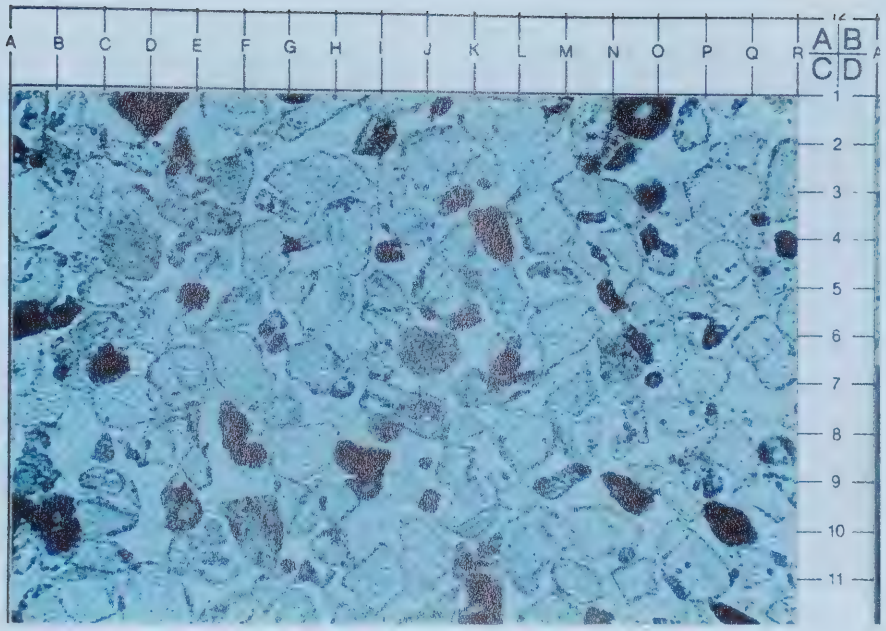

Figure 5.74: Microphotograph of the Sil-1 sand thin section. Sand bulk above the arch. Slot size 0.022 in (0.56 mm). Magnification: 32x

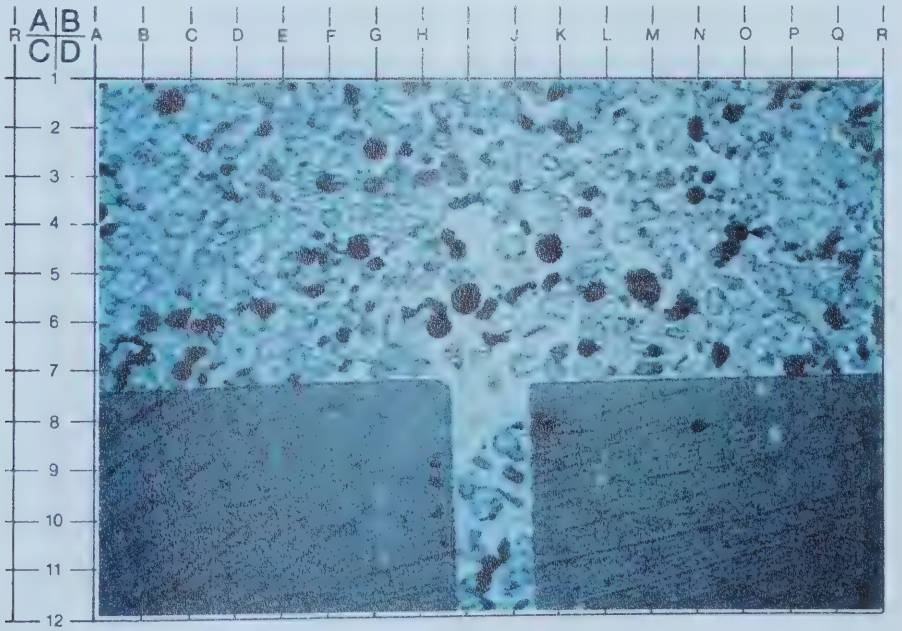

Figure 5.75: Microphotograph of Sil-1 sand. Thin section showing gaps in the sand structure in the vicinity of the slot. Slot size: 0.028in (0.71mm). Magnification: 16x

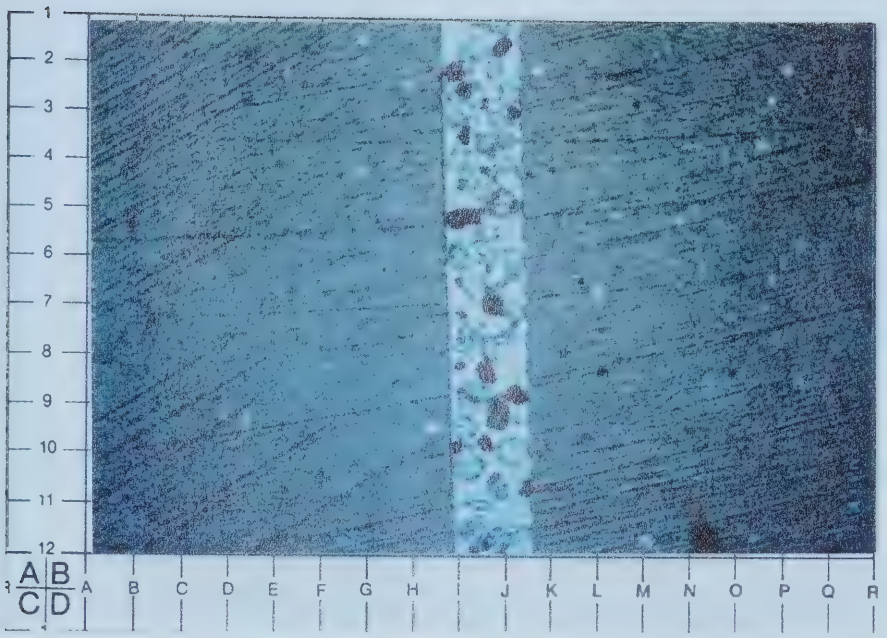

Figure 5.76: Microphotograph of the slot showing grains bridging. Sil-1 sand thin section. Sand Slot size 0.028 in (0.71 mm). Magnification: 16x

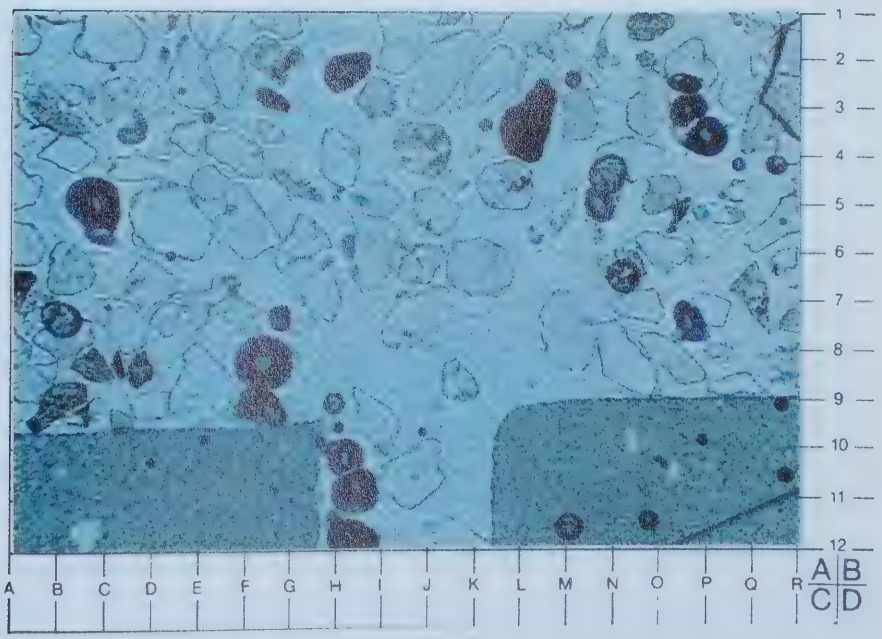

Figure 5.77: Microphotograph of the Sil-1 sand thin section. Incipient sand arch. Slot size 0.028 in (0.56 mm). Magnification: 32x

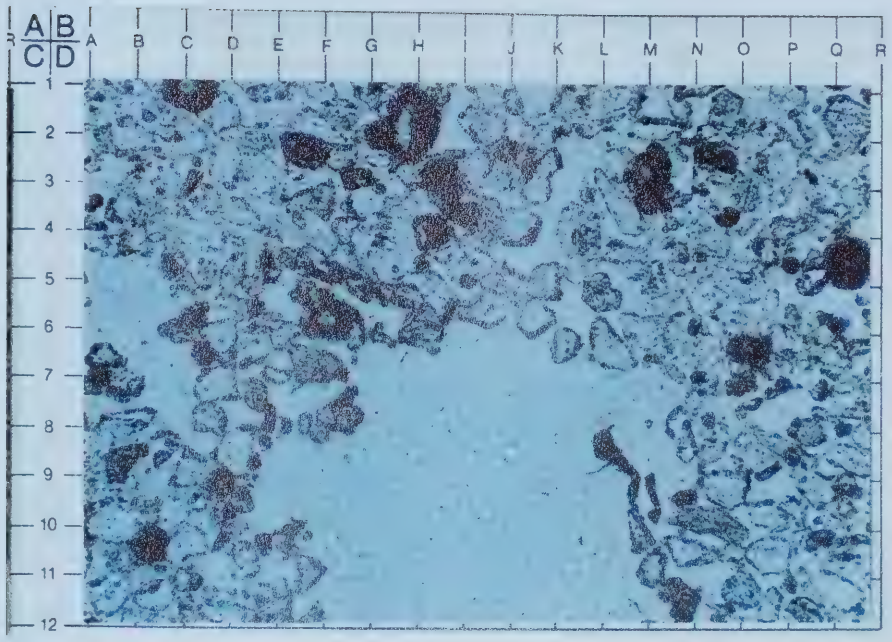

Figure 5.78: Microphotograph of a Husky sand thin section. Arch 1. Slot size 0.028 in (0.56 mm). Magnification: 32x

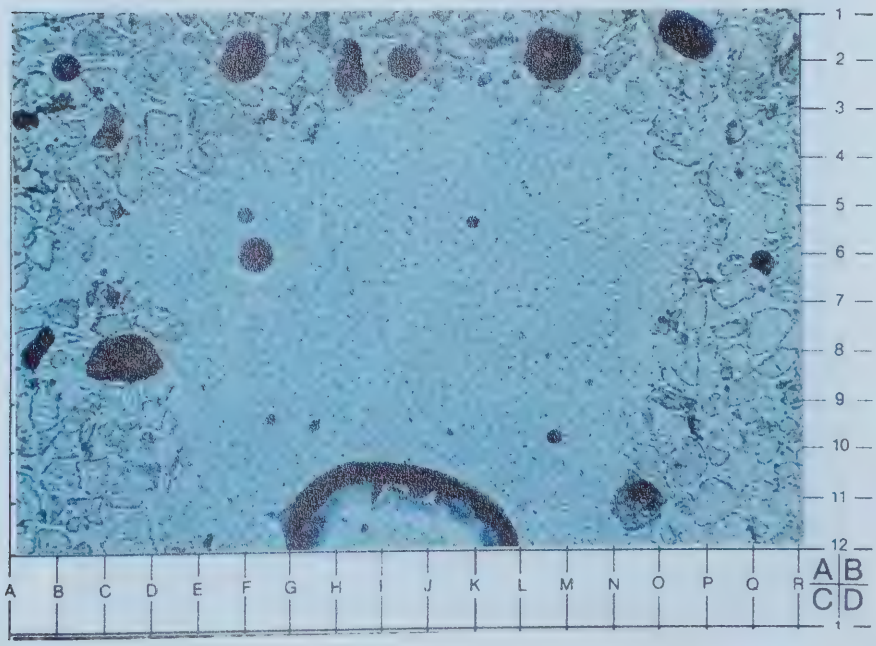

Figure 5.79: Microphotograph of a Husky sand thin section. Arch 2. Slot size 0.028 in (0.56 mm). Magnification: 32x

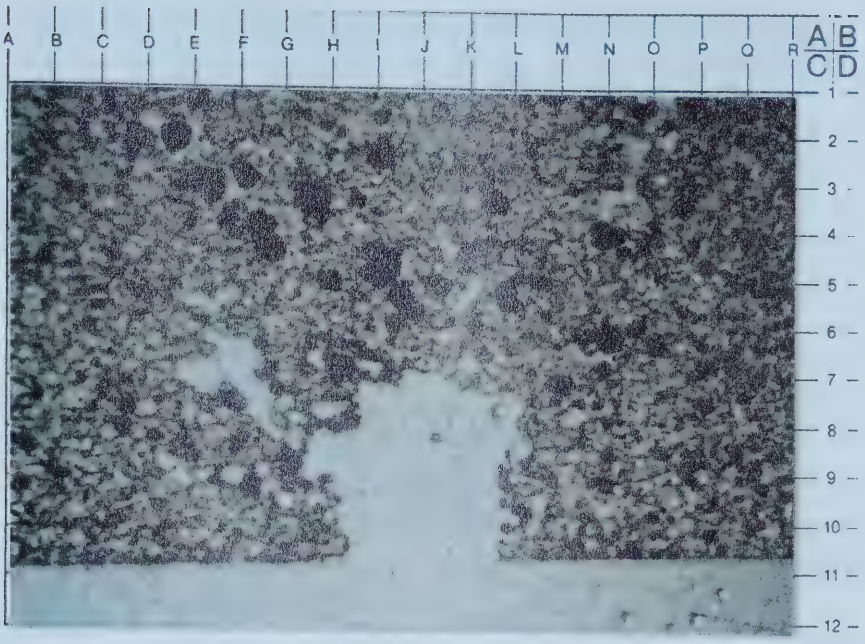

Figure 5.80: Microphotograph of a Husky sand thin section. Arch 1, lower magnification. Slot size 0.028 in (0.56 mm). Magnification: 16x

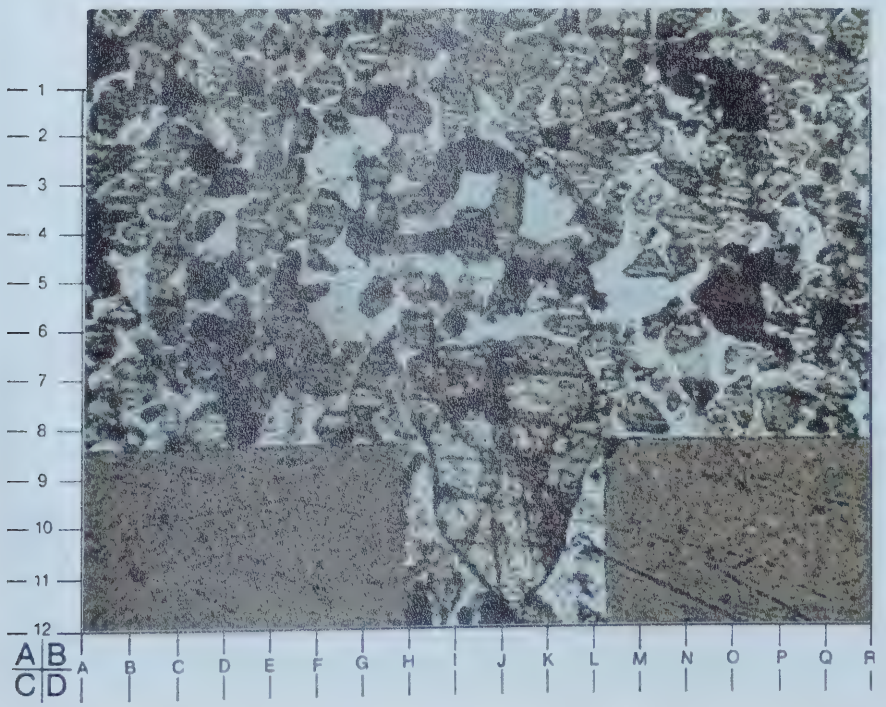

Figure 5.81: Microphotograph of a Husky sand thin section. Sand grain plugging the slot. Slot size 0.028 in (0.56 mm). Magnification: 32x

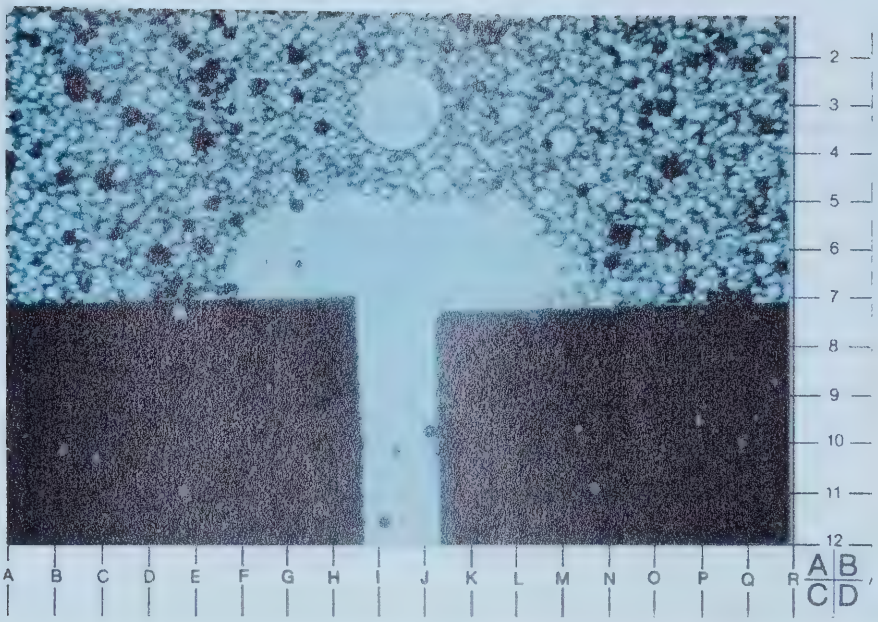

Figure 5.82: Microphotograph of a glass beads with less fines sand. Arch structure and surrounded areas. Slot size 0.028 in (0.56 mm). Magnification: 16x

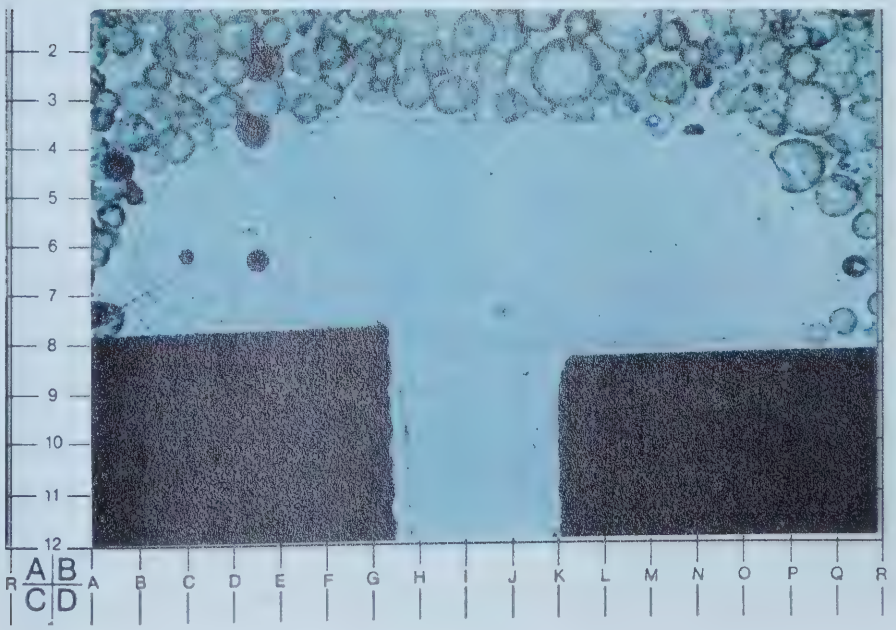

Figure 5.83: Microphotograph of a glass bead with less fines sand. Arch structure at higher magnification. Slot size 0.028 in (0.56 mm). Magnification: 32x

5.4 X-ray Computed Tomography

In order to investigate the effect of sand production on the porosity distribution within the sand pack, a set of CT scanner experiments was performed. Two kinds of samples were examined: dry sand packs and epoxied sand packs.

A detailed description of the procedure followed to perform the tests was given in section 4.2.4.

5.4.1 Dry Sand Tests

Three sands were evaluated: Sil-1, Husky and glass beads with less fines. Two different types of scans were performed, full 2D radiographic imaging and computed tomography (CT) scans. The 2D images were taken with the X-ray penetrating either perpendicular or parallel to the slot length These images enclosed the entire sand pack. The CT images (slices) are cross sections of the pack taken at different heights, usually, 0.1 cm, 1 cm and 5 cm. In this way, the extent of the porosity changes in the sand pack were observe. Table 5.26 summarizes the total quantity of sand produced during these experiments

5.4.1.1 Sil-1 Sand

Figure 5.84 and 5.85 show 2D and cross sectional CT images of the Sil-1 sand pack. In this experiment, approximately 65 % of the pack was produced (Table 5.26). This large production of sand provoked porosity changes in different regions of the sand pack as shown by the 2D images (Figure 5.84). It seems that the largest changes (between 1.6 to 6.4 %) occur in one of the lateral sides of the sand pack (Figure 5.84 (b)). This indicates that sand was preferentially produced from this side. Smaller changes (between 0 and 1.6 %) occurred in the other zones. Furthermore, the porosity alteration appears to be more uniform in the vicinity of the slot (Figure 5.84 (b)). Figure 5.84 (a) shows clearly the convergence of the flow of sand into the slot. The height of the pack after sand production was approximately 10 cm compared to 34.8 cm at the start of the test.

The CT slices (Figure 5.85) support the observations presented by the 2D images. In the slice taken 1 cm above the slot (Figure 5.85 (a)) it is apparent that the changes occur preferentially in one side of the pack, although scattered changes are also observed in the whole cross sectional area. The arrows in Figure 5.85 (a) point out spots with the highest porosity changes (approximately 13%). This could be indicative of the presence of preferential channels in this area, however no further support for this hypothesis was found in any other of the images analyzed. Less porosity changes were observed as the distance from the slot increased (Figure 5.85 (b)).

In summary, the 2D and CT images show that porosity changes occur after sand production. The changes seem to be more uniform in the vicinity of the slot and have the tendency of decreasing further away from the slot.

5.4.1.2 Husky Sand

A very uniform sand pack was observed in the 2D images presented in Figure 5.86, with some localized changes in the vicinity of the slot. This result was somewhat expected since only 24.2 g of sand (approximately 0.7 % of the sand pack) was produced in this experiment. The porosity increases observed in the vicinity of the slot were measured to be mainly between 2.7 to 5.4 %. The variations were present along the slot (Figure 5.86 b) and extended at least 3 mm above it (Figure 5.87a). The porosity increases did not go further than 1 cm inside the pack (Figure 5.87b). A void space with semi-cylindrical shape was observed (Figure 5.86 (a)). This was associated with the presence of an arch in the pack.

5.4.1.3 Glass Beads with Less Fines

Sand production for this test was approximately 1.2 % of the sand pack (Table 5.26). The 2D images indicated that small changes occurred along the sand pack (Figure 5.88). These small changes were mainly located in the area around the slot. In the zone where changes were observed, the porosity variation was estimated to be between 1 to 16.4 %.

The cross section CT slices (Figure 5.89) show more clearly the changes in the pack. As mentioned previously, the most noticeable variations were observed in the area next to the slot (1 mm above). The variations are scattered over the entire cross sectional area with the area right above the slot showing the largest changes (8.2 - 16.4 %). Further from the slot, in the vertical direction, changes become smaller in magnitude (4.1 to 8.2 %).

In general, variations in the porosity of the pack occurred due the sand production. This variation was located mainly in the area around the slot (1 mm above). These variations were located mainly in the area around the slot (1 mm above). The changes decreased with increasing vertical distance from the slot. From the sectional views at 5 cm above the slot, it appears that the Sil-1 (Figure 5.85) sand showed the most changes, followed by the glass beads with lower fines (Figure 5.87) and finally the Husky sand with few changes (Figure 5.89). The larger changes for the Sil-1 sand may be due to the larger quantity of sand produced.

5.4.2 Epoxied Sand Packs

CT cross sectional images were taken of the epoxied sand packs prepared for the thin section tests. The combination of both results (CT images and thin sections) helped to explain the mechanisms involved in the sand production process.

It is important to note that the results obtained from the CT images of the epoxied sand packs cannot be considered as accurate as those obtained in the dry sand tests. As explain in section 4.2.4, a CT scan of a sand pack is normally taken before sand production. In the epoxy test, the sand pack was not flooded with epoxy before sand production started. Therefore, a scan of the upper part of the core was taken as a reference of initial conditions. It was assumed that the disturbance produced by the sand production in this part of the pack was small. This was considered a reasonable assumption since not much sand was produced (less than 10 %) in any of the tests. A scan of the sand free section of epoxied core in Figure 4.22 was also required to calculate the porosity. The entire core was scanned and selected slices are presented.

The Sil-1 sand pack prepared using the 0.028 in (0.71 mm) slot size is not reported in this section since the upper part of the core was irregular in shape and could not be used as a reference for the initial conditions.

5.4.2.1 Sil-1

Figure 5.90 presents the CT images of the epoxied Sil-1 sand pack from the test performed with the 0.022 in (0.56 mm) slot size. The main disturbances occurred around the slot as shown in Figure 5.90(a). These disturbances were still observed 5 mm above the slot (Figure 5.90(b)). The estimated porosity changes were in the order of 5 to 10 %. The changes become less visible when the distance from the slot in the vertical direction increased (Figure 5.90c and d).

In comparison, no visible changes in porosity within the sand pack were observed in the thin sections cut from this pack. Possible explanations are: 1) the thin sections were taken from a zone where the variations were not as important as in other parts of the pack. 3) The CT images overestimated the changes occurring in the sand pack. This last possibility is more unlikely since more area is swept in the CT scanner measurement while the thin sections are taken from selected areas of the core.

Figure 5.91 shows histograms of the porosity within cross sectional slices of the core. The percentage of the surface area of the slice within the porosity increase range (x axis) is shown. Approximately less than 20 % of the surface area in each slice shows any change in porosity.

The most significant porosity changes are in the range of 5-15 % for the Sil-1 sand. The slice 5 mm above the slot presented the most variation. At greater distances, the percentage of porosity changes and affected area decreased.

There is not enough evidence to explain why the CT slice 1 mm above the slot presented less changes than the CT slice 5 mm above. Although the area affected in this slice was the smallest, more contrast was observed in the porosity changes.

5.4.2.2 Husky sand

Two epoxied sand packs were prepared with the Husky sand. Both sand packs were X-ray CT scanned yielding the images presented in Figure 5.92-5.93. The slices taken at 1 mm above the slot were those, which showed the biggest changes in porosity. These changes were concentrated in the area around the slot. As in the Sil-1 case, a histogram for the Husky sand pack II was created (Figure 5.94). The largest changes were between 5-15 % in porosity. The changes were observed within 30 % of the total area of the CT slice.

The effect of sand production on the porosity of the pack became smaller as the vertical distance from the slot increased. Thus at 3 cm from the slot, the maximum variation was approximately 5-10 % in porosity. Only 10 % of the cross sectional area showed porosity changes. The same tendency was observed for both sand packs.

The CT scan observations agree with the observations of the thin sections microphotographs in terms of the enhanced porosity being located around the slot area (Figure 5.81 Section 5.3.2).

The reproducibility of the test was considered to be reasonable since similar results were observed for the two packs prepared with the Husky sand.

5.4.2.3 Glass beads

Figure 5.95 presents the CT cross sectional slices taken of the glass beads sand pack. Practically no changes in the sand pack porosity can be observed in the different slices. Only one spot in the slice scanned at 1 mm above the slot seems to be significant. The porosity change was estimated to be between 5-10 %. The same spot is observed in the CT image taken 2 mm above the slot (Figure 5.95b). This localized porosity increase was not observed in the histogram (Figure 5.96). The histogram at 1 mm and 2 mm were virtually the same. This indicates that, a more detailed histogram of the images is required to detect smaller porosity changes. Less intense changes were observed when the sand pack was scanned at 5 mm and 1 cm above the slot (Figure 5.95). These results agree

with those observed in the thin section tests where a very uniform pack was observed above the arch.

It is interesting to note that although approximately the same quantity of sand was produced during the tests, more changes were observed in the Husky sand packs than in the glass beads sand pack (Figure 5.92 and Figure 5.95). A similar result was observed in the microphotographs of the thin sections. It is important to remember that the glass beads used in this test have the same D_{50} than the Husky sand but lesser fines. It is believed that the fines might be preferentially produced during and after the arch formation leaving more space empty inside the porous matrix which is translate in an increase in the porosity values.

Also, as explain in section , the Husky sand shows more dilation (volume increase), and therefore more increase in porosity when sheared since this sand is more angular than the glass beads.

Summarizing, X-ray CT images showed that porosity changes occur in the pack, specifically in the area near the slot, when sand production takes place. This change depends on the quantity of sand produced and on the morphology of the sand.

A good agreement was found between the thin section observations and the CT scanned images taken to the core before the thin section preparations.

Table 5.26: Dry CT scanner tests. Characteristic of the sand pack and sand produced

Sand	Initial Porosity	Initial mass in the pack (g)	Sand Produced (g)	Sand Produced (%)
Sil-1	43.8	3820.00	2500.49	65.5
Husky	47.9	3500.80	24.80	0.7
GBLF	39.8	2764.00	34.02	1.2

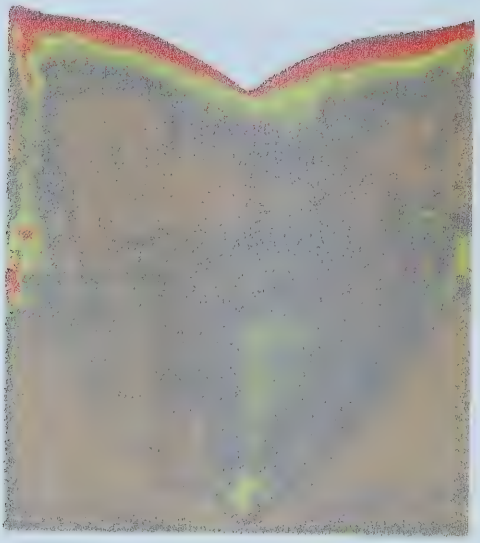

(a) X-ray penetration parallel to the slot

(b) X-ray penetration perpendicular to the slot

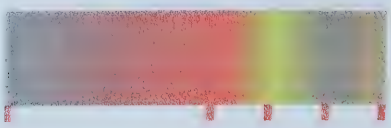

Figure 5.84: Transversal sections of the sand pack. Gravity flow experiments. Sand: Sil-1. Slot size: 0.028 in (0.71 mm).

(a) 1 cm above the slot

(b) 5 cm above the slot

Figure 5.85: Cross section of the sand pack at different heights from the slot. Gravity flow experiments. Sand: Sil-1. Slot size: 0.028 in (0.71 mm).

(a) X-ray penetration parallel to the slot (b) X-ray penetration perpendicular to the slot

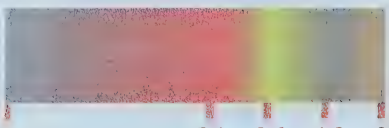

Figure 5.86: Transversal sections of the sand pack. Gravity flow experiments. Sand: Husky. Slot size: 0.028 in (0.71 mm).

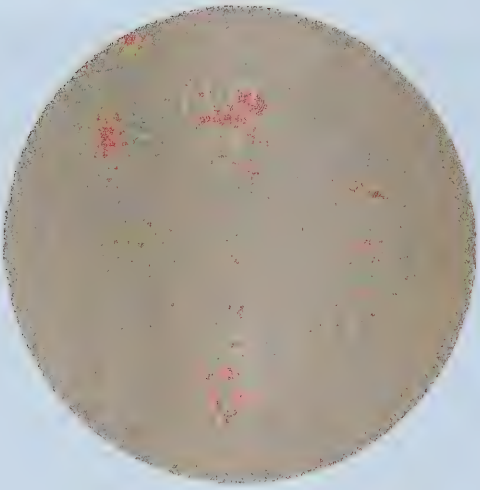

(a) 3 mm above the slot

(b) 1 cm above the slot

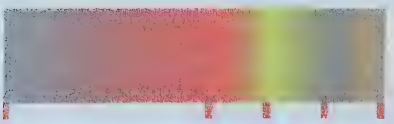

Figure 5.87: Cross section of the sand pack at different heights from the slot. Gravity flow experiments. Sand: Husky. Slot size: 0.028 in (0.71 mm).

(a) X-ray penetration parallel to the slot (b) X-ray penetration perpendicular to the slot

Figure 5.88: Transversal sections of the sand pack. Gravity flow experiments. Sand: Glass Bead less fines. Slot size: 0.028 in (0.71 mm).

(a) 1mm above the slot

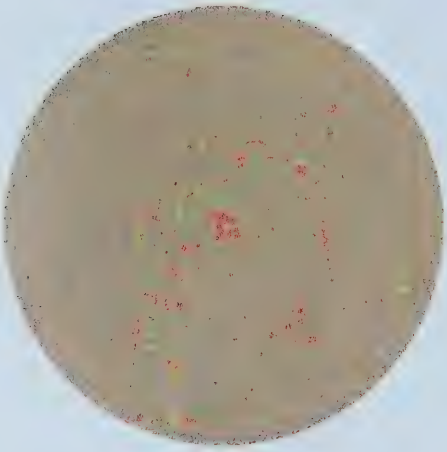

(b) 1 cm above the slot

(c) 5 cm above the slot

Figure 5.89: Cross section of the sand pack at different heights from the slot. Gravity flow experiments. Sand: Glass beads less fines. Slot size: 0.028 in (0.71 mm).

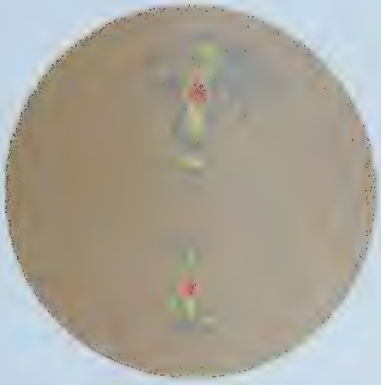

(a) 1mm above the slot

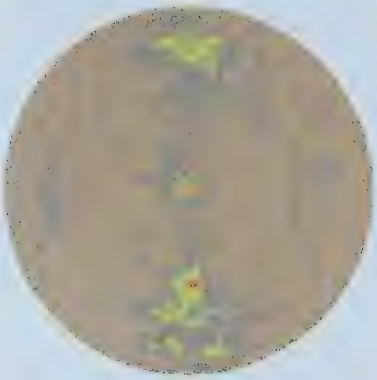

(b) 5 mm above the slot

(c) 1 cm above the slot

(d) 2 cm above the slot

Figure 5.90: Cross section of the sand pack at different heights from the slot. Epoxied core: Sil-1. Slot size: 0.022 in (0.56 mm).

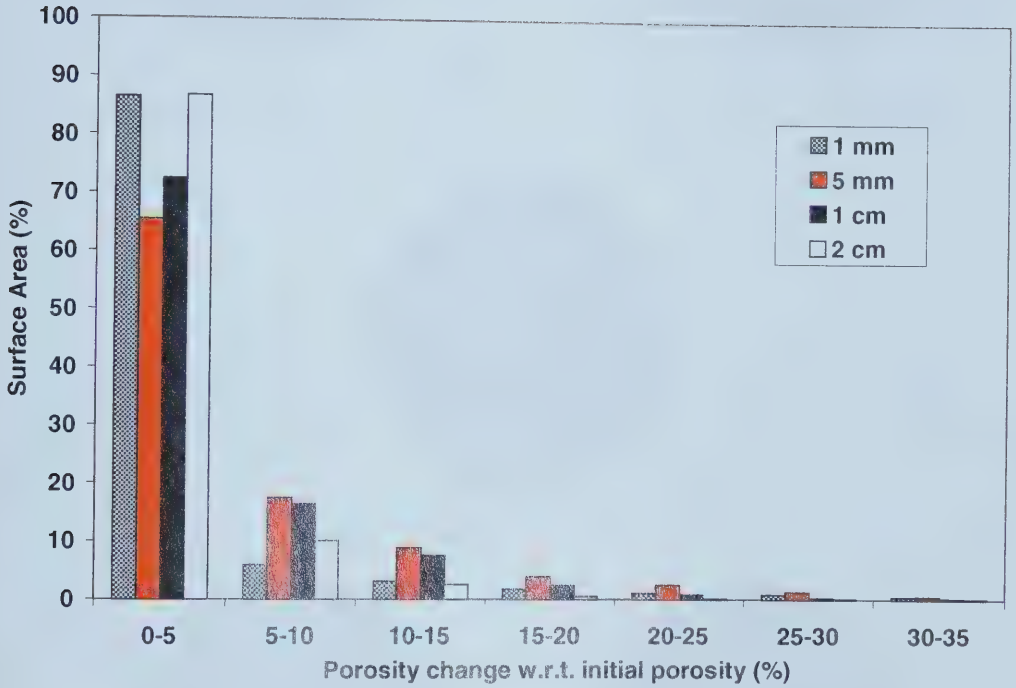

Figure 5.91: Percentage of the surface area of the slice within the indicated porosity change at various locations above the slot. Sil-1. 0.022 in (0.56 mm) slot size

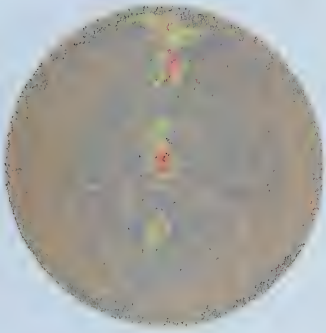

1mm above the slot

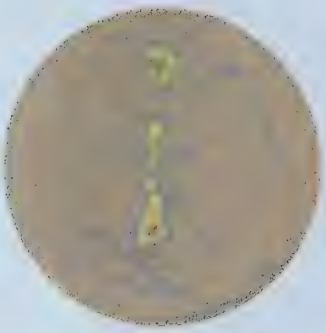

5 mm above the slot

1 cm above the slot

1.5 cm above the slot

3.0 cm above the slot

Figure 5.92: Cross section of the sand pack at different heights from the slot. Epoxied core: Husky sand (I). Slot size: 0.028 in (0.71 mm).

(a) 1mm above the slot

(b) 5 mm above the slot

(c) 1.5 cm above the slot

(d) 3.0 cm above the slot

Figure 5.93: Cross section of the sand pack at different heights from the slot. Epoxied core: Husky sand (II). Slot size: 0.028 in (0.71 mm).

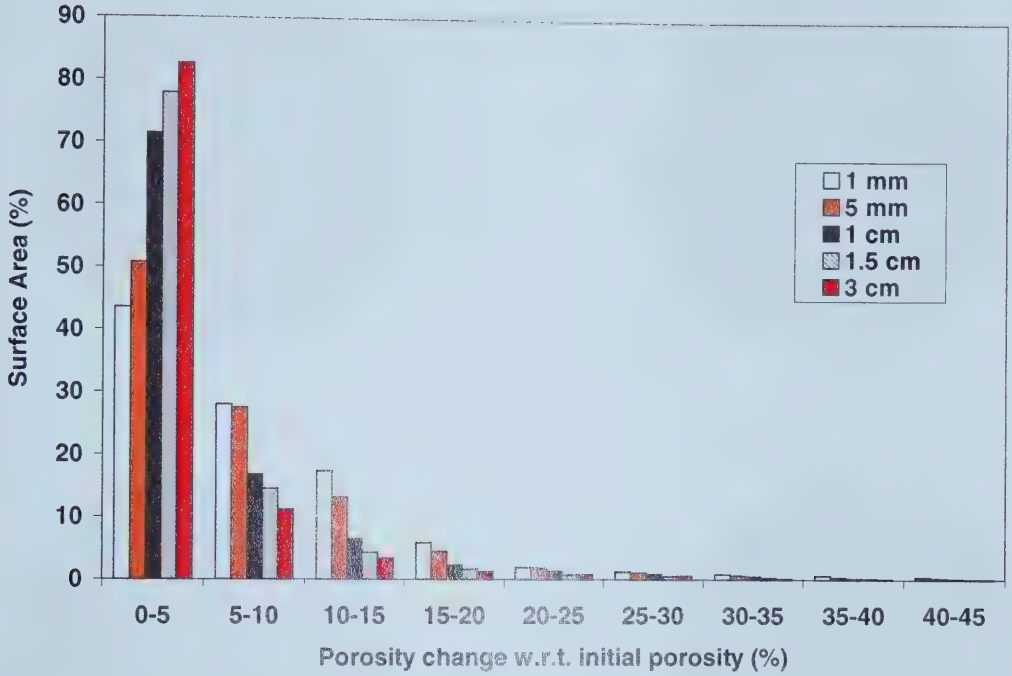

Figure 5.94: Percentage of the surface area of the slice within the indicated porosity change at various locations above the slot. Husky sand. 0.028 in (0.71 mm) slot size.

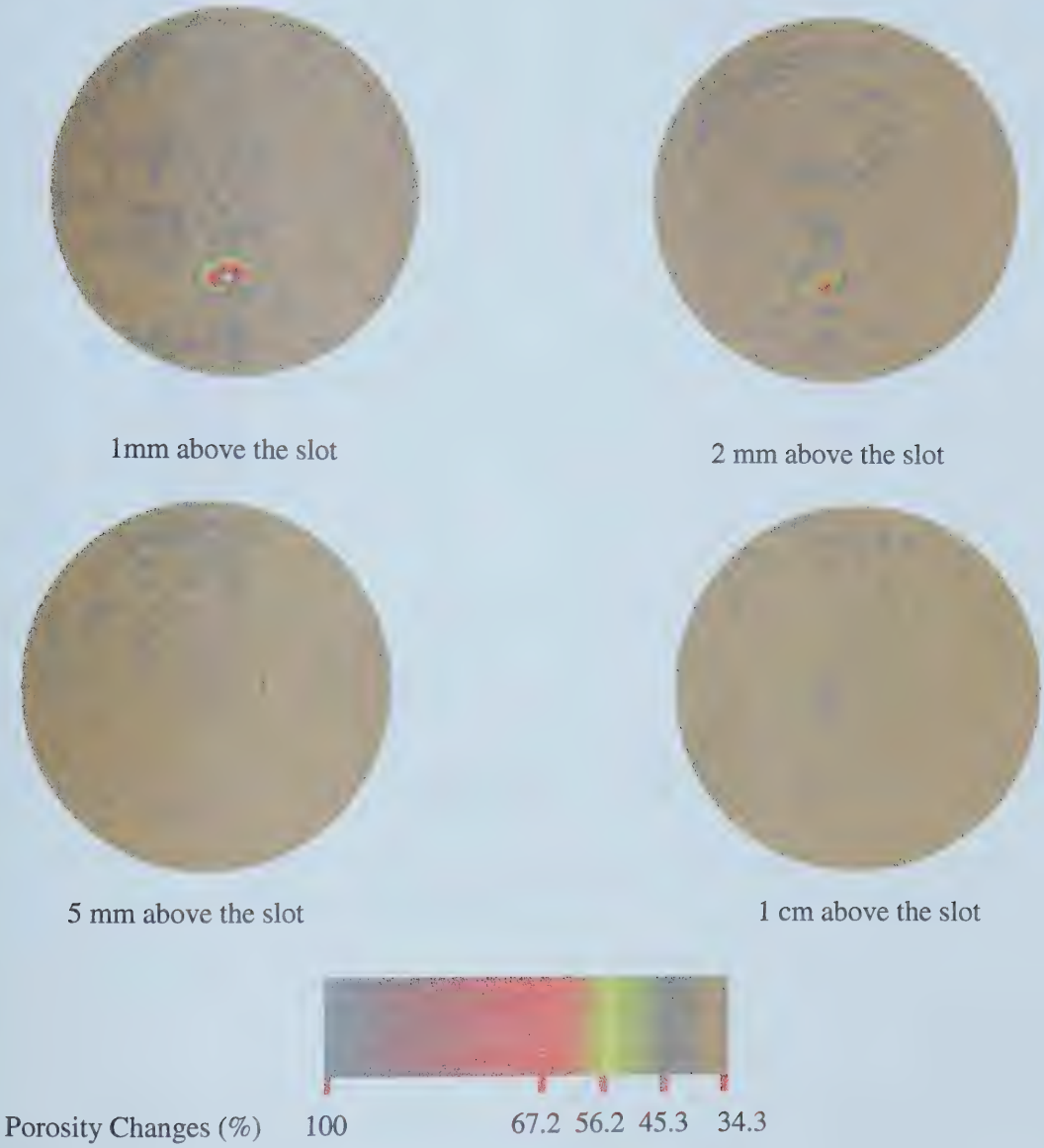

Figure 5.95: Cross section of the sand pack at different heights from the slot. Epoxied core: glass beads less fines. Slot size: 0.028 in (0.71 mm).

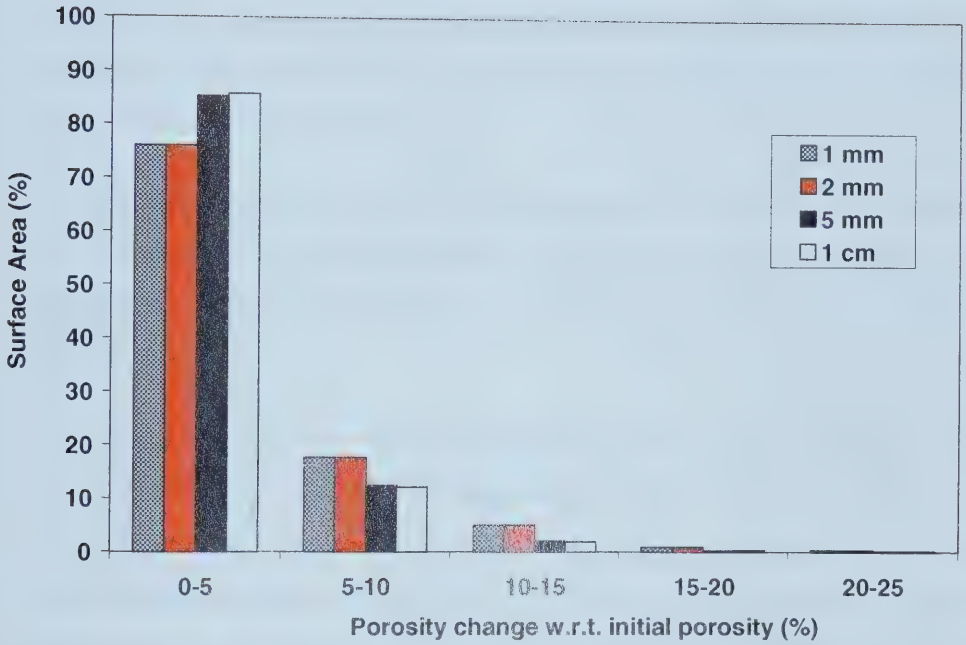

Figure 5.96: Percentage of the surface area of the slice within the indicated porosity change at various locations above the slot. Glass Beads. 0.028 in (0.71 mm) slot size

6 Conclusions

Based on the experimental work conducted, the following conclusions can be drawn:

1. For a given oil flow rate, the sand cut in the produced oil and sand mixture decreased with time. Later periods of sand production were shorter in duration and had lower sand cuts. For certain slot sizes, sand production eventually stopped completely even after producing large quantities of sand.

2. In some cases, significant changes in the permeability and porosity were calculated in the vicinity of the slot. The permeability changes were between 20 to 150 % above the initial permeability. The changes in the permeability and porosity were less away from the slot.

3. Sand production behavior is strongly influenced by the arrangement of the sand grains in the vicinity of the slot. These arrangements include sand bridges, arches, or even sand plugs inside the slot. This process is dynamic as the structures can be formed, then destroyed, and reformed, as shown clearly by pressure and pressure gradient data. This dynamic sand production behaviour is strongly corroborated by thin section observations of the sand arrangement around and in the slot and by CT scanner observations of the dilated regions around the slots.

4. Test results show that the angularity of a sand does not have a significant effect on sand production, under the conditions studied, based on comparisons of the sand production behaviour for Husky sand and glass beads for the same slot width, flow rate and particle size distribution.

5. Sand production appears to be a random process. More sand is produced for larger slot sizes.

6. In the air experiments, the higher initial air flow rate lead to higher sand production in a shorter time.

In conclusion, the results obtained in this study indicate that sand production through the slots can be controlled, depending more on the sand grain sorting than on the morphology of the grains or their average diameter. In addition, a sufficient quantity of sand is produced to enhance the permeability around the slots before sand production is stopped.

7 Recommendations for Future Work

1. The effect of the sand size distribution on sand production though slots should be further investigated. Special attention should be given to the highest percentiles of the size distribution.

2. The influence of the initial flow rate on sand production in a horizontal well should be determined using live heavy oil.

3. Experiments should be carried out to examine the effect of porosity in sand production optimization in the presence of live heavy oil.

4. In order to distinguish between the arching and the slot plugging mechanisms in controlling sand production, experiments with undercut slots should be performed.

5. The effect of confining stress on sand production through the slot should be investigated.

8 References

1 TREMBLAY, B., SEDGWICK, G. and VU, D. "A Review of Cold Production in Heavy Oil Reservoirs". Paper 2008 the 10th European Symposium on Improved Oil Recovery, Brighton, UK, August 18-20,1999.

2 TREMBLAY, B., SEDGWICK, G. and FORSHNER, K. "Simulation of Cold Production in Heavy Oil Reservoirs: Wormhole Dynamics". SPE paper # presented at 3538710th Symposium on Improved Oil Recovery, Tulsa OK, April 21-24, 1996.

3 DUSSEAULT, M.B., GEILKMAN, M. and SPANOS T. "Mechanism of Massive Sand Production in Heavy Oils". Paper presented at the 7th UNITAR conference, Beijing,China, 1998.

4 CHARLEZ A. *Rock Mechanics. Petroleum Aplications.* Volume 2. Editions Technip, Paris, 1997.

5 McCAFFREY, W. and BOWMAN, R. "Recent Successes in Primary Bitumen Production". Paper presented at 8th Annual Heavy Oil and Oil Sands Technical Symposium, March 14 1991.

6 LOUGHEAD, D. and SALTUKLAROGLU, M. "Lloidminster Heavy Oil Production. Why So Unusual?". Ninth Annual Heavy Oil and Oil Sands Technical Symposium, Calgary, Canada. March 11, 1992.

7 HUANG, W., MARCUM B., CHASE M.R. and YU C. "Cold Production Of Heavy Oil From Horizontal Wells In The Frog Lake Field". SPE Reservoir Evaluation & Engineering, December, 1998. pp 551-555

8 METWALLY, M. and SOLANKI, S. "Heavy Oil Reservoir Mechanisms, Lindbergh and Frog Lake Fields, Alberta. Part I: Field Observation and Reservoir Simulation". Paper 95-63 presented at the 46th Annual Technical Meeting of the Petroleum Society of CIM, Banff, Alberta, Canada. May 14-17, 1995.

9 HU, C., LIU, X., WANG, J., SONG, Z., FAN, Z. and YANG F. "Cold Production of Thin-Bedded Heavy Oil Reservoir in Henan Oilfield". SPE paper 50885 presented at the SPE International Conference And Exhibition, Beijing, China, 2-6 November 1998.

10 SMITH, G. "Fluid Flow and Sand Production in Heavy–Oil Reservoirs Under Solution-Gas Drive". SPE Production Engineering,. V 3, No 2, May 1998, pp169-180.

11 MAINI, B. "Foamy Oil Flow In Heavy Oil Production". The Journal of Canadian Petroleum Technology. Vol. 35, No 6, June 1996, pp 21-24.

12 KRAUS, W., McCAFFREY, W. and BOYD, G. "Pseudo-Bubble Point Model For Foamy Oils". Paper No CIM 93-45 presented at the Annual Technical Meeting of the Petroleum Society of CIM. Calgary, Canada. May 9-12, 1993.

13 SHENG, J., HAYES, R., MAINI, B. and TORTIKE, W. "A Proposed Dynamic Model for Foamy Oil Properties". SPE paper 30253 presented at the International Heavy Oil Symposium. Calgary, Alberta, Canada. 19-21 June 1995.

14 MAINI, B., SARMA, H. and GEORGE, A. "Significance Of Foamy-Oil Behaviour In Primary Production Of Heavy Oils." The Journal of Canadian Petroleum Technology. Vol. 32, No 9, November 1993, pp 50-54.

15 ECONOMIDES E. and FERNANDEZ, B."Global Experiences and Practice For Cold Production of Moderate and Heavy Oil". SPE paper 58773 presented at the 2000 SPE International Symposium on Formation Damage Control. Lafayette, Louisiana, 23-24 February 2000.

16 ISLAM, M.R. and GEORGE, A.E. "Sand Control in Horizontal Wells in Heavy Oil Reservoir". SPE paper 18789 presented at the SPE California Regional Meeting, Bakersfield, California, April 5-7, 1989.

17 TOMA P, TREMBLAY, B., HARRIS P. and KORPANY G. "Experimental investigation for reducing the risk of sand inflow in slotted horizontal wells". Paper 94-PET-2 presented at the Energy-Sources Technology Conference and Exhibition. New Orleans, Louisiana, January 23-27, 1994.

18 FJÆr E., HOLT R., HORSRUD P., RAAEN A., RISNES R. *Petroleum Related Rock Mechanics*. Elsevier Scinece Publishers B.V., Netherlands, 1992.

19 CHALATURNIK R., WAGG B., "The mechanism of solid production in unconsolidated heavy-oil reservoirs".SPE paper 23780 presented at the SPE Intl. Symposium On Formation Damage Control. Lafayette, Louisiana, February 26-27, 1992.

20 PENBERTHY W.L. AND SHAUGHNESSY C.M., *Sand Control,* SPE Series on Special Topics, Volume 1, U.S.A., 1992.

21 GEILKMAN M., DUSSEAULT M. and DULLIEN F. "Fluid Production Enhancement by Exploiting Sand Production". SPE/DOE 27797 paper presented at the SPE/DOE Ninth Symposium on Improved Oil Recovery, Tulsa OK, 17-20 April 1994.

22 SQUIRES A. "Inter-Well Tracer Results And Gel Blocking Program". Paper presented at the 10th Annual Heavy Oil And Oil Sands Technical Symposium. March 9, 1993.

23 YEUNG K. "Cold Flow Production of Crude Bitumen at the Burnt Lake Project", Northeastern Alberta". Paper presented at the 1995 UNITAR Intl Conference on Heavy and Tar Sands, Houston, 12-17 February, 1995.

24 TREMBLAY, B. SEDGWICK, G. and Vu, D. "CT imaging of sand production in a Horizontal Sand Pack Using Live Oil ". Paper 98-78 presented at the 49th Annual

Technical Meeting of the Petroleum Society in Calgary, Alberta, Canada, June 8-10, 1998.

25 TREMBLAY, B. SEDGWICK, G. and FORSHNER K. "Modelling of Sand Production from Wells on Primary recovery". The Journal of Canadian Petroleum Technology. Vol 37, No 3, March 1998.

26 TREMBLAY, B. SEDGWICK, G. and Vu, D. "CT Imaging of Wormhole Growth under Solution Gas Drive". SPE Reservoir Eval & and Eng., Vol 2, No 1, February 1999.

27 VAZIRI, H.H. "Mechanics of Fluid and Sand Production from Oil Sand reservoirs". CIM preprint No 86-37-75 presented at the 37th Annual Technical Meeting, Calgary, Alberta, June 8-11, 1986

28 McCORMACK, M.E. "Effective Sand Control – Some AOSTRA experience". Paper presented at the 42nd Petroleum Mechanical Engineering Workshop and Conference, Calgary, Canada. September 21-23, 1986.

29 HALL, C. and HARRISBERGER W. "Stability of Sand Arches: A Key to Sand Control". Journal of Petroleum Technology. July 1970, pp 821-829.

30 TIPPIE, D. and KOHLHAAS, C."Effect of Flow Rate on Stability of Unconsolidated Producing Sands". SPE preprint No 4533 presented at the 48th Annual Fall Meeting, Las Vegas, Nevada. September 30-October 3,1973.

31 BRATLI R., RISNES R. "Stability and Failure of Sand Arches". Society of Petroleum Engineers Journal. April 1981. pp 236-248.

32 McCORMACK M.E. "Mechanisms of Sand Retainment by Wire-Wrapped Screens". Preprint No 56 Presented at the 4th UNITER/UNDP Conference on Heavy Crude and Tar Sands. Edmoton, Alberta, August 7-12, 1988.

33 SELBY, R. and FAROUQ ALI, S.M. CIM Preprint No 87-38-55 presented at the 38th Annual Technical Meeting of the Petroleum Society of CIM. Calgary, Alberta, June 7-10, 1987

34 RISNES R., BRATLI R. and HORSRUD, P. "Sand Stresses Around a Wellbore". Society of Petroleum Engineers Journal. December 1982. pp 883-898.

35 CLEARY, M., MELVAN, J., KOHLHAAS, C. "The effect of Confining Stress and Fluid Properties on Arch Stability in Unconsolidated Sands". SPE Preprint No 8426 presented at the 54th Annual Fall Meeting and Exhibition of the Society of Petroleum Engineers of AIME, Las Vegas, Nevada. September 23-26,1979.

36 MILLER, W.G. "Sand Flor Mechanisms at Well Casing Perforations". MSc Thesis. Department of Civil Engineering. University of Alberta. Fall 1994.

37 MELVAN, J. "The effect of Overburden Stress on the Formation and Stability of Arches in Unconsolidate Sands". MSc Thesis. Colorado School of Mines University. May 1978.

38 DURRETT, J.L., GOLBIN, W., MURRAY, J.W. and TIGHE, R.E. "Seeking a Solution to Sand Control". Journal of Petroleum Technology . December, 1977. pp 1664-1672.

39 STEIN, N., ODEH, A., JONES, L. "Estimating Maximum Sand-Free Production Rates From Friable Sands for Different Well Completion Geometries". Journal of Petroleum Technology. October 1974, pp1156-1158.

40 VAZIRI H.H., PHILLIPS R. AND HURLEY S. "Physical Modelling of Sand Production". Paper No 323. Int. J. Rock Mech & Min. Sci. 34:3-4. 1997

41 BOONE T.J. SMITH, R.J. and GALWAY, R., "Sand Packing Liner Completions in Heavy Oil Reservoirs". Paper presented at the Sixth One Day Conference on Horizontal Well Technology". Calgary, Alberta. November 12, 1997.

42 YUAN Y. "Abacus Simulation on Near Well bore Stresses and Deformation in Heavy Oil Reservoirs in response to Rapid Pressure Drawdown". Report submitted to Alberta Research Council, November 22, 2000.

43 ELSHERIF B. AND TREMBLAY B., Personal communication. February 2001.

44 ÀRPÀD K. *Handbook of Soil Mechanics*, Elsevier Scientific Publishing Company. Budapest 1974. Chapter 2.

45 LAMBE T.W. and WHITMAN R. V. *Series in Soil Engineering: Soil Mechanics.* Edited by T. William Lambe and Robert V. Whitman. Chapter 4.

46 American Society for Testing and Materials, "Standard Test Method for Particle-Size Analysis of Soils". Designation D 442-63 (Reapproved 1990). pp10-16

47 TERZAGHI, K. and PECK, R. B. *Soil Mechanics in Engineering Practice.* John Wiley and Sons, Inc. Chicago, 1967, p 729

48 American Society for Testing and Materials, "Standard Test Method for RubberChemicals-Density". Designation D 1817-96. 346-347.

49 FOLK, R. *Petrology of Sedimentary Rocks.* Hemphill Publishing Company, Austin, Texas, 1974, p 183

50 SELBY, R. "Flow of fines and Sand Production in Unconsolidated Porous Media". MSc Thesis. Department of Mining, Metallurgical and Petroleum Engineering. University of Alberta. Spring 1987.

51 PRYOR, W. A. *Grain Shape* in Procedures in Sedimentology. Robert E. Carver Editor. Georgia,

52 POWERS M. "A new Roundness Scale for Sedimentary Particles". Journal of Sedimentary Petrology. Vol 23, No 2, June 1953. Pp 117-119.

53 HEAD, K.H. *Manual of Soil Laboratory Testing. Volume 2: Permeability, Shear Strength and Compressibility Test.* Pentech Press, London, 1988.

54 American Society for Testing and Materials, "Standard Test Method for Direct Shear test of Soils Under Consolidated Drained Conditions". Designation D 3080-90. 295-300.

55 JOHANSON, J.R. and JENIKE, A.W. "Settlement of Powders in Vertical Channels by Gas Escape". Journal of applied Mechanics, 863-868, December 1972.

56 Mc Carthy C., Personal comunication, February 13th 2001.

57 BIRD, R.B., STEWART, W.E. and LIGHTFOOT, E., "Transport Phenomena". John Wiley & Sons, Inc. USA, 1976

58 TREMBLAY, B. AND OLDAKOWSKI, K. "Modelling of Sand Transport through Wormholes". AACI Report # 9899-6, December 1998.

59 GILLIES, R.G., HILL, K.B., MCKIBBEN, M.J. and SHOOK, C.A. "Solids Transport by Laminar Newtonian Flow", to be published in Powder Technology, 1999.

60 DULLIEN F.A. "Single Phase Flow Through Porous Media and Pore Structure". The Chemical Enginering Journal. 10 (1975). 1-34

61 GEILIKMAN, M.B. and DUSSEAULT, M.B. "Fluid Rate Enhancement from Massive Sand Production in Heavy Oil Reservoirs". Journal of Petroleum Science and Engineering 17 (1997) 5-18.

62 LANGLOIS,W.E. *Slow Viscous Flow,* Collier-Macmillan Canada Ltd., Toronto, 1964

63 KLIMACK, B. *Manufacturer Booklet.* Slotwell Inc.

A APPENDIX: Numerical Simulation of Stress Field around a Slotted Liner [42]

This concise letter report describes a numerical simulation work undertaken by using ABAQUS to compute near-wellbore stresses and deformation as a result of rapid pressure drawdown in heavy oil reservoirs. It describes the numerical model, and computational results generated in ABAQUS.

The simulation considers elastoplastic deformation and its full coupling with fluid flow. A large deformation formulation is used in order to accommodate the possibly large radial displacement at the sand face during the pressure drawdown. A Drucker-Prager constitutive law without a cap is used to describe the elastoplastic deformation. The far-field stresses are isotropic and therefore, an axi-symmetric geometry is computed.

The input parameters are listed in Table A.1. Note that the bubble point pressure and water compressibility are not used in the simulation because a single-phase pore fluid, i.e., bitumen in foamy oil state, is assumed in the simulation. The bubble point pressure of 2.5 MPa is very near the initial reservoir pressure (3 MPa). Therefore, it is assumed that immediately after the pressure drawdown, the foamy oil state prevails.

The mechanical condition at the sand face, as shown in Figure A.1, it initially deforms freely. After a certain period of pressure drawdown, however, the sand face touches the liner so that further radial inward displacement towards the center of the borehole is prohibited because of the large stiffness contrast between the liner and soft reservoir rock. The time (t_1) when the deforming sand face touches the liner varies with the fluid compressibility and reservoir permeability.

Note that for the hydraulic boundary condition at the sand face which controls fluid flow in the formation, it is assumed that the bottomhole pressure is, at any time, in direct communication and thus, in full equilibrium with the pore pressure in the reservoir rock. The temporal variation of the fluid pressure (p_w) at the sand face is shown in Figure A.2.

In the stress-dependent permeability, the following Carmen-Kozeny-type equation describing the variation of permeability with porosity (ϕ) was used:

$$k = A\left(\frac{\phi^3}{(1-\phi)^2}\right) \tag{A.1}$$

with A=25 Darcy which give k=2 Darcy at $\phi=\phi_0=33\%$. A plot showing the variation is shown in Figure A.3. Note that in the ABAQUS simulation, no limit is imposed on the upper end of the porosity value. Therefore, the porosity near the sand face may exceed the theoretical maximum for a continuum particular medium.

The time t_1 (Figure A.1) required for the wellbore to reach the surface of the horizontal liner under the pressure decline conditions in Figure A.2 was: 75.9 minutes for a compressibility of $2.0\text{x}10^{-8}$ Pa^{-1} and 3.03 minutes for a compressibility of $1.0\text{x}10^{-7}$ Pa^{-1}.

The effective stress at the wellbore surface of the horizontal liner when the formation deformation reached the horizontal liner was: 0 MPa and 0.61 MPa at a compressibility of $2.0\text{x}10^{-8}$ Pa^{-1} and $1.0\text{x}10^{-7}$ Pa^{-1} respectively.

Table A.1: Input Parameters Specified by ARC. After Yuan [42]

Parameter	Value
Maximum horizontal stress gradient	0.02 MPa/m
Minimum horizontal stress gradient	0.02 MPa/m
Vertical stress gradient	0.02 MPa/m
Pore pressure gradient	0.006 MPa/m
Depth	500 m
Permeability (absolute)	2 Darcy
Porosity	33%
Oil Viscosity (cP) at saturation pressure	20,000 cP
Foamy Oil compressibility	1) $1.0\text{x}10^{-7}$/Pa, 2) $2.0\text{x}10^{-8}$/Pa
Bubble point pressure	2.5 MPa
Water compressibility	$1.0\text{x}10^{-10}$/Pa
Young's Modulus	500 MPa
Poisson ratio	0.30
Cohesive strength	15 kPa
Peak friction angle (Drucker-Prager)	48.5 degrees
Dilation angle	30 degrees
Biot constant	0.9
Wellbore diameter (drilled hole)	219 mm
Liner outside diameter	140 mm
Initial pressure	3 MPa
Total radial stress decline (drilling)	Total radial stress at wellbore reduced to 3 MPa (Pore pressure maintained at 3 MPa)
Pressure decline (depletion) following drilling	Wellbore pressure decreased to 500 kPa in four minutes
Production phase	Wellbore pressure maintained at 500 kPa for 3 hours

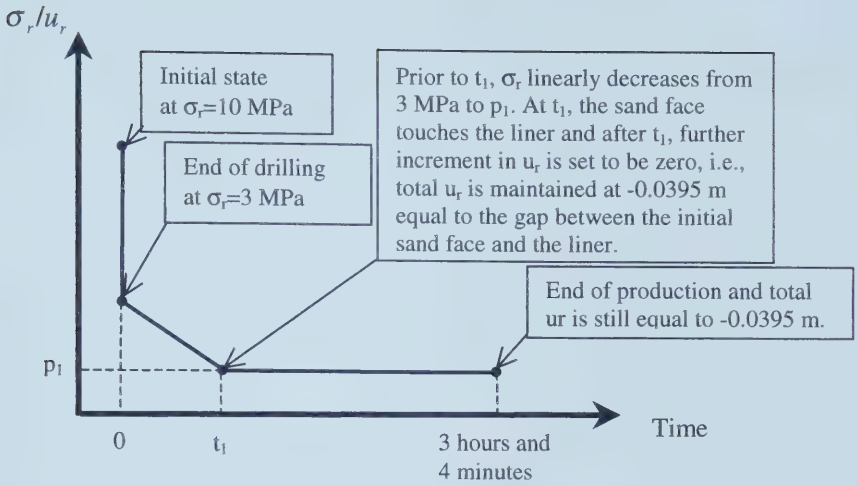

Figure A.1: Mechanical boundary condition at the sand face. u_r is the total radial displacement at the sand face. After Yuan [42]

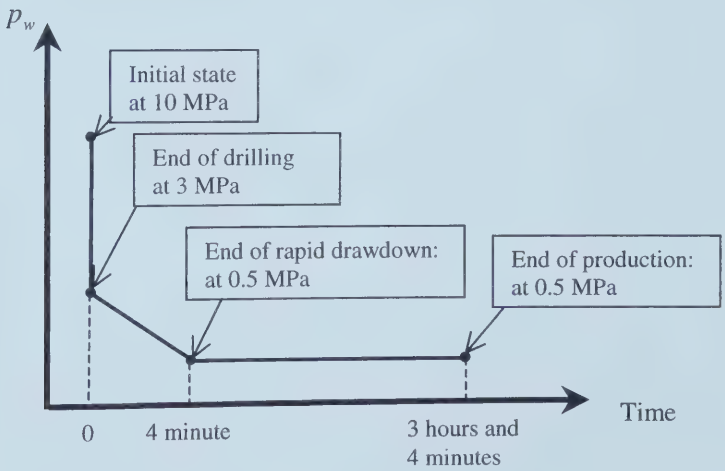

Figure A.2: Hydraulic boundary condition at the sand face. After Yuan [42]

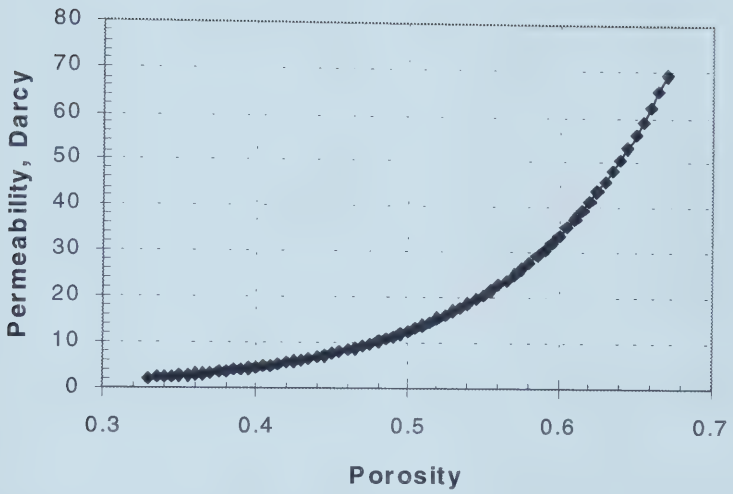

Figure A.3: Variation of the formation permeability with the porosity.

B APPENDIX : Sample Calculations

B.1 Sieve Analysis data

Table B.1: Reproducibility tests of the sieve analysis. Husky sand

U.S. Sieve #	Size mm	Husky	
		Sample 1	Sample 2
18	1.000	100.00	100.00
25	0.710	99.85	99.82
35	0.500	99.50	99.40
45	0.355	99.00	99.03
60	0.250	97.87	97.81
80	0.180	78.93	78.71
120	0.125	30.70	28.98
170	0.090	13.63	12.52
230	0.063	5.79	5.08
325	0.045	2.86	2.43
400	0.038	2.33	2.18

Table B.2: Reproducibility tests of the sieve analysis. Glass Beads Like Husky

U.S.Sieve #	Size mm	Finer Than %		
		Mix 1	Mix 2	Mix 3
35	0.500	99.15	99.21	99.18
45	0.355	98.80	98.85	98.84
60	0.250	96.43	96.31	96.35
70	0.212	90.43	89.56	90.18
80	0.180	76.16	73.98	75.83
100	0.150	45.78	42.12	44.44
120	0.125	32.14	30.41	31.05
170	0.090	13.80	13.68	14.13
230	0.063	4.10	4.29	4.51
325	0.045	0.98	1.09	1.11
400	0.038	0.87	0.97	1.04

Table B.3: Reproducibility tests of the sieve analysis. Glass with less fines

U.S.Sieve #	Size mm	Finer Than %		
		Mix 1	Mix 2	Mix 3
25	0.710	99.91	99.95	99.92
35	0.500	99.50	99.49	99.51
45	0.355	99.30	99.21	99.24
50	0.300	98.99	98.80	98.83
60	0.250	97.87	97.48	97.44
70	0.212	94.34	91.25	92.55
80	0.180	83.83	80.26	79.66
100	0.150	44.98	48.44	39.98
120	0.125	30.12	35.06	30.23
170	0.090	1.76	1.50	1.54
230	0.063	0.54	0.32	0.38
325	0.045	0.15	0.08	0.09
400	0.038	0.10	0.05	0.05

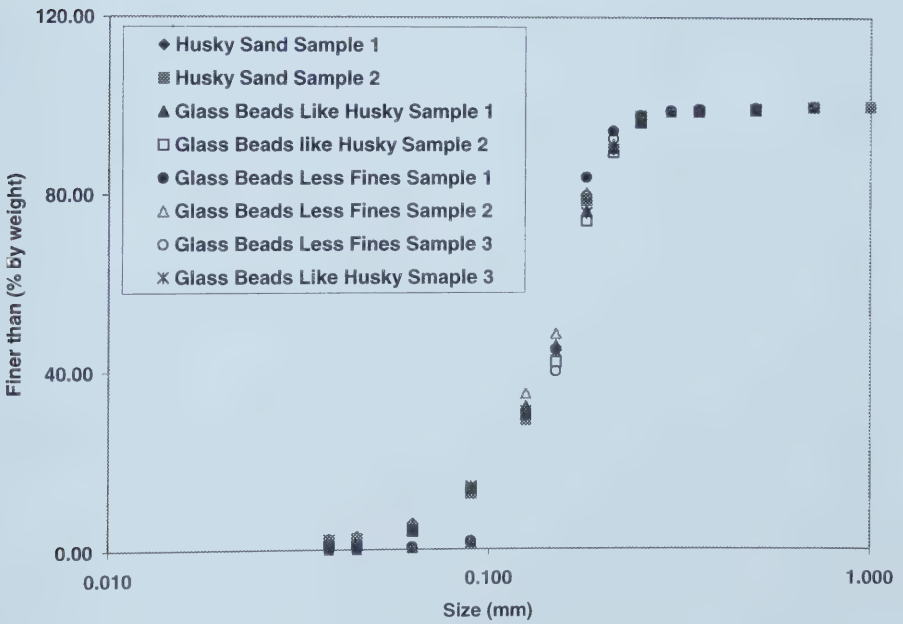

Figure B.1: Size distribution graph: Reproducibility of the sieve analysis for Husky, and glass bead sands.

B.2 Density measurements (From equations 4.3 and 4.4)

Table B.4: Sand density calculations

ρ_{H2O} (22 °C) (g/cc)(from tables)*	0.9978
T_{room} (°C)	22
$\rho_{butanol}$ (22 °C) (g/cc)(from tables)*	0.8058

Sand	Test #	m_p	m_{H2O+p}	m_p	$K + m_p$	ρ (g/cc)	σ	%Desv	%Error
	1	34.5992	63.1541	34.5992	57.7075	0.8075		0.0114	-0.212
Butanol	2	33.7394	61.9353	33.7394	56.5624	0.8076		-0.0114	-0.234
	3	30.9305	58.8081	30.9305	53.4893	0.8074		0.0176	-0.205
	Average					0.8075	0.0001		

Sand	Test #	m_p	$K + m_p$	m_p	m_{s+p}	G	ρ (g/cc)	σ	%Desv
	1	34.8012	59.6386	34.8012	59.9431	76.5721	2.4735		-0.007
GLASS	2	34.5957	57.7075	34.5957	58.8516	74.0106	2.4630		0.416
BEADS	3	34.5987	57.7075	34.5987	55.0568	71.4921	2.4756		-0.093
		34.8012	59.6386	34.8012	54.7031	73.0628	2.4811		-0.315
	Average						2.4733	0.0044	
	1	34.8032	59.6458	34.8032	46.9191	68.0351	2.6255		-0.179
HUSKY	2	33.7394	56.5624	33.7394	58.0573	73.3788	2.6179		0.113
	3	30.9274	53.4893	30.9274	40.5050	60.1138	2.6191		0.066
	Average						2.6208	0.0029	
	1	34.6008	57.7075	34.6008	60.2162	75.4040	2.6122		0.203
SIL-1	2	33.7420	56.5624	33.7420	59.9460	74.7260	2.6318		0.547
	3	30.9255	53.4893	30.9255	59.6974	73.3085	2.5953		-0.849
	Average						2.6175	0.0135	

m_p = mass of picnometer

m_{H2O+p} = mass of water + mass of picnometer

m_{s+p} = mass of sand + mass of picnometer

P = mass of sand = m_{s+p} - m_p

$S = \rho_{butanol}$

$K = mass_{picnometer+butanol} - m_p$

$G = mass_{picnometer + sand + butanol}$

B.3 Effective stress calculations

Table B.5: Effective stress calculations

$P_{prod.}$ (kPa)	101.325
υ	0.3
L (cm)	52.3
c_f	0.525
D (cm)	10.059
1-υ	0.700
4$\mu\upsilon$	0.630
(1-υ)*D/(4L$\mu\upsilon$)	0.085
x (cm)	52.3
$1-e^{-[4\upsilon\mu/(1-\upsilon)](x/D)}$	0.99

where:
$P_{prod.}$ = production pressure
υ =Poisson's ratio
L = length of the pack
c_f = friction coefficient
D = small inner diameter of the cell
x = point where effective stress is calculated, in this case x=L

Slot Size (in)	Sand	q (cm^3/h)	P_{inj} (kPa)	$P_{inj} - P_{prod}$	$\sigma_{eff\ (x)}$ (kPa)
0.022	Sil-1	50	250.27	148.94	12.52
		100	391.64	290.32	24.40
		150	522.60	421.27	35.40
0.028	Sil-1	50	198.17	96.85	8.14
		100	306.66	205.33	17.25
		150	429.56	328.24	27.58
	Husky	50	906.68	805.35	67.67
		100	1991.19	1889.87	158.81
	GBLF	50	731.33	630.00	52.94
		100	1379.33	1278.00	107.39
0.040	Sil-1	50	195.363	94.04	7.90
		100	163.390	62.07	5.22
		150	349.148	247.82	20.82
	Husky	50	879.607	778.28	65.40
		100	1732.505	1631.18	137.07
		150	2490.437	2389.11	200.76

B.4 Shear box test

Table B.6: Data from a typical shear box test. Sand evaluated: Husky

Negatives values in vertical displacement imply setting

m_s (g)	140.63	σ_n (kN/m^2)	40.56	$V_{small\ bars}$	1.12
ρ_s (cm^3)	2.56	L (mm)	9.8048	l (mm)	60.05
V_s (cm^3)	54.93	A (m^2)	0.00361	h (cm)	2.36
m_{load}(Kg)	14.91	PV (cm^3)	28.0756	V_T (cm^3)	83.01
F(N)	146.27	ϕ	33.82	Rate of Displacement (mm/min)	0.10

Time (s)	Room T (°C)	Load (N)	Horizontal Displac.	Vertical Displac.	ΔL (mm)	τ (KPa)	ΔVert. Displac.
0	23.48	0.0000	9.8048	3.7646	0.0000	0.0000	0.0000
40	23.63	2.6828	9.7963	3.7633	0.0085	0.7440	0.0012
60	23.63	9.8349	9.7878	3.7646	0.0170	2.7274	0.0000
80	23.71	16.0913	9.7804	3.7658	0.0243	4.4624	-0.0012
100	23.78	21.4542	9.7671	3.7670	0.0377	5.9496	-0.0024
120	23.63	31.2889	9.7512	3.7670	0.0536	8.6769	-0.0024
140	23.71	49.1669	9.7269	3.7670	0.0779	13.6347	-0.0024
160	23.63	63.4711	9.7001	3.7670	0.1047	17.6015	-0.0024
180	23.71	75.0904	9.6709	3.7694	0.1339	20.8237	-0.0049
200	23.71	85.8186	9.6405	3.7719	0.1643	23.7988	-0.0073
220	23.71	94.7576	9.6100	3.7768	0.1948	26.2777	-0.0122
240	23.56	102.8031	9.5796	3.7817	0.2252	28.5089	-0.0171
260	23.63	109.9552	9.5479	3.7878	0.2568	30.4923	-0.0232
280	23.63	116.2116	9.5175	3.7927	0.2873	32.2273	-0.0281
300	23.78	122.4702	9.4871	3.7975	0.3177	33.9629	-0.0330
320	23.78	128.7266	9.4567	3.8061	0.3481	35.6979	-0.0415
340	23.78	133.1961	9.4274	3.8171	0.3774	36.9373	-0.0525
360	23.78	130.5158	9.4116	3.8195	0.3932	36.1940	-0.0550
380	23.71	139.4548	9.3848	3.8268	0.4200	38.6730	-0.0623
400	23.78	143.9243	9.3520	3.8354	0.4528	39.9124	-0.0708
420	23.71	147.5003	9.3203	3.8464	0.4845	40.9041	-0.0818
440	23.71	151.0763	9.2874	3.8598	0.5173	41.8958	-0.0953
460	23.71	154.6524	9.2546	3.8696	0.5502	42.8875	-0.1050
480	23.63	157.3327	9.2217	3.8806	0.5831	43.6308	-0.1160
500	23.71	160.0153	9.1876	3.8904	0.6172	44.3747	-0.1258
520	23.78	162.6979	9.1535	3.9026	0.6512	45.1186	-0.1380
540	23.78	165.3783	9.1195	3.9160	0.6853	45.8619	-0.1514
560	23.86	166.2717	9.0854	3.9307	0.7194	46.1097	-0.1661
580	23.78	167.1674	9.0501	3.9404	0.7547	46.3581	-0.1759
600	23.78	170.7412	9.0148	3.9514	0.7900	47.3492	-0.1869
620	23.71	171.6369	8.9795	3.9649	0.8253	47.5976	-0.2003
640	23.78	172.5304	8.9454	3.9795	0.8594	47.8453	-0.2150
660	23.78	174.3172	8.9101	3.9917	0.8947	48.3409	-0.2272
680	23.78	175.2130	8.8748	4.0039	0.9300	48.5892	-0.2394
700	23.78	176.1064	8.8395	4.0149	0.9653	48.8370	-0.2504
720	23.78	176.9999	8.8042	4.0272	1.0006	49.0848	-0.2626

Time (s)	Room T (°C)	Load (N)	Horizontal Displac.	Vertical Displac.	ΔL (mm)	τ (KPa)	ΔVert. Displac.
740	23.78	176.9999	8.7689	4.0418	1.0359	49.0848	-0.2772
760	23.71	176.9999	8.7348	4.0565	1.0700	49.0848	-0.2919
780	23.71	176.9999	8.7007	4.0699	1.1041	49.0848	-0.3053
800	23.71	177.8933	8.6654	4.0809	1.1394	49.3326	-0.3163
820	**23.78**	**177.8933**	**8.6313**	**4.0931**	**1.1735**	**49.3326**	**-0.3285**
840	**23.71**	**177.8933**	**8.5960**	**4.1053**	**1.2088**	**49.3326**	**-0.3408**
860	23.71	176.9999	8.5607	4.1200	1.2441	49.0848	-0.3554
880	23.71	176.1064	8.5254	4.1334	1.2794	48.8370	-0.3688
900	23.71	176.1064	8.4913	4.1444	1.3134	48.8370	-0.3798
920	23.71	175.2130	8.4560	4.1566	1.3487	48.5892	-0.3921
940	23.63	172.5304	8.4195	4.1676	1.3853	47.8453	-0.4030
960	23.63	172.5304	8.3854	4.1810	1.4193	47.8453	-0.4165
980	23.56	170.7412	8.3489	4.1933	1.4559	47.3492	-0.4287
1000	23.56	169.8477	8.3136	4.2030	1.4912	47.1014	-0.4385
1020	23.56	168.0609	8.2783	4.2140	1.5265	46.6059	-0.4495
1040	23.48	166.2717	8.2430	4.2238	1.5618	46.1097	-0.4592
1060	23.56	163.5914	8.2065	4.2336	1.5983	45.3664	-0.4690
1080	23.48	161.8022	8.1712	4.2433	1.6336	44.8702	-0.4788
1100	23.48	160.0153	8.1347	4.2519	1.6701	44.3747	-0.4873
1120	23.63	157.3327	8.0982	4.2604	1.7066	43.6308	-0.4959
1140	23.63	154.6524	8.0616	4.2665	1.7431	42.8875	-0.5020
1160	23.63	152.8632	8.0263	4.2739	1.7784	42.3913	-0.5093
1180	23.63	149.2872	7.9886	4.2812	1.8162	41.3996	-0.5166
1200	23.63	145.7111	7.9509	4.2861	1.8539	40.4079	-0.5215
1220	23.56	141.2416	7.9144	4.2861	1.8904	39.1685	-0.5215
1240	23.63	136.7721	7.8778	4.2910	1.9270	37.9290	-0.5264
1260	23.63	132.3026	7.8401	4.2922	1.9647	36.6896	-0.5276
1280	23.63	128.7266	7.8024	4.2958	2.0024	35.6979	-0.5313
1300	23.71	126.0463	7.7658	4.2983	2.0389	34.9546	-0.5337
1320	23.71	123.3637	7.7281	4.3007	2.0767	34.2106	-0.5362
1340	23.71	120.6811	7.6904	4.2958	2.1144	33.4667	-0.5313
1360	23.78	118.8942	7.6539	4.2958	2.1509	32.9712	-0.5313
1380	23.71	117.1073	7.6173	4.2946	2.1875	32.4757	-0.5301
1400	23.71	116.2116	7.5808	4.2934	2.2240	32.2273	-0.5288
1420	23.71	115.3181	7.5455	4.2934	2.2593	31.9795	-0.5288
1440	23.71	114.4247	7.5090	4.2934	2.2958	31.7317	-0.5288
1460	23.78	114.4247	7.4725	4.2934	2.3323	31.7317	-0.5288
1480	23.71	114.4247	7.4360	4.2934	2.3688	31.7317	-0.5288
1500	23.78	114.4247	7.4007	4.2946	2.4041	31.7317	-0.5301
1520	23.63	114.4247	7.3629	4.2958	2.4419	31.7317	-0.5313
1540	23.63	114.4247	7.3276	4.2958	2.4772	31.7317	-0.5313
1560	23.71	114.4247	7.2911	4.2971	2.5137	31.7317	-0.5325
1580	23.71	114.4247	7.2558	4.2958	2.5490	31.7317	-0.5313
1600	23.78	114.4247	7.2193	4.2934	2.5855	31.7317	-0.5288
1620	23.71	115.3181	7.1840	4.2922	2.6208	31.9795	-0.5276
1640	23.78	114.4247	7.1475	4.2934	2.6573	31.7317	-0.5288
1660	23.78	114.4247	7.1109	4.2934	2.6938	31.7317	-0.5288
1680	23.86	114.4247	7.0744	4.2946	2.7304	31.7317	-0.5301
1700	23.78	115.3181	7.0391	4.2958	2.7657	31.9795	-0.5313
1720	23.71	114.4247	7.0026	4.2971	2.8022	31.7317	-0.5325
1740	23.71	115.3181	6.9661	4.2983	2.8387	31.9795	-0.5337
1760	23.71	114.4247	6.9308	4.2983	2.8740	31.7317	-0.5337
1780	23.63	115.3181	6.8943	4.2971	2.9105	31.9795	-0.5325

Time (s)	Room T (°C)	Load (N)	Horizontal Displac.	Vertical Displac.	ΔL (mm)	τ (KPa)	ΔVert. Displac.
1800	23.63	115.3181	6.8578	4.2958	2.9470	31.9795	-0.5313
1820	23.63	115.3181	6.8225	4.2958	2.9823	31.9795	-0.5313
1840	23.56	115.3181	6.7872	4.2971	3.0176	31.9795	-0.5325
1860	23.56	114.4247	6.7506	4.2971	3.0542	31.7317	-0.5325
1880	23.56	114.4247	6.7141	4.2983	3.0907	31.7317	-0.5337
1900	23.56	114.4247	6.6788	4.2995	3.1260	31.7317	-0.5349
1920	23.48	115.3181	6.6435	4.3007	3.1613	31.9795	-0.5362
1940	23.41	115.3181	6.6070	4.3007	3.1978	31.9795	-0.5362
1960	23.48	115.3181	6.5717	4.3007	3.2331	31.9795	-0.5362
1980	23.56	114.4247	6.5352	4.3007	3.2696	31.7317	-0.5362
2000	23.56	114.4247	6.4987	4.2995	3.3061	31.7317	-0.5349
2020	23.48	115.3181	6.4634	4.2983	3.3414	31.9795	-0.5337
2040	23.48	115.3181	6.4281	4.2995	3.3767	31.9795	-0.5349
2060	23.56	114.4247	6.3915	4.2995	3.4133	31.7317	-0.5349
2080	23.56	115.3181	6.3562	4.2995	3.4486	31.9795	-0.5349
2100	23.63	114.4247	6.3197	4.3007	3.4851	31.7317	-0.5362
2120	23.63	114.4247	6.2832	4.3007	3.5216	31.7317	-0.5362
2140	23.56	113.5312	6.2479	4.3020	3.5569	31.4840	-0.5374
2160	23.56	114.4247	6.2126	4.3032	3.5922	31.7317	-0.5386
2180	23.63	114.4247	6.1761	4.3044	3.6287	31.7317	-0.5398
2200	23.48	114.4247	6.1396	4.3068	3.6652	31.7317	-0.5423
2220	23.48	114.4247	6.1043	4.3068	3.7005	31.7317	-0.5423
2240	23.48	115.3181	6.0677	4.3068	3.7371	31.9795	-0.5423
2260	23.56	114.4247	6.0312	4.3068	3.7736	31.7317	-0.5423
2280	23.48	114.4247	5.9959	4.3056	3.8089	31.7317	-0.5411
2300	23.33	114.4247	5.9606	4.3044	3.8442	31.7317	-0.5398
2320	23.33	114.4247	5.9241	4.3056	3.8807	31.7317	-0.5411
2340	23.48	114.4247	5.8876	4.3056	3.9172	31.7317	-0.5411
2360	23.56	114.4247	5.8523	4.3056	3.9525	31.7317	-0.5411
2380	23.56	114.4247	5.8158	4.3056	3.9890	31.7317	-0.5411
2400	23.56	114.4247	5.7805	4.3068	4.0243	31.7317	-0.5423
2420	23.56	114.4247	5.7452	4.3068	4.0596	31.7317	-0.5423
2440	23.63	114.4247	5.7074	4.3068	4.0974	31.7317	-0.5423
2460	23.63	113.5312	5.6721	4.3081	4.1327	31.4840	-0.5435
2480	23.63	113.5312	5.6356	4.3081	4.1692	31.4840	-0.5435
2500	23.63	113.5312	5.6003	4.3081	4.2045	31.4840	-0.5435
2520	23.63	113.5312	5.5626	4.3081	4.2422	31.4840	-0.5435
2540	23.56	113.5312	5.5273	4.3093	4.2775	31.4840	-0.5447
2560	23.56	113.5312	5.4907	4.3093	4.3140	31.4840	-0.5447
2580	23.63	113.5312	5.4542	4.3093	4.3506	31.4840	-0.5447
2600	23.63	113.5312	5.4189	4.3093	4.3859	31.4840	-0.5447
2620	23.63	113.5312	5.3824	4.3093	4.4224	31.4840	-0.5447
2640	23.63	113.5312	5.3459	4.3093	4.4589	31.4840	-0.5447
2660	23.63	113.5312	5.3094	4.3093	4.4954	31.4840	-0.5447
2680	23.63	114.4247	5.2741	4.3093	4.5307	31.7317	-0.5447
2700	23.71	113.5312	5.2376	4.3081	4.5672	31.4840	-0.5435
2720	23.71	114.4247	5.2010	4.3081	4.6038	31.7317	-0.5435
2740	23.78	114.4247	5.1657	4.3081	4.6391	31.7317	-0.5435
2760	23.71	113.5312	5.1304	4.3068	4.6744	31.4840	-0.5423
2780	23.63	113.5312	5.0939	4.3068	4.7109	31.4840	-0.5423
2800	23.63	114.4247	5.0586	4.3068	4.7462	31.7317	-0.5423
2820	23.63	113.5312	5.0221	4.3068	4.7827	31.4840	-0.5423

Time (s)	Room T (°C)	Load (N)	Horizontal Displac.	Vertical Displac.	ΔL (mm)	τ (KPa)	ΔVert. Displac.
2840	23.63	114.4247	4.9856	4.3068	4.8192	31.7317	-0.5423
2860	23.71	113.5312	4.9503	4.3068	4.8545	31.4840	-0.5423
2880	23.71	113.5312	4.9150	4.3068	4.8898	31.4840	-0.5423
2900	23.78	113.5312	4.8785	4.3068	4.9263	31.4840	-0.5423
2920	23.71	113.5312	4.8432	4.3068	4.9616	31.4840	-0.5423
2940	23.71	113.5312	4.8066	4.3081	4.9982	31.4840	-0.5435
2960	23.71	113.5312	4.7713	4.3081	5.0335	31.4840	-0.5435
2980	23.71	112.6355	4.7336	4.3081	5.0712	31.2356	-0.5435
3000	23.56	112.6355	4.6983	4.3081	5.1065	31.2356	-0.5435
3020	23.48	113.5312	4.6630	4.3081	5.1418	31.4840	-0.5435
3040	23.56	113.5312	4.6265	4.3081	5.1783	31.4840	-0.5435
3060	23.56	113.5312	4.5912	4.3081	5.2136	31.4840	-0.5435
3080	23.56	112.6355	4.5547	4.3081	5.2501	31.2356	-0.5435
3100	23.48	112.6355	4.5181	4.3081	5.2867	31.2356	-0.5435
3120	23.48	112.6355	4.4828	4.3093	5.3220	31.2356	-0.5447
3140	23.41	112.6355	4.4475	4.3093	5.3573	31.2356	-0.5447
3160	23.48	113.5312	4.4110	4.3093	5.3938	31.4840	-0.5447
3180	23.48	113.5312	4.3745	4.3105	5.4303	31.4840	-0.5459
3200	23.41	113.5312	4.3392	4.3105	5.4656	31.4840	-0.5459
3220	23.41	112.6355	4.3027	4.3105	5.5021	31.2356	-0.5459
3240	23.48	112.6355	4.2662	4.3105	5.5386	31.2356	-0.5459
3260	23.48	112.6355	4.2309	4.3105	5.5739	31.2356	-0.5459
3280	23.41	112.6355	4.1943	4.3105	5.6104	31.2356	-0.5459
3300	23.41	112.6355	4.1578	4.3105	5.6470	31.2356	-0.5459
3320	23.41	112.6355	4.1225	4.3105	5.6823	31.2356	-0.5459
3340	23.41	113.5312	4.0872	4.3117	5.7176	31.4840	-0.5472
3360	23.33	112.6355	4.0507	4.3117	5.7541	31.2356	-0.5472
3380	23.41	112.6355	4.0142	4.3117	5.7906	31.2356	-0.5472
3400	23.33	112.6355	3.9789	4.3117	5.8259	31.2356	-0.5472
3420	23.41	112.6355	3.9424	4.3117	5.8624	31.2356	-0.5472
3440	23.41	112.6355	3.9058	4.3117	5.8989	31.2356	-0.5472
3460	23.33	112.6355	3.8705	4.3117	5.9342	31.2356	-0.5472
3480	23.33	112.6355	3.8352	4.3129	5.9695	31.2356	-0.5484
3500	23.41	112.6355	3.7987	4.3129	6.0061	31.2356	-0.5484
3520	23.48	112.6355	3.7622	4.3129	6.0426	31.2356	-0.5484
3540	23.56	111.7421	3.7269	4.3129	6.0779	30.9878	-0.5484
3560	23.48	112.6355	3.6904	4.3117	6.1144	31.2356	-0.5472
3580	23.41	112.6355	3.6551	4.3117	6.1497	31.2356	-0.5472
3600	23.48	112.6355	3.6198	4.3117	6.1850	31.2356	-0.5472
3620	23.41	112.6355	3.5833	4.3117	6.2215	31.2356	-0.5472
3640	23.56	111.7421	3.5468	4.3117	6.2580	30.9878	-0.5472
3660	23.56	112.6355	3.5114	4.3117	6.2933	31.2356	-0.5472
3680	23.56	111.7421	3.4749	4.3117	6.3299	30.9878	-0.5472
3700	23.56	111.7421	3.4396	4.3105	6.3652	30.9878	-0.5459
3720	23.56	111.7421	3.4031	4.3105	6.4017	30.9878	-0.5459
3740	23.56	112.6355	3.3678	4.3105	6.4370	31.2356	-0.5459
3760	23.56	111.7421	3.3313	4.3105	6.4735	30.9878	-0.5459
3780	23.48	112.6355	3.2960	4.3105	6.5088	31.2356	-0.5459
3800	23.48	112.6355	3.2607	4.3105	6.5441	31.2356	-0.5459
3820	23.56	112.6355	3.2242	4.3093	6.5806	31.2356	-0.5447
3840	23.71	111.7421	3.1877	4.3093	6.6171	30.9878	-0.5447
3860	23.63	111.7421	3.1524	4.3093	6.6524	30.9878	-0.5447
3880	23.63	111.7421	3.1171	4.3093	6.6877	30.9878	-0.5447

Time (s)	Room T (°C)	Load (N)	Horizontal Displac.	Vertical Displac.	ΔL (mm)	τ (KPa)	ΔVert. Displac.
3900	23.56	111.7421	3.0793	4.3093	6.7255	30.9878	-0.5447
3920	23.48	111.7421	3.0440	4.3081	6.7608	30.9878	-0.5435
3940	23.48	110.8486	3.0087	4.3081	6.7961	30.7400	-0.5435
3960	23.48	110.8486	2.9722	4.3081	6.8326	30.7400	-0.5435
3980	23.56	111.7421	2.9357	4.3081	6.8691	30.9878	-0.5435
4000	23.63	110.8486	2.9004	4.3068	6.9044	30.7400	-0.5423
4020	23.56	110.8486	2.8639	4.3068	6.9409	30.7400	-0.5423
4040	23.48	110.8486	2.8273	4.3068	6.9775	30.7400	-0.5423
4060	23.56	110.8486	2.7933	4.3068	7.0115	30.7400	-0.5423
4080	23.56	110.8486	2.7567	4.3056	7.0481	30.7400	-0.5411
4100	23.56	110.8486	2.7202	4.3056	7.0846	30.7400	-0.5411
4120	23.56	110.8486	2.6849	4.3056	7.1199	30.7400	-0.5411
4140	23.56	111.7421	2.6484	4.3056	7.1564	30.9878	-0.5411
4160	23.48	111.7421	2.6131	4.3044	7.1917	30.9878	-0.5398
4180	23.48	110.8486	2.5766	4.3044	7.2282	30.7400	-0.5398
4200	23.41	110.8486	2.5413	4.3044	7.2635	30.7400	-0.5398
4220	23.48	110.8486	2.5060	4.3032	7.2988	30.7400	-0.5386
4240	23.56	110.8486	2.4695	4.3032	7.3353	30.7400	-0.5386
4260	23.48	110.8486	2.4342	4.3032	7.3706	30.7400	-0.5386
4280	23.48	110.8486	2.3976	4.3032	7.4072	30.7400	-0.5386
4300	23.56	109.9552	2.3611	4.3020	7.4437	30.4923	-0.5374
4320	23.48	109.9552	2.3258	4.3020	7.4790	30.4923	-0.5374
4340	23.48	110.8486	2.2905	4.3020	7.5143	30.7400	-0.5374
4360	23.48	110.8486	2.2528	4.3020	7.5520	30.7400	-0.5374
4380	23.48	109.9552	2.2175	4.3007	7.5873	30.4923	-0.5362
4400	23.56	109.9552	2.1810	4.3007	7.6238	30.4923	-0.5362
4420	23.56	109.9552	2.1444	4.3007	7.6604	30.4923	-0.5362
4440	23.48	109.9552	2.1091	4.2995	7.6957	30.4923	-0.5349
4460	23.48	109.9552	2.0738	4.2995	7.7310	30.4923	-0.5349
4480	23.48	109.9552	2.0373	4.2983	7.7675	30.4923	-0.5337
4500	23.56	109.9552	2.0008	4.2983	7.8040	30.4923	-0.5337
4520	23.56	109.9552	1.9643	4.2983	7.8405	30.4923	-0.5337
4540	23.56	109.9552	1.9290	4.2983	7.8758	30.4923	-0.5337
4560	23.56	109.955	1.8925	4.2971	7.9123	30.4923	-0.5325
4580	23.56	109.955	1.8559	4.2971	7.9488	30.4923	-0.5325
4600	23.56	109.062	1.8206	4.2971	7.9841	30.2445	-0.5325
4620	23.56	109.955	1.7841	4.2958	8.0207	30.4923	-0.5313

B.5 Calculation of the air flow rate

Two assumptions were made to calculate the air flow rate. The first one is that the air flow was turbulent. This assumption was based on rough calculations during the calibration of the capillary tube using a flowmeter. The second assumption is that the capillary tube can be considered "hydraulically smooth". Therefore the friction factor is given by the following equation [18]:

$$f = \frac{0.0791}{\mathrm{Re}^{1/4}} \tag{B.1}$$

where Re is the dimensionless parameter Reynolds number given by:

$$\mathrm{Re} = \frac{Dv\rho}{\mu} \tag{B.2}$$

D = diameter of the pipe
v = average fluid velocity
ρ = density of the fluid
μ = viscosity of the fluid

The velocity of the air at the entrance of a pipe can be calculated from [57]:

$$2\frac{fL}{D} = \ln\frac{p_2}{p_1} - \frac{1}{2}\left[\left(\frac{p_2}{p_1}\right)^2 - 1\right]\frac{RT_1}{Mv_1^2} \tag{B.3}$$

where: L = the length of the pipe
D = the diameter of the pipe
P_2 = the pressure at the end of the capillary tube
P_1 = the pressure at the entrance of the capillary tube
R = the universal gas constant
T_1 = temperature at the entrance of the capillary tube
M = the molecular weight of the air
v_1 = velocity of the air at the entrance of the capillary tube

Substituting B.2 into B.1 and then into B.3, an equation as a function of v, the unknown variable is obtained:

$$0 = \ln\frac{p_2}{p_1} - \frac{1}{2}\left[\left(\frac{p_2}{p_1}\right)^2 - 1\right]\frac{RT_1}{Mv_1^2} - 0.1582\frac{L}{D}\left(\frac{\mu}{Dv\rho}\right)^{1/4} \quad \text{(B.4)}$$

Using the real gas equation, the air density was calculated as:

$$\rho = \frac{pM}{ZRT} \quad \text{(B.5)}$$

where Z is the compressibility factor which depends on pressure. Data obtained from tables [64] for Z at 20 °C was plotted in Figure B.2. A second degree polynomial was fitted to the Z factor data with a regression coefficient of 0.9999:

$$Z = 3x10^{-10}p^2 - 4x10^{-6}p + 1 \quad \text{(B.6)}$$

The viscosity of the air was assumed to be constant within the same range of temperature and pressure used in this experimental work.

The iteration tool called "solver" in excel was used in the fluid velocity calculation.

Once v_1 is calculated and knowing the pressures p_1 and p_2, the velocity of the fluid at the end of the capillary tube, v_2, can be found using the mass balance equation:

$$p_2v_2 = p_1v_1 \quad \text{(B. 7)}$$

Therefore, the air flow rate was calculated as:

$$Q_A = v_2A \quad \text{(B. 8)}$$

where A = the area of the pipe
Q_A = air flow rate
v_2 = velocity at the end of the capillary tube

Table B.7 to B.10 present the data and calculations to determine Q_A. Table B.8 shows the average pressure drop, inlet pressure and outlet pressure for each sand pack at the different air delivery pressures. The calculations were made at two different temperatures representing the range in temperature during the experiments.

Table B.7: Constants used in the air flow rate calculations

L (m)	0.55
D (m)	1.40×10^{-3}
A (m^2)	1.53×10^{-6}
M (g/mol)	28.97
μ (Pa.s)(20 C, Patm)	1.8×10^{-5}
R($mPam^3K^{-1}mol^{-1}$)	8314.51

Table B.8: Data for air flow rate calculations. ADP = air delivery pressure

ADP (psi)	Sand	ΔP (kPa)	p_2 (kPa)	p_1 (kPa)	T (K)	Z factor	ρ (Kg/m^3)
10	Sil-1	32.00	108.52	140.52	295	0.9995	1.4714
		32.00	108.52	140.52	300	0.9995	1.4469
	Husky	32.25	113.19	145.44	295	0.9995	1.5281
		32.25	113.19	145.44	300	0.9995	1.5026
20	Sil-1	81.29	119.87	201.16	295	0.9994	1.8970
		81.29	119.87	201.16	300	0.9994	1.8654
	Husky	79.26	127.86	207.12	295	0.9993	1.9795
		79.26	127.86	207.12	300	0.9993	1.9465
40	Sil-1	174.71	165.99	340.70	295	0.9990	2.9952
		174.71	165.99	340.70	300	0.9990	2.9453
	Husky	172.90	163.79	336.69	295	0.9990	2.9585
		172.90	163.79	336.69	300	0.9990	2.9091
60	Sil-1	232.07	221.99	454.06	295	0.9987	3.9977
		232.07	221.99	454.06	300	0.9987	3.9310
	Husky	232.24	223.99	456.23	295	0.9987	4.0223
		232.24	224.99	457.23	300	0.9987	3.9669
80	Husky	301.40	283.07	584.47	295	0.9983	5.1318
		301.40	283.07	584.47	300	0.9983	5.0463

p_2 (kPa) and p_1 (kPa) are absolute pressures

Table B.9: Air flow rate calculations

Sand	$\ln\left(\frac{p_2}{p_1}\right)$	$\frac{1}{2}\left[\left(\frac{p_2}{p_1}\right)^2 - 1\right]$	$\frac{RT_1}{M}$	$0.1582\frac{L}{D}\left(\frac{\mu}{D\rho}\right)^{0.25}$	v_1 (m/s)
Sil-1	-0.2584	-0.2018	84666.22	19.05	47.70
	-0.2584	-0.2018	86101.24	19.13	48.05
Husky	-0.2507	-0.1972	84666.22	18.87	47.35
	-0.2507	-0.1972	86101.24	18.95	47.69
Sil-1	-0.5177	-0.3225	84666.22	17.88	63.07
	-0.5177	-0.3225	86101.24	17.96	63.54
Husky	-0.4824	-0.3095	84666.22	17.69	62.15
	-0.4824	-0.3095	86101.24	17.77	62.61
Sil-1	-0.7191	-0.3813	84666.22	15.95	72.21
	-0.7191	-0.3813	86101.24	16.02	72.75
Husky	-0.7206	-0.3817	84666.22	16.00	72.13
	-0.7206	-0.3817	86101.24	16.07	72.66
Sil-1	-0.7156	-0.3805	84666.22	14.84	74.77
	-0.7156	-0.3805	86101.24	14.90	75.32
Husky	-0.7114	-0.3795	84666.22	14.82	74.75
	-0.7091	-0.3789	86101.24	14.87	75.28
Husky	-0.7250	-0.3827	84666.22	13.94	77.27
	-0.7250	-0.3827	86101.24	14.00	77.84

The velocity v_2 was calculated by using Equation B.7 substituting the velocity v_1 in Table B.9 and p_1 and p_2 from Table B.8. The air flow rate was then calculated by using equation B.8. This flow rate was averaged for the two different sand packs since the values of the velocity v_2 calculed in table B.9 were similar. The average air flow rates are listed in Table 4.10 as a function of the injection pressure.

Table B.10: Z factor for air at different pressures[64]. Temperature 20 °C.

Z	p (atm)	p (Kpa)
1.0000	0.01	1.01
0.9999	0.10	10.13
0.9998	0.40	40.53
0.9996	1.00	101.33
0.9975	7.00	709.28
0.9965	10.00	1013.25
0.9889	40.00	4053.00
0.9861	70.00	7092.75
0.9884	100.00	10132.50

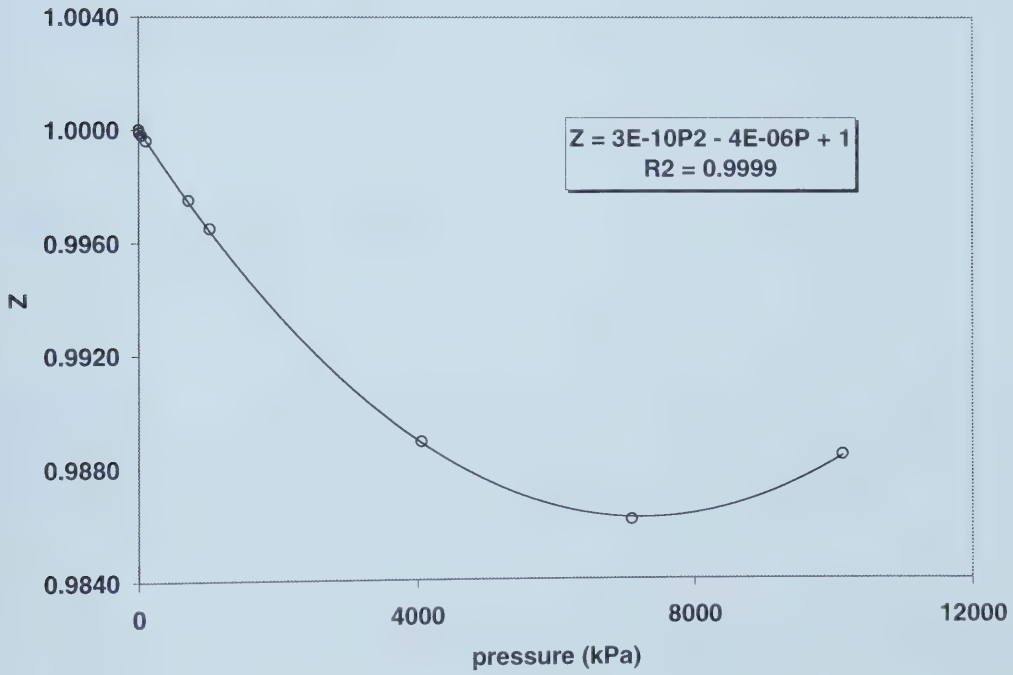

Figure B.2: Z factor versus pressure for air @ 20 °C

B.6 Calibration of the pump

The pump was calibrated by measuring the exact volume of oil delivered for a given period of time. This was done for the three flow rates evaluated in the liquid experiments and for both pump cylinders.

For an accurate measurement of the volume delivered by the pump a similar procedure to the one used for determining the density of the sands based on the ASTM method D1817 [48] was used. The main difference was the use of water to determine the volume of the picnometer instead of 1-butanol.

A Weld's specific gravity bottle (picnometer) was used. First the volume of the picnometer was found. This is done by weighing the vessel when empty and dry, and again when completely filled with water.

The volume can be found as follow:

$$V = \frac{w}{\rho_{H_2O}} \tag{B.9}$$

where: V = volume of the picnometer
w = weight of water
ρ_{H2O} = water density

Secondly, the oil was delivered into the dry picnometer. A chronometer was used to measure the time during which the sample was collected. The sample is weighed in the vessel, which is then filled with water and reweighed. The sample weight times the density of the water is divided by the weight of water that the sample displaced.

The pump flow rate can be calculated by either:

1. Using the oil density measured at the analytical laboratory of ARC to calculate the oil volume using B.9 or
2. Determining the density of the oil with the data obtained and using the weight of the sample to determine the volume

The flow rate is then calculated by dividing the volume found in either way by the time of sampling. Table B.11 and Table B.12 show the data found during these tests and Figure B.3 and B.4 show the calibration curves for pumps 1 and 2 respectively.

Table B.11: Pump 1 calibration data

q (cc/h)	Test #	Pdry	P_{H2O}	P_{dry}	$P_{drv+sample}$	$P_{drv+sample+H2O}$	t (min)	ρ (g/cc)	V (cc)	q (cc/h)	q from ρ
50	1	31.63	63.62	31.64	37.35	63.48	7	0.9727	5.8704	50.32	50.23
	2	31.65	63.60	31.65	36.50	63.48	6	0.9741	4.9788	49.79	49.78
	3	31.65	63.59	31.65	39.68	63.41	10	0.9763	8.2246	49.35	49.45
	Average							0.9744		49.82	49.82
100	1	31.63	63.58	31.64	44.87	63.21	8.1	0.9704	13.6341	100.621	100.21
	2	31.65	63.57	31.63	40.48	63.35	5.4	0.9762	9.0660	100.734	100.92
	3	31.64	63.57	31.64	40.4	63.39	5.4	0.9781	8.9559	99.824	100.21
	Average							0.9736		100.39	100.45
150	1	31.64	63.59	31.63	56.06	62.95	10	0.9731	25.104	150.63	150.44
	2	31.64	63.58	31.62	43.85	63.23	5	0.9720	12.582	150.99	150.62
	3	31.64	63.54	31.63	43.8	63.21	5	0.9727	12.512	150.15	149.88
	Average							0.9726	16.73	150.59	150.31

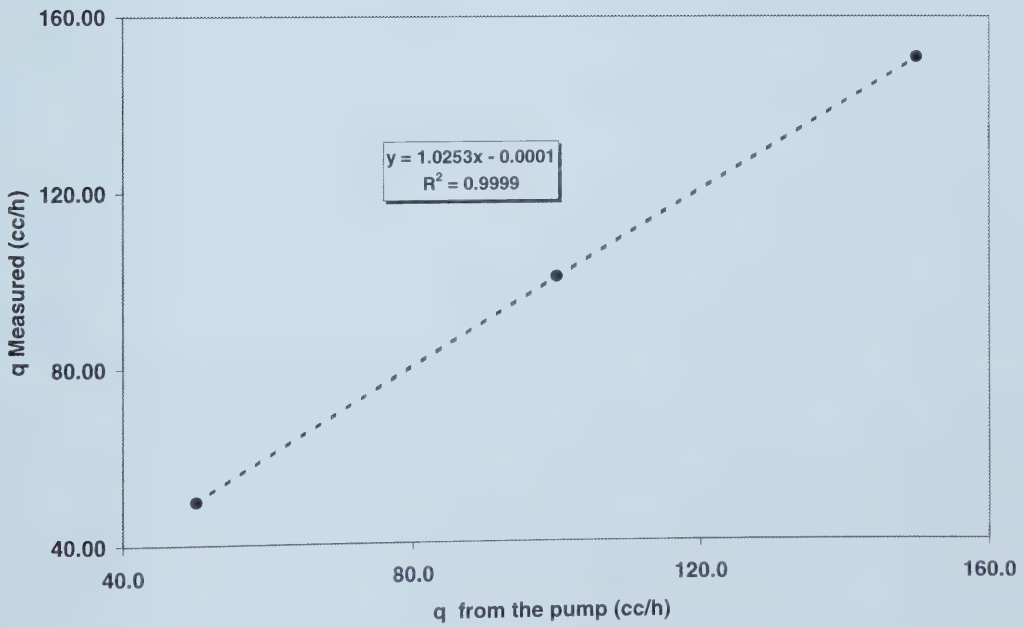

Figure B.3: Calibration graph for pump 1

Table B.12: Pump 2 calibration data

q (cc/h)	Test #	Pdry	P_{H2O}	P_{dry}	$P_{dry+sample}$	$P_{dry+sample+H2O}$	t (min)	ρ (g/cc)	V (cc)	q (cc/h)	q from ρ
50	1	31.63	63.60	31.66	37.54	63.49	7.0	0.975	6.03	51.69	51.73
	2	31.63	63.61	31.64	38.17	63.45	8.0	0.973	6.71	50.34	50.26
	3	31.63	63.58	31.64	34.86	63.52	4.0	0.977	3.30	49.44	49.57
	Average							0.975		50.49	50.52
100	1	31.65	63.57	31.64	38.29	63.37	4.1	0.971	6.85	100.275	99.88
	2	31.65	63.58	31.63	38.19	63.41	4.0	0.976	6.72	100.828	100.99
	3	31.66	63.56	31.62	38.13	63.36	4.0	0.974	6.68	100.227	100.22
	Average							0.974		100.44	100.36
150	1	31.63	63.61	31.64	43.86	63.3	5.0	0.973	12.56	150.75	150.50
	2	31.63	63.59	31.64	43.89	63.3	5.0	0.974	12.57	150.87	150.87
	3	31.64	63.61	31.64	43.82	63.3	5.0	0.973	12.51	150.15	150.01
	Average							0.974	12.55	150.59	150.46

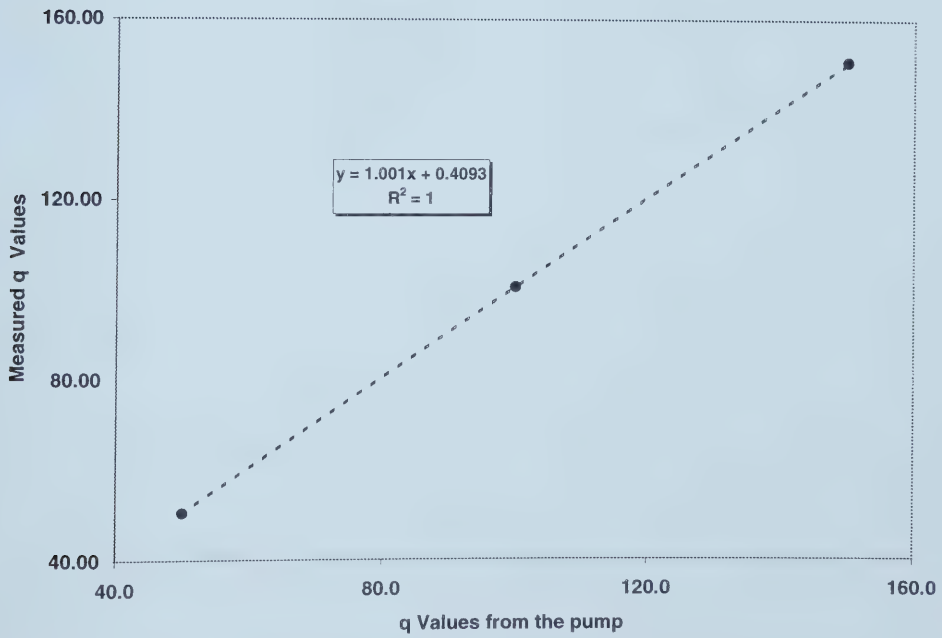

Figure B.4: Calibration graph for pump 2

B.7 Calculation of porosity in the pack

The porosity of the pack was calculated knowing the mass of the sand, its density and the total volume of the pack. This volume was calculated from the dimensions of the vessel and the total height of the sand in the cell.

The vessel was composed of a cylindrical and a converging section as shown in Figure 4.18. An example of a porosity calculation for the liquid Run 5 is given below:

R_L (cm)	10.318	where: R_L = Radius of the large cylinder
r_S (cm)	5.30	r_S = Radius of the small cylinder
m_s (g)	24960	m_s = Sand mass
ρ_s (g/cm^3)	2.621	ρ_s = Sand density
V_s(cm^3)	9523.795	V_S = Sand volume
h_{cz} (cm)	10.16	h_{cz}= Height of the converging zone
$h_{sand\ in\ the\ cylinder}$ (cm)	40.50	$h_{sand\ in\ the\ cylinder}$ = Sand height
$h_{small\ cylinder}$ (cm)	0.84	$h_{small\ cylinder}$ = Small cylinder height
$V_{converging\ zone}$ (V_{cz}) (cm^3)	1953.832	$V_{Converging\ zone}$ = Converging zone volume
$V_{small\ cylinder}$ (cm^3)	66.754	$V_{small\ cilynder}$ = Small cylinder volume
$V_{cylinder}$ (cm^3)	13544.25	$V_{cylinder}$ = Cylinder volume
V_T (cm^3)	15564.83	V_T = Total volume
PV	6041.038	PV = Pore volume
ϕ	0.388	ϕ = Porosity

$$\phi = \frac{PV}{V_T} \tag{B.1}$$

$$PV = V_T - V_S \tag{B.2}$$

$$V_T = V_{cz} + V_{cylinder} + V_{smallcylinder} \tag{B.3}$$

$$V_{cz} = \frac{1}{3}\pi h_{cz}\left[R_L{}^2 + R_L r_S + r_S^2\right]$$

(B.4)

$$V_s = \frac{m_s}{\rho_s} \tag{B.5}$$

B.8 Compressibility Tests

B.8.1 Procedure

1. Once the pack was saturated with oil, the outlet valve was closed.

2. Oil was injected at a constant rate.

3. Some time was allowed for readings to stabilize.

Pressure readings were taken by the data acquisition system during the test; the pump volume was measured from the displacement of the pump piston.

B.8.2 Calculations

For low gas saturation, the total compressibility of the air and oil within the sand pack may be written as:

$$c_T = S_o c_o + S_g c_g \tag{B.6}$$

where: c_T = the total compressibility
S_o = the oil saturation
c_o = the oil compressibility
S_g = the gas saturtation
c_g = the gas compressibility

From the definition of isothermal compressibility, the gas compressibility is given by:

$$c_g = -\frac{1}{V}\frac{\partial V}{\partial p}\Big|_T \tag{B.7}$$

Since the tests were performed at pressures close to atmospheric, the ideal gas equation can be used:

$$V = \frac{nRT}{p} \tag{B.8}$$

where: V = gas volume
n = number of moles
R= universal gas constant
T = temperature
p = pressure

The partial derivative of the previous expression with respect to p is:

$$\frac{\partial V}{\partial p} = -\frac{nRT}{p^2} \tag{B.9}$$

Substituting (B.8) and (B.9) in (B.7) we obtain for the compressibility of the gas:

$$c_g = \frac{1}{p} \tag{B.10}$$

Therefore from (B.7), assuming that the oil compressibility can be neglected, we can calculate the volume of air present in the pack using (B.10) for the gas compressibility as follows:

$$V = -p\frac{\Delta V}{\Delta p} \tag{B.11}$$

The differential pressure was taken at three different ports along the cell to verify the values obtained.

A sample calculation taking the data show in Table B.13 is given below:

$\Delta V_{\text{oil injected}} = -\Delta V_{\text{gas compressed}} = 22.00$ cc

$p = 176.814$ kPa

$PV = 6041.04$ cc

For the port at the top of the cell, the differential pressure (Δp_1) was = **158.94 kPa.** Therefore the gas volume @ **15.435 kPa** (initial pressure) was:

$$V_{@15.435} = (176.814 + 101.325)kPa\,\frac{22cc}{158.94kPa} = 38.499cc$$

The volume of gas in the pack at atmospheric pressure can be found using Boyle's law:

$$V_{@\,atm} = \frac{V_{@\,15.435}\, p_f}{p_{atm}} \tag{B.12}$$

Therefore substituting values in (B.8):

$$V_{@\,atm} = \frac{38.499cc(15.435 + 101.325)kPa}{101.325kPa} = 44.364cc$$

The percentage of air in the pack taking the PV calculated in B.3 is:

$$\%Air = \frac{V_{air}}{PV} * 100 = \frac{44.364}{6041.04} * 100 = 0.734$$

The maximum quantity of air accepted in the sand pack was 1% at atmospheric pressure.

The pressures measured in ports 2 and 5, identified as P_2 and P_3 respectively, were done as a check measurement. It can be observed in Table B.13 that they are close to each other with a maximum difference of 7.34 %.

In these calculations the compressibility of the oil was neglected. Therefore the actual gas saturation should be lower than the one presented. In addition, since the pressure during the test is significantly larger than atmospheric pressure, the gas saturation in the pack will be lower.

B.9 Determination of absolute permeability

The absolute permeability to oil of a sand pack was calculated using Darcy's law for linear flow. The pressure drop readings were taken at the central part of the cell where a differential transducer identified as ΔP_1 was connected. The core was flooded with silicone oil at a constant flow rate.

From Darcy's linear flow equation, the permeability can be calculated as follow:

$$k = \frac{Q\Delta L\mu}{A\Delta P} \tag{B.13}$$

where: Q = the volumetric flow rate
ΔL = length of a section of the sand pack
A = the cross sectional area perpendicular to the flow
ΔP = the pressure drop across the sand pack segment with length ΔL
μ = the viscosity of the flowing fluid in this case synthetic oil

The permeability was calculated at different times and an average was taken as the core permeability.

Sample data and values calculated are showing in Table B.14.

Table B.13: Sample data for compressibility test. Oil Run # 5: Husky Oil sand. Slot size 0.028 in

Room T (C)	26.92	**For ΔP_1**	
Slot size (in)	0.02800	$V_{@\ 15.435}$ (cc)	38.4984
Pump initial reading (cm^3)	631.208	$V_{@\ atm.\ P}$ (cc)	44.3629
Pump final reading (cm^3)	653.208	**% Air**	**0.7344**
Date of the test	06/19/00	**For ΔP_2**	
μ for $T_{average}$ (cP)	13099.35	$V_{@\ 15.435}$ (cc)	37.9950
ΔV (cc)	22.00	$V_{@\ atm.\ P}$ (cc)	41.9310
Δp_1 (kPa)	158.94	**% Air**	**0.6941**
Δp_2 (kPa)	158.15	**For Δp_3**	
Δp_3 (kPa)	156.65	$V_{@\ 15.435}$ (cc)	39.6685
PV (cc)	6041.04	$V_{@\ atm.\ P}$ (cc)	45.0149
		% Air	**0.7452**

Time (s)	p_1 (kPa)	p_2 (kPa)	p_3 (kPa)	T cell (°C)
0	17.8708	13.6563	24.4846	27.02
20	17.9721	13.5066	24.3123	27.02
40	94.2768	17.7067	25.2086	27.02
60	171.2984	36.5563	28.3801	27.02
80	204.4951	56.1565	32.2071	27.02
100	215.9360	72.2062	36.4471	27.02
120	219.4100	84.8559	40.6878	27.02
140	219.4100	94.7056	44.7555	27.02
160	217.7752	102.9559	48.9620	27.02
180	216.1406	109.8054	52.9955	27.02
200	214.9150	115.6057	56.9251	27.02
460	200.9197	152.1052	98.0192	27.02
220	213.1790	120.6555	60.7173	26.95
240	211.6456	125.0558	64.4063	26.95
260	209.8083	128.9058	67.9572	26.95
280	209.5004	132.4058	71.4390	26.95
300	208.4795	135.6055	74.7834	27.02
320	206.6402	138.3550	77.9896	27.02
340	206.1298	140.8556	81.1263	27.02
360	204.4951	143.0557	84.1603	27.02
380	203.6786	145.1052	87.0562	27.02
400	203.7800	147.2052	89.9521	27.02
420	202.8623	148.9552	92.7790	27.02
440	201.9426	150.5050	95.4336	26.95
520	199.4896	155.7055	105.3623	26.95

Time (s)	p_1 (kPa)	p_2 (kPa)	p_3 (kPa)	T cell (°C)
580	197.3464	158.8049	111.8781	26.95
640	195.5071	160.9049	117.7042	26.95
700	194.5875	162.8047	122.9785	26.87
760	193.0561	164.5547	127.8741	26.87
820	192.3410	165.8555	132.3213	26.87
880	191.5227	166.7549	136.2167	26.87
940	191.2168	167.4549	139.6643	26.87
1000	189.3776	168.2054	142.7674	26.87
1060	189.4808	169.0552	145.5943	26.87
1120	188.4579	169.6054	148.3521	26.80
1180	187.8460	169.7552	150.6963	26.80
1240	186.8231	170.1052	152.8683	26.80
1300	186.1081	170.2549	154.7989	26.80
1360	186.1081	170.4552	156.6256	26.80
1420	185.2918	170.8052	158.3149	26.87
1480	185.1904	171.0055	159.9700	26.80
1540	184.8826	171.1046	161.3489	26.80
1600	184.8826	171.2048	162.6246	26.87
1660	183.8616	171.3049	163.7622	26.87
1720	183.9649	171.3049	164.8656	26.87
1780	183.1465	171.4051	165.8993	26.87
1840	183.0452	171.5548	166.7962	26.87
2020	182.1256	171.9048	169.6915	26.80
2320	180.6955	171.6549	172.0706	26.80
2620	179.8772	171.7055	174.3806	26.80
2920	179.0608	171.4051	175.6557	26.80
3220	179.5712	171.2553	176.5178	26.80
3520	178.6516	170.9053	177.2417	26.80
3820	177.9366	170.6555	177.6553	26.80
4120	176.9157	170.2549	177.7586	26.80
4420	176.3020	170.0050	177.9999	26.80
4720	176.2006	169.8048	178.1380	26.87
5020	175.2809	169.5549	178.1380	26.73
5320	175.2809	169.3050	178.0347	26.73
5620	174.4646	168.9055	177.9657	26.73
5920	174.4646	168.7548	177.8276	26.73
6220	173.5449	168.4048	177.7586	26.73
6520	173.5449	168.4048	177.6212	26.80
6820	173.1358	167.9546	177.3450	26.80
7120	173.0345	168.0052	177.2766	26.87
7420	173.1358	168.3552	177.3108	26.87
7720	173.5449	168.4553	177.4831	26.87
8020	173.5449	168.8053	177.8276	26.95
8320	174.3613	168.9550	177.9999	26.95
8620	174.4646	169.3546	177.9999	26.95
8920	174.4646	169.3050	178.4483	27.02
9220	174.5659	169.8553	179.1724	27.02
9520	175.2809	170.0546	179.2756	27.02

Time (s)	p_1 (kPa)	p_2 (kPa)	p_3 (kPa)	T cell (°C)
9820	175.2809	170.3551	179.4137	27.09
10120	175.2809	170.6555	179.6892	27.09
10420	176.2006	171.0055	180.2067	27.17
10720	176.2006	171.5052	180.7235	27.17
11020	176.8143	171.8047	181.1371	27.17

Table B.14: Sample data and calculations for permeability tests. Oil run # 5: Husky Sand. Slot size: 0.028 in (0.712 mm)

$T_{cell\ average}$ (°C)	27.88
Slot Size (in)	0.02800
ΔL (cm)	9.5
A (cm^2)	334.426
Date of the test	08/22/00
$\mu_{average}$ (cP)	12427.46
Q (cm^3/h)	20
Q (cm^3/s)	0.005556
$k_{average}$(darcies)	4.42

Elapse Time (s)	Date and Time	Time (s)	Δp_1(kPa) Corrected	T cell (°C)	μ (cP)	$k_{in\ the\ pack}$ darcies
966968400	20:00.0	0	47.2091	27.094	12550.34	4.25
966968700	25:00.0	300	47.1155	27.094	12550.34	4.26
966969000	30:00.0	600	47.1062	27.094	12550.34	4.26
966969300	35:00.0	900	47.1155	27.241	12527.15	4.25
966969600	40:00.0	1200	47.0128	27.167	12538.72	4.26
966969900	45:00.0	1500	47.1062	27.314	12515.62	4.25
966970200	50:00.0	1800	46.9006	27.314	12515.62	4.27
966970500	55:00.0	2100	46.8537	27.388	12504.13	4.27
966970800	00:00.0	2400	46.8352	27.388	12504.13	4.27
966971100	05:00.0	2700	46.8912	27.461	12492.68	4.26
966971400	10:00.0	3000	46.9286	27.461	12492.68	4.26
966971700	15:00.0	3300	46.8819	27.461	12492.68	4.26
966972000	20:00.0	3600	46.9099	27.388	12504.13	4.26
966972300	25:00.0	3900	46.9286	27.535	12481.27	4.25
966972600	30:00.0	4200	46.9473	27.535	12481.27	4.25
966972900	35:00.0	4500	46.9941	27.608	12469.91	4.24
966973200	40:00.0	4800	46.9941	27.608	12469.91	4.24
966973500	45:00.0	5100	47.0313	27.535	12481.27	4.24

Elapse Time (s)	Date and Time	Time (s)	Δp_1(kPa) Corrected	T cell (°C)	μ (cP)	$k_{in\ the\ pack}$ darcies
966973800	50:00.0	5400	47.0875	27.608	12469.91	4.23
966974100	55:00.0	5700	47.0782	27.608	12469.91	4.24
966974400	00:00.0	6000	47.1342	27.681	12458.58	4.23
966974700	05:00.0	6300	47.1342	27.755	12447.29	4.22
966975000	10:00.0	6600	47.1904	27.755	12447.29	4.22
966975300	15:00.0	6900	47.1997	27.681	12458.58	4.22
966975600	20:00.0	7200	47.2184	27.608	12469.91	4.22
966975900	25:00.0	7500	47.3026	27.461	12492.68	4.22
966976200	30:00.0	7800	47.2839	27.461	12492.68	4.22
966976500	35:00.0	8100	47.2931	27.461	12492.68	4.22
966976800	40:00.0	8400	47.3306	27.681	12458.58	4.21
966977100	45:00.0	8700	47.3493	27.755	12447.29	4.20
966977400	50:00.0	9000	47.3868	27.902	12424.84	4.19
966977700	55:00.0	9300	47.4241	27.828	12436.05	4.19
966978000	00:00.0	9600	47.4148	27.902	12424.84	4.19
966978300	05:00.0	9900	47.4428	27.975	12413.67	4.18
966978600	10:00.0	10200	47.4428	28.049	12402.55	4.18
966978900	15:00.0	10500	47.4802	27.902	12424.84	4.18
966979200	20:00.0	10800	47.4615	27.902	12424.84	4.19
966980400	40:00.0	12000	47.5270	27.902	12424.84	4.18
966981600	00:00.0	13200	47.5457	27.902	12424.84	4.18
966982800	20:00.0	14400	47.5737	27.975	12413.67	4.17
966984000	40:00.0	15600	47.5737	28.049	12402.55	4.17
966985200	00:00.0	16800	47.5457	28.049	12402.55	4.17
966986400	20:00.0	18000	47.5457	28.049	12402.55	4.17
966987600	40:00.0	19200	47.4615	28.196	12380.41	4.17
966988800	00:00.0	20400	47.2931	27.975	12413.67	4.20
966990000	20:00.0	21600	47.1250	27.828	12436.05	4.22
966991200	40:00.0	22800	46.8912	27.975	12413.67	4.23
966992400	00:00.0	24000	46.7135	27.902	12424.84	4.25
966993600	20:00.0	25200	46.5452	27.902	12424.84	4.27
966994800	40:00.0	26400	46.3488	27.828	12436.05	4.29
966996000	00:00.0	27600	46.1807	27.828	12436.05	4.31
966997200	20:00.0	28800	45.9843	27.902	12424.84	4.32
966998400	40:00.0	30000	45.7972	27.902	12424.84	4.34
966999600	00:00.0	31200	45.6758	27.902	12424.84	4.35
967000800	20:00.0	32400	45.4980	27.902	12424.84	4.37
967002000	40:00.0	33600	45.3858	27.975	12413.67	4.37
967003200	00:00.0	34800	45.1427	28.049	12402.55	4.39
967004400	20:00.0	36000	45.0118	27.975	12413.67	4.41
967005600	40:00.0	37200	44.8062	28.049	12402.55	4.43
967006800	00:00.0	38400	44.5911	27.975	12413.67	4.45
967008000	20:00.0	39600	44.3386	28.049	12402.55	4.47
967009200	40:00.0	40800	44.1517	27.975	12413.67	4.50
967010400	00:00.0	42000	43.9741	28.049	12402.55	4.51
967011600	20:00.0	43200	43.6841	28.122	12391.46	4.54
967012800	40:00.0	44400	43.4692	28.049	12402.55	4.56

Elapse Time (s)	Date and Time	Time (s)	Δp_1(kPa) Corrected	T cell (°C)	μ (cP)	$k_{in\ the\ pack}$ darcies
967014000	00:00.0	45600	43.2167	28.122	12391.46	4.58
967015200	20:00.0	46800	42.9643	28.049	12402.55	4.62
967016400	40:00.0	48000	42.7585	28.122	12391.46	4.63
967017600	00:00.0	49200	42.7118	28.122	12391.46	4.64
967018800	20:00.0	50400	42.3752	28.196	12380.41	4.67
967020000	40:00.0	51600	42.2349	28.196	12380.41	4.69
967021200	00:00.0	52800	41.9638	28.122	12391.46	4.72
967022400	20:00.0	54000	41.7767	28.196	12380.41	4.74
967023600	40:00.0	55200	41.6458	28.196	12380.41	4.75
967024800	00:00.0	56400	41.4869	28.196	12380.41	4.77
967026000	20:00.0	57600	41.2344	28.196	12380.41	4.80
967027200	40:00.0	58800	41.1690	28.196	12380.41	4.81
967028400	00:00.0	60000	41.0942	28.196	12380.41	4.82
967029600	20:00.0	61200	41.0382	28.196	12380.41	4.82
967030800	40:00.0	62400	41.0008	28.196	12380.41	4.83
967032000	00:00.0	63600	41.0475	28.269	12369.40	4.82
967033200	20:00.0	64800	40.8044	28.269	12369.40	4.85
967034400	40:00.0	66000	40.7203	28.269	12369.40	4.86
967035600	00:00.0	67200	40.7015	28.343	12358.43	4.86
967036800	20:00.0	68400	40.7390	28.269	12369.40	4.86
967038000	40:00.0	69600	40.8886	28.269	12369.40	4.84
967039200	00:00.0	70800	41.0288	28.196	12380.41	4.83
967040400	20:00.0	72000	41.0942	28.269	12369.40	4.81
967041600	40:00.0	73200	41.1504	28.269	12369.40	4.81
967042800	00:00.0	74400	41.2626	28.269	12369.40	4.79
967044000	20:00.0	75600	41.4215	28.269	12369.40	4.78
967045200	40:00.0	76800	41.5337	28.269	12369.40	4.76
967046400	00:00.0	78000	41.8984	28.269	12369.40	4.72
967047600	20:00.0	79200	42.7210	28.269	12369.40	4.63
Average values				**27.88**	**12427.85**	**4.42**

University of Alberta Library
0 1620 1395 4902
B45452